

VOLUME 79 SEPTEMBER 11, 1975 NUMBER 19

JPCHAX

THE JOURNAL OF

PHYSICAL

CHEMISTRY



PUBLISHED BIWEEKLY BY THE AMERICAN CHEMICAL SOCIETY

New physical chemistry references.

Wiley-Interscience.

Electrons in Metals

An Introduction to Modern Topics

C.M. Hurd

Concise answers "what is a metal?" Explains fundamental concepts simply, facilitating understanding by those new to the field. A consultant who reviewed the book before publication said, "It is a unique work which gathers together in one place much of the material needed to understand metals." 0-471-42220-7 1975 352 pp. (tent.) \$19.50

Advances in General Physics, Vols. 31, 32, 33

edited by **I. Prigogine & Stuart A. Rice**

Vol. 31: Non-Simple Liquids:

A Topical Volume in Advances

Covers theory of molecular models for water, structure of polar fluids, kinetic theory of dense polyatomic fluids, low-energy electron status in liquid metals, more. 0-471-69933-0 1975 496 pp. (tent.) \$29.95 (tent.)

Vol. 32: Proceedings of the Conference on Instability and Dissipative Structures in Hydrodynamics

Explores mechanism of instabilities in non-linear systems, stellar evolutionary stability in relation to spectral theory, magnetic fields and convections, other topics. 0-471-69934-9 1975 336 pp. (tent.) \$27.50

Vol. 33: Advances in Chemical Physics

Updates transition state stabilization energy as a measure of chemical reactivity, thermodynamics of evolving chemical systems and approach to equilibrium. 0-471-69935-7 1975 480 pp. (tent.) \$32.00

Phonons and Resonances in Solids

Baldassare Di Bartolo & Richard C. Powell

Treats the thermal vibrations of crystalline solids and their effects on the spectra of these materials. Concentrates on symmetry considerations and experimental techniques. An ideal learning reference aid. 0-471-21275-X 1975 500 pp. (tent.) \$19.95 (tent.)

Chemical Infrared Fourier Transform Spectroscopy

Peter R. Griffiths

A Volume in Chemical Analysis: A Series of Monograph on Analytical Chemistry and Its Applications, P.J. Elvin J.D. Winefordner, Advisory Editors
Gives you easy access to the theory, instrumentation, and chemical applications of infrared Fourier transform spectroscopy. Covers the Michelson interferometer, computing techniques, signal-to-noise ratio. Details dual-beam FTS, the principle behind the new GC-IR instrument introduced by Spectrotherm Corp. 0-471-32786-7 1975 352 pp. (tent.) \$24.95

Separation Methods in Chemical Analysis

James M. Miller

A better understanding of common separation methods useful in approaching laboratory problems. Details gas and liquid chromatography, distillation, liquid-liquid extraction, and zone electrophoresis. An ideal basic reference to everyday problems. 0-471-60490-9 1975 309 pp. \$14.95

Membranes in Separations

Sun-Tak Hwang & Karl Kammermeyer

Volume 7 in the Wiley Series on Techniques of Chemistry, Arnold Weissberger, Advisory Editor
Provides a unified treatment of all membrane separation methods. Covers specific applications in biomedicine, industry, and analytical chemistry. Concise definition terminology and concepts clarify confusing existing views. 0-471-93268-X 1975 559 pp. \$35.50

Deformation Kinetics

A.S. Krausz & H. Eyring

Full discussion of the thermally activated plastic deformation and fracture processes. Provides an understanding of the physical principles and the analytical methods of the interpretation of molecular processes. 0-471-24983-1 1975 576 pp. (tent.) \$24.95 (tent.)



Treatise on Analytical Chemistry, Vol. 11

Part 1: Theory and Practice

edited by **I.M. Kolthoff & Philip J. Elving**,

with the assistance of **Ernest B. Sandell**

Practical reference to apparatus, techniques, and operations. Covers classical methods of analysis, and the gravimetric and titrimetric techniques. 0-471-49967-6 1975 752 pp. (tent.) \$39.50

Progress in Inorganic Chemistry, Vol. 21

edited by **Stephen J. Lippard**

Detailed information on metal carbonyls, polynuclear complexes with aminoalcohols and iminoalcohols as ligands, much more. 0-471-54091-9 1975 304 pp. (tent.) \$22.50

The Measurement of Airborne Particles

Richard D. Cadle

A Volume in the Wiley Series on Environmental Science and Technology, R.L. Metcalf, James N. Pitts Jr., Werner Stumm, Advisory Editors

Wew help for the selection, development, and use of airborne measurement equipment. Shows what's being manufactured in aerosol measurement equipment, along with design criteria. Full discussion of the theory, techniques, and equipment for the measurement of particles suspended in gases - especially air.

0-471-12910-0 1975 347 pp. (tent.) \$18.95 (tent.)

The Organic Chemistry of Electrolyte Solutions

sohn E. Gordon

A Volume in the Interscience Monographs Series on Organic Chemistry, George A. Olah, Advisory Editor Comprehensive coverage of the chemical, structural, Spectroscopic, and dynamic aspects of electrolyte Solutions. Data regarding simple to exotic solutions - Such as polyelectrolytes, micelles, now at your fingertips in one guide. 0-471-31620-2 1975 496 pp. (tent.) 19.95 (tent.)

The Observation and Analysis of tellar Photospheres

avid F. Gray

introduction to the observational aspects of stellar Atmospheres. Includes material on observation equip-

ment, analytical techniques, and the principles of data collection in spectrophotometry. 0-471-32380-2 1975 480 pp. (tent.) \$24.95

Theory of Molecular Relaxation

Applications in Chemistry and Biology

Francis K. Fong

Stimulating, radically new approach to understanding relaxation phenomena. Contains detailed descriptions of radiationless processes, account of the recently proposed molecular model for the primary light reaction in photosynthesis. 0-471-26555-1 1975 320 pp. (tent.) \$15.95

Marine Corrosion

Francis L. LaQue

sponsored by the Electrochemical Society, Inc.

A Volume in the Wiley Series on Corrosion, N. Hackerman, C.V. King, F.L. LaQue, & Z.A. Foroulis, Advisory Editors

Describes the practical problems encountered in marine environments and solutions provided by modern technology. 0-471-51745-3 1975

352 pp. \$22.50

Molecular Scattering:

Physical and Chemical Applications

edited by **K.P. Lawley**

Volume 30 in the Wiley Series on Advances in Chemical Physics, I. Prigogine & S.A. Rice, Advisory Editors

Collection of up-to-date articles on reactive scattering, electronic excitation in collisions between neutrals, classical S-matrix in molecular collision, scattering of positive ions by molecules, etc. 0-471-51900-6 1975 592 pp. (tent.) \$49.50 (tent.)

Prices subject to change without notice.

Write Dr. Robert Badger, Dept. 976.

Include author, title, and **book number** for prompt service.

WILEY-INTERSCIENCE

a division of JOHN WILEY & SONS, INC.
605 Third Avenue, New York, N.Y. 10016



In Canada: John Wiley & Sons, Canada, Ltd.

22 Worcester Road, Rexdale, Ontario 092-45277-W1

ห้องสมุด กรมวิทยาศาสตร์

THE JOURNAL OF PHYSICAL CHEMISTRY

BRYCE CRAWFORD, Jr., *Editor*
STEPHEN PRAGER, *Associate Editor*
ROBERT W. CARR, Jr., **FREDERIC A. VAN-CATLEDGE**, *Assistant Editors*

EDITORIAL BOARD: C. A. ANGELL (1973-1977), F. C. ANSON (1974-1978),
V. A. BLOOMFIELD (1974-1978), J. R. BOLTON (1971-1975), L. M. DORFMAN (1974-1978),
H. L. FRIEDMAN (1975-1979), E. J. HART (1975-1979), W. J. KAUFMANN (1974-1978),
R. L. KAY (1972-1976), D. W. McCLURE (1974-1978), R. M. NOYES (1973-1977),
J. A. POPLE (1971-1975), B. S. RABINOVITCH (1971-1975), S. A. RICE (1969-1975),
F. S. ROWLAND (1973-1977), R. L. SCOTT (1973-1977), A. SILBERBERG (1971-1975),
J. B. STOTHERS (1974-1978), W. A. ZISMAN (1972-1976)

AMERICAN CHEMICAL SOCIETY, 1155 Sixteenth St., N. W., Washington, D. C. 20036

Books and Journals Division

D. H. MICHAEL BOWEN *Director*

CHARLES R. BERTSCH *Head, Editorial Processing Department*
BACIL GUILLEY *Head, Graphics and Production Department*
SELDON W. TERRANT *Head, Research and Development Department*

©Copyright, 1975, by the American Chemical Society. Published biweekly by the American Chemical Society at 20th and Northampton Sts., Easton, Pa. 18042. Second-class postage paid at Washington, D.C., and at additional mailing offices.

All manuscripts should be sent to *The Journal of Physical Chemistry*, Department of Chemistry, University of Minnesota, Minneapolis, Minn. 55455.

Additions and Corrections are published once yearly in the final issue. See Volume 78, Number 26 for the proper form.

Extensive or unusual alterations in an article after it has been set in type are made at the author's expense, and it is understood that by requesting such alterations the author agrees to defray the cost thereof.

The American Chemical Society and the Editor of *The Journal of Physical Chemistry* assume no responsibility for the statements and opinions advanced by contributors.

Correspondence regarding accepted copy, proofs, and reprints should be directed to Editorial Processing Department, American Chemical Society, 20th and Northampton Sts., Easton, Pa. 18042. Department Head: CHARLES R. BERTSCH. Associate Department Head: MARIANNE C. BROGAN, Assistant Editors: CELIA B. MCFARLAND, JOSEPH E. YURVATI.

Advertising Office: Centcom, Ltd., 50 W. State St., Westport, Conn. 06880.

Business and Subscription Information

Send all new and renewal subscriptions *with payment to*: Office of the Controller, 1155 16th Street, N.W., Washington, D.C. 20036. Subscriptions should be renewed promptly to avoid a break in your series. All correspondence and telephone calls regarding

changes of address, claims for missing issues, subscription service, the status of records, and accounts should be directed to Manager, Membership and Subscription Services, American Chemical Society, P.O. Box 3337, Columbus, Ohio 43210. Telephone (614) 421-7230. For microfiche service, contact ACS Microfiche Service, 1155 16th St. N.W., Washington, D.C. 20036. Telephone (202) 872-4444.

On changes of address, include both old and new addresses with ZIP code numbers, accompanied by mailing label from a recent issue. Allow four weeks for change to become effective.

Claims for missing numbers will not be allowed (1) if loss was due to failure of notice of change in address to be received before the date specified, (2) if received more than sixty days from date of issue plus time normally required for postal delivery of journal and claim, or (3) if the reason for the claim is "issue missing from files."

Subscription rates (hard copy or microfiche) in 1975: \$20.00 for 1 year to ACS members; \$80.00 to nonmembers. Extra postage \$4.50 in Canada and PUAS, \$5.00 other foreign. Supplementary material (on microfiche only) available on subscription basis, 1975 rates: \$15.00 in U.S., \$19.00 in Canada and PUAS, \$20.00 elsewhere. All microfiche airmailed to non-U.S. addresses; air freight rates for hard-copy subscriptions available on request.

Single copies for current year: \$4.00. Rates for back issues from Volume 56 to date are available from the Special Issues Sales Department, 1155 Sixteenth St., N.W., Washington, D.C. 20036.

Subscriptions to this and the other ACS periodical publications are available on microfilm. For information on microfilm write Special Issues Sales Department at the address above.

Notice to Authors last printed in the issue of July 3, 1975

THE JOURNAL OF
PHYSICAL CHEMISTRY

Volume 79, Number 19 September 11, 1975

JPCHAx 79(19) 1985-2076

ISSN 0022-3654

- Unimolecular Decomposition Rates of Cyclobutanone, 3-Oxetanone, and Perfluorocyclobutanone. An RRKM Calculation of Internally Converted Hot Molecules George M. Breuer, Roger S. Lewis, and Edward K. C. Lee* 1985
- Radiolysis of 0.4 M Sulfuric Acid Solutions with Fission Fragments from Dissolved Californium-252. Estimated Yields of Radical and Molecular Products that Escape Reactions in Fission Fragment Tracks Ned E. Bibler 1991
- A Reevaluation of the Ultrasonic Absorption Spectra of Aqueous Samarium(III) Sulfate Solutions Michael M. Farrow, Neil Purdie,* and Edward M. Eyring 1995
- Complex Solubilities of the Silver Halides in Aprotic Solvents Containing Sulfur and Oxygen Mark Salomon 2000 ■
- Regular Solution Theory and the Surface Tension of Molten Salt Mixtures D. A. Nissen* and B. H. Van Domelen 2003
- Vaporization Kinetics of Solid and Liquid Silver, Sodium Chloride, Potassium Bromide, Cesium Iodide, and Lithium Fluoride Curtis T. Ewing and Kurt H. Stern* 2007
- Thermal Instability in Synthetic Hydroxyapatites H. Catherine W. Skinner,* J. Steven Kittelberger, and Ralph A. Beebe 2017
- Stability of Polymer Lattices Prepared Using Mixtures of Anionic and Nonionic Surfactants Hiroshi Ono,* Eiki Jidai, and Akira Fujii 2020
- Photohydrogenation of Ethyne and Ethene on the Surface of Titanium Dioxide A. H. Boonstra* and C. A. H. A. Mutsaers 2025
- Polarized Single-Crystal Spectra of the Phenazine-Iodine Charge-Transfer Complex Basil G. Anex* and Govind Prasad 2028
- Carbon-13 Spin Relaxation and Methyl Rotation Barriers in the Methylethylenes Scott W. Collins, Terry D. Alger, David M. Grant,* Karl F. Kuhlmann, and James C. Smith 2031
- Electron Spin Resonance of the [16]Annulene Anion Radical. Ion Association in Hexamethylphosphoramide Jesús Gilberto Concepción and Gershon Vincow* 2037
- Electron Spin Resonance Studies on the 1,3,5,7-Tetramethylcyclooctatetraene Anion Radical Jesús Gilberto Concepción and Gershon Vincow* 2042
- Rate of Electron Exchange between Ferrocene and Ferricenium Ion from Nuclear Magnetic Resonance Studies Edward Shih Yang, Man-Sheung Chan, and Arthur C. Wahl* 2049
- Spin-Orbit Coupling in Organic Molecules C. A. Masmanidis, H. H. Jaffé,* and R. L. Ellis 2052
- Analysis of Free Diffusion in a Binary System When the Diffusion Coefficient Is a Function of the Square Root of Concentration John G. Albright and Donald G. Miller* 2061
- Enthalpy of Dilution of Aqueous Solutions of Some Bis Quaternary Ammonium Ganglionic and Neuromuscular Blocking Agents S. Agharkar and S. Lindenbaum* 2068 ■

20.7.1.2518

■ Supplementary material for this paper is available separately, in photocopy or microfiche form. Ordering information is given in the paper.

* In papers with more than one author, the asterisk indicates the name of the author to whom inquiries about the paper should be addressed.

AUTHOR INDEX

- | | | | |
|----------------------------------|------------------------------|--------------------------------|-----------------------------|
| Agharkar, S., 2068 | Eyring, E. M., 1995 | Lewis, R. S., 1985 | Salomon, M., 2000 |
| Albright, J. G., 2061 | Farrow, M. M., 1995 | Lindenbaum, S., 2068 | Skinner, H. C. W.,
2017 |
| Alger, T. D., 2031 | Fujii, A., 2020 | Masmanidis, C. A.,
2052 | Smith, J. C., 2031 |
| Anex, B. G., 2028 | Grant, D. M., 2031 | Miller, D. G., 2061 | Stern, K. H., 2007 |
| Beebe, R. A., 2017 | Jaffé, H. H., 2052 | Mutsaers, C. A. H. A.,
2025 | Tsuchida, E., 2072 |
| Bibler, N. E., 1991 | Jidai, E., 2020 | Nishikawa, H., 2072 | Van Domelen, B. H.,
2003 |
| Boonstra, A. H., 2025 | Kittelberger, J. S.,
2017 | Nissen, D. A., 2003 | Vincow, G., 2037, 2042 |
| Breuer, G. M., 1985 | Kuhlmann, K. F.,
2031 | Ono, H., 2020 | Wahl, A. C., 2049 |
| Chan, M.-S., 2049 | Lee, E. K. C., 1985 | Prasad, G., 2028 | Yang, E. S., 2049 |
| Collins, S. W., 2031 | | Purdie, N., 1995 | |
| Concepcion, J. G.,
2037, 2042 | | | |
| Ellis, R. L., 2052 | | | |
| Ewing, C. T., 2007 | | | |

THE JOURNAL OF PHYSICAL CHEMISTRY

Registered in U. S. Patent Office © Copyright, 1975, by the American Chemical Society

VOLUME 79, NUMBER 19 SEPTEMBER 11, 1975

Unimolecular Decomposition Rates of Cyclobutanone, 3-Oxetanone, and Perfluorocyclobutanone. An RRKM Calculation of Internally Converted Hot Molecules¹

George M. Breuer, Roger S. Lewis, and Edward K. C. Lee*

Department of Chemistry, University of California, Irvine, California 92664 (Received February 11, 1975)

Publication costs assisted by the University of California

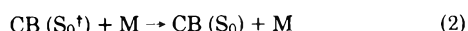
Specific rate constants for the unimolecular decomposition of cyclobutanone (CB), 3-oxetanone (OXTN), and perfluorocyclobutanone (PFCB) have been calculated by the general RRKM computer program of Hase and Bunker. PFCB is calculated to react slower and OXTN faster than CB for a given photoactivation energy. The calculation supports the internal conversion mechanism in the photolysis of PFCB, and it predicts that the observable pressure quenching of the internally converted intermediate in the photolysis of OXTN would occur above 1 atm. For CB and PFCB, the experimental values can be fitted to the calculated values using a stepladder deactivation model for 3–6 kcal/mol lost per collision for the CB (S_0^+)–propylene pair. Conversion of photoactivation energy to product translation is discussed.

Introduction

The RRKM (Rice–Ramsperger–Kassel–Marcus) theory has been developed to the point where it gives fairly reliable specific rate constants, $k(E)$, in many applications involving unimolecular reactions,^{1,2} although non-RRKM kinetic behavior has been found recently in several systems indicating the failure of the standard assumption of random lifetime distribution.^{3–5} We shall not be concerned presently with the latter aspect. Instead, we restrict ourselves to the former, calculation of the rates by the general RRKM computer program of Hase and Bunker which has recently become available.⁶ Because of our recent experimental studies of photoactivated molecules which undergo rapid $S_1 \rightarrow S_0$ internal conversion process to give monoenergetic, vibrationally hot, ground state molecules, we have chosen to study three model molecules, cyclobutanone (CB),⁷ 3-oxetanone (OXTN),⁸ and perfluorocyclobutanone (PFCB).⁹ Hot cyclobutanone molecules decompose to ethylene and ketene,

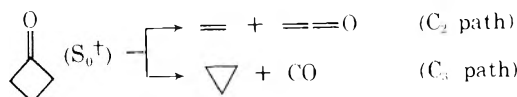


unless collisionally deactivated by a collision partner, M



The observed decomposition rate constants, $k_{\text{obsd}}(E)$, evaluated for various internal excitation energies (E), agreed reasonably well with the calculated rate constants,^{7a} $k_{\text{calcd}}(E)$, obtained from the semiclassical approximation procedure developed by Rabinovitch et al.¹⁰ Since the cycloreversion reaction (1) is known to be a “concerted” process ($\sigma 2s + \sigma 2a$) allowed by the conservation of orbital symmetry,¹¹ we expect 3-oxetanone and perfluorocyclobutanone to behave similarly. We wish to compare the specific unimolecular rate constants calculated for varying energies and activated complex models in the above three molecules featuring changes in the substituent groups and consequent changes in the vibrational frequencies. The calculation predicts that the internally converted OXTN produced by photoactivation at ~ 320 nm would have a unimolecular decomposition lifetime as short as 10^{-10} sec and the pressure quenching can only be observed experimentally above 1 atm.⁸ The calculated rates for PFCB agree well with the photochemically observed quenching rates of a PFCB intermediate which has been suggested to be the internally converted PFCB (S_0^+),^{9b} and the calculation quantitatively lends additional support for the proposed mechanism.

We define C_2 and C_3 path for cyclobutanone to be as shown below:

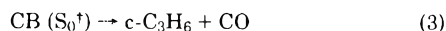


Computational Procedure

Cyclobutanone (CB). Figure 1 shows a simplified energy diagram for the unimolecular decomposition of cyclobutanone. The notations used by Robinson and Holbrook are adopted here for convenience.^{3b} The version of the general RRKM program employed in this study requires postulation of an activated complex (or critical configuration) model for which the principle moments of inertia (I_a , I_b , and I_c), the vibrational frequencies, and E_0 , the difference in zero point energies between the molecule and the complex (i.e., the activation energy at 0°K) are specified. The principle moments of inertia were calculated from the atomic masses and coordinates by a program supplied by Hase. The ground state of cyclobutanone is planar. Four of the activated complex models used are shown along with the bond length used in calculating the atomic coordinates in Figure 2. The frequencies for the complex were then calculated to fit the thermal A factor as experimentally determined¹² ($E_a = 52.0$ kcal/mol and $A = 3.6 \times 10^{14}$ sec⁻¹ at 641°K) using the absolute rate theory (ART). A computer program of W. L. Hase calculates the A factor by ART for a set of estimated frequencies and also computes the difference between the activation energy (E_a) and E_0 . The known experimental frequencies for the CB molecule¹³ and the calculated frequencies for the four activated complex models are listed in Table I, together with each set of three moments of inertia. Two other "trial models" were studied, both using the same moments of inertia as the hot molecule and both allowing the b_2 ring mode, ν_{19} (see Table I), to become zero as the "reaction coordinate"; one called "upper limit" case (UL) reduced all of the frequencies except the ring puckering vibration, ν_{27} (see Table I), by a constant factor of 14.79% while the other, "lower limit" case (LL), reduced *only* the ring puckering frequency to 8.8 from 71.8 cm⁻¹. The b_2 ring vibration mode has been chosen, somewhat arbitrarily, as the reaction coordinate. The program is largely insensitive to the mode chosen.

In the RRKM program, semiclassical state counting¹⁴ was employed because of the high energies and relatively low frequencies involved in the calculation. No correction was made for anharmonicity in the vibrations. The program then calculates the specific rate constant as a function of total vibrational excitation energy ($E = E_{h\nu} + E_{th}$) and also the total translational energy of the decomposition products, assuming no exothermicity from the activated complex.

In addition to the C_2 decomposition channel (1), there is a C_3 decomposition channel (3) which involves the decarbonylation process



This C_3 decomposition process is known to be two orders of magnitude slower than the primary C_2 decomposition process in pyrolysis.^{12b} Hase's ART program was used to fit frequencies of the activated complex to give the observed thermal rate constant^{12b} $k = 2.34 \times 10^{14} \exp(-58,000/RT)$ sec⁻¹ at 641°K, assuming no change of the moments of inertia in the activated complex. Three "models" were used

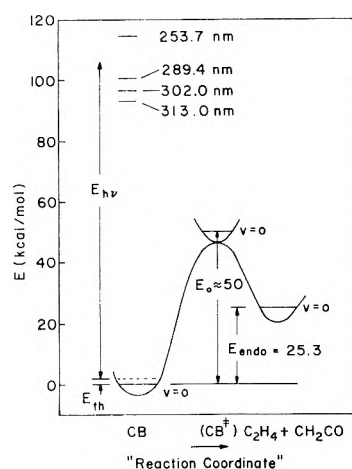


Figure 1. Simplified energetics diagram for CB (S_0^{\dagger}).

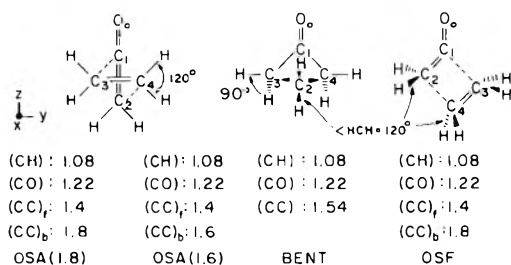


Figure 2. Assumed structures for four activated complexes of CB. OSA refers to "orbital symmetry allowed" and OSF refers to "orbital symmetry forbidden". Bond lengths are in ångström units.

here; in all three, as before, the frequency of the b_2 mode ring vibration (no. 19) at 850 cm⁻¹ was assumed to become zero as the "reaction coordinate". It is, of course, not necessary and is indeed unlikely that the same mode would be the reaction coordinate for both C_2 and C_3 decomposition pathways; as noted before the choice is not particularly important in terms of the calculated results. In the "upper limit" case, all of the vibrational frequencies except the ring puckering vibration (ν_{27}) at 71.8 cm⁻¹ were decreased by a constant factor of 12.1%. In the "lower limit" case, the ring puckering frequency only was reduced to 13.6 cm⁻¹. In the "most probable" case, perhaps better called the intermediate case, the five ring vibration frequencies, with the exception of the sixth mode corresponding to the "reaction coordinate", were reduced by a constant factor of 32.9%. For the C_3 decomposition process, the RRKM program as described above for the C_2 decomposition rate calculation was used to compute the rates as a function of the vibrational excitation energy.

Perfluorocyclobutanone (PFCB) and 3-Oxetanone (OXTN). As it will be shown later, it was found in the rate calculation for cyclobutanone that various values of the moments of inertia corresponding to different activated complex geometries yielded only minor variations of the unimolecular rate constants, within a factor of 2. Because of this insensitivity, the same moments of inertia were used for the activated complex as for the hot molecule for the PFCB and OXTN calculation.

Three moments of inertia of PFCB were calculated assuming geometries similar to the planar ground state of CB,^{13b} since neither an infrared nor microwave analysis is presently available. For the same reason, the molecular vi-

TABLE I: Frequencies (cm^{-1})^a and Moments of Inertia ($\text{amu} \text{ \AA}^2$)^b for Cyclobutanone C_2 Path

Vibrn no. ^c	Molecule	Activated complex			
		OSA (1.8)	OSA (1.6)	Bent	OSF
18 ring (b_2)	1124	766	748	774	791
24 CH_2 rock (b_1)	1073	1073	1073	1073	1073
7 ring (a_1)	956	598	580	606	623
13 CH_2 rock (a_2)	902	902	902	902	902
8 ring (a_1)	850	492	474	500	517
19 ring (b_2)	850	0	0	0	0
12 CH_2 twist (a_2)	829	829	829	829	829
25 CH_2 rock (b_1)	735	735	735	735	735
9 ring (a_1)	670	312	294	320	337
20 CO wag (b_2)	454	454	454	454	454
26 CO wag (b_1)	395	395	395	395	395
27 ring (b_1)	71.8 ^d	43.7	42.4	44.0	45.7
I_{xz}	142.06 ^b	93.55	90.10	110.80	149.00
I_{yy}	105.17 ^b	103.70	92.18	86.54	117.00
I_{zz}	46.87 ^b	49.51	41.40	56.35	42.57
$(I_a I_b I_c)^{1/2}$	836.86	693.04	586.38	735.06	861.46

^a Vibration numbering and fundamental frequencies given in ref 13a. ^b Moments of inertia given in ref 13b. ^c Frequencies which remain unchanged above 1200 cm^{-1} with vibrational number in parentheses are 3004 (21), 2978 (22), 2978 (1), 2975 (10), 2933 (2), 2933 (4), 1816 (3), 1479 (4), 1476 (5), 1402 (6), 1402 (15), 1332 (16), 1242 (17), 1209 (23), and 1200 (11). ^d A harmonic frequency which gives the same vibrational partition function (at 641°K) as with the observed anharmonic frequencies.

TABLE II: Frequencies (cm^{-1}) and Moments of Inertia ($\text{amu} \text{ \AA}^2$) for Perfluorocyclobutanone and 3-Oxetanone C_2 Path

PFCB ^d			OXTN ^e		
Vibrn no. ^a	Molecule	Complex	Vibrn no. ^b	Molecule ^b	Complex
8 ring (a_1)	(950)	612	6 ring (a_1)	832	444
9 ring (a_1)	(700)	450	7 ring (a_1)	683	363
11 CH_2 twist (a_2)	(935)	435	14 ring (b_2)	1076	573
18 ring (b_2)	(660)	425	15 ring (b_2)	955	0
19 ring (b_2)	(1000)	0	21 ring (b_1)	140	75
27 ring (b_1)	(50)	32.3			
I_{xx}	431.72	431.72	I_{xx}	137.08 ^c	137.08
I_{yy}	372.00	372.00	I_{yy}	101.97 ^c	101.97
I_{zz}	532.34	532.34	I_{zz}	41.66 ^c	41.66
$(I_a I_b I_c)^{1/2}$	9246	9246	$(I_a I_b I_c)^{1/2}$	763.10	763.10

^a Vibration numbering given in ref 13a. ^b Vibration numbering and fundamental frequencies given in ref 17. ^c Moments of inertia given in ref 16. ^d Frequencies which remain unchanged with vibrational number in parentheses are 1434 (1), 1366 (2), 1820 (3), 700 (4), 567 (5), 293 (6), 364 (7), 1250 (10), 435 (12), 200 (13), 1250 (14), 435 (15), 270 (16), 260 (17), 450 (20), 1250 (21), 1250 (22), 337 (23), 200 (24), 200 (25), and 350 (26). ^e Frequencies which remain unchanged with vibrational number in parentheses are 2931 (1), 1847 (2), 1457 (3), 1134 (4), 979 (5), 2962 (8), 111 (9), 1102 (10), 2924 (11), 1430 (12), 1250 (13), 488 (16), 2956 (17), 1284 (18), 1049 (19), and 401 (21).

brational frequencies of PFCB were estimated from those assigned for CB and perfluorocyclobutane.¹⁵ Fortunately, the moments of inertia¹⁶ and vibrational frequency assignments¹⁷ of OXTN were available for the planar ground state.

The frequencies of the activated complex were calculated to fit the experimental A factor of CB¹² using Hase's ART program, since again no thermal A factors for PFCB and OXTN are presently available. The frequencies and moments of inertia used are listed in Table II. Since the thermochemical and thermal kinetic data for either of these molecules are not experimentally available, we decided to use the same E_0 value used for CB (see Figure 1).

Results and Discussion

Cyclobutanone (C_2 Path). Figure 3 shows a plot of cal-

culated values of the specific rate constant (k_{RRKM}) as a function of total molecular excitation energy for six different activated complex models. Also, experimental values^{7a} of the mean collision frequency at the half-quenching pressure ($\omega_{1/2}$) obtained at 313.0, 302.0, 289.4, and 253.7 nm are shown for comparison. In the energy ranges covered, the values of k_{RRKM} for all six models come within a factor of 2 for a given energy, indicating relative insensitivity to the choice of the activated complex models used here. There is an agreement at high energies between the values of $k(E)$ calculated from the semiclassical approximation formulation^{7a} and the values of k_{RRKM} calculated for OSA (1.8) which can be regarded as the "most probable" (MP) one. OSA (1.8) refers to the "orbital symmetry allowed" model, 1.8 Å separation of nascent double bond centers, and OSF refers to the "orbital symmetry forbidden" model in Figure

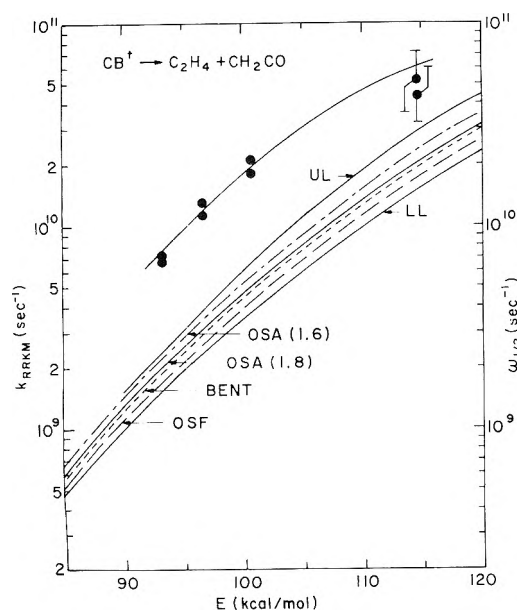


Figure 3. (Left) Calculated specific rate constants of the C_2 path of CB for various activated complex models vs. excitation energy. (Right) Observed mean collision frequencies at the half-quenching pressure ($\omega_{1/2}$) vs. excitation energy (ref 7a).

2. We can certainly regard the "upper limit" (UL) and the "lower limit" (LL) values to represent the two extreme cases. For this reason we chose to limit our activated complex models to the MP, UL, and LL cases in subsequent calculations.

Assuming that the factor of 2~3 discrepancy between the observed values of $\omega_{1/2}$ and the calculated values of k_{RRKM} is due to the inefficient collisional deactivation by propylene which was used as the collision partner (M), we have calculated the values of average energy loss per collision (Δ) for the multistep deactivation scheme given in Appendix. Keeping many terms in the kinetic analysis (stepladder model) and numerically fitting the experimental points of $\omega_{1/2}$ to k_{RRKM} , the values of Δ at 313.0- and 253.7-nm excitation have been obtained for the three models, and they are shown in Table III. These values are reasonable and are in agreement with similar values calculated for other systems.¹⁸ The average energy loss per collision, however, is not constant for both 253.7- and 313.0-nm excitation, 6 and 3 kcal/mol per collision, respectively. It should be noted that we have neglected the possibility of activating collisions in this model, since they should be less probable for these high photoactivation energies and large collision partners¹⁹ (and therefore large Δ 's). Calculations on other systems show a decreasing effect of deleting activating collisions as more complex collision partners are involved, although there may be a factor of 2 or 3 difference in Δ when helium is used.^{18b}

The general RRKM program also calculates the amount of internal energy of the complex which is converted to translational energy during the reaction. This is accomplished for a given initial energy by determining the probability that various quantities of energy are contained in the vibrational mode which becomes the reaction coordinate. Figure 4 shows the relative translational energy distribution for the three models, MP, UL, and LL, at two wavelengths, 253.7 and 313.0 nm. The plots are somewhat curved on semilogarithmic paper, but are fairly closely approximated by a simple exponential function. Thus an ex-

TABLE III: Energy Loss per Collision (Δ) for CB^+ (M = Propylene)

λ_{ex} , nm	$E = E_{hv} + E_{th}$, kcal/mol	Δ , kcal/mol/collision	Condition
313.0	93.2	3.7	Upper limit
313.0	93.2	3.1	OSA (1.8)
313.0	93.2	2.4	Lower limit
253.7	114.6	9.2	Upper limit
253.7	114.6	5.9	OSA (1.8)
253.7	114.6	4.1	Lower limit

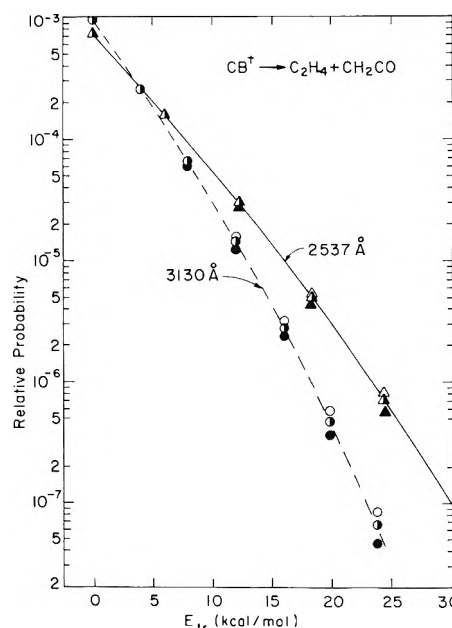


Figure 4. Relative probability for the translational energy distribution for the C_2 path of CB: (filled symbols) upper limit; (half-filled symbols) OSA (1.8); (open symbols) lower limit.

ponential fit to the initial portion of the relative probability function should give an approximate value for the average value of the energy put into translation of the two decomposition fragments, neglecting the energy available between the activated complex and the products, ~24.7 kcal/mol. The data in Table IV summarize the values of the average translational energy, $\langle E_{tr} \rangle$, calculated from the probability function generated by the program.

From the results tabulated we can see that at 313.0 nm, only about 3.0 kcal/mol of the activated complex energy is put into translation of the product fragments, and at 253.7 nm only about 3.9 kcal/mol is available in translation, only 0.9 kcal/mol more than at 313.0 nm. Only about 6% of the activated complex energy is put into translation on the average, corresponding approximately to the expectation based on the internal degrees of freedom involved within the principle of equipartitioning of energy. If we assume that, in addition to the activated complex energy put into translation, all of the "exothermicity" from the complex to the products, 24.7 kcal/mol, is also converted into translational energy, then the energy distributed among the products is 33.3 kcal/mol at 313.0 nm, 36.5 kcal/mol at 302.0 nm, 40.5 kcal/mol at 289.4 nm, and 53.8 kcal/mol at 253.7 nm. Two major problems occur in the translational energy

TABLE IV: Values of Average Translational Energy (kcal/mol) vs. λ_{ex} (nm)^a for Cyclobutanone C₂ Path

Model C ₂	λ_{ex}			
	313.0 nm	302.0 nm	289.4 nm	253.7 nm
Upper limit	2.89	3.04	3.21	3.80
OSA (1.6)	3.00	3.15	3.34	3.93
OSA (1.8)	3.01	3.16	3.34	3.93
Bent	3.01	3.16	3.34	3.94
OSF	3.01	3.16	3.35	3.94
Lower limit	3.08	3.23	3.41	4.00

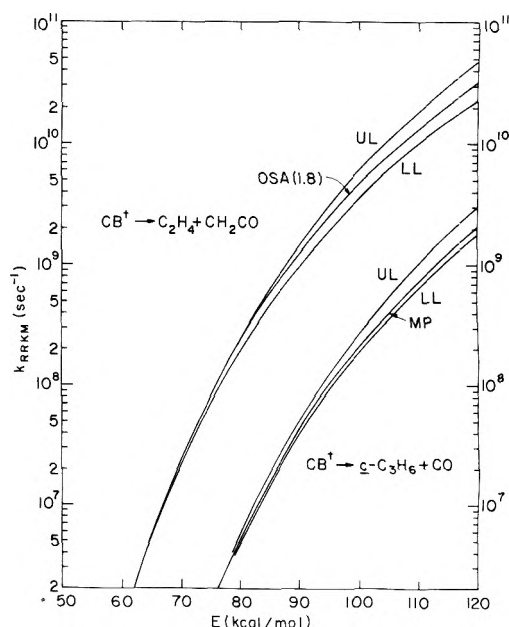
^a Internal energies of activated complex available for translation are 39.3 (313.0 nm), 42.7 (302.0 nm), 46.8 (289.4 nm), and 60.7 kcal/mol (253.7 nm).

calculations done in the program. First, when there is an "exothermicity" from the activated complex, the fraction of that energy which goes into product translation energy will depend on the shape of the potential surface in that region, an unknown quantity. Secondly, for complex molecules the reaction path does not correspond to a single vibrational mode but to a combination of modes; thus the energy from several modes may appear as translation and not just the energy contained in the single mode selected as the reaction path. It is hoped that future theoretical treatments will deal more closely with these problems in light of the importance of determining the deposition of energy in such kinetic systems.

Cyclobutanone (C₃ Path). Figure 5 shows the values of calculated RRKM rate constants of the C₃ path for three activated complex models, MP, UL, and LL, and they are compared to those calculated for the C₂ path. The ratio of the rate constants for the C₂ path to those for the C₃ path ranges from 538 at 60 kcal/mol to 15.3 at 120 kcal/mol for the "most probable" model; the ratios at other energies are 170 at 65, 90.7 at 70, 59.8 at 75, 44.3 at 80, 35.1 at 85, 29.2 at 90, 25.0 at 95, 22.0 at 100, 19.7 at 105, 18.0 at 110, and 16.5 at 115 kcal/mol. It should be noted that the C₂ path dominates the C₃ path by at least a factor of 15 for the photoactivation wavelength range of 313.0 to 253.7 nm, or $E_{hv} + E_{th}$ of 93.2 to 114.6 kcal/mol. Therefore, the calculation suggests that the quantum yield of the C₃ products resulting solely from the decomposition of CB (S_0^+) must be less than 0.03, less than $1/10$ of the total C₃ quantum yield, since the observed quantum yields of the C₂ products are ~ 0.71 at 313.0 nm ($C_3/C_2 \approx 0.4$) and ~ 0.55 at 253.7 nm ($C_3/C_2 \approx 0.8$).^{7a} This conclusion is consistent with the observations made in the photoactivation studies of alkyl-substituted cyclobutanones, 2-*n*-propylcyclobutanone and the *cis* and *trans* isomers of 2,3-dimethylcyclobutanone²⁰ and 2,4-dimethylcyclobutanone.²¹

Table V summarizes the data for the calculation of the amount of activated complex energy which goes into translation of the fragments *c*-C₃H₆ and CO. As before, these data are obtained from an exponential fit to the initial portion of the relative probability curve similar to Figure 4. These data are very similar to those for the C₂ path (see Table IV), as might be expected, particularly at these high energies. Again, about 7–8% of the activated complex energy becomes available for translation, as expected.

PFCB and OXTN (C₂ Path). Calculated specific rate constants for the C₂ path of PFCB and OXTN are com-

**Figure 5.** Calculated specific rate constants for the C₃ path of CB as compared to those for the C₂ path.**TABLE V: Values of Average Translational Energy (kcal/mol) vs. λ_{ex} (nm)^a for Cyclobutanone C₃ Path**

Model C ₃	λ_{ex}			
	313.0 nm	302.0 nm	289.4 nm	253.7 nm
Upper limit	2.65	2.81	2.99	3.58
Most probable	2.74	2.90	3.09	3.69
Lower limit	2.80	2.96	3.15	3.76

^a Internal energies of the activated complex available for translation are 33.0 (313.0 nm), 36.7 (302.0 nm), 40.8 (289.4 nm), and 54.7 kcal/mol (253.7 nm).

pared to those of CB in Figure 6. The value of k_{RRKM} for PFCB is 3 orders of magnitude smaller than that for CB at 60 kcal/mol and it is 1 order of magnitude smaller at 120 kcal/mol. One expects this kind of behavior, since the density of states ratio (activated complex/molecule) should be much higher for CB than for PFCB which has more low-frequency vibrations, although the density of states for CB should be much lower than that for PFCB. Again, as expected, the values of k_{RRKM} for OXTN is 1–1.5 orders of magnitude higher than that for CB, because OXTN has six fewer vibrational modes than CB. This suggests that the collisional deactivation of the photoactivated OXTN (S_0^+) would require about 10 times higher pressure than that required for the photoactivated CB (S_0^+).

Three experimental points for PFCB in Figure 6 were obtained using the gas kinetic collision diameter for PFCB of 6.0 Å and the "strong" collision assumption which cannot be strictly valid. Of course, the fact that these points are about a factor of 2 higher than the corresponding calculated values suggests that there is a low efficiency of collisional deactivation as has been observed in the case of CB. However, we shall not attempt a detailed comparison, because of the assumptions employed in the calculation which make the calculations for PFCB and OXTN less reliable than that for CB; (a) A factors for the decompositions

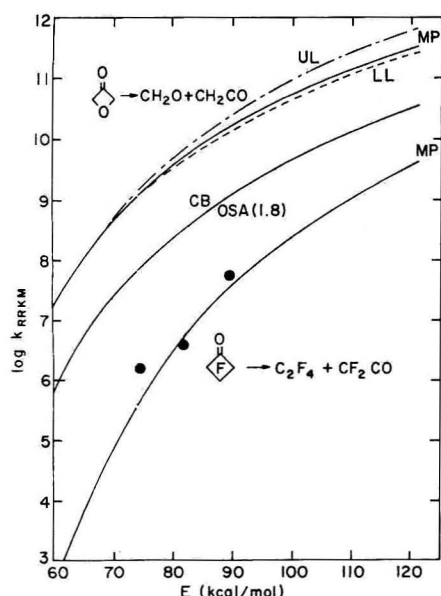


Figure 6. Calculated specific rate constants for the C_2 path of PFCB and OXTN. Three filled points are experimental values of PFCB ($E_0 = 3.7$ kcal/mol).^{9b}

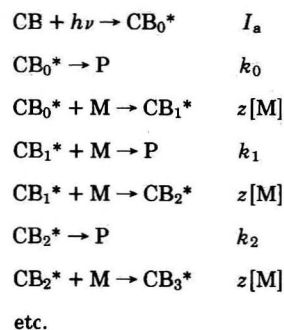
of PFCB and OXTN were assumed to be the same as the A factor for CB and (b) E_a 's for PFCB and OXTN were assumed to be the same as E_a for CB. However, since the C_2 path for CB and its isomers is allowed by the orbital symmetry conservation rules,^{11,21} we should not expect much change for the values of the A factor and E_a for PFCB and OXTN.

A review of the experimental rate data (see Benson and O'Neal)²² suggests that the A factors should be within a factor of 4 or 5 for the three molecules, CB, PFCB, and OXTN, but that the E_a values could be off as much as (but probably less than) 20%, causing larger deviations from the calculation done here. We believe that the influence of F substitution for H as well as the influence of O substitution for CH_2 in determining the values of k_{RRKM} are real.

The present calculation certainly validates the internal conversion mechanism in the photolysis of PFCB,^{9b} while it helps in designing the pressure quenching experiments so that the presence of short-lived hot ground state of OXTN can be established in the photolysis of OXTN.⁸

Appendix

The multistep deactivation scheme for the hot cyclobutanone where up transitions are neglected is



where an asterisk indicates the vibrationally hot species, the subscripts 0, 1, 2, ..., n indicate the number of collisions

suffered by the vibrationally hot species which loses Δ kcal/mol per collision, and P and M are the decomposition product and the collision partner, respectively. I_a , k_n , z , and $[\text{M}]$ have the usual meanings. Application of the steady state approximation to CB_0^* , CB_1^* , CB_2^* , etc., gives the following expression for the rate of product formation:

$$\frac{1}{I_a} \frac{dP}{dt} = \frac{k_0}{k_0 + zM} + \frac{k_1 z M}{(k_0 + zM)(k_1 + zM)} + \frac{k_2 z^2 M^2}{(k_0 + zM)(k_1 + zM)(k_2 + zM)} + \dots$$

At the half-quenching pressure, $M_{1/2}$, we obtain

$$\left\{ \frac{dP}{dt} \right\}_{M_{1/2}} = \frac{1}{2} \left\{ \frac{dP}{dt} \right\}_0 = \frac{1}{2} I_a$$

Hence, if we adopt $\omega_{1/2} = zM_{1/2}$, we obtain

$$\frac{1}{2} = \frac{k_0}{k_0 + \omega_{1/2}} + \frac{k_1 \omega_{1/2}}{(k_0 + \omega_{1/2})(k_1 + \omega_{1/2})} + \frac{k_2 \omega_{1/2}^2}{(k_0 + \omega_{1/2})(k_1 + \omega_{1/2})(k_2 + \omega_{1/2})} + \dots$$

We can find the value of Δ for a given set of k_0 , k_1 , k_2 , ..., k_n values and $\omega_{1/2}$ from the above expression, since $E_0 = h\nu$, $E_1 = h\nu - \Delta$, $E_2 = h\nu - 2\Delta$, ...

References and Notes

- (1) This research has been supported by NSF Grant GP 41407X. The earlier support by the Office of Naval Research is gratefully acknowledged.
- (2) (a) R. A. Marcus and O. K. Rice, *J. Phys. Colloid Chem.*, **55**, 894 (1951); (b) R. A. Marcus, *J. Chem. Phys.*, **20**, 355 (1952).
- (3) See for recent reviews (a) B. S. Rabinovitch and D. W. Setser, *Adv. Photochem.*, **3**, 1 (1964); (b) P. J. Robinson and K. A. Holbrook, "Unimolecular Reactions", Wiley-Interscience, New York, N.Y., 1972; (c) W. Forst, "Theory of Unimolecular Reactions", Academic Press, New York, N.Y., 1973.
- (4) D. L. Bunker and W. L. Hase, *J. Chem. Phys.*, **59**, 4621 (1973).
- (5) (a) H. H. Harris and D. L. Bunker, *Chem. Phys. Lett.*, **11**, 433 (1971); (b) D. L. Bunker, *J. Chem. Phys.*, **57**, 332 (1972); (c) C. T. Ting and F. S. Rowland, *J. Phys. Chem.*, **74**, 4080 (1970); (d) J. D. Rynbrandt and B. S. Rabinovitch, *J. Chem. Phys.*, **54**, 2275 (1971); (e) Y.-N. Tang and Y. Y. Su, *ibid.*, **57**, 4048 (1972); (f) J. G. Moehlmann, J. T. Gleaves, J. W. Hudgens, and J. D. McDonald, *J. Chem. Phys.*, **60**, 4790 (1974).
- (6) The program of D. L. Bunker and W. L. Hase is available through Quantum Chemistry Program Exchange (No. QCPE-234), Department of Chemistry, Indiana University.
- (7) (a) N. E. Lee and E. K. C. Lee, *J. Chem. Phys.*, **50**, 2094 (1969); (b) J. C. Hemminger and E. K. C. Lee, *ibid.*, **56**, 5284 (1972); (c) J. Metcalfe, H. A. J. Carless, and E. K. C. Lee, *J. Am. Chem. Soc.*, **94**, 7235 (1972).
- (8) G. M. Breuer and E. K. C. Lee, unpublished work.
- (9) (a) R. S. Lewis and E. K. C. Lee, *J. Chem. Phys.*, **61**, 3434 (1974); (b) *J. Phys. Chem.*, **79**, 187 (1975).
- (10) (a) D. W. Setser and B. S. Rabinovitch, *Can. J. Chem.*, **40**, 1425 (1962); (b) G. Z. Whitten and B. S. Rabinovitch, *J. Chem. Phys.*, **38**, 2466 (1963).
- (11) (a) R. B. Woodward and R. Hoffmann, *Angew. Chem., Int. Ed. Engl.*, **8**, 781 (1969); (b) H. A. J. Carless and E. K. C. Lee, *J. Am. Chem. Soc.*, **92**, 4482 (1970).
- (12) (a) M. N. Das, F. Kern, T. D. Coyle, and W. D. Walters, *J. Am. Chem. Soc.*, **76**, 6271 (1954); (b) A. T. Blades, *Can. J. Chem.*, **47**, 615 (1969); (c) T. H. McGee and A. Schleifer, *J. Phys. Chem.*, **76**, 963 (1972); (d) A. T. Blades and H. S. Sandhu, *ibid.*, **77**, 1316 (1973); (e) T. H. McGee and A. Schleifer, *ibid.*, **77**, 1317 (1973).
- (13) (a) K. Frei and H. H. Gunthard, *J. Mol. Spectrosc.*, **5**, 218 (1960); (b) L. H. Scharpen and V. W. Laurie, *J. Chem. Phys.*, **49**, 221 (1968).
- (14) (a) G. Z. Whitten and B. S. Rabinovitch, *J. Chem. Phys.*, **38**, 2466 (1963); **41**, 1883 (1964); (b) D. C. Tardy and B. S. Rabinovitch, *ibid.*, **48**, 1427 (1968).
- (15) W. C. Harris and D. B. Yang, *J. Chem. Phys.*, **60**, 4175 (1974).
- (16) J. S. Gibson and D. O. Harris, *J. Chem. Phys.*, **57**, 2318 (1972).
- (17) J. R. Durig, A. C. Morrisey, and D. O. Harris, *J. Mol. Struct.*, **6**, 375 (1970).
- (18) (a) R. Atkinson and B. A. Thrush, *Proc. Roy. Soc. (London), Ser. A*, **316**, 131 (1970); (b) B. S. Rabinovitch, H. F. Carroll, J. D. Rynbrandt, J. H. Georgakakos, B. A. Thrush, and R. Atkinson, *J. Phys. Chem.*, **75**, 3376 (1971); (c) M. G. Toper and R. W. Carr, Jr., *ibid.*, **58**, 757 (1973); (d) S. W. Orchard and B. A. Thrush, *Proc. R. Soc. (London), Ser. A*, **329**, 233 (1972).

- (19) (a) D. C. Tardy and B. S. Rabinovitch, *J. Chem. Phys.*, **45**, 3720 (1966); (b) D. C. Tardy and B. S. Rabinovitch, *J. Chem. Phys.*, **48**, 1282 (1968).
- (20) H. A. J. Carless and E. K. C. Lee, *J. Am. Chem. Soc.*, **94**, 1 (1972).
- (21) (a) H. A. J. Carless, J. Metcalfe, and E. K. C. Lee, *J. Am. Chem. Soc.*, **94**, 7221 (1972); (b) J. Metcalfe, H. A. J. Carless, and E. K. C. Lee, *ibid.*, **94**, 7235 (1972).
- (22) S. W. Benson and H. E. O'Neal, *Nat. Stand. Ref. Data Ser.*, Nalt. Bur. Stand., **21** (1970). We have compared the values of A factor and E_a for the hydrocarbons and their perfluoro analogs, ethane, cyclobutane, cyclobutene, and vinylcyclopropane. Also, the cyclopropane-ethylene oxide, cyclobutane-oxetane, and cyclopentene-2,5-dihydrofuran pairs were compared.

Radiolysis of 0.4 M Sulfuric Acid Solutions with Fission Fragments from Dissolved Californium-252. Estimated Yields of Radical and Molecular Products that Escape Reactions in Fission Fragment Tracks^{1,2}

Ned E. Bibler

E. I. du Pont de Nemours & Co., Savannah River Laboratory, Aiken, South Carolina 29801 (Received January 16, 1975)

Publication costs assisted by the U.S. Energy Research and Development Administration

Radiolysis of 0.4 M sulfuric acid solutions at very high linear energy transfer (LET) values (~ 400 eV/Å) was studied with fission fragments from dissolved ^{252}Cf . This isotope irradiates the solution with both fission fragments and α particles. Visible and uv absorption spectroscopy were used to determine $G(\text{Fe}^{3+})$ in 10^{-3} M Fe^{2+} , $G(\text{Ce}^{3+})$ in 10^{-4} M Ce^{4+} – 10^{-3} M Ce^{3+} , and $G(\text{Ce}^{3+})$ in 10^{-4} M Ce^{4+} – 10^{-3} M Ce^{3+} containing 10^{-3} M (and 10^{-2} M) Tl^+ . Values for $G(\text{H}_2)$ were determined manometrically. Experiments with α particles (LET ≈ 9 eV/Å) from dissolved ^{244}Cm verified the technique and measured 100 eV yields (G values) for pure α radiolysis. Experiments with mixtures of ^{244}Cm and ^{252}Cf established that the effects of fission fragments and α particles are independent. The following results were obtained for $G(\text{Fe}^{3+})$, $G(\text{Ce}^{3+})$, $G(\text{Ce}^{3+})$ in 0.001 M Tl^+ , and $G(\text{H}_2)$, respectively: for ^{244}Cm 5.1, 2.9, 3.3, 1.3; for ^{252}Cf 4.4, 2.7, 2.9, 1.8; for fission fragments 3.3, 2.4, 2.4, 2.1. Interpretation of the fission fragment yields leads to the following estimates for the respective species escaping track reactions: $G(\text{H}_2) = 2.1$, $G(\text{H}_2\text{O}_2) = 0.96$, $G(\text{HO}_2) = 0.5$, $G(\text{OH}) = 0$, and $G(\text{H}) = 0$.

Introduction

In previous studies of fission fragment radiolysis of aqueous solutions, nuclear reactors have been used to induce fission in dissolved ^{235}U .³⁻⁷ Because of this and other technical difficulties, few such studies have been performed. Systems suitable for estimating the yields of radical and molecular species that escape track reactions have not been examined even though fission fragments have the highest LET of all particles available to radiation chemists.⁸ This paper describes results of radiolysis experiments with dissolved ^{252}Cf , a nuclide that decays by spontaneous fission. Solutions of pure 0.4 M H_2SO_4 or solutions of 0.4 M H_2SO_4 containing Fe^{2+} or Ce^{4+} ions were irradiated, and the radiolytic effects of fission fragments were determined. Because the radiation chemistry of these systems has been interpreted in terms of the yields of molecular and radical products for other types of radiation,⁹ the present results were used to estimate these yields for fission fragment radiolysis.

Experimental Section

Californium-252 was produced by successive neutron capture by ^{239}Pu and purified by a series of solvent extraction and ion-exchange techniques.¹⁰ Major impurities from the final product were nonradioactive zinc and iron in

quantities almost equal to that of ^{252}Cf . The necessary concentrations of ^{252}Cf were about 10^{-3} lower than that of added solutes. Thus, these impurities did not affect the radiation chemistry of the systems studied. Solutions were prepared with triply distilled water and reagent grade chemicals; $\text{Ce}(\text{HSO}_4)_4$ was recrystallized before use. Also, in the experiments with $\text{Ce}(\text{HSO}_4)_4$, the solutions were exposed to ^{60}Co γ radiation for further purification and for production of $\text{Ce}(\text{III})$ before ^{252}Cf was added. All experiments were performed at 20–25° with air-saturated solutions.

The evolution of radiolytically generated gases from 0.4 M H_2SO_4 was measured remotely in a shielded cell. Solutions containing ~ 800 μg of ^{252}Cf were prepared by dissolving freshly precipitated $\text{Cf}(\text{OH})_3$ with 5 ml of 0.4 M H_2SO_4 . The procedure for collecting and analyzing the evolved gases has been described previously.¹¹

Spectrophotometric experiments were performed in a glove box using ~ 4 μg of ^{252}Cf . The solution to be irradiated (~ 3 ml) was placed in a carefully cleaned 1-cm optical cell. ^{252}Cf was concentrated by sorption on several beads of Dowex 50W-X8 cation resin. The beads were washed, and ^{252}Cf was removed with ~ 500 μl of 3 M $(\text{NH}_4)_2\text{SO}_4$ in 0.4 M H_2SO_4 . This solution was added to the cell, and the cell was then positioned in a Coleman Model 101 spectrophotometer in the glove box. The optical density was recorded

automatically as a function of time on a chart outside the glove box. Independent experiments established that $(\text{NH}_4)_2\text{SO}_4$ did not affect the chemistry.

Radiolysis of the following solutions in 0.4 M H_2SO_4 was studied: 10^{-3} M Fe^{2+} , 10^{-4} M Ce^{4+} – 10^{-3} M Ce^{3+} , and 10^{-4} M Ce^{4+} – 10^{-3} M Ce^{3+} containing Tl^+ . The concentration of Fe^{3+} was calculated from its absorbance at 304 nm and an extinction coefficient of $2197 \text{ M}^{-1} \text{ cm}^{-1}$. For Ce^{4+} , the respective values were 320 nm and $5610 \text{ M}^{-1} \text{ cm}^{-1}$.

To verify the above techniques, several α radiolysis experiments on these systems were performed in the same manner using dissolved ^{244}Cm as the α source. The results agreed with published values.¹²

Californium-252 decays by α emission as well as by spontaneous fission. The total absorbed dose is due to α particles, fission fragments, and β particles from decay of the fission fragments. Energy absorption from α particles and fission fragments (both have small ranges of 0.002–0.004 cm^{13,14}) was calculated from their average energies (6.11¹⁵ and 185.7¹⁶ MeV, respectively), their specific activities [1.15×10^9 and 3.68×10^7 disintegrations/(min μg), respectively¹⁷], and the ^{252}Cf concentration determined by absolute neutron and α counting. The β energy absorbed was calculated from the estimated specific activity for fission product β particles in equilibrium with ^{252}Cf [2.2×10^8 disintegrations/(min μg)¹⁸], their estimated average energy (1.3 MeV¹⁸), and the fraction absorbed. This fraction was 73%, as calculated from the equation for energy transmitted from a radioactive solution in an infinite absorbing cylinder 1 cm in diameter.¹⁹ Calculation of the dose in the ^{244}Cm experiments has been described previously.¹¹

The observed 100-eV yields calculated for ^{252}Cf radiolysis are assumed to be linear combinations of three radiolysis yields:

$$G_{\text{obsd}} = F_{\alpha}G_{\alpha} + F_{\beta}G_{\beta} + F_{\text{ff}}G_{\text{ff}} \quad (1)$$

The coefficients, F_{α} , F_{β} , and F_{ff} , are the respective fractions of energy deposited by α particles, β particles, and fission fragments. For ^{252}Cf solutions, these fractions are 0.500, 0.015, and 0.485, respectively. Values for G_{α} were determined by experiments with ^{244}Cm ; values for G_{β} were taken from the literature. This equation was tested (as shown later) and found to be valid.

Results and Discussion

Gas Evolution Studies. In these experiments, ^{252}Cf concentrations were nominally 0.1 mg/ml, corresponding to a dose rate of 2.2×10^{18} eV/(min ml) and a total dose of 4×10^{20} eV/ml. Figure 1 shows the time dependence of the amount of gas evolved at constant pressure for a typical experiment. The gas was composed of H_2 , O_2 , and traces of the fission fragments ^{88}Kr , ^{87}Kr , ^{133}Xe , and ^{135}Xe . Table I summarizes the 100-eV yields in all the experiments.

For calculating $G(\text{H}_2)_{\text{ff}}$ from eq 1, the values chosen for $G(\text{H}_2)_{\alpha}$ and $G(\text{H}_2)_{\beta}$ were 1.27¹¹ and 0.45,²⁰ respectively. The average result, 2.1 with a standard deviation of 0.1, agrees with that determined by Sowden,³ but is slightly higher than those of other workers.^{4–6}

Spectrophotometric Studies. For these experiments, ^{252}Cf concentrations were nominally 1 $\mu\text{g}/\text{ml}$, corresponding to a dose rate of 10^{16} eV/(ml min) and a total dose of 10^{18} eV/ml.

Fe^{2+} System. To test the validity of eq 1, irradiations were performed with both ^{252}Cf and ^{244}Cm present as radiation sources. In effect, this changes the values for F in

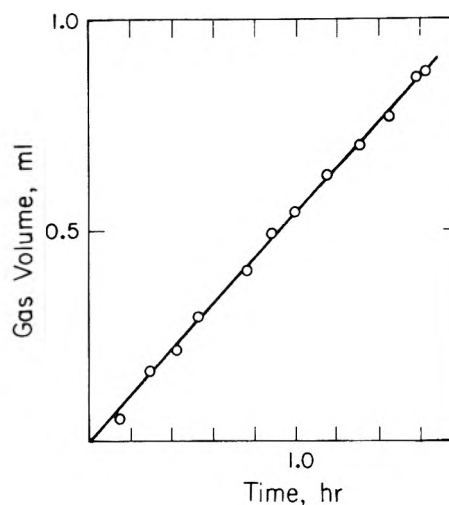


Figure 1. Gas evolution from a 0.4 M H_2SO_4 solution of 0.115 mg/ml ^{252}Cf ; $P = 756$ mm, $T = 28^\circ$. Composition of gas is 77% H_2 , 23% O_2 , and traces of ^{87}Kr , ^{88}Kr , ^{135}Xe , and ^{133}Xe .

TABLE I: 100-eV Yields of Gaseous Products from ^{252}Cf Radiolysis of 0.4 M H_2SO_4^a

$G(\text{gas})_{\text{obsd}}$	$G(\text{H}_2)_{\text{obsd}}$	$G(\text{O}_2)_{\text{obsd}}$	$G(\text{H}_2)_{\text{ff}}$
2.22	1.72	0.50	2.22
2.05	1.65	0.40	2.08
1.99	1.62	0.37	2.02
2.41	1.74	0.67	2.26

^a [^{252}Cf] in all experiments was nominally 0.1 mg/ml.

eq 1. The total α dose was equal to that from ^{244}Cm and ^{252}Cf .

Equation 1 can be rearranged to give

$$G_{\text{obsd}} - F_{\alpha}G_{\alpha} - F_{\beta}G_{\beta} = F_{\text{ff}}G_{\text{ff}}$$

If eq 1 is valid, a plot of $(G_{\text{obsd}} - F_{\alpha}G_{\alpha} - F_{\beta}G_{\beta})$ vs. F_{ff} should be linear with (0,0) intercept and a slope of G_{ff} .

Figure 2 shows values of $(G_{\text{obsd}} - F_{\alpha}G_{\alpha} - F_{\beta}G_{\beta})$ plotted against F_{ff} for several experiments with different amounts of ^{244}Cm and ^{252}Cf . Values chosen for $G(\text{Fe}^{3+})_{\alpha}$ and $G(\text{Fe}^{3+})_{\beta}$ were 5.10^{21,12} and 15.5,²² respectively. Least-squares analysis indicates that the results are linear with a correlation of 0.98. Thus, eq 1 is valid for determining 100-eV yields for fission fragment radiolysis. From the slope, $G(\text{Fe}^{3+})_{\text{ff}}$ is 3.1 (Figure 2).

Several experiments were performed with only dissolved ^{252}Cf present. Figure 3 shows the time dependence of the optical density for a typical experiment. The average value for $G(\text{Fe}^{3+})_{\text{obsd}}$ for seven experiments was 4.38 ± 0.15 and for $G(\text{Fe}^{3+})_{\text{ff}}$, 3.28 ± 0.35 . This latter result agrees well with the above value obtained from the slope, and also agrees with the single published value of 3.0 ± 0.9 .⁷ The decrease of $G(\text{Fe}^{3+})$ with radiations of increasing LET is shown in Figure 4. The average LET of ^{252}Cf fission fragments was approximated to be equal to that for ^{235}U fission fragments (400 eV/Å).⁷ Clearly the lowest value for $G(\text{Fe}^{3+})$ is with fission fragments of high LET. This is consistent with the interpretation that higher LET values favor molecular product formation at the expense of radical formation and thus reduce $G(\text{Fe}^{3+})$.⁷

Ce^{4+} System. This system was studied with α radiolysis with ^{244}Cm in addition to radiolysis with ^{252}Cf . Results

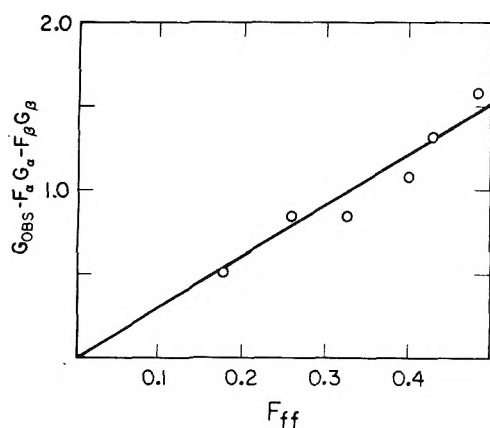


Figure 2. Test of the equation $G_{\text{obsd}} = F_{\alpha}G_{\alpha} + F_{\beta}G_{\beta} + F_H G_H$ with results of radiolysis of $10^{-3} M \text{Fe}^{2+}$ in aqueous $0.4 M \text{H}_2\text{SO}_4$ solution and different concentrations of ^{244}Cm and ^{252}Cf .

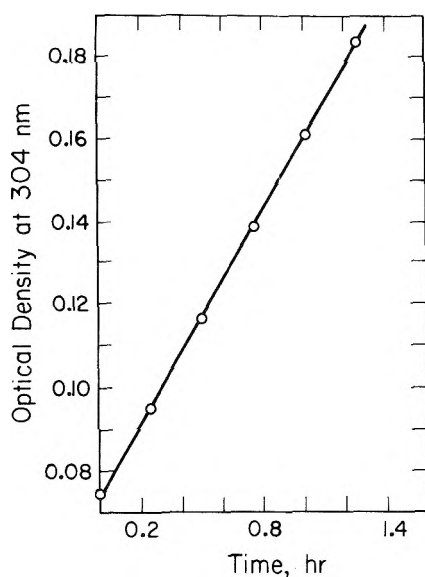


Figure 3. Optical density increase at 304 nm from Fe^{3+} production in $10^{-3} M \text{Fe}^{2+}$ in aqueous $0.4 M \text{H}_2\text{SO}_4$ solution containing $0.67 \mu\text{g/ml } ^{252}\text{Cf}$.

with ^{244}Cm agreed with published values and verified the experimental technique.¹² Figure 5 shows the time dependence of the optical density for a typical experiment with ^{252}Cf . Table II presents results for all experiments. The values for $G(\text{Ce}^{3+})_{\text{ff}}$ are consistently lower than those for $G(\text{Ce}^{3+})_{\alpha}$. Previous studies have shown that $G(\text{Ce}^{3+})$ increases with increasing LET,⁸ but then at very high LET, decreases with increasing LET.⁹ The above results also indicate this behavior.

Estimate of Radical and Molecular Yields. The above 100-eV yields can now be used to estimate yields of radical and molecular products from fission fragment radiolysis of water. These are not initial values, but only the yields of those radicals or products that survive or escape reactions in fission fragment tracks. These surviving species then diffuse away from the tracks and are detected either by their subsequent reactions with dissolved solutes (Fe^{2+} , Fe^{3+} , Ce^{4+} , or Ce^{3+}), or by their formation of stable molecules, e.g., H_2 . From established mechanisms for radiolytic oxidation of Fe^{2+} or reduction of Ce^{4+} in $0.4 M \text{H}_2\text{SO}_4$, the following relations have been derived for acid solutions:⁹

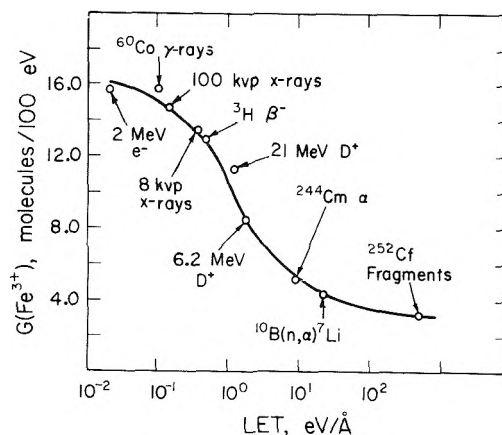


Figure 4. Variation of $G(\text{Fe}^{3+})$ with LET. All data from ref 8, except for ^{244}Cm and ^{252}Cf which were determined in this work.

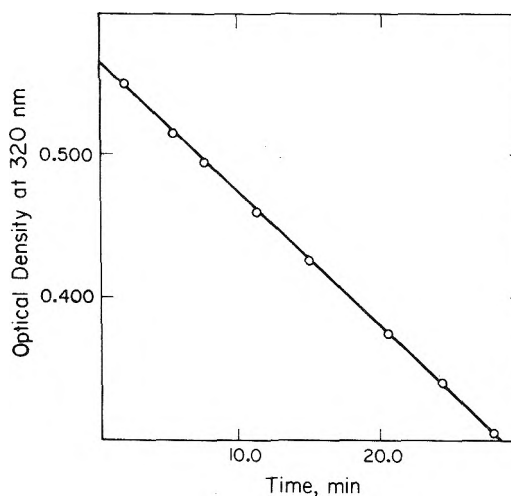


Figure 5. Optical density decrease at 320 nm from Ce^{4+} reduction in $1.01 \times 10^{-4} M \text{Ce}^{4+}$ and $\sim 10^{-3} M \text{Ce}^{3+}$ in aqueous $0.4 M \text{H}_2\text{SO}_4$ containing $2.6 \mu\text{g/ml } ^{252}\text{Cf}$.

$$G(\text{Fe}^{3+}) = 3[G(\text{H}) + G(\text{HO}_2)] + G(\text{OH}) + 2G(\text{H}_2\text{O}_2) \quad (2)$$

$$G(\text{Ce}^{3+}) = G(\text{H}) + G(\text{HO}_2) - G(\text{OH}) + 2G(\text{H}_2\text{O}_2) \quad (3)$$

In the presence of 10^{-3} or $10^{-2} M \text{Ti}^+$

$$G(\text{Ce}^{3+}) = G(\text{H}) + G(\text{HO}_2) + G(\text{OH}) + 2G(\text{H}_2\text{O}_2) \quad (4)$$

It is reasonable to assume that LET affects only the distribution and quantity of reactive intermediates and not their chemical reactions. Therefore, the above equations can be applied to results from ^{252}Cf radiolysis. When these are solved simultaneously for fission fragment radiolysis, $G(\text{OH}) = 0.0$, $G(\text{H}) + G(\text{HO}_2) = 0.45$, and $G(\text{H}_2\text{O}_2) = 0.97$. A value of 0.0 for $G(\text{OH})$ was also determined at $\text{LET} \approx 18 \text{ eV}/\text{\AA}$ by Collinson, Dainton, and Kroh⁹ by radiolysis with partially degraded α particles from ^{210}Po . They also reported $G(\text{H}_2\text{O}_2) = 1.2$ and $G(\text{H}) + G(\text{HO}_2) = 0.63$.

An estimate of $G(\text{H})$ can be made from eq 5 derived by combining eq 2 with eq 6 based on mass balance.

$$G(\text{H})_{\text{ff}} = 0.25[G(\text{Fe}^{3+})_{\text{ff}} - 2G(\text{H}_2)_{\text{ff}}] \quad (5)$$

$$2G(\text{H}_2) = G(\text{OH}) + 2G(\text{H}_2\text{O}_2) + 3G(\text{HO}_2) - G(\text{H}) \quad (6)$$

With observed values for $G(\text{Fe}^{3+})_{\text{ff}}$ and $G(\text{H}_2)_{\text{ff}}$, $G(\text{H})_{\text{ff}}$ is estimated to be -0.26 ± 0.14 at a 95% confidence level. As

TABLE II: 100-eV Yields for Radiolysis of $10^{-4} M \text{Ce}^{4+}$ – $10^{-3} M \text{Ce}^{3+}$ ^a

α radiolysis ^b			²⁵² Cf radiolysis ^b		
[Tl ⁺], M	No. of expt	$G(\text{Ce}^{3+})$	No. of expt	$G(\text{Ce}^{3+})_{\text{obsd}}$	$G(\text{Ce}^{3+})_{\text{ff}}$
0	2	2.89 ± 0.16	6	2.67 ± 0.04	2.45 ± 0.18^c
10^{-3}	2	3.34 ± 0.04	3	2.94 ± 0.09	2.37 ± 0.19^d
10^{-2}	2	3.14 ± 0.04	3	2.86 ± 0.09	2.41 ± 0.19^d

^a [²⁵²Cf] in all experiments is nominally 1 $\mu\text{g}/\text{ml}$. ^b Uncertainties in each determination are standard deviations. ^c $G(\text{Ce}^{3+})_{\beta} = 2.39$ (ref 23). ^d $G(\text{Ce}^{3+})_{\alpha} = 7.92$ (ref 23).

it is impossible for $G(\text{H})_{\text{ff}}$ to be negative, it therefore must be zero. Other published values for $G(\text{Fe}^{3+})_{\text{ff}}$ and $G(\text{H}_2)_{\text{ff}}$ are 3.0⁷ and 2.0,³ 1.6,⁵ 1.7,⁶ and 1.8,⁶ respectively. These, when substituted into eq 5, also indicate that $G(\text{H})_{\text{ff}}$ is negative, and thus must be zero. Apparently, H atoms as well as OH radicals do not escape fission fragment tracks to react with solutes at millimolar concentrations. Reactions for removal of H atoms and OH radicals in the tracks are

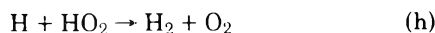
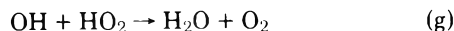
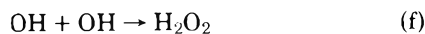
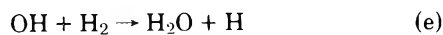
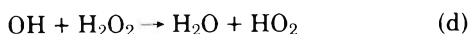
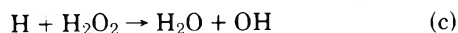
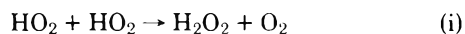


Figure 6 shows the variation with LET of 100-eV yields for radical and molecular products. Data for the solid lines were compiled by Allen.²⁴ The dotted lines connect the points determined for fission fragments with their respective solid lines. The increase in $G(\text{HO}_2)$ is consistent with H and OH radicals not escaping the fission fragment tracks but reacting with H_2O_2 (reactions c and d). This leads to the observed decrease in $G(\text{H}_2\text{O}_2)$ at very high LET values.⁹

Negative values for $G(\text{H})_{\text{ff}}$, in addition to indicating that $G(\text{H})_{\text{ff}}$ is zero, suggest that some radiolytic oxidation product of H_2O has not been included in eq 6. A reasonable possibility is molecular oxygen. To date all published fission fragment radiolysis studies^{3,5,6} as well as this one have detected O_2 along with H_2 . Also O_2 has been observed in α radiolysis.^{11,12} Possible track reactions for the formation of O_2 are (g) and (h) along with



With O_2 included, eq 5 becomes

$$2G(\text{H}_2) = G(\text{OH}) + 2G(\text{H}_2\text{O}_2) + 3G(\text{HO}_2) + 4G(\text{O}_2) - G(\text{H}) \quad (7)$$

With $G(\text{H})_{\text{ff}}$ equal to zero, eq 7 predicts that $G(\text{O}_2)_{\text{ff}}$ is 0.3. This is slightly larger than the value of 0.17 observed in α radiolysis.^{11,12} Data in Table I indicate a value of 0.8 for $G(\text{O}_2)_{\text{ff}}$ using a value of 0.17 for α ^{11,12} and 0.00 for β radiolysis. Although agreement is not good, and although it is highly improbable that $G(\text{O}_2)_{\text{ff}}$ could be as large as 0.8, the hypothesis of O_2 formation is still feasible.

A final implication of the fission fragment radiolysis

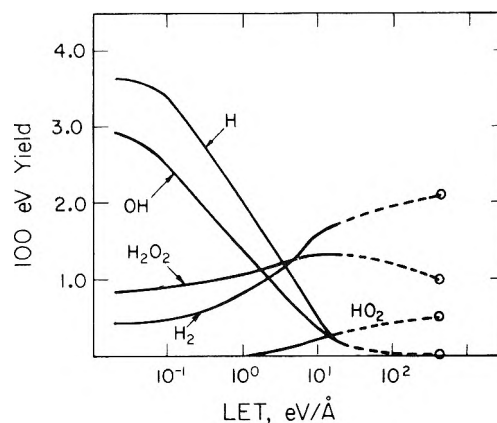


Figure 6. Variation of molecular and radical yields with LET in radiolysis of aqueous 0.4 M H_2SO_4 . Solid lines taken from ref 24.

studies is that the observed 100-eV yield for water decomposition may be larger than that for α radiolysis of such solutions. The larger values of $G(\text{H}_2)_{\text{ff}}$ indicate that $G(-\text{H}_2\text{O})_{\text{ff}}$ may be as high as 4.0 or 4.2 compared to 3.2 to 3.5 for α radiolysis.¹² Evidence for a value of 4.2 for α radiolysis has been obtained by using 0.1 M NH_4CNS as scavenger.¹² Vladimirova suggests the larger scavenger concentrations suppress reactions a, c, d, and e.¹² Perhaps the concentration and distribution of radicals in fission fragment tracks favor this behavior at millimolar scavenger concentrations. Clearly, more experiments at very high LET are necessary to verify if this is truly the case.

Acknowledgment. The author wishes to express appreciation to A. R. Boulogne for purification of the ²⁵²Cf and assistance in performing experiments in the shielded facility. Also, M. L. Hyder and D. H. Stoddard are thanked for their helpful and stimulating discussions.

References and Notes

- (1) Work done under USAEC Contract No. AT(07-2)-1.
- (2) Presented in part at the 5th International Congress of Radiation Research, July 14–20, 1974, Seattle, Wash.
- (3) R. G. Sowden, *Trans. Faraday Soc.*, **55**, 2084 (1959).
- (4) R. M. Bidwell, L. P. D. King, and W. R. Wyckoff, *Nucl. Sci. Eng.*, **1**, 452 (1956).
- (5) J. W. Boyle and H. A. Mahlman, *Nucl. Sci. Eng.*, **2**, 492 (1957).
- (6) J. W. Boyle, C. J. Hohanadel, T. J. Sworski, J. A. Ghormley, and W. F. Kieffer, *Proc. Int. Conf. Peaceful Uses At. Energy*, **7**, 576 (1956).
- (7) L. Ehrenberg and E. Saeland, Joint Establishment for Nuclear Energy Research, JENER Publications No. 8 (1954).
- (8) E. J. Henley and E. R. Johnson, "The Chemistry and Physics of High Energy Reactions", University Press, Washington, D.C., 1969, p 254.
- (9) E. Collinson, F. S. Dainton, and J. Kroh, *Proc. R. Soc. (London)*, *Ser. A*, **265**, 407 (1962).
- (10) J. L. Crandall, "Californium-252 Neutron Sources", to be published in the Proceedings of the ANS National Topical Meeting on Applications of ²⁵²Cf, Austin, Texas, Sept 11, 1972.
- (11) N. E. Bibler, *J. Phys. Chem.*, **78**, 211 (1974).

- (12) M. V. Vladimirova, *Adv. Chem. Ser.*, No. 81, 280 (1968).
(13) I. G. Draganic' and Z. D. Draganic', "The Radiation Chemistry of Water", Academic Press, New York, N.Y., 1971, p 150.
(14) K. V. Marsh and J. A. Miskel, *J. Inorg. Nucl. Chem.*, 21, 15 (1961).
(15) C. M. Lederer, J. M. Hollander, and I. Perlman, "Table of Isotopes", 6th ed, Wiley, New York, N.Y., 1968, p 149.
(16) S. L. Whetstone, Jr., *Phys. Rev.*, 131, 1232 (1963).
(17) D. Metta, H. Diamond, R. F. Barnes, J. Milsted, J. Gray, Jr., D. J. Henderson, and C. M. Stevens, *J. Inorg. Nucl. Chem.*, 27, 33 (1965).
(18) D. H. Stoddard, personal communication.
(19) B. T. Price, C. C. Horton, and F. T. Spinney, "Radiation Shielding", Pergamon Press, New York, N.Y., 1957, p 228.
(20) Reference 11, p 142.
(21) Determined with ^{244}Cm in this work.
(22) Reference 8, p 281.
(23) T. J. Sworski, *Radiat. Res.*, 4, 483 (1956).
(24) A. O. Allen, "The Radiation Chemistry of Water and Aqueous Solutions", Van Nostrand, Princeton, N.J., 1961, p 58.

A Reevaluation of the Ultrasonic Absorption Spectra of Aqueous Samarium(III) Sulfate Solutions

Michael M. Farrow, Neil Purdie,*¹ and Edward M. Eyring

Department of Chemistry, University of Utah, Salt Lake City, Utah 84112 (Received September 21, 1974; Revised Manuscript Received June 20, 1975)

Publication costs assisted by the Directorate of Chemical Sciences, Air Force Office of Scientific Research

Measurements of the ultrasonic absorption spectra of aqueous samarium sulfate solutions have been repeated using an optical-acoustic method over the frequency range 15–250 MHz. Considerably more data points were obtained with the new method, and the data have been analyzed in terms of a single and a double relaxation over both a constant and a variable nonrelaxational background absorption. The double relaxation analyses provide the best correspondence between theory and experiment. The overall ion association process has been treated as a two-step kinetic mechanism yielding four rate constants correlated with both relaxation times. The results are discussed in terms of the internal consistency of the two-step model. Comparisons are made with theoretical predictions of the rate constants for the diffusion-controlled first step and with previously reported values for the rate constants for the second and rate-determining step.

Introduction

Ultrasound absorption measurements on aqueous solutions of trivalent rare earth salts were first made some 20 years ago.² The rare earth sulfates in particular have attracted much attention since 1965 from numerous investigators, and the inevitable controversies have arisen.³ An unusual variation in the plot of the specific rate constant for the rate-controlling step vs. atomic number was interpreted either as a change in mechanism or as a change in cation coordination number.³ On the other hand, experimental data were consistently reproducible over the frequency range from 5 to about 250 MHz, in whole or in part, but the data were relatively sparse and were always³ fitted to the equation for a single relaxation. Since the frequency of maximum absorption for the "observed" single relaxation was dependent upon the cation, this relaxation was unanimously attributed to substitution for coordinated water on the cation by the approaching sulfate ion in accordance with the last and rate-determining step in the multistep mechanism for complex formation.⁴ Ultrasound absorption measurements have not been made at frequencies greater than 250 MHz for the rare earth sulfates so the faster step(s) involving outer-sphere ion pairing could not be characterized and the pragmatic approach of calculating the outer ion-pair formation constant has always been used in the kinetic analysis of the slowest step.³

From two distinct experimental observations, the fact

arises that the relaxation(s) involving the faster step(s) may be contributing to the observed low-frequency relaxation. In the first reports of sound absorption measurements on rare earth sulfates^{5,6} attention was drawn to a slight broadening of the low-frequency "single" relaxation curve at frequencies above 100 MHz, indicative of a faster relaxation of low amplitude. Insufficient experimental data precluded a complete analysis in terms of multiple relaxations, there being only three or four absorption measurements in excess of 100 MHz. Measurements up to 6 GHz on divalent metal sulfates⁷ had been used to successfully locate the faster relaxations for these systems in the frequency range 400–600 MHz. If this faster step is diffusion controlled, then the 3:2 rare earth sulfate solutions would be expected to relax at higher frequencies at formal concentrations equivalent to the 2:2 sulfates. In actuality, the 2:2 salt concentrations are typically 10 times greater than those used for the 3:2 electrolytes, which would conceivably lower the 3:2 relaxation frequencies to a range <400 MHz. The inevitable conclusion is reached that the ultrasound absorption spectra of the rare earth sulfate solutions are composites of multiple relaxations in which case it is invalid to assume that each relaxation time is characterized by only two rate constants.

This concern over the validity of introducing unwarranted assumptions to simplify the kinetic equations when relaxations are obviously coupled has been expressed numer-

ous times but not tested analytically.⁸ The purpose of the present work was to collect sufficient data over the frequency range of the relaxations in order that the existence of multiple relaxations might be established. Another objective was to perform the complete analysis using the exact rate equations, so that the results from both methods might be compared.

Experimental Section

Ultrasound absorption measurements were made using an optical-acoustic technique, comparable to the old Debye-Sears method,⁹ in which the white light source was replaced by an argon-ion laser. Details of the instrumentation and procedures for measurement are described elsewhere.¹⁰ The argon-ion laser was operated on the green line at 514.5 nm. The acoustic transducer was a 5-MHz fundamental frequency X-cut quartz crystal, and measurements were made at all odd harmonics up to 205–245 MHz. Precision on the measured absorption coefficient α at each frequency was better than $\pm 2\%$.

Solutions were prepared using deionized redistilled water, and samarium sulfate hydrate (American Potash & Chem. Corp.). Concentrations were determined by ion exchange and titration of the eluant sulfuric acid with standard potassium hydroxide. Solutions were thermostatted for the measurements at $25 \pm 0.1^\circ$.

Results

Total sound absorption data, expressed as $(\alpha/f^2)_T$ neper $\text{sec}^2 \text{cm}^{-1}$, are given in Table I along with the uncertainties in each measurement. On the present equipment a value of $21.7 \pm 0.5 \times 10^{-17}$ neper $\text{sec}^2 \text{cm}^{-1}$ was obtained for pure water over the entire frequency range of the measurements. This value is in excellent agreement with previous literature values. Absorptions measured at the highest frequencies are still in excess of the nonrelaxational absorption due to pure water alone. Accordingly the data were fitted to a general equation

$$(\alpha/f^2)_T = \sum_{i=1}^r \left\{ \frac{A_i}{1 + (f/f_i)^2} \right\} + B \quad (1)$$

which is a summation of relaxational terms (in parentheses) where A_i are the relaxation amplitudes, f_i are the relaxation frequencies, and B is a background/solvent absorption term. The number of contributing single relaxations is given by r .

Experimental error in $(\alpha/f^2)_T$ and the uncertainty in r compounds the difficulty of fitting the experimental data to $(2r + 1)$ parameters. The following specific cases were considered: (1) $r = 1$ and B is a variable nonrelaxational absorption due to the solvent alone, or a result of structural changes in the solvent brought about by the added electrolyte; (2) $r = 2$ and $B = 21.7 \times 10^{-17}$ neper $\text{sec}^2 \text{cm}^{-1}$; (3) $r = 2$ and B is a variable nonrelaxational absorption as described in case 1. Included in case 1 is the condition where $r = 1$ and $B = 21.7 \times 10^{-17}$ neper $\text{sec}^2 \text{cm}^{-1}$. Case 2 is considered separately, but it is no more than a particular condition of case 3. At this juncture it is necessary to point out that precision in the data is inadequate to distinguish between two and three relaxations. Furthermore, the variation in B was limited to $\pm 3\%$ of the value for the pure solvent, since a change of ca. $+3\%$ has been reported¹¹ for 0.1 M MnSO_4 , i.e., a more concentrated, but less charged electrolyte. Values of B less than 21.7×10^{-17} neper $\text{sec}^2 \text{cm}^{-1}$ have been reported numerous times for uni-univalent elec-

TABLE I: Experimental Frequencies and Total Absorption Data as $(\alpha/f^2)_T$ neper $\text{sec}^2 \text{cm}^{-1}$

f , MHz	$10^{17}(\alpha/f^2)_T$	f , MHz	$10^{17}(\alpha/f^2)_T$
$C = 3.522 \times 10^{-2} M$			
15.04	281.0 ± 23.8	115.3	61.5 ± 0.4
25.00	235.0 ± 9.2	125.3	56.3 ± 0.09
35.00	203.0 ± 4.8	135.5	52.4 ± 0.2
45.00	165.0 ± 6.2	145.5	49.4 ± 0.3
55.14	136.0 ± 1.7	155.5	45.8 ± 0.2
65.25	116.7 ± 0.6	165.5	43.4 ± 0.09
75.24	99.0 ± 0.3	185.7	40.2 ± 0.05
85.30	86.0 ± 0.6	205.7	36.2 ± 0.15
95.31	74.7 ± 0.4		
$C = 2.347 \times 10^{-2} M$			
15.01	199.0 ± 8.0	105.4	51.3 ± 0.2
25.04	167.0 ± 5.0	115.4	46.2 ± 0.2
34.99	142.5 ± 2.5	125.5	44.8 ± 0.2
45.00	177.1 ± 0.5	135.5	42.1 ± 0.2
55.00	97.7 ± 1.0	155.6	37.1 ± 0.1
65.25	82.4 ± 0.5	175.7	34.4 ± 0.2
75.27	71.0 ± 0.6	195.7	31.7 ± 0.3
85.28	63.6 ± 0.9	215.8	30.0 ± 0.05
95.34	55.5 ± 0.2		
$C = 1.712 \times 10^{-2} M$			
15.12	175.0 ± 12.0	125.1	40.3 ± 0.4
25.00	144.0 ± 15.0	135.2	37.7 ± 0.2
35.12	120.0 ± 4.0	145.5	36.4 ± 0.15
45.11	99.5 ± 1.1	155.6	34.3 ± 0.05
55.11	82.5 ± 1.8	165.5	33.2 ± 0.069
65.21	71.2 ± 0.4	175.5	31.1 ± 0.075
75.21	62.7 ± 0.4	185.7	30.0 ± 0.11
85.21	55.5 ± 0.3	195.8	29.5 ± 0.092
95.33	50.1 ± 0.2	205.8	28.6 ± 0.091
105.8	46.4 ± 0.2	215.9	28.0 ± 0.085
115.2	42.0 ± 0.4		
$C = 1.170 \times 10^{-2} M$			
15.00	115.0 ± 17.0	115.3	34.6 ± 0.27
18.00	115.0 ± 4.0	125.4	32.8 ± 0.15
25.00	102.0 ± 5.0	135.5	31.5 ± 0.094
33.99	88.0 ± 2.0	145.4	30.6 ± 0.15
35.00	83.5 ± 1.6	165.6	28.6 ± 0.11
45.00	70.8 ± 1.4	175.0	27.7 ± 0.60
55.00	59.9 ± 0.98	175.5	28.0 ± 0.91
60.00	55.1 ± 2.2	175.7	27.5 ± 0.044
75.23	46.3 ± 0.94	185.7	27.0 ± 0.066
85.30	42.8 ± 0.31	195.7	26.5 ± 0.048
95.28	39.1 ± 0.16	205.8	26.3 ± 0.095
100.00	37.7 ± 0.43	246.3	24.6 ± 0.18
105.3	36.3 ± 0.18		

trolytes,¹² but a change of -3% is observed only when solute concentrations are in excess of 0.5 M. A decision on the best correspondence between theory and experiment was based upon which of these cases produced the *minimum* absolute root mean square (rms) deviation defined as

$$s = \left[\left\{ \sum_{i=1}^n [(\alpha/f^2)_{T,\text{expt}} - (\alpha/f^2)_{T,\text{calcd}}]^2 W_T \right\} / (n - p) \right]^{1/2} \quad (2)$$

where n is the number of experimental frequencies, W_T is a weighting factor based upon the standard deviation of indi-

vidual absorption measurements introduced to account for the relative precision in $(\alpha/f^2)_T$, and p is the number of dependent parameters A_i , f_i , and B required in each case to determine $(\alpha/f^2)_{T, \text{calcd}}$. Rather than solve eq 1 directly, a simulation procedure was used and the actual calculations were carried out on the equivalent expression

$$\{(\alpha/f^2)_T - B\}cf = \sum_{i=1}^r \left| \frac{2(A_{\text{EXCESS}})(f/f_i)}{1 + (f/f_i)^2} \right| \quad (3)$$

where c is the velocity of sound and $(\alpha_{\text{EXCESS}}\lambda)_i$ is the (chemical) absorption per wavelength in excess of the nonrelaxational background.

In case 1 a standard converging grid search for values of A_i and f_i which gave the minimum s for each B was made, as B was incremented until an overall minimum in s was obtained. Typical values of A_i , f_i , and B , and the values which correspond to the minimum s for case 1, are given in Table II. For cases 2 and 3 an iterative grid search technique was used, in which two 10×10 grids were set up whose initial wide limits spanned the approximate ranges of each relaxation frequency and each relaxation amplitude. Equation 3 was solved for all experimental frequencies using all combinations of points in the high-frequency grid for each point in the low-frequency grid. New narrower limits were set symmetrically around the points in each grid which gave the best correspondence between $(\alpha/f^2)_{T, \text{calcd}}$ and $(\alpha/f^2)_{T, \text{expt}}$ in the previous cycle and the grid search continued, by successive convergences until s was minimized. Convergence was usually accomplished in seven to eight passes. On repeating the grid search for each new value of B , the initial grids were reset to the initial limits. The resultant parameters corresponding to the best fit, expressed as the rms deviation between theoretical and calculated curves for cases 2 and 3, are given in Table III. Within the prescribed limits of B there is no basis on which to favor case 2 over case 3. To obtain the minimum rms deviation of comparable magnitude to the double relaxation analysis for the most concentrated solution, the value of B had to be increased to 24.3×10^{-17} neper $\text{sec}^2 \text{cm}^{-1}$, which is approximately the value expected from the small amplitude of the higher frequency absorption determined in the double relaxation analysis. However, one cannot directly compare the values of s for case 1 with those for cases 2 and 3 since the number of adjustable parameters differ.

Ultrasound absorption spectra are shown for two solution concentrations in Figure 1. The data are presented as absorption in excess of the pure solvent, case 2, in terms of the normalized excess absorption coefficient per wavelength $(\alpha_{\text{chem}}\lambda)$ in nepers, equal to $(\alpha_T - \alpha_S)\lambda$, where α_S is the absorption coefficient for the pure solvent calculated from $B = (\alpha_S/f^2)$. The relationship between the maximum $(\alpha_{\text{chem}}\lambda)_i$ and A_i is that $A_i = (2\alpha_{\text{chem}}\lambda)_i/cf_i$ where c is the velocity of sound. The open circles in Figure 1 are the experimental absorptions, and the solid lines are the computer simulated total excess absorption curve and the calculated single relaxation curves, respectively.

Errors in the relaxation frequencies and amplitudes for the double relaxation analysis are difficult to estimate, so we have resorted to a comparison of this real experimental situation with the theoretical simulation presented by Rassing and Lassen.¹³ In terms of the data, the number of experimental frequencies taken is similar in both cases, but the precision in our experimental absorption data is better than their assumed value of $\pm 2\%$. The amplitude of the high-frequency absorption is small enough that the overall

TABLE II: Absorption Parameters from Simulated Computer Analysis as a Single Relaxation Over a Variable Background Absorption^a

$10^2 C$, M	f_1 , MHz	$10^{17} A_1$, neper $\text{sec}^2 \text{cm}^{-1}$	$10^{17} B$, neper $\text{sec}^2 \text{cm}^{-1}$	10^5rms
3.522	44.6	285.3	24.50	5.1
2.347	43.1	196.4	23.00	6.2
1.712	43.5	161.5	22.35	6.1
1.170	42.4	106.0	21.70	4.9

^a Errors in f_1 are $\pm 5\%$, in $A_1 \pm 1\%$.

TABLE III: Absorption Parameters from Simulated Computer Analysis as a Double Relaxation Over a Variable Background^a

$10^2 C$, M	f_1 , MHz	$10^{17} A_1$, neper $\text{sec}^2 \text{cm}^{-1}$	f_2 , MHz	$10^{17} A_2$, neper $\text{sec}^2 \text{cm}^{-1}$	10^5rms
$B = \{(\alpha/f^2)_{\text{water}} - 3\%\} = 21.05 \times 10^{-17}$ neper $\text{sec}^2 \text{cm}^{-1}$					
3.522	178.2	6.3	44.59	279.8	7.57
2.347	142.9	6.0	41.89	194.0	6.94
1.712	122.7	5.2	42.65	157.6	7.12
1.170	109.4	4.9	38.64	108.3	5.60

$B = \{(\alpha/f^2)_{\text{water}}\} = 21.7 \times 10^{-17}$ neper $\text{sec}^2 \text{cm}^{-1}$					
3.522	178.2	6.0	43.95	282.9	6.71
2.347	142.9	4.7	41.78	195.5	6.61 ^b
1.712	122.7	5.2	40.91	162.8	6.55 ^b
1.170	106.4	3.9	38.64	107.6	4.60 ^b

$B = \{(\alpha/f^2)_{\text{water}} + 3\%\} = 22.35 \times 10^{-17}$ neper $\text{sec}^2 \text{cm}^{-1}$					
3.522	177.2	4.3	44.27	283.0	6.42 ^b
2.347	136.9	3.4	41.86	196.5	6.84
1.712	118.2	4.0	40.26	166.4	6.72
1.170	106.4	1.6	38.64	110.2	6.13

^a Errors in f_1 and A_1 are $\pm 20\%$, errors in f_2 are $\pm 5\%$, in $A_2 \pm 3\%$.
^b Best fit.

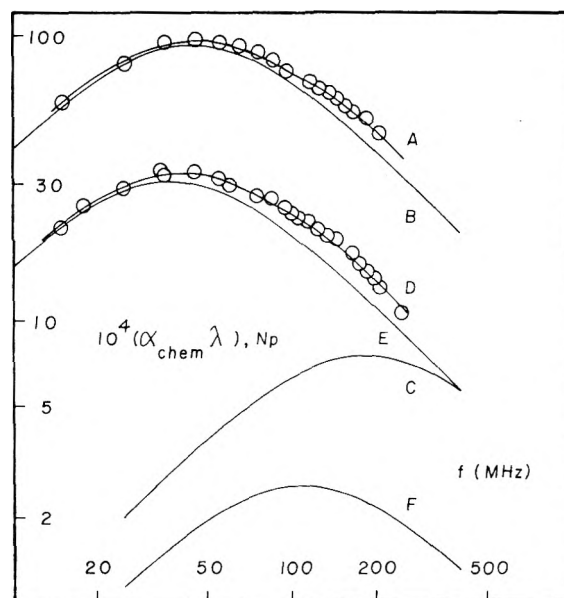


Figure 1. Excess ultrasound absorption spectra for samarium sulfate solutions plotted as $10^4 (\alpha_{\text{chem}}\lambda)$ neper vs. frequency in MHz. A, B, and C are the computer-simulated double and composite single relaxation curves for $C = 3.522 \times 10^{-2} M$. D, E, and F are the corresponding curves for $C = 1.170 \times 10^{-2} M$.

TABLE IV: Parameters Calculated from Equilibrium Constant^a in the Evaluation of θ

$10^2 C, M$	β^b	$10^2 \mu, M^c$	$10^3 [\overline{\text{Sm}^{3+}}]$	$10^2 [\overline{\text{SO}_4^{2-}}]$	γ_1^{12}	DER ^c	$10^3 \theta$
3.522	1.924	12.172	2.676	3.790	0.147	-0.005	5.940
2.347	1.897	8.491	2.417	2.589	0.157	-0.018	4.363
1.712	1.874	6.430	2.157	1.928	0.169	-0.028	3.534
1.170	1.843	4.612	1.836	1.354	0.190	-0.039	2.821

^a Equilibrium constant is 4.55×10^3 , ref 14. ^b β is the degree of association expressed in terms of a total metal ion concentration, $2C$. ^c μ is the ionic strength of the solutions. ^d DER is the partial derivative $(\partial \ln \Pi_f / \partial \ln \beta)_C$.

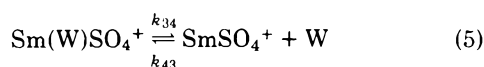
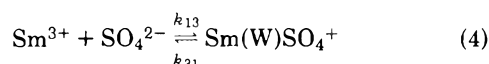
TABLE V: Rate Constants and Stepwise Equilibrium Constants for SmSO_4^+ Formation

	Method of analysis				
	Eq 7	Eq 5-6	Ref 15 (3-step) ^a	Ref 16 (2-step)	Theor (2-step)
k_{13}	1.6×10^{11}	1.5×10^{11}	$K_{12} = 436$		1.3×10^{11}
k_{31}	1.3×10^8	2.4×10^8	$K_{23} = 1.5$		1.7×10^8
K_{13}	1230	625		365	765
k_{34}	2.3×10^8	2.9×10^8	3.3×10^8	4.1×10^8	
k_{43}	9.4×10^7	5.2×10^7	6.3×10^7	3.4×10^7	
K_{34}	2.4	5.6	5.3	12.1	
K_T (kinetic)	4185	4125	4556	4782	
K_T (conduct)	4550	4550	4550	4550	

^a For the 3-step mechanism $K_T(\text{kinetic}) = K_{12}(1 + K_{23} + K_{23}K_{34})$.

absorption curve could be approximated to a single relaxation in which case f_2 can be established with a high degree of certainty. We chose to use an error of $\pm 5\%$ in f_2 and $\pm 3\%$ in A_2 , consistent with their single relaxation analysis. For both f_i and A_i an error of at least $\pm 20\%$ is considered appropriate in accord with their two relaxation model.

The overall analysis suggests that two closely coupled relaxations are contributing to the total absorption. We have chosen to proceed with the assumption that the kinetic interpretation of the data can be made in terms of a two-step mechanism:



In previous treatments of a two-step mechanism $K_{13} = k_{13}/k_{31}$ was calculated from theory and the assumption was introduced that $k_{13}, k_{31} \gg k_{34}, k_{43}$ in which case the rate equations were simplified to

$$\tau_1^{-1} = 2\pi f_1 = k_{13}\theta + k_{31} \quad (6)$$

$$\tau_2^{-1} = 2\pi f_2 = \left[\frac{\theta}{\theta + K_{13}^{-1}} \right] k_{34} + k_{43} \quad (7)$$

where τ_1, τ_2 and f_1, f_2 are the relaxation times and frequencies, respectively, and

$$\theta = \Pi_f \left\{ [\overline{\text{Sm}^{3+}}] + [\overline{\text{SO}_4^{2-}}] + [\overline{\text{SO}_4^{2-}}] \left(\frac{\partial \ln \Pi_f}{\partial \ln \beta} \right)_C \right\}$$

In the expression for θ , $\Pi_f = \gamma_1^{12}$ where γ_1 is the activity coefficient of a univalent ion, the bars refer to equilibrium concentrations, and β and C are the degree of association and the analytical salt concentration, respectively. The expansion of the partial derivative term and the iterative calculation of θ have been adequately described³ and bear no

repetition here. Results of the calculations are given in Table IV.

The outcome of this analysis was that $k_{31} \leq k_{34}$ which negates the assumption that the relaxations are noninterfering and that the relaxation times are characterized by only two rate constants as in eq 5 and 6.

The exact solution of the rate equations requires that we solve the roots of the secular determinant for a two-step mechanism in which both relaxation times are correlated with all four rate constants, according to

$$(\tau_{1,2})^{-1} = \frac{1}{2} \{ S \pm (S^2 - 4P)^{1/2} \} \quad (8)$$

where the positive sign corresponds with τ_1^{-1} , the negative with τ_2^{-1} , $S = (k_{13}\theta + k_{31} + k_{34} + k_{43})$ and $P = [k_{13}\theta(k_{34} + k_{43}) + k_{31}k_{43}]$. Two concentrations and four frequencies are sufficient to solve eq 8. Knowing $\tau_1^{-1} = 2\pi f_1$, and $\tau_2^{-1} = 2\pi f_2$, S and P can be calculated from the ultrasound absorption curves using the equations $S = 2\pi(f_1 + f_2)$ and $P = 4\pi^2 f_1 f_2$. A straightforward simultaneous solution of two equations for S and two equations for P gives as a result the four rate constants.

The resultant specific rate constants for the two-step mechanism are given in Table V. A criterion for estimating the internal consistency of the rate data is to calculate the overall association constant for the process using $K_T = K_{13}(1 + K_{34})$, and to compare this with the value obtained conductimetrically¹⁴ (see Table V). Also given in Table V are previous results, and the results obtained from the present data when the assumption that $k_{13}, k_{31} \ll k_{34}, k_{43}$ is introduced.

Discussion

The backward rate constants k_{31} and k_{43} are the only two which change significantly between the approximate and rigorous analysis. In both treatments $k_{31} \approx k_{34}$ so the

rate data from the more rigorous solutions should be accepted over all previous results.³

Of the four rate constants most of the interest and much of the controversy is centered around k_{34} . Since the low relaxation frequency is observed to increase with atomic number (Z) and to maximize around Sm–Eu–Gd, the most significant coupling between relaxations is typified by the present example. According to the multistep mechanism the higher frequency relaxation is independent of the cation so the decrease in k_{34} of about 30% from the value ($3.3 \times 10^8 \text{ sec}^{-1}$) obtained previously for Sm in the approximated calculation¹⁵ is representative of the largest change which can be expected for any ion in the rare earth series. The tendency therefore would be to lower the maximum¹⁵ in the plot of k_{34} vs. Z bringing it into closer correspondence with the plot of the thermodynamic formation constants K_T vs. Z . If the same factors influence both K_T and k_{34} , the thermodynamic reason for the unusual variation in K_T , i.e., a coordination number change, would suffice to account for the variation in k_{34} without resorting to a kinetic reason such as a mechanistic change.¹⁶

The value in Table V of $k_{13} = 1.6 \times 10^{11} \text{ M}^{-1} \text{ sec}^{-1}$ probably represents the upper limit for the diffusion-controlled outer ion-pair formation rate constant since for $k_{13} > 2 \times 10^{11} \text{ M}^{-1} \text{ sec}^{-1}$, the rate constants for step 2 are both calculated to be negative. Another system for which k_{13} approaches this order of magnitude is the recombination of the proton with a Lewis base,¹⁷ e.g., OH^- , F^- , SO_4^{2-} . Errors in experimental f_1 values, which are substantial because of the low absorbance amplitude of the higher frequency relaxations, could conceivably introduce an error of as great as a factor of two in k_{13} . Such a change in k_{13} makes $k_{43} > k_{34}$, and leaves k_{34} essentially unaltered.

k_{13} can be calculated from diffusion theory. Since a two-step model was used the distance of closest approach \bar{a} in forming the outer ion pair was taken to be 6.10 \AA , equal to the sum of the ionic radii and one water molecule diameter. Using the Debye¹⁸ equation

$$k_{13} = \frac{4\pi NZ_A Z_B e_0^2 (D_A + D_B)}{10^3 \epsilon k T [\exp(Z_A Z_B e_0^2 / \epsilon k T \bar{a}) - 1]} \quad (9)$$

where Z_A , Z_B , $D_A = 1.82 \times 10^{-5} \text{ sec}^2 \text{ cm}^{-1}$, and $D_B = 2.13 \times 10^{-5} \text{ sec}^2 \text{ cm}^{-1}$ are the ion charges and diffusion coefficients,¹⁹ respectively, and the remaining symbols have their usual significance, k_{13} is equal to $1.3 \times 10^{11} \text{ M}^{-1} \text{ sec}^{-1}$. Considering the uncertainties in such parameters as the dielectric constant of the solvent in the vicinity of the ions and in \bar{a} , a theoretical value for k_{13} for Sm(W)SO_4^+ of $10^{11} \text{ M}^{-1} \text{ sec}^{-1}$ is not unacceptable and in good agreement with the value from experiment.

The value calculated from kinetics for the overall thermodynamic association constant is in good agreement with

the conductimetric value so the rate data are internally self-consistent. k_{31} can also be calculated from theory using the Eigen²⁰ equation

$$k_{31} = (3Z_A Z_B e_0^2 / \epsilon \bar{a} k T) \times \{(D_A + D_B) / [1 - \exp(-Z_A Z_B e_0^2 / \epsilon \bar{a} k T)]\} \quad (10)$$

and a value of $1.7 \times 10^8 \text{ sec}^{-1}$ is obtained again in good agreement with experiment. The only unsatisfactory correspondence between theory and experiment is in $K_{13} = k_{13}/k_{31}$, 765 and 1230, respectively. A value of $\bar{a} = 5 \text{ \AA}$ would give a theoretical value of 1120 for K_{13} , but the lack of correspondence is best left as due to the uncertainty in k_{13} experimental.

In summary, in the reevaluation of the ultrasonic absorption spectra of aqueous samarium sulfate solutions the experimental data can be fitted by the equation for two closely coupled relaxations. A more rigorous interpretation of the rate data as a two-step mechanism demonstrates little change in the rate constant of particular interest, i.e., k_{34} , which mitigates our concerns over the validity of assumptions introduced in earlier analyses,^{3,16} at least with respect to this rate constant.

Acknowledgment. This work was supported by the Directorate of Chemical Sciences, Air Force Office of Scientific Research, Grant No. AFOSR 73-2444A.

References and Notes

- (1) Work done while author was on sabbatical leave from Department of Chemistry, Oklahoma State University, Stillwater, Okla. 74074.
- (2) K. Tamm, G. Kurtze, and R. Kaiser, *Acustica*, **4**, 380 (1954).
- (3) Reviewed in N. Purdie and M. M. Farrow, *Coord. Chem. Rev.*, **11**, 189 (1973).
- (4) H. Diebler and M. Eigen, *Z. Phys. Chem. (Frankfurt am Main)*, **20**, 229 (1959).
- (5) N. Purdie and C. A. Vincent, *Trans. Faraday Soc.*, **63**, 2745 (1967).
- (6) J. J. Grescek, M. S. Thesis, University of Maryland, 1966.
- (7) K. Fritsch, C. J. Montrose, J. L. Hunter, and J. F. Dill, *J. Chem. Phys.*, **52**, 2242 (1970).
- (8) Reference 3, and references to S. Petrucci therein.
- (9) P. Debye and F. W. Sears, *Proc. Natl. Acad. Sci. USA*, **18**, 410 (1932).
- (10) M. M. Farrow, S. Olsen, N. Purdie, and E. M. Eyring, manuscript in preparation.
- (11) L. G. Jackopin and E. Yeager, *J. Phys. Chem.*, **74**, 3766 (1970).
- (12) K. G. Breitschwerdt and H. K. Kistenmacher, *J. Chem. Phys.*, **56**, 4800 (1972).
- (13) J. Rassing and H. Lassen, *Acta Chem. Scand.*, **23**, 1007 (1969).
- (14) F. H. Spedding and S. Jaffe, *J. Am. Chem. Soc.*, **76**, 882 (1954).
- (15) M. M. Farrow and N. Purdie, *J. Solution Chem.*, **2**, 513 (1973).
- (16) J. Reidler and H. B. Silber, *J. Phys. Chem.*, **77**, 1275 (1973).
- (17) M. Eigen and L. DeMaeyer in "Techniques of Organic Chemistry", Vol. VIII, A. Weissberger, Ed., Part II, Interscience, New York, N.Y., 1963, p 1034.
- (18) P. Debye, *Trans. Electrochem. Soc.*, **82**, 265 (1942).
- (19) Ion mobilities from R. A. Robinson and R. H. Stokes, "Electrolyte Solutions", 2nd ed (revised), Butterworths, London, 1971, p 463, which are easily converted to diffusion coefficients as in H. Eyring and E. M. Eyring, "Modern Chemical Kinetics", Reinhold, New York, N.Y., 1963, pp 84–85.
- (20) Reference 17, p 1032.

Complex Solubilities of the Silver Halides in Aprotic Solvents Containing Sulfur and Oxygen

Mark Salomon

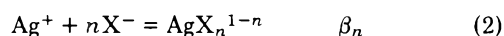
Power Sources Technical Area, U.S. Army Electronics Technology and Devices Laboratory (ECOM), Fort Monmouth, New Jersey 07703
(Received April 14, 1975)

Publication costs assisted by the U.S. Army Electronics Technology and Devices Laboratory

The complex solubilities of the silver halides AgCl, AgBr, and AgI have been determined in dimethyl sulfite (DMS), ethylene sulfite (ES), and tetramethylene sulfoxide (TMSO). It is found that anion solvation in several aprotic solvents decreases according to $H_2O > DMS > ES > DMSO \sim PC > TMSO_2 > TMSO$. The reason for the greater anion solvation in dimethyl sulfite compared to ethylene sulfite is attributed to the introduction of a 1,3-nonbonded interaction in the cyclic structure upon coordination with the anion. The present results are discussed in terms of the nature of bonding about the sulfur atom and the resulting effects on the reactivity of the open chain and cyclic structures.

Introduction

It has been known for some time¹ that, unlike water, aprotic solvents are poor solvators for anions. The present paper is a continuation of our previous work² on the nature of ion solvation in aprotic solvents. In particular, we are concerned with those factors influencing the solvation of anions. The nature of the complex solubilities of the silver halides, AgX (X = Cl, Br, I), has proved to be of value in analyzing these factors. The reactions of interest are



and



From these equations several qualitative conclusions can be made. If we choose a solvent which favors the solvation only of Ag^+ , then it is expected that the solubility product, K_{s0} , will increase, the stability constant, β_n , will decrease, and K_{s2} should remain virtually unchanged. If a solvent is selected which favors only anion solvation, then it is expected that K_{s0} would increase and that both β_n and K_{s2} would decrease. The magnitude of K_{s2} can therefore be used as a relative measure of the solvating ability of the particular solvent under investigation.

In the present paper, the equilibrium constants for the above reactions are determined in dimethyl sulfite (DMS), ethylene sulfite (ES), tetramethylene sulfoxide (TMSO), and a 1.123 M solution of TMSO in propylene carbonate (PC). Finally these results are discussed in relation to the rates of $(RO)_2SO$ hydrolysis in alkaline and acidic (aqueous) solutions.

Experimental Section

Materials. Tetrapropylammonium perchlorate, chloride, bromide, and iodide (TPAP, TPACl, TPABr, and TPAI, respectively) were purified by the methods described by Mann.³ All solvents were purified by fractional distillation under vacuum; details on purification of PC, TMSO, DMS, and ES can be found in ref 2, 4, 5, and 6, respectively. The purified solvents were stored in an argon-filled drybox over type 4A molecular sieves. Karl Fischer titrations showed

these solvents to contain not more than 50 ppm water, by weight ($<0.004 M$). All electrolyte solutions reported here are of a constant ionic strength of 0.0500 M and were prepared in the drybox. TPAP was used as the inert electrolyte to maintain the ionic strength.

Method. The solubility and stability constants representing eq 1-3 were obtained from potentiometric titration data as described previously.² The titrant was 50 mM $AgClO_4$ in the given solvent except for ethylene sulfite where a 14.64 mM $AgClO_4$ titrant was used. In a 50 mM $AgClO_4$ solution, ES tended to become cloudy after 24 hr of storage; the 14.64 mM solution was considerably more stable. The nature of this cloudiness was not investigated but was assumed to be due to hydrolysis with the residual water and precipitation of Ag_2SO_3 .

The titration cell is identical with the one described earlier.² The indicator electrode was a coiled, etched silver wire and the reference electrode was a silver wire in 50 mM $AgClO_4$ (14.64 mM in ethylene sulfite). The cell and 15 or 20 ml of TPAX + TPAP solution⁷ was fitted with a Gilmont 2-ml microburet containing the titrant and removed from the drybox and placed in a water bath thermostated at $25 \pm 0.1^\circ$. Magnetic stirring was maintained throughout the titration. A Doric Model DS-100 integrating microvoltmeter was used for the emf measurements.

Results

The experimental concentrations⁷ used to calculate the equilibrium constants are C_X , C_{Ag} , and $[Ag^+]$. C_X and C_{Ag} are the total halide and silver concentrations and $[Ag^+]$ is the silver ion concentration. The latter is obtained from the Nernst equation

$$E = E' + RT/F \ln [Ag^+] \quad (4)$$

where E is the measured emf and E' is a formal potential and contains contributions from the liquid junction and nonideality of the electrolyte solutions. E' is assumed to remain constant because of the use of a constant ionic strength media. The emf values in TMSO solutions were stable to within ± 0.2 mV and in DMS and ES to within ± 0.5 mV. E' values were obtained from the region of the titration curve where $C_{Ag} > C_X$ and had standard deviations of 1-2 mV. The stability constants were obtained using the

TABLE I: Experimental Molar Equilibrium Constants at 25°

Solvent	Salt	$-\log K_{s0}$	$\log \beta_2$	$\log \beta_3$	$\log K_{s2}$
PC/TMSO (1.123 M) [0.721] ^a	AgCl	15.26 ± 0.02	16.56 ± 0.01	17.17 ± 0.14	1.30 ± 0.02
	AgBr	15.52 ± 0.02	16.38 ± 0.01	17.49 ± 0.05	0.85 ± 0.02
	AgI	16.61 ± 0.10	17.98 ± 0.02		1.37 ± 0.01
TMSO [1.263]	AgCl	11.24 ± 0.01	13.82 ± 0.01		2.58 ± 0.01
	AgBr	11.35 ± 0.01	13.48 ± 0.01	14.60 ± 0.09	2.13 ± 0.01
	AgI	11.82 ± 0.08	14.01 ± 0.05		2.20 ± 0.09
DMS [3.321]	AgCl	16.53 ± 0.09	14.04 ± 0.07		-2.49 ± 0.11
	AgBr	18.08 ± 0.42	16.91 ± 0.10		-1.17 ± 0.43
	AgI	20.32 ± 0.37	19.68 ± 0.50		-0.64 ± 0.63
ES [1.422]	AgCl	18.47 ± 0.01	18.30 ± 0.07		-0.17 ± 0.06
	AgBr	19.92 ± 0.02	19.99 ± 0.01	22.29 ± 0.03	0.07 ± 0.02
	AgI	21.03 ± 0.02	21.71 ± 0.01		0.68 ± 0.02

^a Bracketed values are the Debye-Hückel A factors in $M^{1/2} K^{3/2}$.

TABLE II: Standard Molar Equilibrium Constants at 25°

Solvent	Salt	$-\log K_{s0}^\circ$	$\log \beta_2^\circ$	$\log K_{s2}^\circ$
PC/TMSO (1.123 M)	AgCl	15.3	16.6	1.3
	AgBr	15.6	16.4	0.9
	AgI	16.7	18.0	1.4
TMSO	AgCl	11.3	13.9	2.6
	AgBr	11.4	13.6	2.1
	AgI	11.9	14.1	2.2
DMS	AgCl	16.8	14.3	-2.5
	AgBr	18.3	17.1	-1.2
	AgI	20.5	19.9	-0.6
ES	AgCl	18.6	18.4	-0.2
	AgBr	20.0	20.1	0.1
	AgI	21.1	21.2	0.7
H ₂ O	AgCl	9.8	5.3	-4.5
	AgBr	12.3	7.3	-5.0
	AgI	16.1	10.7	-5.4
DMSO	AgCl	10.6	12.2	1.6
	AgBr	10.6	11.7	1.1
	AgI	11.6	12.8	1.2
TMSO ₂ (30°)	AgCl	18.1	19.8	1.7
	AgBr	18.4	19.7	1.3
PN/SO ₂ (3.30 M)	AgCl	10.4	7.9	-2.5
	AgBr	11.5	9.1	-2.4
	AgI	13.7	11.4	-2.3

data in the unsaturated solutions by an iterative least-squares method in which the relative error function, U , is minimized.² For i data points, U is defined by

$$U = \sum_i (1 - y_i/fy_i)^2 \quad (5)$$

where

$$y_i = (C_{Ag,i} - [Ag^+]_i)/[Ag^+]_i \quad (6)$$

and

$$fy_i = \sum_i^n \beta_n [X^-]_i^n \quad (7)$$

The standard deviations for the β_n 's were calculated by Sil-lén's pit-mapping method.⁸ The solubility products were calculated from each data point in the saturated solutions using the Newton-Raphson iterative method to solve the equation

$$(C_X - C_{Ag} + [Ag^+])/[Ag^+] = K_{s0}/[Ag^+]^2 +$$

$$\sum_2^n (n-1)\beta_n (K_{s0}/[Ag^+])^n \quad (8)$$

The final K_{s0} is taken as the average from all points in the saturated region. The refined β_n 's and K_{s0} 's and their standard deviations are given in Table I. In Table II, the standard equilibrium constants are given. The activity coefficients were calculated from the Davies equation⁹

$$\log \gamma_{\pm} = -\frac{A\mu^{1/2}}{1 + \mu^{1/2}} + 0.3A\mu \quad (9)$$

and ion-pair formation was assumed to be negligible. In eq 9, A is the Debye-Hückel factor and μ is the ionic strength. The A factors are given in brackets in Table I (units are $M^{1/2} K^{3/2}$). The standard deviations are not included in Table II but are expected to be about 10% higher than the experimental values due to the uncertainty in the use of eq 9. Also included in Table II for comparison are data for water,¹⁰ dimethyl sulfoxide,¹¹ and tetramethylene sulfone (TMSO₂).¹² Table III lists the standard free energies of transfer, ΔG_t° (ion), of single ions from water to the aprotic solvent. These values are based on our previous assumption that $\Delta G_t^\circ(\text{AgCl}_2^-) \approx -\Delta G_t^\circ(\text{AgBr}_2^-)$.² The reliability of this assumption appears to be satisfactory as the ΔG_t° (ion) values for PC, DMSO, DMF, AN, TMSO₂, and AC are within ± 2 kcal/mol (and always of correct sign) of those obtained by more conventional methods.^{1,13}

Discussion and Conclusions

On the basis of the magnitudes of K_{s2} in Table II and from those compiled elsewhere,¹¹ it can be concluded that the ability of a solvent to solvate a halide ion increases according to

$$\text{TMSO} < \text{TMSO}_2 \sim \text{DMF} \sim \text{PN} \sim \text{DMSO} \sim$$

$$\text{PC} < \text{ES} < \text{DMS} < \text{SO}_2 < \text{H}_2\text{O} \quad (10)$$

The position of SO₂ in eq 10 is based on our previous results for a 3.30 M SO₂ solution in PN^{2a} and it is possible that the solvation of halides in pure SO₂ is stronger than in water. The unique ability of SO₂ and the organic sulfites to solvate the halide anions must be due to the expansion of the outer valence shell of sulfur above an octet: i.e., the 3d orbitals of sulfur must, in part, accommodate the extra electrons of the halide anion. Moffit¹⁴ was the first to theoretically demonstrate the importance of the sulfur 3d orbit-

TABLE III: Standard Free Energies of Transfer of Single Ions from Water to Aprotic Solvent

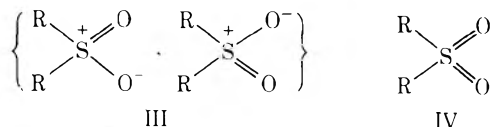
Solvent	$\Delta G_{\text{t}}^{\circ}(\text{ion})^a$						
	Ag ⁺	Cl ⁻	Br ⁻	I ⁻	AgCl ₂ ⁻	AgBr ₂ ⁻	AgI ₂ ⁻
PC	5.5	8.7	5.9	1.0	1.3	-1.3	-8.2
PC/TMSO (1.123 M)	-1.9	9.5	6.4	2.7	1.6	-1.6	-6.5
TMSO	-9.2	11.3	8.0	3.5	1.7	-1.7	-6.9
DMSO	-8.9	10.0	6.6	2.8	1.7	-1.7	-6.2
TMSO ₂ (30°)	1.4	12.8	7.0		1.6	-1.6	
DMS	4.9	4.6	3.3	1.5	1.9	-1.9	-5.3
ES	4.9	7.1	5.7	2.0	1.2	-1.2	-5.5
PN	-2.0	9.5	7.0	3.5	1.2	-1.2	-4.7
PN/SO ₂ (3.30 M)	-3.0	3.8	1.9	-0.2	1.2	-1.2	-3.6
PN/THT (0.10 M)	-8.9	10.1	6.2	2.2	2.6	-2.6	-8.1
PC/THT (0.09 M)	-5.7	8.8	6.0	2.6	1.4	-1.4	-5.0
DMF	-2.8	10.2	6.9		1.7	-1.7	
AN	-3.5	8.2	5.4	1.4	1.5	-1.5	-6.6
AC	5.7	9.9	7.0	3.9	1.7	-1.7	-4.6

^a $\Delta G_{\text{t}}^{\circ}(\text{ion})$ values are in kcal/mol at 25° based on the molar scale. Symbols not defined in text are PN = propionitrile; AN = acetonitrile; DMF = dimethyl formamide; AC = acetone.

als. The diffuse 3d orbitals of sulfur are contracted by highly electronegative substituents so that substantial overlap can occur between the 2p orbitals of oxygen and the sulfur's 3d orbitals.¹⁵ The significant structures of dimethyl sulfoxide are I and II and the S-O bond is much weaker than in the sulfones, SO₂, and SO₃ because of the large contribution by structure I.^{14,16} The hybridization of sulfur in

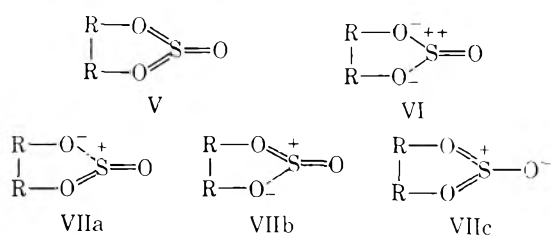


DMSO is therefore either sp³ (I) or sp³d (II) and in the presence of a halide, X⁻, structure I becomes dominant and because the 3d orbitals are no longer available, DMSO is a poor solvator for X⁻. Introducing additional oxygens about the sulfur results in sp³d hybridization which can form two π bonds in SO₂ and the sulfones, and sp³d² hybridization which can form three π bonds in SO₃.^{14,15} In the dialkyl sulfone, the important resonating structures appear to be III and IV.¹⁴ Were it not for steric hindrance (R₂SO₂ is a



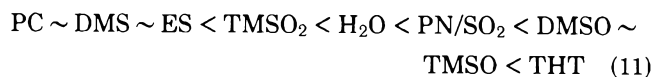
distorted tetrahedron), X⁻ ions might otherwise be expected to be strongly solvated via structure III. In SO₂ for which structures similar to III and IV can be written, X⁻ ions are strongly coordinated to the sulfur. Our previous CNDO calculations^{2c} confirmed the importance of structure III in the O₂S-Cl⁻ complex.

In SO₃ the sulfur can have sp³d or sp³d² hybridization and, by analogy, the possible contributing structures to



ethylene sulfite are V-VIIc. Structures VIIa-c are highly likely based on the fact that ethylene sulfite is free of any ring strain.^{17,18} Structure V appears to be unimportant for reasons discussed below. Structure VI is considered to be unimportant since the excess negative charges on the endocyclic oxygens would lead to ring strain via a 1,3-nonbonded interaction. However, it is suggested that VI is important when the sulfur interacts with the X⁻ nucleophile. In this case the transfer of charge to the endocyclic oxygens results in a 1,3-nonbonded interaction which introduces ring strain. In dimethyl sulfite, the buildup of charge on the oxygens could simply result in an increase of the RO-S-OR angle. We can cite two pieces of chemical evidence for this mechanism. The first is the present results which show that DMS solvates anions more strongly than does ES. The second is based on the rates of hydrolysis of DMS and ES in aqueous acidic and alkaline media.^{18,19} In alkaline solution, the rate of ES hydrolysis is 360 times faster than that of DMS whereas in acidic solution, DMS is hydrolyzed 22 times faster than ES. In the latter case, the rates of hydrolysis are first order with respect to [H⁺] and are catalyzed by the halides in the order Br⁻ > Cl⁻. The high reactivity of ES in alkaline solution was originally thought to be due to ring strain¹⁹ but later work^{17,18} showed that the heats of hydrolysis of ES and DMS were identical thereby eliminating ring strain as an important factor. In addition, ring strain could not explain the reversal of the rates of hydrolysis in acid solution. This complex behavior can however be reconciled by reference to the simple valence bond structures VI-VII. In alkaline solution, the nucleophilic attack by OH⁻ on VI results in a 1,3-nonbonded interaction in cyclic ES resulting in ring strain and a decrease in stability. This effect, as discussed above, is absent in the open chain DMS. In acidic solution, the hydrolysis is initiated by protonation of an endocyclic oxygen¹⁹ which effectively removes the high electron density. Ring strain is thereby absent in acidic solution even when the sulfur is under nucleophilic attack by X⁻.

In our previous work on S-O containing solvents,² we have suggested that the coordination site for Ag⁺ is the sulfur atom. This conclusion was based, in part, on the large negative values for $\Delta G_{\text{t}}^{\circ}(\text{Ag}^+)$ as shown in Table III. The order of increasing stability of Ag⁺ is, from Table III



Those solvents on the left-hand side of H_2O in eq 11 are considered to coordinate Ag^+ via the oxygen atom while those on the right-hand side of H_2O coordinate Ag^+ via the sulfur. The fact that Ag^+ is strongly coordinated to DMSO, TMSO, and SO_2 indicates the importance of the structures II and IV (for SO_2). $TMSO_2$ should also strongly coordinate Ag^+ , but is sterically hindered as discussed above. If V was an important contributor to the overall structure of ES and DMS, then these solvents would be expected to be on the right-hand side of H_2O in eq 11; since they appear on the left-hand side, it is concluded that V is unimportant and that Ag^+ is coordinated via an oxygen. Recently Ahrland and Björk²⁰ have presented spectroscopic evidence showing that in the solvate $Ag(DMSO)_2ClO_4$, the oxygen in DMSO is the site for Ag^+ coordination. We have not yet resolved this finding for the solvates and the large negative values of $\Delta G_t^\circ(Ag^+)$ for the solutions.

Supplementary Material Available. Listings of the experimental data (concentrations and emf's) will appear following these pages in the microfilm edition of this volume of the journal. Photocopies of the supplementary material from this paper only or microfiche (105 × 148 mm, 24× reduction, negatives) containing all of the supplementary material for the papers in this issue may be obtained from the Business Office, Books and Journals Division, American Chemical Society, 1155 16th St., N.W., Washington, D.C. 20036. Remit check or money order for \$4.50 for pho-

tocopy or \$2.50 for microfiche, referring to code number JPC-75-2000.

References and Notes

- (1) (a) A. J. Parker, *Quart. Rev., Chem. Soc.*, **16**, 163 (1962); (b) *Chem. Rev.*, **69**, 1 (1969).
- (2) (a) M. Salomon and B. K. Stevenson, *J. Phys. Chem.*, **77**, 3002 (1973); (b) M. Salomon, *ibid.*, **78**, 1817 (1974); (c) *ibid.*, **79**, 429 (1975).
- (3) C. K. Mann, *Adv. Electroanal. Chem.*, **3**, 57 (1969).
- (4) G. J. Janz and R. P. T. Tomkins, "Nonaqueous Electrolytes Handbook", Vol. I, Academic Press, New York, N.Y., 1972.
- (5) N. P. Yao, E. D'Orsay, and D. N. Bennion, *J. Electrochem. Soc.*, **115**, 999 (1968).
- (6) P. G. Sears and W. C. O'Brien, *J. Chem. Eng. Data*, **13**, 112 (1968).
- (7) See paragraph at end of text regarding supplementary material.
- (8) L. G. Sillén, *Acta Chem. Scand.*, **16**, 159 (1962).
- (9) C. W. Davies, "Ion Association", Butterworths, London, 1962.
- (10) D. D. Wagman, W. H. Evans, V. B. Parker, I. Halow, S. M. Bailey, and R. H. Schumm, *Nat. Bur. Stand., Techn. Note*, **270-4** (May 1969).
- (11) M. K. Chantooni and I. M. Kolthoff, *J. Phys. Chem.*, **77**, 1 (1973).
- (12) R. L. Benoit, A. L. Beauchamp, and M. Deneux, *J. Phys. Chem.*, **73**, 3268 (1969).
- (13) (a) C. M. Criss and M. Salomon, "Physical Chemistry of Organic Solvent Systems", A. K. Covington and T. Dickinson, Ed., Plenum Press, New York, N.Y., 1973, chapter 2.4. (b) B. G. Cox, G. R. Hedwig, A. J. Parker, and D. W. Watts, *Aust. J. Chem.*, **27**, 477 (1974).
- (14) (a) W. E. Moffit, *Proc. R. Soc. (London), Ser. A*, **200**, 409 (1950); (b) H. P. Koch and W. E. Moffit, *Trans. Faraday Soc.*, **47**, 7 (1951).
- (15) (a) D. P. Craig, A. Maccoll, R. S. Nyholm, L. E. Orgel, and L. E. Sutton, *J. Chem. Soc.*, 332 (1954); (b) D. P. Craig and E. A. Magnusson, *ibid.*, 4895 (1956).
- (16) V. I. Baranovskii, Yu. N. Kukushkin, N. S. Panina, and A. I. Panin, *Russ. J. Inorg. Chem.*, **18**, 844 (1973).
- (17) N. Pagdin, A. K. Pine, J. G. Tillett, and H. F. van Woerden, *J. Chem. Soc.*, 3835 (1962).
- (18) R. E. Davies, *J. Am. Chem. Soc.*, **84**, 599 (1962).
- (19) (a) C. A. Bunton, P. B. D. de la Mare, and J. G. Tillett, *J. Chem. Soc.*, 4754 (1958); (b) *ibid.*, 1766 (1959); (c) J. G. Tillett, *ibid.*, 37 (1962).
- (20) S. Ahrland and N.-O. Björk, *Acta Chem. Scand., Sect. A*, **28**, 823 (1974).

Regular Solution Theory and the Surface Tension of Molten Salt Mixtures

D. A. Nissen* and B. H. Van Domelen

Sandia Laboratories, Albuquerque, New Mexico 87115 (Received March 5, 1975)

Publication costs assisted by the U.S. Energy Research and Development Administration

The isothermal surface tension of a number of binary molten salt mixtures of the same charge type can be calculated from equations based on regular solution theory with excellent agreement between the experimental and calculated values of the surface tension.

Introduction

The properties of a large number of molten salt solutions can be predicted to a close approximation by regular solution theory.¹⁻³ We showed in an earlier paper⁴ that, by the use of regular solution theory, it was possible to calculate an isothermal surface tension curve for the LiCl-KCl molten salt system which agreed very closely with our experimental curve. It seemed reasonable to assume that this same approach would be feasible for the calculation of the surface tension of other binary molten salt systems. Consequently, the isothermal surface tension curves for a number of molten salt mixtures of the same charge type were calcu-

lated using an equation whose derivation is based on the assumption of regular solution behavior of these mixtures. The purpose of this paper is to present the results of these calculations and to discuss some of the assumptions involved in the calculations themselves.

The term "regular solution" was used by Hildebrand⁵ to describe a class of mixtures which exhibited nonideal behavior but did show certain similarities. These mixtures have been studied rather extensively, both theoretically and experimentally.⁶⁻⁸ Briefly, regular solutions differ from ideal solutions in that, in the former, the configurational entropy is not independent of the mutual disposition of the

several kinds of molecules, or, in other words, regular solutions have a nonzero heat of mixing. For a binary mixture which has the properties of a regular solution, the enthalpy of mixing is given by⁵

$$\Delta H = wx_1x_2 \quad (1)$$

In this equation x_1 and x_2 are the mole fractions of components 1 and 2, and w is the interchange energy or interaction parameter. This parameter, which is defined for pairwise interactions,⁹⁻¹¹ is a measure of the deviation from ideal solution behavior, i.e., for an ideal solution $w = 0$.

The surface tension of regular solutions has been placed on a firm theoretical foundation by Guggenheim⁷ and Prigogine.¹¹ They have shown that, when each molecule in the liquid is treated as though it were arranged on a lattice (quasi-lattice model) and there is a random distribution of the molecules in both the bulk and surface of the liquid (zerth approximation), in spite of the nonzero heat of mixing, the surface tension of the mixture is given by

$$\begin{aligned} \gamma = \gamma_1 + \frac{kT}{a} \ln \frac{x_1'}{x} + \frac{wl}{a} [(x_2')^2 - (x_2)^2] - \\ \frac{wm}{a} (x_2)^2 = \gamma_2 + \frac{kT}{a} \ln \frac{x_2'}{x_2} + \\ \frac{wl}{a} [(x_1')^2 - (x_1)^2] - \frac{wm}{a} (x_1)^2 \quad (2) \end{aligned}$$

For details of the calculation of the surface tension as a function of the bulk composition, we refer the reader to ref 7, p 179 and ref 11, p 176.

In this equation, γ_i is the surface tension of the pure i th component at the temperature of the experiment, x_i is the mole fraction of the i th component, the primes referring to the surface layer, w is the interaction parameter in the theory of regular solutions, l and m refer to the fraction of nearest neighbors which occupy the lattice plane and an adjacent lattice plane, respectively, and satisfy the relationship $l + 2m = 1$. For a simple cubic lattice, $Z = 6$ and $m = 1/6$, in a close packed lattice, $Z = 12$ and $m = 1/4$. The parameter a is the mean surface area of the molecules and is given by

$$a = \frac{1}{2} \left[\left(\frac{v_1}{N} \right)^{2/3} + \left(\frac{v_2}{N} \right)^{2/3} \right] \quad (3)$$

where N is Avogadro's number and v_i is the molar volume of the i th component.

In keeping with the assumptions in the derivation of eq 2, we shall assume that the molten salt mixtures discussed here can be considered, on a time-averaged basis, as though they were composed of ion pairs or neutral molecules rather than as assemblage of individual anions and cations.

Experimental Section

Since the purpose of this study was to compare the calculated isothermal surface tension curve of a binary mixture with experimental data, one of our primary concerns was the accuracy of the experimental data. Thus, we considered only those studies for which the data were presented either in tabular form or as equations. We tried also to select mixtures for which data were reported by one or more investigators or, if this was not possible, to use only data from an investigator whose work could be cross checked. For those cases in which two or more investigators reported data on the same system, the data were all plotted and the best curve drawn through the data points. Al-

TABLE I: Values of the Interaction Parameter and Mean Molecular Surface Area for Several Binary Molten Salt Systems

Systems	$w = 4\Delta H_{0.5}$, ^a cal/mol	a , cm ² $\times 10^{16}$	T , °C
NaCl-KCl	-522	17.3	825
LiCl-KCl	-4200	16.3	800
NaNO ₃ -KNO ₃	-442	19.2	400
LiNO ₃ -KNO ₃	-1900	18.2	350
LiNO ₃ -CsNO ₃	-3000	20.2	425
NaNO ₃ -CsNO ₃	-1280	20.9	425
AgNO ₃ -NaNO ₃	+600	17.7	350
AgNO ₃ -KNO ₃	-450	18.9	350
AgNO ₃ -RbNO ₃	-1190	19.6	350

^a References 13-15.

though the information was not always available, we would estimate the precision of the data given in the cited papers to be about 0.5%. Because of the good agreement between data presented by different investigators for the same system, we would estimate the accuracy of the experimental data to be about 1-2%. Data on the molar volume of each salt, which was used to calculate the mean molecular surface area, were taken from Janz' tabulation.¹²

We were also attempting to define the limits of applicability of regular solution theory to the calculation of surface tension curves, so we tried to select as wide a variety of cation pairs as possible for which surface tension and heat-of-mixing data were available. The following mixtures are treated: LiCl-KCl,⁴ NaCl-KCl,^{16,17} LiNO₃-KNO₃,¹⁸ NaNO₃-KNO₃,^{17,18} NaNO₃-CsNO₃,¹⁸ LiNO₃-CsNO₃,¹⁸ AgNO₃-NaNO₃,¹⁷⁻¹⁹ AgNO₃-KNO₃,¹⁷⁻¹⁹ AgNO₃-RbNO₃.¹⁸

In order to calculate the surface tension of a binary mixture using eq 2, it is necessary that we have a value for the interaction parameter w . Referring to eq 1, it can be seen that w can readily be obtained from heat-of-mixing data. For our calculations, we have used values of the interaction parameter taken from the heat-of-mixing studies of Kleppa and Hersh.¹³⁻¹⁵ These are listed in Table I, along with the mean molecular surface area and the temperature. The values of the interaction parameter shown in Table I were evaluated at $x_1 = x_2 = 0.5$ and, in keeping with common practice, are shown as $4\Delta H_{0.5}$. The calculated and experimental values of the surface tension are shown in Table II. The percent deviation of the calculated value of the surface tension from the experimental value is shown in the fourth column.

Discussion

With the exception of the (Ag-M)NO₃ mixtures, it is evident from the excellent agreement between the calculated and experimental values of the surface tension of the molten salt mixtures shown in Table II that the assumption of regular solution behavior in the calculation of surface tension is quite realistic.

In Figure 1 we have plotted the calculated and experimental isothermal surface tension curve for two different molten salt mixtures, LiNO₃-KNO₃ and NaNO₃-CsNO₃. This figure was included in order to demonstrate graphically the agreement between not only the experimental and calculated values of the surface tension, but also the shapes of the surface tension-composition curves themselves. The excellent agreement between both the experimental and

TABLE II: Comparison of Calculated and Experimental Values of the Surface Tension of Various Binary Molten Salt Systems

A. NaCl-KCl $T = 825^\circ$				F. NaNO ₃ -CsNO ₃ $T = 425^\circ$			
Mole % KCl	$\gamma(\text{calcd})$, dyn/cm	$\gamma(\text{exptl})$, dyn/cm ^{a,b}	Δ , %	Mole % CsNO ₃	$\gamma(\text{calcd})$, dyn/cm	$\gamma(\text{exptl})$, dyn/cm ^d	Δ , %
20	109.5	109.5	0.0	20	104.1	103.5	0.6
40	105.5	105.2	0.3	40	98.9	97.7	1.2
60	102.0	101.8	0.2	60	95.5	94.5	1.1
80	99.1	98.8	0.3	80	92.8	92.3	0.5
B. LiCl-KCl $T = 800^\circ$				G. AgNO ₃ -NaNO ₃ $T = 350^\circ$			
Mole % KCl	$\gamma(\text{calcd})$, dyn/cm	$\gamma(\text{exptl})$, dyn/cm ^c	Δ , %	Mole % NaNO ₃	$\gamma(\text{calcd})$, dyn/cm	$\gamma(\text{exptl})$, dyn/cm ^{b,d,e}	Δ , %
20	107.2	107.3	-0.1	20	135.6	131.9	2.8
40	101.4	102.9	-1.4	40	130.6	126.5	3.2
60	99.2	98.7	0.5	60	125.6	121.9	3.0
80	98.1	98.1	0.0	80	120.7	118.5	1.8
C. NaNO ₃ -KNO ₃ $T = 400^\circ$				H. AgNO ₃ -KNO ₃ $T = 350^\circ$			
Mole % KNO ₃	$\gamma(\text{calcd})$, dyn/cm	$\gamma(\text{exptl})$, dyn/cm ^{b,d}	Δ , %	Mole % KNO ₃	$\gamma(\text{calcd})$, dyn/cm	$\gamma(\text{exptl})$, dyn/cm ^{b,d,e}	Δ , %
20	111.6	111.4	0.2	20	131.8	125.8	4.8
40	110.0	110.0	0.0	40	124.9	118.4	5.5
60	108.8	108.8	0.0	60	119.5	115.0	3.9
80	107.8	107.8	0.0	80	114.9	112.7	4.8
D. LiNO ₃ -KNO ₃ $T = 350^\circ$				I. AgNO ₃ -RbNO ₃ $T = 350^\circ$			
Mole % KNO ₃	$\gamma(\text{calcd})$, dyn/cm	$\gamma(\text{exptl})$, dyn/cm ^d	Δ , %	Mole % RbNO ₃	$\gamma(\text{calcd})$, dyn/cm	$\gamma(\text{exptl})$, dyn/cm ^d	Δ , %
20	108.7	108.6	0.1	20	126.9	121.1	4.8
40	108.0	107.7	0.3	40	118.6	113.9	4.1
60	108.1	108.2	-0.1	60	113.2	109.5	3.4
80	109.1	109.5	-0.4	80	109.0	106.5	2.3
E. LiNO ₃ -CsNO ₃ $T = 425^\circ$							
Mole % CsNO ₃	$\gamma(\text{calcd})$, dyn/cm	$\gamma(\text{exptl})$, dyn/cm ^d	Δ , %				
20	97.2	95.7	1.6				
40	92.9	92.7	0.2				
60	91.9	91.5	0.4				
80	91.0	90.9	0.1				

^a Reference 16. ^b Reference 17. ^c Reference 4. ^d Reference 18. ^e Reference 19.

calculated values of the surface tension, as well as the form of the curves, although the two experimental surface-tension curves are noticeably different in shape, is evident.

In our calculations of the surface tension of molten salt mixtures, we have assumed that: (1) the molar volume v_i is a linear function of a concentration of the i th component, or more correctly, that the surface area occupied by each molecule can be adequately represented by the mean value, as calculated from eq 3; (2) the temperature dependence of the interaction parameter is negligible; and (3) the concentration dependence of w is also negligible. The excellent agreement between the experimental and calculated values of the surface tension for a majority of the systems considered would appear to indicate the reasonableness of these assumptions, which are discussed further below.

While the molar volume is a linear function of composi-

tion for LiCl-KCl and NaCl-KCl,²⁰ the system AgNO₃-NaNO₃ does show a small positive deviation from additivity, $\sim 1.5\%$.²¹ Since a variation of 10% in the value of a causes less than 1% change in the calculated values of the surface tension, this deviation is trivial and certainly cannot be responsible for the observed difference between the calculated and experimental values of the surface tension for the AgNO₃-NaNO₃ mixture.

Except for a small correction resulting from volume changes upon mixing, the excess entropy of mixing of a regular solution [$x_1x_2(\partial w/\partial T)$] is zero and, as a consequence, the interaction parameter should be almost temperature independent. Heat-of-mixing studies¹³ have shown that the enthalpies of mixing in a number of molten salt systems exhibit only a slight temperature dependence. One would thus expect the assumption of negligible temperature de-

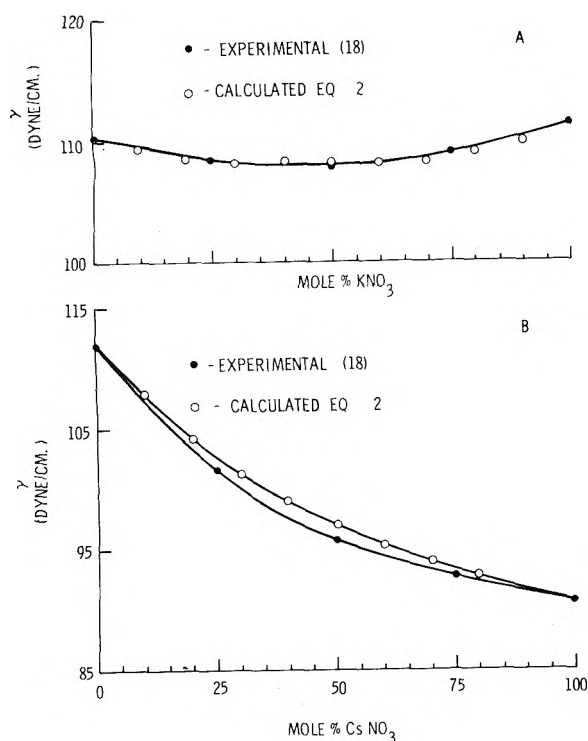


Figure 1. A comparison of calculated and experimental surface tension data for (A) LiNO₃-KNO₃ ($T = 350^\circ$) and (B) NaNO₃-CsNO₃ ($T = 425^\circ$).

pendence of the interaction parameter to be a reasonable one.

The assumption of concentration independence of the interaction parameter, as required by regular solution theory, is incorrect as the heat-of-mixing data of Kleppa and Hersh show.¹³⁻¹⁵ For most of the mixtures listed in Table II, the change in the value of the interaction parameter with concentration is less than 20% of the value at 0.5 mole fraction, where the interaction parameter is evaluated. This corresponds to a change of less than 2% in the calculated value of the surface tension. The only exception is the AgNO₃-KNO₃ mixture which shows a 33% variation in the value of w over that calculated for the equimolar composition. However, we doubt that this can explain the large difference shown in Table II between the experimental and calculated values of the surface tension. If the regular solution assumption is correct and the deviation can, in fact, be attributed to the pronounced concentration dependence of the interaction parameter, one would surely expect that, at the equimolar composition, where this parameter is evaluated, the two values of the surface tension would correspond and the difference would become more pronounced as the composition departed from this value. This is not what we see. Therefore, we must seek another explanation.

We should note in passing that the choice of a value for the parameter m , the fraction of nearest neighbors which occupy the adjacent lattice plane, is trivial, causing less than a 1% change in the calculated value of the surface tension.

Because of the pronounced deviation of the calculated values of the surface tension from the experimental values for the three (Ag-M)NO₃ systems shown in Table II, much larger than can be accounted for by inaccuracies in the experimental data, we suspect that the assumptions implicit in eq 2 were somewhat unrealistic for these mixtures. This

TABLE III: Polarizability of Various Cations

Ion	$10^{24}\alpha,$ cm ³	Ion	$10^{24}\alpha,$ cm ³
Li ⁺	0.300	Rb ⁺	1.98
Na ⁺	0.41	Cs ⁺	3.34
K ⁺	1.33	Ag ⁺	2.40

view is strengthened by the results of heat-of-mixing studies on these systems by Kleppa,^{15,22} which indicate that non-coulombic effects, such as formation of covalent bonds or van der Waal's interactions, related to the polarizability of the silver ion, may play a significant role.

If the differences between the calculated and experimental values of the surface tension are related to the polarizability of the cation, one might expect to observe significant deviations for systems which have a highly polarizable cation, other than silver. Table III shows the polarizability of various cations taken from the data of Tessman, Kahn, and Shockley.²³

It is evident from the data of Table III that, if polarizability of the cation is put forward as the explanation for the difference between the experimental and calculated results for the surface tension of the (Ag-M)NO₃ mixtures, one might also expect to see significant deviations in both the (Cs-Li)NO₃ and (Cs-Na)NO₃ systems; these were not observed.

It has been suggested¹⁴ that there are significant contributions from covalently bonded structures in silver ion containing melts. If this is indeed the case, it would seem to be reasonable that the assumptions of regular solution theory are no longer applicable; namely, that distributions and orientations are random.⁵ Unfortunately, there are not enough reliable surface tension data for other silver-containing systems to explore this anomaly in more detail.

Conclusion

We have shown that, by assuming the simplest realistic model of molten salt solutions, i.e., regular solution behavior, it is possible to calculate the isothermal surface tension curve of a molten salt mixture which is within 2%, i.e., within experimental error, of that derived from experimental measurements. In order to perform this calculation, it is only necessary that we know the surface tension and density of the pure components and the interaction parameter, which can be obtained from heat-of-mixing studies.

For those molten mixtures in which one might assume the formation of covalently bonded structures, the assumptions of regular solution theory appear to break down. As a result, pronounced deviations between the calculated and experimental values of the isothermal surface tension begin to become apparent.

References and Notes

- (1) J. Lumsden, "Thermodynamics of Molten Salt Mixture", Academic Press, New York, N.Y., 1966, p 1.
- (2) S. Sternberg and C. Herdlicka, *Rev. Roum. Chem.*, **13**, 13 (1968).
- (3) H. Bloom and B. J. Welch, *Discuss. Faraday Soc.*, **32**, 115 (1961).
- (4) D. A. Nissen and R. W. Carlsten, *J. Electrochem. Soc.*, **121**, 500 (1974).
- (5) J. H. Hildebrand, *J. Am. Chem. Soc.*, **51**, 66 (1929).
- (6) G. S. Rushbrooke, "Introduction to Statistical Mechanics", Oxford University Press, London, 1949.
- (7) E. A. Guggenheim, "Mixtures", Oxford University Press, London, 1952, p 29.
- (8) J. H. Hildebrand and R. L. Scott, "The Solubility of Non-Electrolytes", Reinhold, New York, N.Y., 1950.

- (9) E. A. Guggenheim, ref 8, p 23.
(10) G. N. Lewis and M. Randall, "Thermodynamics", 2nd ed, McGraw-Hill, New York, N.Y., 1961, p 283.
(11) R. Defay, I. Prigogine, A. Bellemans, and D. H. Everett, "Surface Tension and Adsorption", Wiley, New York, N.Y., 1966, p 171.
(12) G. S. Janz and C. G. Dykhuis, "Molten Salts", Vol. 1, U.S. Department of Commerce, National Bureau of Standards Reference Data Series, 1969.
(13) O. J. Kleppa and L. S. Hersh, *J. Chem. Phys.*, **34**, 351 (1961).
(14) L. S. Hersh and O. J. Kleppa, *J. Chem. Phys.*, **42**, 1309 (1965).
(15) O. J. Kleppa, R. B. Clark, and L. S. Hersh, *J. Chem. Phys.*, **35**, 175 (1961).
(16) G. Bertozzi, *J. Phys. Chem.*, **69**, 2606 (1965).
(17) J. L. Dahl, Ph.D. Thesis, Iowa State College, 1957.
(18) G. Bertozzi and G. Sternheim, *J. Chem. Phys.*, **68**, 2908 (1964).
(19) H. Bloom, F. G. Davis, and D. W. James, *Trans. Faraday Soc.*, **56**, 1179 (1960).
(20) E. R. Van Artsdalen and I. S. Yaffee, *J. Phys. Chem.*, **59**, 118 (1955).
(21) G. E. Blomgren, *J. Phys. Chem.*, **66**, 1500 (1962).
(22) O. J. Kleppa and L. S. Hersh, *Discuss. Faraday Soc.*, **32**, 99 (1961).
(23) J. R. Tessman, A. H. Kahn, and W. Shockley, *Phys. Rev.*, **92**, 890 (1958).

Vaporization Kinetics of Solid and Liquid Silver, Sodium Chloride, Potassium Bromide, Cesium Iodide, and Lithium Fluoride

Curtis T. Ewing and Kurt H. Stern*

Chemistry Division, Naval Research Laboratory, Washington, D.C. 20375 (Received January 22, 1975)

Publication costs assisted by the Naval Research Laboratory

Vacuum vaporization rates of Ag, LiF, NaCl, KBr, and CsI have been measured over a several hundred degree range from the low temperature solid to well above the melting point. Ag vaporizes at the equilibrium rate over the entire temperature range. NaCl, KBr, and CsI exhibit an anomalously low vaporization coefficient for the solid near the melting point with a subsequent rapid rise just above the melting point, whereas for LiF, the coefficient is nearly constant over the entire temperature range. For all the salts, vaporization rates of solid and liquid are equal at the melting point. Mechanisms which account for these observations are discussed.

Introduction

The vaporization kinetics of crystalline solids and of liquids has been studied by many workers for a long time. The object of such studies is to determine the vaporization mechanism by comparing the experimental vacuum vaporization rate with the rate predicted by the Knudsen equation¹ from the kinetic theory of gases. The latter corresponds to the (experimental) equilibrium vaporization rate. The attainment of such a rate (which is the theoretical maximum) for the vaporization from a surface directly into a vacuum implies that all steps of the process prior to desorption are at equilibrium.² When lower rates are found (and assuming that no artifacts such as surface contamination and heat transfer are responsible), one attempts to interpret these in terms of a mechanism in which some steps are kinetically hindered.

Substances studied in the solid and liquid states have usually been quite different. Although the reasons for this are not really clear, the result has been that theories of solid and liquid vaporization have emphasized different features of the process: imperfections, such as kinks and ledges for the solid,³ and geometric factors, such as hindered rotation,⁴ for the liquid. For both solid and liquid vaporization, the nature of the surface region is important since molecules must pass through it on their way from the condensed phase to the vapor. It seemed to us that more insight into the vaporization process might be obtained by studying the kinetics for both the solid and liquid phases of

the same substance over a wide range of temperature. For example, in passing through the melting point, the nature and composition of the vapor phase remains virtually unchanged and the effect of the solid \rightarrow liquid transition on the kinetics should become evident.

If a detailed theory is to be constructed, it is most readily and critically tested if the thermodynamic and structural properties of the substances concerned are accurately known and if they lend themselves to model building. The alkali halides suit this purpose. We selected several of these to encompass the spectrum of masses and sizes from largest to smallest: CsI, KBr, NaCl, LiF. These salts also cover a range with respect to vapor composition: CsI vapor is almost purely monomeric, whereas LiF contains appreciable concentrations of dimer and trimer. However, although the composition of the equilibrium vapor is well known, the composition of the vapor under free evaporation has only been measured over solid NaCl and LiF, covering a short temperature range. This will be discussed later. Silver was selected as an example of a substance whose vapor is monatomic.

The equilibrium vaporization rates necessary for the interpretation of the kinetic results were reported for the same substances in our previous paper.⁵ The effects of variations in solid surface structure, as well as the numerous precautions which are required to avoid rates limited by nonchemical processes, e.g., heat transfer, were previously studied for solid NaCl.⁶ Additional studies are presented in this paper.

Theory

The maximum rate at which a substance may vaporize into a vacuum is, according to the classical Knudsen theory,¹ equal to the rate at which impinging molecules strike the surface from the equilibrium vapor. For the case of a single vaporizing species of molecular weight M , the mass flux given by the Knudsen equation is

$$J_{\text{eq}} = \frac{1}{4}\rho\bar{c} = P_{\text{eq}}(M/2\pi RT)^{1/2} \quad (1a)$$

where ρ is the density, \bar{c} is the average velocity, and P_{eq} is the equilibrium vapor pressure. The corresponding molar flux is

$$J_{\text{eq}} = P_{\text{eq}}(2\pi MRT)^{-1/2} \quad (1b)$$

When the evaporation rate is less than the maximum (equilibrium) rate, the difference is expressed in terms of the ratio $J/J_{\text{eq}} = \alpha$. The precise treatment of this ratio by various authors⁷⁻⁹ in terms of "vaporization coefficients", "condensation coefficients", and "sticking coefficients" has given rise to somewhat different meanings attributed to these terms. We postpone a discussion of these till later, except to point out that all vaporization kinetics proceeds from a consideration of this ratio.

The vaporization energy ΔE_v° for equilibrium conditions is defined by

$$d \ln J_{\text{eq}}/d(1/T) = -\Delta E_v^\circ/R \quad (2)$$

and that corresponding for free evaporation by

$$d \ln J/d(1/T) = -\Delta E_a/R \quad (3)$$

Alternatively, the flux can be converted to the Langmuir pressure P^* where

$$P^* = J(2\pi RT/M)^{1/2} \quad (4)$$

If the standard state is the same as that at equilibrium, activation parameters derived from the temperature dependence of P^* can be directly compared to the corresponding thermodynamic functions. For the thermodynamic enthalpy of vaporization

$$d \ln P_{\text{eq}}/d(1/T) = -\Delta H_v^\circ/R \quad (5)$$

and for the activation enthalpy

$$d \ln P^*/d(1/T) = -\Delta H^*/R \quad (6)$$

It also follows directly that

$$d \ln \alpha/d(1/T) = (\Delta H_v^\circ - \Delta H^*)/R \quad (7)$$

From eq 6, 7, and 9

$$\Delta H^* = \Delta E_a + RT/2 \quad (8)$$

The determination of the activation entropy is more difficult since it requires a knowledge or assumption of surface concentrations. This topic has been discussed by Somorjai and Lester.¹⁰ A different approach has been suggested by Rosenblatt.¹¹

When the vapor phase consists of more than a single species, the flux equations must be modified. The mass flux of each species is given by

$$J_i = [N_i^{1/2}/\sum N_i^{1/2}]J \quad (9)$$

where $i = 1$ for monomer, 2 for dimer, etc. In order to determine the mole fraction of each species N_i , the composition of the vapor must be known. For NaCl, the degree of

dimerization under free evaporation has been measured by Lester and Somorjai¹² and by Eisenstadt et al.¹³ Both of these studies report somewhat less dimerization than the equilibrium values in the JANAF tables.¹⁴ However, the monomer/dimer ratios are close to the equilibrium values of Miller and Kusch,¹⁵ Eisenstadt, Rao, and Rothberg,¹³ and Akishin et al.¹⁶ It seems reasonable to conclude, therefore, that although the monomer/dimer ratios are not known as accurately as we would like, the available evidence indicates that the molecular composition of the flux emanating from a salt under vacuum does not differ greatly from that of the equilibrium vapor. We have therefore assumed in this work that the molecular composition of the alkali halide vapors is independent of pressure.

The partial Langmuir pressures are then given by

$$P_i^* = J_i(2\pi RT/M_i)^{1/2} \quad (10)$$

and the activation enthalpy for the vaporization of the i th species by

$$\Delta H_i^* = (d \ln P_i^*/dT)RT^2 \quad (11)$$

The overall activation enthalpy is

$$\Delta H^* = \sum (N_i \Delta H_i^*) \quad (12)$$

Corresponding equations hold for equilibrium vaporization.

Collisional Effects (at $l/a = 0$) and the Rate of Vaporization. For the rate information obtained in this study, apparent mean free paths (λ , based on observed fluxes) varied over several orders of magnitude from values in excess of 100 to values less than 0.01 cm. Many experiments were made with Knudsen numbers (λ/D) above unity, and intermolecular collisions above the vaporizing surface should theoretically have been unimportant. However, for many other experiments, particularly those at high temperatures, apparent Knudsen numbers extended well below unity with vaporization rates exceeding 1000 mg cm⁻² min⁻¹. The actual Knudsen number and mean free path at the vaporizing surface depend, of course, on the rate at which gas-phase molecules are formed and the rate at which they diffuse away from the surface; but for the low mean free paths encountered in this work, the possibility did exist that flow near the vaporizing surface could approach hydrodynamic conditions.

For the conditions under which the experiments were performed, the flux from the vaporizing surface is analogous to the flux of gas through a thin-edge orifice into an evacuated space. It has been shown conclusively in studies by Searcy and Schulz,¹⁷ by Carlson et al.,¹⁸ by Wey and Wahlbeck,¹⁹ and by Ewing and Stern⁵ that mass flows in the intermediate and in the near hydrodynamic regions are always equal to or larger than those which would be predicted from the Knudsen equation. It is, therefore, unlikely for our experimental conditions that gas-phase collisions can restrict the flow from the free salt surface.

It was also recognized that a small fraction of the vapor molecules at $l/a = 0$ may be reflected back onto the vaporizing surface from the walls of the larger tube surrounding the sample. Studies of Coleman and Egerton²⁰ indicate that this effect should not have reduced the observed rate by more than 1%. Precautions taken to eliminate the possibility of any significant rate reduction from vapor clouds or from other factors related to instrument parameters are described in a previous study⁶ of sodium chloride.

Clausing Effects. The apparent steady-state rate of va-

porization from a surface decreases systematically as the vaporizing surface recedes from the top of the crucible. This results from the Clausing effect where molecules are randomly reflected off the walls and back into the vaporizing surface. The desired rate was, of course, that with the salt surface flush with the top of the crucible ($l/a = 0$); and for each isothermal experiment this value was obtained either by extrapolating observed rates to zero time or by recording the initial rate. The magnitude of the change in rate with increase in l/a is a rather complex function of several parameters: the length-to-radius ratio (l/a) of the channel, the meniscus shape, the flow conditions existing in the channel, and the vaporization coefficient. A supporting study (to be presented in a later section) was made of these parameters and their effect on the change in rate and on the change in the escape probability.

When $\alpha = J/J_{e0}$ is less than unity and when the effluent molecules pass through a finite cylindrical channel above the vaporizing surface, the observed escape probability, K_c , will be higher than the theoretical Clausing value, K_T . In this case a fraction K_T of the molecules leaving the surface escapes, and a fraction $(1 - K_T)$ is returned to the vaporizing surface. The surface adsorbs a fraction $\alpha(1 - K_T)$ of the returning molecules and re-emits a fraction $(1 - \alpha)(1 - K_T)$. This wall reflection, surface adsorption, and reemission continues with progressively smaller fractions of molecules. Under conditions where intermolecular collisions are unimportant, Sandry and Stevenson²¹ derived the equation

$$K_c = K_T \sum_{n=0}^{\infty} [(1 - \alpha)(1 - K_T)]^n \quad (13)$$

Experimental Section

Free-evaporation fluxes were obtained isothermally by heating small crucibles with samples of the alkali halide and determining the loss of weight with time. The instrument used was an automatic recording Mettler thermobalance which has been described in detail elsewhere.²² The samples were surrounded by a larger chamber maintained at an apparent vacuum of 10^{-5} Torr or lower. Temperatures were precisely measured with a platinum-10% rhodium thermocouple, the junction of which was in direct thermal contact with the base of the sample crucible. The thermobalance and the associated experimental system were previously used for a preliminary study on sodium chloride,⁶ and the extensive precautions taken in that study to assure furnace isothermality and the reliability of both temperature and weight determinations were repeated in the present study.

All evaporation experiments for LiF, CsI, and KBr in both solid and liquid phases were made using single lots of optical grade single crystals procured from the Harshaw Chemical Co. Cation impurities in all lots, analyzed spectroscopically, were typically less than 10 ppm; silicon was present in concentrations of 50–100 ppm. These concentrations are sufficiently low so as to have no influence on the kinetics.⁶ In the case of NaCl, identical kinetic information was obtained for materials from three sources—boules specially grown at the Naval Research Laboratory, optical grade single crystals from Harshaw Chemical Co., and polycrystalline samples obtained by shaping solidified melts of an ultrapure grade of powder from Alfa Inorganics. Spectrochemical analyses of all boules or lots of NaCl have been reported.⁶ Salts used in this study were generally of comparable purity, with negligible cation impurities.

The crystals to be vaporized were formed by cleaving with a razor blade, by machining, or by cutting with diamond string saws. For CsI, where vaporization was studied as a function of crystallographic orientation, faces were generally oriented to within $\pm 0.5^\circ$ of the desired plane. The vaporization rate from the crystal face of an alkali halide was found to be independent of surface preparation. Surfaces which were ground, cleaved, scraped, or cut gave identical results. Test surface dimensions of crystals were measured with micrometers before, and often after, the experiments. It was shown in a previous study⁶ that the probability of significant coverage of a salt surface by contaminants such as pump oil or water is low. Even at low temperatures, during vaporization multiple layers of the salt are stripped off in the time that one monolayer of adsorbed impurity would be expected to form.

The standard technique of cementing samples with gold paste (or silver paste in the case of CsI) into graphite was selected as in the previous study⁶ because this crucible material has a high thermal conductivity and a high surface emissivity for the receipt of radiant energy from the furnace. A machined crucible usually contained a few milligrams of volatiles and was pre-fired at 1000° to constant weight. For each weight-loss determination, a crystal was cemented with its vaporizing surface flush with the top of the crucible and the assembly preheated for several hours to constant weight at 350 – 550° . Since vaporization rates are often said to be influenced by trace contaminants, a number of comparative tests were made at temperatures below 600° . Rates were measured for NaCl and LiF crystals tightly wrapped with platinum-10% rhodium and palladium foils. At temperatures above 770° , rates were measured for NaCl in graphite and tantalum-10% tungsten without gold paste. It was shown quite conclusively with all these tests that rates observed with crystals cemented into graphite were not influenced by the graphite, by the gold, or by any other material in the cementing paste.

Crucibles for the liquid determinations were generally precision machined with uniform diameters from high-purity Poco graphite or tantalum-10% tungsten. Tops were generally flared to a larger diameter with polished horizontal surfaces sloping at a small angle from an outside lip to the sharp edge of the crucible diameter. This type of reservoir at the top of the crucible permitted an addition of salt in excess of that required to fill the crucible. The starting material for a liquid experiment was always a single crystal shaped and loaded into the cell under a controlled dry atmosphere. For an experimental determination of flux, the cell with sample was preheated, while under high vacuum, to constant weight at a temperature near the melting point, then melted, and heated rapidly to the desired run temperature.

For measurements at high temperatures and high rates, an excess of salt in the reservoir at the top of the crucible allowed for evaporation during the preheating period, so that an isothermal state could be reached with a low l/a . For runs at intermediate and low rates, the point at which the larger salt meniscus in the reservoir receded by vaporization into the uniform diameter hole ($l/a = 0$) was identified on the recorder by a sharp change in the slope of the weight trace.

Determination of Flux at $l/a = 0$ from Experimental Weight Traces. For isothermal experiments at both very high and very low rates, the steady-state rate of vaporization was accurately obtained directly from the slope of the

weight vs. time trace. At the high-rate end of the measurement range, hydrodynamic (streaming) conditions in the channel above the vaporizing surface completely override all Clausius effects and the weight loss becomes linear with time. The same linearity or effective linearity is observed at very low rates for quite a different reason. Weight losses are low and corresponding escape probabilities change very slowly with time. Actually, the initial rate was satisfactory for most of the experimental work in the solid state.

For experimental conditions intermediate between those described above, the rate changes appreciably as the vaporizing surface rapidly recedes from the top of the crucible, and the steady-state rate of vaporization was obtained by extrapolating observed rates to $l/a = 0$. The extrapolation procedure was complicated by the change with time of the force exerted by the effluent vapor and the corresponding change in the required correction to the observed weight. The computer program for fitting and extrapolating (or interpolating) weight trace information to $l/a = 0$ was designed to correct apparent rates for change in the force on the crucible, and for change in the escape probability.

Results

Heat-Transfer Processes and the Rate of Vaporization. The experimental studies reported in this paper involved extremely rapid evaporation rates (up to $1100 \text{ mg cm}^{-2} \text{ min}^{-1}$) which are several orders of magnitude above those normally encountered in such studies. Vaporization is an endothermic process, and often at such high rates, control is not exerted by the vaporizing step but by some heat-transfer process between the source of the heat and the vaporizing surface.

For the free-evaporation of single crystals of sodium chloride, potassium bromide, and cesium iodide (Figures 7, 8, and 9), there is a pronounced lowering (of the rate, and, therefore) of the vaporization coefficient, as the melting point of each salt is approached. It was recognized that this unexpected behavior could be produced by a rate-controlling heat-transfer process or by some other experimental artifact, as well as by changes in the vaporization mechanism. To clarify this situation, a series of free-evaporation measurements was made near the melting point for single-crystalline sodium chloride at a temperature of 780° . Samples for these tests were precision machined with different lengths and diameters. The results are presented graphically in Figure 1 where the mass rate J (at $l/a = 0$) is plotted as a function of length for crystal diameters of 0.3, 0.5, and 0.74 cm. The scatter of points is typical of the reproducibility obtained at this temperature, and rates are independent of both diameter and length.

As a supplement to this study, several cylindrical crystals of NaCl were machined with a drilled hole in one end so that the bare crystal could be positioned directly on the thermocouple and stick of the Mettler thermobalance. Relatively low vaporization rates per unit area (approaching $1/10$ th of the expected J) were observed for these samples at 780° . Actually, a major part of the required heat for this low rate could have been supplied by conduction from the thermocouple and stick, so the experiments demonstrate rather clearly that essentially no heat is transmitted directly by radiation from the furnace either to the bulk crystal or to the vaporizing surface. Hence, conduction through the crystal is the predominant mechanism of heat transfer, and the absence of any change in rate with length or diameter (Figure 1) precludes any self-cooling of the heat-transfer surface or rate control by a heat-transfer process.

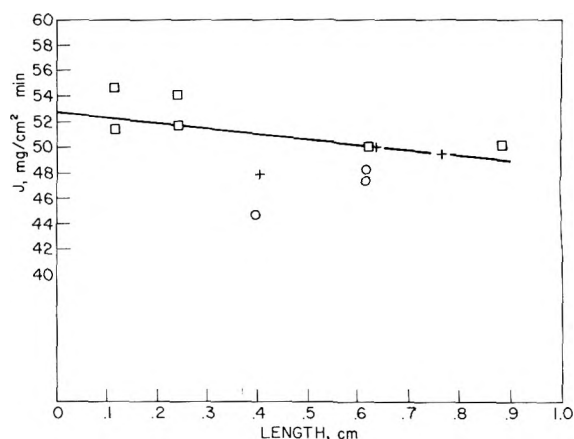


Figure 1. Effect of diameter and length of sample on the vaporization rate of crystalline sodium chloride: O, 0.30-cm diameter; □, 0.50-cm diameter; +, 0.74-cm diameter.

Even though experimental evaporation rates for the liquid alkali halides at temperatures well above their melting points were generally more reproducible than those near the melting point, the observed rates were still very high, and it was again important to show experimentally that vaporization kinetics is involved and not some form of heat-transfer control. Therefore, for each liquid salt, rates for the full temperature range were customarily observed with crucibles of two diameters—0.25 and 0.50 cm. Comparable rates for each salt were again found within experimental error to be independent of the diameter of the crucible. Another experimental fact is also important in this respect. At temperatures well above the melting point, it will be shown later in this article that the flow is hydrodynamic or near hydrodynamic and escape probabilities approach unity at all values of l/a . Weight traces for experiments in this region were generally observed to be linear. The rate was found to be independent of sample length up to lengths of 1.5 cm (i.e., l/a values from 0 to 10).

The experimental facts presented in this section, we believe, demonstrate conclusively that there is no control by a heat-transfer process for either the solid or liquid alkali halide and that significant self-cooling of the vaporizing surface is absent.

Escape Probabilities and Meniscus Shape at Low Flows. Measurements at higher temperatures were done on liquids, and we were initially concerned over the possibility that the measured flux at $l/a = 0$ could depend on the meniscus type and the meniscus area. Sandry and Stevenson²¹ have shown mathematically that the observed rate of vaporization from a convex (nonwetting) meniscus is very sensitive (particularly at low values of l/a) to the ratio of surface to cross-sectional area; and, conversely, that the effective rate (escape probability-area product) from both a concave and a flat meniscus is virtually independent of this area ratio. Free-evaporation measurements for each salt and for silver were always measured in two types of crucibles—generally Poco graphite and tantalum-10% tungsten. One would expect from surface energy considerations that the meniscus in Poco should be virtually flat and that in the refractory alloy it should be concave. This was experimentally confirmed by visual observations of thermally quenched samples and by the fact that the rate per unit cross-sectional area was always independent of both the size and the type of crucible.

Escape Probabilities and Vaporization Coefficients at

Low Flows. A series of experiments was performed to test the validity of eq 13 for that limiting case where intermolecular collisions are unimportant and vaporization coefficients are low. Several cylindrical samples of sodium chloride were prepared and cemented into graphite crucibles with the vaporizing surface flush with the top of the crucible. Interchangeable graphite cylinders (with an internal diameter equal to the diameter of the salt crystal) were also prepared so that they could be readily attached above the salt samples to provide well-defined l/a ratios of approximately 0.5, 1, 1.5, and 2. Escape probabilities for the several different l/a ratios were carefully measured at 780° where α is approximately 0.23. The results are presented in Figure 2, where experimental escape probabilities are compared with those computed from eq 13. The experimental values are a few percent higher than those predicted, but are generally in satisfactory agreement.

In the lower temperature range, experimental and theoretical escape probabilities were observed for several of the salts. Figure 3 presents for LiF a comparison of experimental escape probabilities with corresponding values calculated from eq 13. The agreement between observed and predicted values is again good. Although these results are important in that they verify the mathematical predictions of Sandry and Stevenson,²¹ they also significantly increased the reliability and reproducibility of computerized extrapolation procedures which were often required to generate J at $l/a = 0$.

Escape Probabilities and Vaporization Coefficients at High Flows. It should be recognized that eq 13 is strictly valid only under conditions involving relatively low flow rates where intermolecular collisions are unimportant. As the temperature and vaporization rates increase, the apparent mean free path of the vapor decreases rapidly, and if the channel above the vaporizing surface is of sufficient length,⁵ flow will move into the transition and finally into the hydrodynamic⁵ region. As the flow approaches the hydrodynamic state, one would expect streaming conditions to override all Clausing reflections. Experimentally, this does occur and is shown dramatically in Figure 4. In this figure, the ratio of the experimental K to the calculated K_c (eq 13) for each salt is plotted vs. the apparent mean free path (calculated from apparent Langmuir pressures at vaporizing surfaces). As the temperature and vaporization rates increase, intermolecular collisions and streaming become progressively more important and the escape probability ratio, K/K_c , increases from unity to approximately 1.5. At the higher ratios, the experimental K is unity at all values of l/a , suggesting a well-developed hydrodynamic flow in the channel above the vaporizing surface.

Calibration of the Thermobalance with Metallic Silver. Free-evaporation fluxes were measured for silver (Handy and Harmon 99.999% purity) over an extended temperature range from about 910 to 1330° . Container materials included Poco graphite and tantalum-10% tungsten with diameter variation from 0.20 to 0.50 cm. An Arrhenius plot of the results is presented in Figure 5, where flux obtained under vacuum is compared to a smoothed curve of the flux in the equilibrium vapor. Saturation values were obtained from the selected vapor-pressure information of Nesmeyanov²³ which agree accurately with several vapor-pressure studies²⁴⁻²⁸ published since this compilation was issued.

An interesting phenomenon with silver was observed at lower temperatures. Below 1100° , the observed flux at a particular temperature was initially on the dashed curve

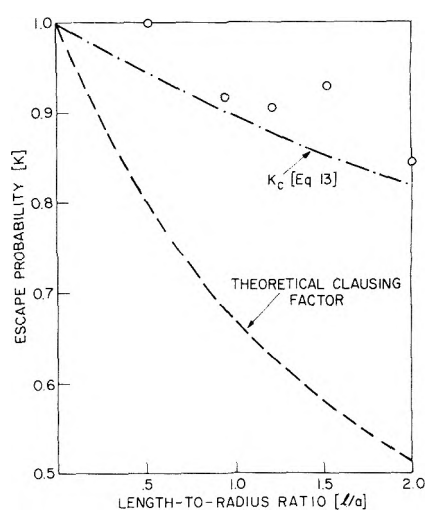


Figure 2. Escape probabilities for crystalline sodium chloride at 780° ($\alpha = 0.23$) from cylindrical channels (with well-defined l/a ratios) above the vaporizing surface: O, experimental escape probability.

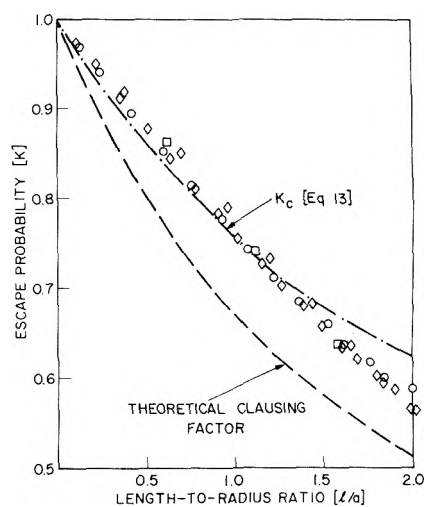


Figure 3. Escape probabilities for LiF at 890° ($\alpha = 0.64$) vs. l/a : O, experimental values for 0.39-cm diameter sample; square, experimental values for 0.13-cm diameter; diamond, experimental values for 0.26-cm diameter.

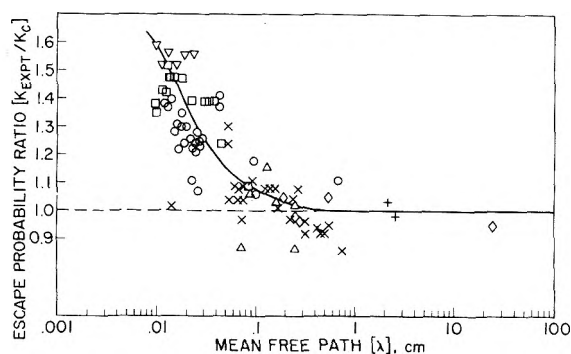


Figure 4. Escape probability ratio (K_{expt}/K_c) vs. mean free path for NaCl, KBr, LiF, CsI, and Ag: O, NaCl liquid; square, KBr liquid; X, LiF liquid; inverted triangle, CsI liquid; diamond, NaCl solid; +, LiF solid; triangle, Ag liquid.

(Figure 5); but after a short preheating of the sample to around 1150° , a value 30–40% higher was obtained. The higher value after preheating was consistent and reproducible, but would gradually drop, and after several hours, re-

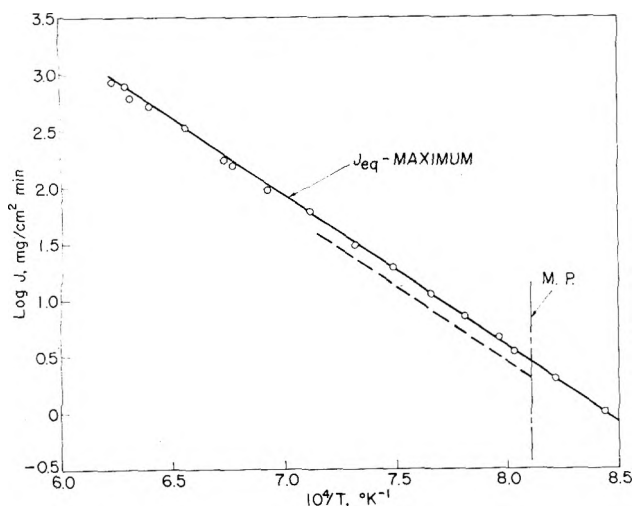


Figure 5. Arrhenius plot of experimental vaporization fluxes for silver and comparison with maximum equilibrium fluxes: (---) for discussion see text.

turn to its base value on the dashed curve. It is well known that oxygen (probably in the form of Ag_2O) is soluble²⁹ in molten silver. We believe that the dashed curve represents the flux for an equilibrium solution of oxygen in silver and that the oxygen is removed by preheating the sample under vacuum above 1150° . Therefore, all experimental points below 1160° on Figure 5 represent values obtained after preheating samples to 1150° .

The experimental measurements extend over a substantial temperature range covering both liquid and solid states, with the vaporization coefficient being unity over the entire range. This is consistent with what has been predicted and measured for monatomic metals.³⁰⁻³⁵ These results for silver cover a range of flow conditions equivalent to those required for the alkali halide work, and we believe that they provide additional and important evidence that the observed vaporization coefficients for the alkali halides at high flow rates are real and not due to some instrumental artifact.

Vaporization Rate of Single Crystals. Dislocation Density and Crystal Orientation. Vaporization rates for sodium chloride were previously⁶ shown to be independent of dislocation densities which differ by two orders of magnitude. In that paper,⁶ the authors studied vaporization rates from the three crystalline faces of sodium chloride and concluded that free-evaporation rates are the same for all three crystallographic planes. The same type of study was performed for crystalline cesium iodide and the experimental results for the (100), (110), and (111) faces are shown in an Arrhenius plot (Figure 6). It is again clearly shown that free-evaporation rates are independent of orientation.

Free Evaporation of the Alkali Halides. For each salt, experimental fluxes were obtained for a large number of crystalline and liquid samples under a variety of experimental conditions. In the solid region, samples were formed from larger crystals by cleaving, cutting, or machining into various shapes, and by cementing these with a conducting gold paste into high-purity Poco graphite crucibles. The vaporization surface of samples varied from an area of 0.12 to 0.70 cm^2 . In the liquid region, crucibles, as previously described in this paper, were prepared from Poco graphite, tantalum-10% tungsten, and platinum-10% rhodium with diameters of 0.25 and 0.50 cm.

Experimental free-evaporation fluxes for the four salts

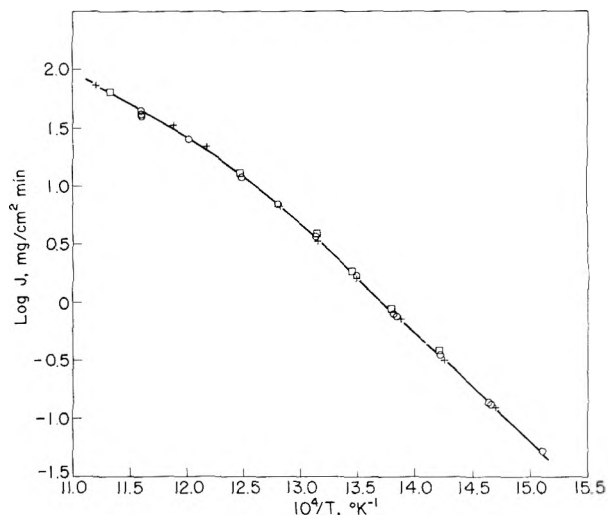


Figure 6. Arrhenius plot at low temperatures of experimental vaporization fluxes from (100), (110), and (111) crystallographic surfaces of cesium iodide crystals: O, (100) surface; □, (110) surface; +, (111) surface.

are presented in Arrhenius plots (Figures 7-10), and for each salt, free-evaporation values are compared directly with corresponding fluxes in the equilibrium vapor. The equilibrium values are those measured directly at this laboratory⁵ by the Knudsen method on the same thermobalance. The Arrhenius type of plot illustrates very clearly some distinctive characteristics of evaporation in this family of materials. It also permits a visual comparison of activation energies with corresponding thermodynamic energies of vaporization. Three of the salts (sodium chloride, potassium bromide, and cesium iodide) exhibit an unexpected minimum in the vaporization coefficient at the melting point. Lithium fluoride, on the other hand, exhibits a smooth transition from solid to liquid state.

The free-evaporation curves for sodium chloride, potassium bromide, and cesium iodide are similar in many respects; and since the minimum in the vaporization curve was most extensively studied for sodium chloride, the characteristics of this type of evaporation can best be discussed in terms of the NaCl results. In the temperature region below 665° , the free-evaporation flux for NaCl is less than the maximum observed under equilibrium conditions; but the vaporization coefficient, the activation energy, and other kinetic quantities are essentially independent of temperature.

The temperature independence of kinetic quantities does not hold at higher temperatures. Above 665° , the steady-state rate of evaporation (see Figure 7) falls away progressively from the maximum rate in a manner similar to that observed by Davy and Somorjai³⁶ for ice crystals. The evaporation rate at the melting point is the same for both liquid and solid, but as the temperature is increased, the rate rises rapidly and levels off such that the rate and vaporization coefficient become more or less consistent with extensions of the low-temperature values. The characteristic tailing off of the rate from its equilibrium value at higher temperatures in the liquid state is typical of the results for all the alkali halides.

The most notable characteristic of the free-evaporation of NaCl, KBr, and CsI is the nearly constant slope of $\log J$ vs. $1/T$ at lower temperature and the progressively decreasing slope as the melting point is approached. The radical

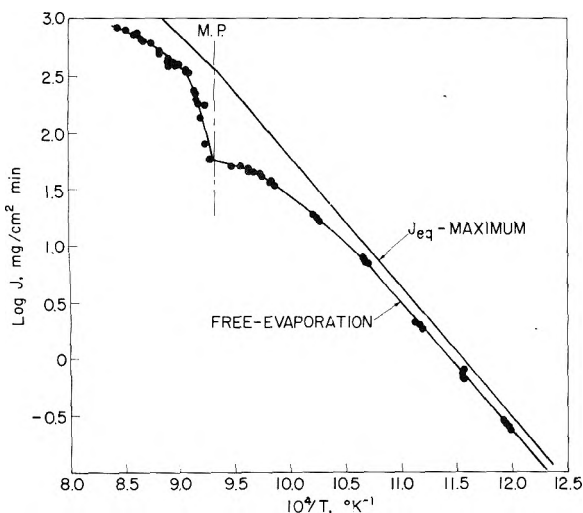


Figure 7. Arrhenius plot of experimental vaporization fluxes for sodium chloride and comparison with maximum equilibrium fluxes.

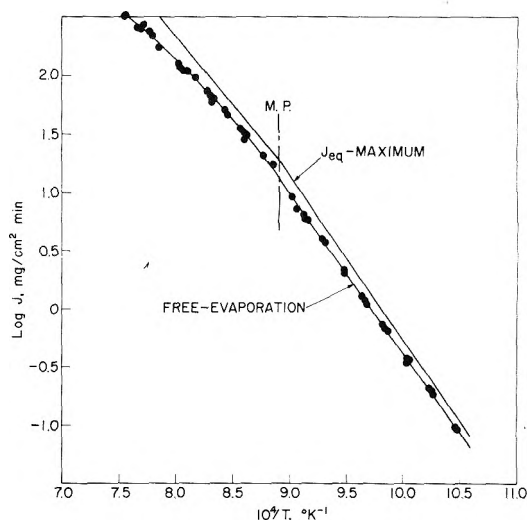


Figure 10. Arrhenius plot of experimental vaporization fluxes for lithium fluoride and comparison with maximum equilibrium fluxes.

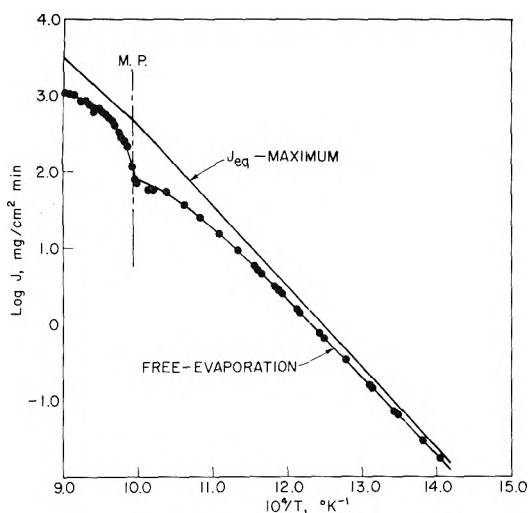


Figure 8. Arrhenius plot of experimental vaporization fluxes for potassium bromide and comparison with maximum equilibrium fluxes.

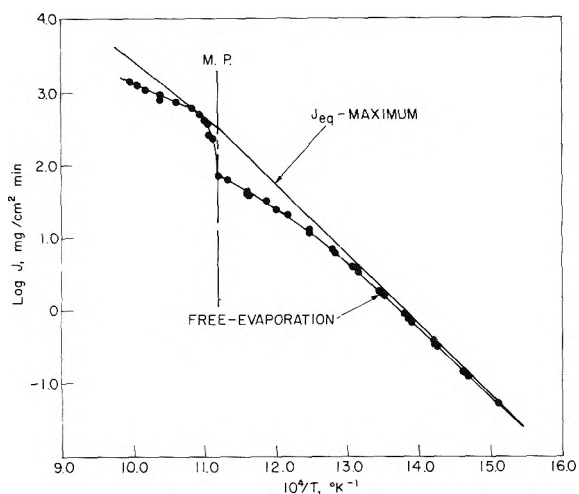


Figure 9. Arrhenius plot of experimental vaporization fluxes for cesium iodide and comparison with maximum equilibrium fluxes.

change in slope suggests a change in mechanism; so additional experiments were performed with NaCl in an effort to better define the mechanisms of vaporization in each temperature region. Crystalline samples were shaped to give apparent surface to cross-sectional area ratios of approximately 2 and 3. Results of free-evaporation tests with these samples are plotted in Figure 11 and are compared both with the free-evaporation flux at unit area ratios and with the flux in the equilibrium vapor. It will be noted that in the lower temperature range where the slopes are parallel, the free-evaporation flux is completely independent of the actual area of the vaporizing surface. In contrast, at temperatures approaching the melting point, the measured flux is directly dependent on area; and as the ratio of surface to cross-sectional area is increased, the flux approaches an upper limit consistent with a rough linear extension of the low-temperature results. We will present in a later section the importance of these results as evidence of vaporization mechanisms.

The free-evaporation flux for lithium fluoride (Figure 10), in complete contrast to that for the other alkali halides, exhibits no significant minimum at the melting point. Flux and activation energy both show smooth transitions between the liquid and solid states. This fact has important implications with regard to the mechanism of vaporization and the importance of bulk-to-surface steps in the consecutive reactions leading to vaporization.

Evaporation from single-crystalline LiF, as with NaCl, was shown experimentally to be independent of the actual surface area. Lithium fluoride in the liquid state, at least for a reasonable temperature range above the melting point, exhibits vaporization which is characteristic of the crystalline alkali halides at lower temperatures, and one would suspect that the flux in this range should also be independent of surface area. In response to such a possibility, free-evaporation results were obtained in this region with crucibles of different size and different wetting characteristics. Lithium fluoride in tantalum-10% tungsten forms a wetting, and in Poco, a nonwetting meniscus. There was some spread in experimental results (Figure 10), but no trend was observed that could be in any way associated with the size or shape of the meniscus. Meniscus shapes at measurement temperatures are not known, but the evapo-

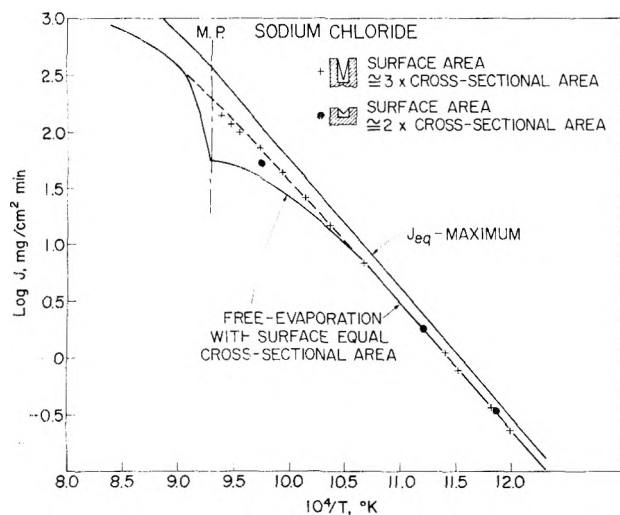


Figure 11. Effect of apparent surface area on experimental vaporization fluxes for sodium chloride.

ration results do tend to substantiate the supposition that rate in the liquid state is also independent of surface area.

Discussion

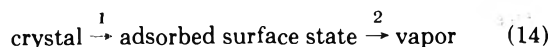
We first summarize the results obtained in this work which must be accounted for by any proposed vaporization model. (1) For all the substances studied, the vacuum vaporization rate is continuous through the melting point, i.e., the rates of the solid just below and the liquid just above the melting point are equal. (2) The vaporization rate of solid and liquid silver equals the equilibrium rate over the entire temperature range studied. (3) Two different types of behavior were observed for the four alkali halides studied. (a) For LiF (Figure 10), the overall vaporization coefficient α is somewhat less than unity and nearly independent of temperature over the entire range, except for the high-temperature liquid where α decreases slowly with rising temperature. (b) The results for NaCl, KBr, and CsI (Figures 7-9) have certain features in common. For the low-temperature solid (flat crystals) α is somewhat less than unity and nearly independent of temperature, although there seems to be a tendency for it to approach unity at low temperatures. This tendency is most evident for CsI which has $\alpha = 1$ at the lowest temperature measured. As the melting point is approached, α progressively decreases, reaching its minimum at the melting point. Above the melting point, α rises very rapidly over a 10-20° range up to a maximum value which is unity for CsI, but less than unity for NaCl and KBr. Above the maximum, α decreases slowly with increasing temperature. (4) For solid LiF over the entire temperature range and for low-temperature solid NaCl, the rate of vaporization for a given cross-sectional area is independent of the actual crystal area. However, for high-temperature solid NaCl, and probably for KBr and CsI, the rate per unit cross section can be raised to a maximum (corresponding to a linear extension of the low-temperature $\log J$ vs. $1/T$ plot) by increasing the surface to cross-sectional area ratio. An extrapolation of this maximum rate into the liquid range intersects the observed maximum rate of the liquid. (5) For both solid CsI and NaCl, the observed vaporization rate is independent of crystallographic orientation.

A comparison of our results with those of previous studies is possible only for NaCl and LiF in the "low-tempera-

ture solid" range. There are no free-evaporation measurements for CsI and KBr, and no high-temperature measurements for NaCl and LiF. Our disagreement with the results of Lester and Somorjai¹² for NaCl, particularly with respect to the effect of dislocation density, has been discussed previously.⁶

The vaporization kinetics of low-temperature solid LiF has previously been measured by Howlett, Lester, and Somorjai.³⁷ In contrast to their results for NaCl¹² they found a rate independent of dislocation density. This is also our finding. However, their value of α is only 0.17, compared to 0.75 obtained in this work. We have no explanation for this discrepancy, but believe that our values are correct since they meet the liquid value at the melting point.

In a previous paper,⁶ we accounted for the vaporization of solid NaCl in terms of a simple, two-step mechanism:



In terms of this model, the curvature of the $\log J$ vs. $1/T$ plot near the melting point for NaCl was accounted for by a change from 2 to 1 as the rate-determining step. The corresponding $\log J$ plots for solid LiF and Ag remain linear with $\Delta H^* \approx \Delta H_v^\circ$, and the same model implies for these substances that the desorption step² is rate determining to the melting point and that the surface has its equilibrium concentration of adsorbed molecules. A unity value of α is to be expected for silver and other heavy metals since practically every time an atom strikes a lattice of the same species, it will stick.⁸ For LiF the measured rate, corresponding to $\alpha \approx 0.75$, must be the maximum rate attainable since the flux cannot be increased by increasing the surface/cross-sectional area ratio. (Thermodynamics requires that the flux across any plane parallel to the vaporization surface cannot exceed the flux corresponding to the maximum equilibrium vaporization rate.)

The description of the vaporization process for solid LiF also applies to the low-temperature range of NaCl, KBr, and CsI. The four salts in this region differ primarily in the actual values of the activation parameters (which parallel the thermodynamic ones), and in the quantitative details of the desorption process. Several important properties for each salt crystal in the low-temperature solid region are presented in Table I. In each case, the activation enthalpy, the vaporization enthalpy, and the condensation coefficient are average values for the temperature range over which the quantities are reasonably constant. The activation enthalpy and its equilibrium counterpart could have been readily obtained with eq 9-12, using free-evaporation fluxes in this article and equilibrium fluxes from our previous study.⁶ However, respective enthalpies for the various species differ by only a few kilocalories, so that the enthalpy for the formation of 1 mol of real vapor is rather insensitive to changes in the composition of the vapor. In fact, ΔH_v° and ΔH^* , as computed directly from eq 2 and 3, respectively, and eq 8, are (within experimental error) equivalent to those obtained from eq 9-12. Therefore, the former, more direct method was arbitrarily selected to obtain the enthalpy values. Activation and thermodynamic vaporization enthalpies for each salt differ by only 1-3 kcal. The two quantities are directly related mathematically by eq 7, and the observed difference reflects an apparent small change in the experimental vaporization coefficient with temperature.

The last column in Table I lists the entropy difference

TABLE I: A Comparison of Activational and Thermodynamic Enthalpies of Vaporization for Single-Crystalline LiF, NaCl, KBr, and CsI

Salt	Av temp. °C	ΔH^* , kcal mol ⁻¹	ΔH_v° , kcal mol ⁻¹	α	$\Delta S^* - \Delta S_v^\circ$, cal deg ⁻¹ mol ⁻¹
LiF	760	63.4	66.1	0.75	-3.18
NaCl	600	52.9	54.1	0.74	-1.97
KBr	480	47.5	49.5	0.79	-3.09
CsI	440	43.6	44.9	0.88	-2.07

between the formation of the activated complex and the vapor molecule (using eq 15). Compared to typical values of ΔS_v° for the alkali halides, ~ 40 cal deg⁻¹ mol⁻¹, this difference is quite small and is consistent with the activated complex being almost a vapor molecule. Moreover, the values of $(\Delta S^* - \Delta S_v^\circ)$ are so small for the four salts that no great differences in configuration exist between activated complex and gas. Similarly, no great differences in $(\Delta H^* - \Delta H_v^\circ)$ are evident. However, both ΔH^* and ΔH_v° for LiF are considerably higher than for the other salts. It follows that at any particular temperature, the molar vaporization rate of LiF should be less than that of the other salts. (Since ΔS_v° is approximately the same for all the salts, differences in ΔH_v° correspond to differences in ΔG_v° .) Thus, if the rate of the bulk-to-surface step and/or the number of desorption sites are approximately the same for all the salts, desorption is more likely to remain rate determining for LiF as the temperature is raised because the desorption rate is quantitatively lower than that for the other salts.

As the melting point is approached, NaCl, KBr, and CsI differ markedly from LiF. The only other system for which such a marked decrease in α has been observed is ice. Davy and Somorjai³⁶ only carried out their ice measurements to a maximum temperature of -40° . They attribute the decrease in α to a gradual depletion of molecules in a mobile surface layer below its equilibrium value. For the alkali halides, a similar interpretation seems appropriate. Confirming evidence is provided by the results obtained with shaped NaCl crystals: the value of α at higher temperatures when the vaporizing surface of the crystal is flat drops below that predicted from a linear extrapolation of lower temperature values. However, α may be increased to a value quantitatively consistent with the lower temperature values by shaping the crystal so as to triple the actual surface to cross-sectional area ratio.

Two plausible mechanisms may be advanced to account for the marked decrease in α as the melting point is approached: (a) the concentration in the mobile surface layer is reduced below its equilibrium value as one of the bulk-to-surface steps becomes slow compared to the desorption step; (b) the number of desorption sites is reduced below its equilibrium value by some effect related to the coexistence of solid and liquid structure at the surface. Either of these mechanisms would explain the increase in rate observed when there is an increase in the ratio of the actual surface area to the cross-sectional area. Unfortunately, not enough is known about the structure of crystal surfaces near the melting point or the nature of desorption sites to distinguish between the two mechanisms.

We consider next the vaporization of the liquid. When a silver crystal melts, the major effect is the disruption of long-range order in the bulk phase. Since desorption is rate

determining in both states, the only change in the vaporization rate is that resulting from the change in desorption energy, i.e., the change in the activational enthalpy upon melting is the same as that for the equilibrium vaporization.

The situation for LiF, at all except the highest temperatures measured, is similar to that for Ag as far as the enthalpy relations are concerned. However, α is less than unity over the entire temperature range. This effect can be interpreted in a number of ways which do not differ greatly; for example, by a theory of Eyring which attributes values of $\alpha < 1$ to hindered rotation^{4,38} or that of Bradley³⁹ which considers some fraction of molecules to be unsuitably arranged spatially for incorporation into the condensed phase. Such an effect may also be interpreted in terms of an activational entropy of vaporization.

$$\Delta S^* = R \ln \alpha + (\Delta H^* - \Delta H_v^\circ)/T + \Delta S^\circ \quad (15)$$

If $\Delta H^* \approx \Delta H_v^\circ$ and α does not differ much from unity, ΔS^* will only be slightly less than ΔS° . In terms of activated complex theory, the activated complex will only be very slightly more bound to the surface than a gas molecule. This result is quite consistent with Searcy's² arguments that the activated complex in desorption is essentially a vapor molecule.

What at first sight seems remarkable is that the results for solid and liquid LiF are the same. Yet the present results show that as long as desorption is rate determining, the only difference between desorption from a solid and from a liquid surface is the difference in the activation enthalpies which equals the corresponding difference in the thermodynamic enthalpies. This result is quite different from that of Burns⁴⁰ for Al_2O_3 , Ga_2O_3 , and In_2O_3 , in which vaporization is dissociative. In that case, $\alpha \approx 0.3$ below the melting point and unity in the liquid.

In the high-temperature liquid region, α for each of the four salts gradually but progressively falls away from its lower temperature value in the liquid state. Since it is not likely that the nature and energies of the interactions of mobile layer molecules with the underlying substrate would change with temperature, we conclude that the effect is similar to that for the high-temperature solid, i.e., a gradual decrease of mobile layer concentration below its equilibrium value. This model is quite consistent with the generally accepted picture of a liquid surface as providing a rather abrupt transition between bulk and vapor. Thus the topmost layer of the bulk liquid is only slightly less densely populated than the bulk liquid,⁴¹ the molecules in this layer exchanging freely with the mobile layer of more gas-like molecules just above it. Only at very high vaporization rates is this exchange rate insufficient to populate the mobile layer up to its equilibrium concentration.

We have discussed the characteristic drop in the evaporation coefficient for solid NaCl, KBr, or CsI as the melting point of the salt is approached. These substances in the liquid state at temperatures near their respective melting points also exhibit behavior different from that found for LiF. When a flat crystal of one of these substances melts, the surface area apparently remains nearly constant and the vaporization rate immediately above the melting point is equal to that of the solid just below. However, as the temperature rises, the vaporization rate rises extremely rapidly, until approximately 10 – 20° above the melting point, the rate corresponds (according to our model) to that from a fully liquid surface with a mobile layer having its

equilibrium concentration, or nearly so. It remains to account for this region of rapid increase. Although our ideas are rather speculative, they are consistent with knowledge about the continuity of solid and liquid states gained by Ubbelohde and coworkers⁴² using a variety of techniques. Thus for many substances (although not for the alkali halides, specifically), there is evidence that just as the solid becomes increasingly disordered when the melting point is approached, so the liquid retains some solid structure above the melting point. It is therefore conceivable that the rapid increase in vaporization rate above the melting point results from the melting of solid-like regions in the liquid which retain some of the vaporization characteristics of the solid just below the melting point.

At the melting point, the molar vaporization rate for all the salts is practically the same. For those salts whose vaporization rates below the melting point are greater than that of LiF, this comes about because the overall rate near the melting point is now limited by the number of desorption sites and/or by the rate of bulk-to-surface step. The virtual independence of the rate on temperature in this region suggests that the measured flux is near the maximum for a solid in this family of materials.

Finally, we consider the possibility of interpreting the overall vaporization coefficient α in terms of a sticking coefficient S and a factor n which measures the departure of the surface concentration (both for solids and liquids) from its equilibrium value. The experimental results for solid LiF to the melting point and for solid NaCl, KBr, and CsI at lower temperatures, where $\Delta H^* = \Delta H^\circ$ and where the magnitude of α for a given cross-sectional area is independent of the actual crystal area, suggests the possible existence of a sticking coefficient S different from unity. A coefficient of this type could arise from the following model. At equilibrium, vaporization and condensation fluxes are equal and

$$J_{v,eq} = S J_{c,eq} \quad (16)$$

where $J_{c,eq}$ is the flux for the equilibrium vapor impinging on a unit area of the surface, i.e., it is the flux defined by eq 1a. The coefficient S is the fraction of this flux which sticks or condenses on impact.

If the energetic or configurational barriers to free-evaporation are the same as those at equilibrium, and if desorption is the rate-determining step, then

$$J_{v,0} = J_{v,eq} = S J_{c,eq} \quad (17)$$

The nonunity value of S results where (at equilibrium) all the impinging molecules do not stick to the surface. In this case $S = \alpha$ and the interpretation given for eq 15 applies.

When, as for high-temperature solid NaCl, KBr, and CsI and for the high-temperature liquid, desorption is no longer rate determining, we have shown that the most reasonable interpretation of the concomitant decrease in α is a change in the rate-determining step. Desorption becomes so rapid that some prior step becomes rate controlling and the concentration of surface molecules is reduced below its equilibrium value. If the concept of a sticking coefficient at lower temperature is valid, one would expect this phenomenon to also be present at higher temperatures. The general equation combining both models would then become

$$J_{v,0} = n J_{v,eq} = S n J_{c,eq} \quad (18)$$

where n is defined as the ratio of the actual surface concen-

tration to the equilibrium surface concentration. Since $J_{v,0}$ and $J_{c,eq}$ are the measured quantities, the product $S n$ would be equal to the observed vaporization coefficient α calculated from a Knudsen and a free-evaporation experiment carried out at the same temperature. At temperatures where $n < 1$, S could be determined by a linear extrapolation of the low temperature $\log \alpha$ vs. $1/T$ plot, and n is calculated from the experimental α and S .

Acknowledgments. We wish to thank Dr. F. L. Carter and Mr. W. Sadler for orienting and X-raying single crystals, and Dr. A. R. Ruffa for helpful discussions.

Appendix I. Nomenclature

a	characteristic dimension of vaporizing surface; for circular cross section, this is the radius and for square cross section, one-half the minimum linear dimension
D	diameter
ΔE	change in internal energy
ΔE_a	activation energy in Arrhenius equation, kcal mol ⁻¹
ΔH	enthalpy change for the formation of 1 mol of vapor, kcal mol ⁻¹
J	flux, mg cm ⁻² min ⁻¹
\bar{J}	flux, mol cm ⁻² sec ⁻¹
l	length of channel above the vaporizing surface
M	molecular weight
N	mole fraction in vapor
P	vapor pressure
R	gas constant
S	sticking coefficient
ΔS	entropy change for the formation of 1 mol of vapor, cal deg ⁻¹ mol ⁻¹
T	absolute temperature, °K
α	vaporization coefficient
λ	mean free path
ρ	density

Subscripts

eq	quantity at equilibrium
i	any molecular species
v, n	vaporization quantity
0	vaporization into vacuum
c	condensation quantity

Superscripts

*	activation quantity or Langmuir pressure
o	standard state, 1 atm for gas

References and Notes

- (1) M. Knudsen, *Ann. Phys.*, **47**, 697 (1915).
- (2) A. W. Searcy in "Chemical and Mechanical Behavior of Inorganic Materials", A. W. Searcy, D. V. Ragone, and U. Colombo, Ed., Wiley, New York, N.Y., 1970, Chapter 6.
- (3) O. Knacke, R. Schmolke, and I. N. Stranski, *Z. Kristallogr.*, **109**, 184 (1957).
- (4) J. F. Kincaid and H. Eyring, *J. Chem. Phys.*, **6**, 620 (1938).
- (5) C. T. Ewing and K. H. Stern, *J. Phys. Chem.*, **78**, 1998 (1974).
- (6) C. T. Ewing and K. H. Stern, *J. Phys. Chem.*, **77**, 1442 (1973).
- (7) R. J. Ackerman, R. J. Thorn, and G. H. Winslow in "The Characterization of High Temperature Vapors", J. L. Margrave, Ed., Wiley, New York, N.Y., 1967, Chapter 14.
- (8) F. M. Wanlass and H. Eyring, *Adv. Chem. Ser.*, No. **33**, 140 (1961).
- (9) R. C. Paule and J. L. Margrave, "The Characterization of High Temperature Vapors", Wiley, New York, N.Y., 1967, Chapter 6.
- (10) G. A. Somorjai and J. E. Lester, *Prog. Solid State Chem.*, **4**, 1 (1967).
- (11) G. M. Rosenblatt in "Heterogeneous Kinetics at Elevated Temperatures", G. R. Belton and W. L. Worrell, Ed., Plenum Press, New York, N.Y., 1970, pp 209-229.
- (12) J. E. Lester and G. A. Somorjai, *J. Chem. Phys.*, **49**, 2940 (1968).

- (13) M. Eisenstadt, V. S. Rao, and G. M. Rcthberg, *J. Chem. Phys.*, **30**, 604 (1959).
- (14) D. R. Stull and H. Prophet, *Natl. Stand. Ref. Data Ser., Natl. Bur. Stand., No. 37* (1971).
- (15) R. C. Miller and P. Kusch, *J. Chem. Phys.*, **25**, 860 (1956).
- (16) P. A. Akishin, L. N. Gorokhov, and L. N. Sidorov, *Zhur. Fiz. Khim.*, **33**, 2822 (1959).
- (17) A. W. Searcy and D. A. Schulz, *J. Chem. Phys.*, **38**, 772 (1963).
- (18) K. D. Carlson, P. W. Gilles, and R. J. Thorn, *J. Chem. Phys.*, **38**, 2725 (1963).
- (19) S. J. Wey and P. G. Wahlbeck, *J. Chem. Phys.*, **57**, 2932 (1972).
- (20) F. F. Coleman and A. Egerton, *Phil. Trans. A.*, **234**, 177 (1934).
- (21) T. D. Sandry and F. D. Stevenson, *J. Chem. Phys.*, **53**, 151 (1970).
- (22) H. G. Wiedemann, *Chem. Ing. Tech.*, **36**, 1105 (1964).
- (23) An. N. Nesmeyanov, "Vapour Pressure of the Element", Publishing House of the USSR Academy of Sciences, Moscow, 1961.
- (24) P. C. Marx, E. T. Chang, and N. A. Gokcen, *High Temp. Sci.*, **2**, 140 (1970).
- (25) S. K. Tarby and V. S. Robinson, III, *Trans. Met. Soc. AIME*, **242**, 719 (1968).
- (26) J. Bohdansky and H. E. J. Schins, *J. Phys. Chem.*, **71**, 215 (1967).
- (27) H. E. J. Schins, R. W. M. van Wijk, and B. Dorpema, *Z. Metallkd.*, **330** (1971).
- (28) I. Ansara and E. Bonnier, *Conf. Int. Metall. Beryllium, [Commun.]*, **3rd**, 1965, 17 (1966).
- (29) E. W. R. Steacie and F. M. G. Johnson, *Proc. R. Soc. (London)*, **112**, 542 (1926).
- (30) O. Knacke and I. N. Stranski, *Prog. Met. Phys.*, **6**, 181 (1956).
- (31) J. P. Hirth and G. M. Pound, *Prog. Mater. Sci.*, **11**, 1 (1963).
- (32) M. Volmer and I. Estermann, *Z. Phys.*, **7**, 13 (1921).
- (33) K. Neumann and K. Schmoll, *Z. Phys.*, **2**, 215 (1954).
- (34) R. B. Holden, R. Speiser, and H. L. Johnson, *J. Am. Chem. Soc.*, **70**, 3897 (1948).
- (35) R. P. Burns, A. L. Jason, and M. G. Inghram, *J. Chem. Phys.*, **40**, 2739 (1964).
- (36) J. G. Davy and G. A. Somorjai, *J. Chem. Phys.*, **55**, 3624 (1971).
- (37) D. L. Howlett, J. E. Lester, and G. A. Somorjai, *J. Phys. Chem.*, **75**, 4049 (1971).
- (38) E. M. Mortensen and H. Eyring, *J. Phys. Chem.*, **64**, 846 (1960).
- (39) R. S. Bradley and P. Volans, *Proc. R. Soc., Ser. A*, **217**, 508 (1953).
- (40) R. P. Burns, *J. Chem. Phys.*, **44**, 3307 (1966).
- (41) W. Lu, M. S. Jhon, T. Ree, and H. Eyring, *J. Chem. Phys.*, **46**, 1075 (1967).
- (42) For a summary see A. R. Ubbelohde, *J. Chem. Phys.*, **61**, 58 (1964).

Thermal Instability in Synthetic Hydroxyapatites

H. Catherine W. Skinner,*

Department of Surgery, Yale University, New Haven, Connecticut 06510

J. Steven Kittelberger,

Xerox Corporation, 114 Webster, New York 14580

and Ralph A. Beebe

Department of Chemistry, Amherst College, Amherst, Massachusetts 01002 (Received September 18, 1974; Revised Manuscript Received June 19, 1975)

Hydrothermally synthesized hydroxyapatites, $\text{Ca}_{10}(\text{PO}_4)_6(\text{OH})_2$, were subjected to pyrolysis at atmospheric pressure and under vacuum (10^{-3} and 10^{-7} Torr, H_2O pressure). At high vacuum evolved gases were observed with a mass spectrometer as the sample temperature was raised $10^\circ/\text{min}$ from room temperature to 800° . A dehydration peak was observed at 705° . All treated samples exhibited an absence of ir bands assigned to (OH) stretching and librational modes indicating a loss of (OH) from the structure. X-Ray analysis gave broadened diffraction maxima for samples pyrolyzed under vacuum conditions. In addition, maxima from a second phase appeared, which were identified as $\beta\text{-Ca}_3(\text{PO}_4)_2$. Dehydroxylated apatite is considered an intermediate in the reaction $\text{Ca}_{10}(\text{PO}_4)_6(\text{OH})_2 \rightarrow 2\text{Ca}_3(\text{PO}_4)_2 + \text{Ca}_4\text{P}_2\text{O}_9 + \text{H}_2\text{O}$.

Hydroxyapatite, $\text{Ca}_{10}(\text{PO}_4)_6(\text{OH})_2$ (HA), is considered the mineral model for the inorganic phase of bones and teeth. There has been and is great interest in the substance per se as well as in the mineral-biological tissue reactions. Generalized chemical and physical properties and the crystal structures of apatites have been known for a long time.¹⁻³ Equilibrium phase diagrams for the $\text{CaO-P}_2\text{O}_5\text{-H}_2\text{O}$ system have contributed toward our understanding of the reactions and idiosyncracies of the pure phase HA.^{4,5} HA is the stable calcium phosphate phase over large portions of the diagram but the HA-fluid phase field has a restricted compositional range, H_2O as well as $\text{CaO/P}_2\text{O}_5$ (Figure 1 field 5). We report here on investigations into the stability of well-crystallized stoichiometric HA synthesized by hydrothermal techniques.

Two samples of HA were synthesized at 450° and 22,000 lb/in.² H_2O pressure in standard hydrothermal equipment

from different bulk starting compositions.⁴ Sample SM₂ had $\text{Ca/P} = 1.5$, H_2O 75 wt %; SM₁ had $\text{Ca/P} = 1.5$, 50% H_2O . SM₂ plots in field 5 (Figure 1) and SM₁ in field 4. The samples were held at temperature and pressure for 70 days, sufficient time to assure attainment of the equilibrium. The samples produced well-crystallized HA with sharp X-ray diffraction patterns (Figure 2), and differ only in having been synthesized in different phase fields. SM₂ contained crystalline HA plus fluid; SM₁ contained HA plus $\beta\text{-Ca}_2\text{P}_2\text{O}_7$ plus fluid.

The HA phase of these samples (hand-picked in the case of SM₁) was subjected to pyrolysis at atmospheric pressure, and under vacuum at two partial pressures of H_2O (measured at 10^{-7} and 10^{-3} Torr). At the high vacuum, we employed a thermal desorption spectrometer⁶ equipped to raise the sample temperature at a linear rate of $10^\circ/\text{min}$. The spectrometer included a quadrupole mass spectrome-

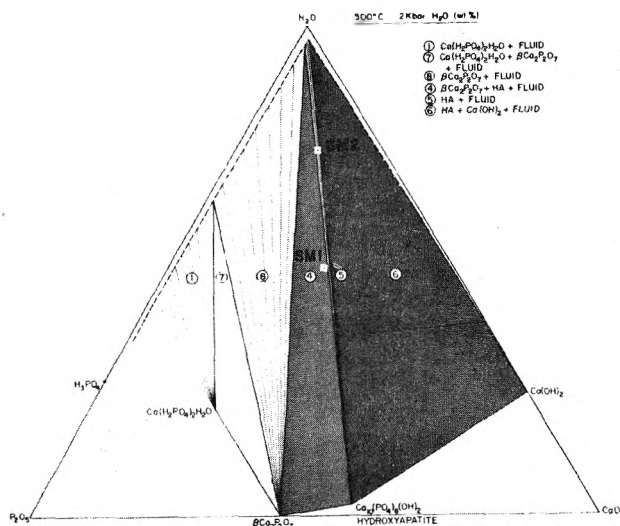


Figure 1. Equilibrium phase diagram for $\text{CaO-P}_2\text{O}_5\text{-H}_2\text{O}$ at 500° . 30,000 lb/in.² H_2O pressure showing bulk composition of samples SM1, SM2.

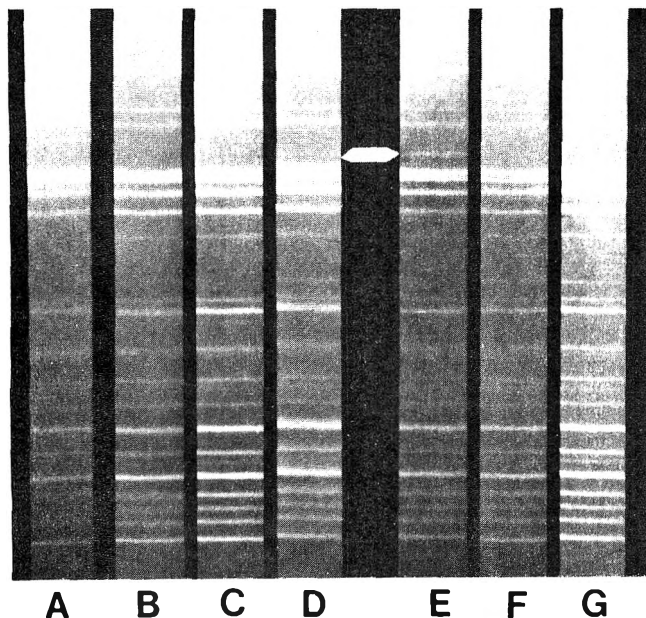


Figure 2. Portions of Guinier X-ray powder diffraction photographs from d_{hkl} approximately 3.5 Å at bottom to 1.67 Å at top: (A) low-temperature precipitated "apatite"; (B) SM2 hydrothermally synthesized hydroxyapatite before pyrolysis; (C) SM2 pyrolyzed in a muffle furnace to 850° ; (D) SM2 pyrolyzed under vacuum ($\sim 10^{-6}$ Torr) to 850° ; (E) SM1 pyrolyzed under vacuum ($\sim 10^{-6}$ Torr) to 850° ; (F) SM1 hydrothermally synthesized hydroxyapatite before pyrolysis; (G) SM1 pyrolyzed in a muffle furnace to 850° . Calculated unit cell parameters (in Å) for SM2 samples: (B) 9.429 (3), 6.886 (3) $V = 530.0 \text{ \AA}^3$; (C) 9.421 (1), 6.896 (1) $V = 530.1 \text{ \AA}^3$; (D) 9.459 (2), 6.915 (2) $V = 535.8 \text{ \AA}^3$.

ter for continuous monitoring of gaseous decomposition products. After initial pump-down to 5×10^{-7} Torr at room temperature, each sample was heated to 850° at $10^\circ/\text{min}$. The samples were held at 850° for 15 min and then cooled to room temperature under vacuum over a period of approximately 2 hr. The partial pressure of water varied from 5 to 10×10^{-7} Torr over the approximately 3 hr total experimental time. During the period of linear temperature rise, discrete peaks recorded in a $P_{\text{H}_2\text{O}}$ vs. time trace indicated discrete hydration processes.⁷ For both

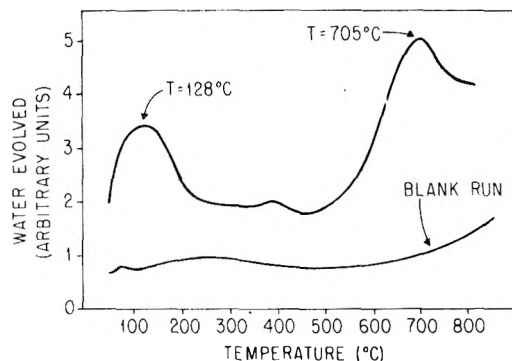


Figure 3. Temperature programmed dehydration spectrum for SM2 hydroxyapatite (upper curve). The lower curve shows the water evolution in the apparatus with no hydroxyapatite present.

SM1 and SM2 a peak occurs in the dehydration spectrum between 675 and 800° . The thermal dehydration plot for SM2 (Figure 3) illustrates the results with the peak maximum at 705° . We attribute the low-temperature peak to desorption from the apatite sample surface, and the high-temperature peak to dehydroxylation. At the conclusion of each experiment the samples were transferred with minimum exposure to the atmosphere into capped vials. Pyrolysis at atmospheric pressure (3 hr at 1000°) was made in a standard muffle furnace. All pyrolyzed samples were submitted to X-ray and infrared examination.

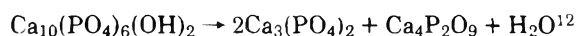
Infrared spectra of all pyrolyzed samples (in KBr pellets) differed from the starting material in not showing absorption bands at 3570 and 633 cm^{-1} , bands which have been unambiguously assigned to (OH) stretching and librational modes in HA. This result implies a loss of (OH) from that site in the structure. PO_4 bands in the $500\text{-}600\text{-}$ and $1000\text{-}1200\text{-cm}^{-1}$ regions were somewhat broadened. These features are well known.⁸ A curious feature was the appearance, at 1950 and 2020 cm^{-1} , of a pair of very sharp bands. These bands increase in intensity and sharpness with decreasing partial pressure of water during pyrolysis. Fowler⁹ has identified several low-intensity bands in this region as overtones and combinations of orthophosphate stretching modes. Our samples before pyrolysis also showed low-intensity bands in this region. The sharpness of the 1950- and 2020-cm^{-1} bands after pyrolysis suggests that they are characteristic of pyrolysis products. Further work leading to definite assignment of this pair of bands is in progress; contamination due to organic constituents has been ruled out.

Muffle furnace pyrolyzed SM1 and SM2 samples exhibited sharp, single-phase, apatite diffraction patterns (Figure 2C,G). X-Ray diffraction patterns of the high-vacuum pyrolyzed SM2 show markedly broadened maxima (Figure 2D). Somewhat broadened maxima were also noted in the low-vacuum pyrolyzed sample. SM1 did not exhibit line broadening under either of these conditions. However, diffraction maxima, in addition to those of HA, appeared in both high- and low-vacuum pyrolyzed SM1 samples. The maxima were used to identify the second phase as tricalcium phosphate ($\beta\text{-Ca}_3(\text{PO}_4)_2$). A maximum belonging to tricalcium phosphate is barely discernible on the broadened SM2 pattern in the same position. (See arrow between Figure 2D and E.)

The original hydrothermal SM1 and SM2 samples grown in different phase fields at the same temperature and pressure have discrete unit cell parameters.¹⁰ The parameters of the HA phase calculated from diffraction data up to 80°

2θ show minor differences (Figure 2, legend). After vacuum pyrolysis the parameters, and therefore the unit cell volume, increase, suggesting crystal structure alteration.

The fact that HA is sensitive to partial pressures of H_2O is not unexpected. In a truly anhydrous system HA should not appear.¹¹ The reaction is

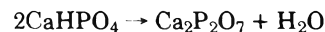


The breakdown of HA and the appearance of $Ca_3(PO_4)_2$ has been documented on our samples. $Ca_4P_2O_9$ has not been identified, possibly because the three most intense diffraction maxima of $Ca_4P_2O_9$ overlap those of HA. However, it is also true that major crystal structural changes involving the PO_4 group would be required to nucleate and form $Ca_4P_2O_9$. The major fraction of the vacuum-pyrolyzed material remains "apatitic" with increased unit cell volume. Increased unit cell volume is anticipated as both $Ca_3(PO_4)_2$ and $Ca_4P_2O_9$ have unit cell volumes greater than HA: $Ca_3(PO_4)_2 = 3495 \text{ \AA}^3$, $Ca_4P_2O_9 = 795 \text{ \AA}^3$, HA = 529 \AA^3 .

The formation of anhydrous calcium phosphates from HA involves not only dehydroxylation but major structural transformations. After atmospheric pyrolysis (1000° for 3 hr) HA dehydroxylates (loss of $3570 + 633\text{-cm}^{-1}$ ir bands) but no other structural changes are indicated. After 72 hr at 1000° no further structural changes were noted. Atmospheric $p(H_2O)$ is sufficient to maintain apatite structure elements even after prolonged heating at 1000° . However, after vacuum pyrolysis (3 hr to 850°) both dehydroxylation and structural changes were indicated (broadened diffraction maxima). The effect of vacuum is to decrease the stability of HA accelerating the breakdown reaction.

The dehydroxylated apatite phase is probably a metastable intermediate in the breakdown of HA and might be called "oxyapatite". The term oxyapatite has been in the

literature for a long time¹³ designating apatites which do not exhibit OH bands in ir but have the apatite structure. The dehydroxylated apatite phase is probably analogous to the phase $\gamma\text{-}Ca_2P_2O_7$ in the reaction



$\gamma\text{-}Ca_2P_2O_7$ was shown¹⁴ to be metastable relative to the $\beta\text{-}Ca_2P_2O_7$ modification. The reaction is extremely sluggish due to the necessary conversion of PO_4 to P_2O_7 groups. The kinetics of this¹⁵ reaction and the HA conversion must depend on $p(H_2O)$ as well as temperature.

Acknowledgment. We wish to acknowledge grant support from the National Institutes of Health for both the hydrothermal synthesis work (H. C. W. Skinner, DE 2716) and the dehydration studies (R. A. Beebe, DE 2819).

References and Notes

- (1) H. C. Hodge, M. LeFevre, and W. F. Bale, *Ind. Eng. Chem., Anal. Ed.*, **10**, 156 (1938).
- (2) S. B. Hendricks, M. D. Jefferson, and V. M. Mosley, *Z. Anorg. Chem.*, **81**, 352 (1932).
- (3) J. R. VanWazer, "Phosphorus and Its Compounds", Vol. I, Wiley-Interscience, New York, N.Y., 1966, p 513.
- (4) H. C. W. Skinner, *Amer. J. Sci.*, **273**, 545 (1973).
- (5) H. J. Bassett, *J. Chem. Soc.*, **601**, 2929 (1958).
- (6) C. W. Anderson, R. A. Beebe, and J. S. Kittelberger, *J. Phys. Chem.*, **78**, 1631 (1974).
- (7) R. J. Cetanovic and Y. Amenomiya, *Catal. Rev.*, **6**, 21 (1972).
- (8) C. B. Baddiel and E. E. Berry, *Spectrochim. Acta*, **22**, 1407 (1966).
- (9) B. Fowler, *Inorg. Chem.*, **13**, 194 (1974).
- (10) H. C. W. Skinner, *Appl. Spectrosc.*, **22**, No. 5, 414 (1968). Calculations have been programmed to discriminate and exclude phases other than apatite.
- (11) G. Tromel and H. Moller, *Z. Chem.*, **206**, 227 (1932); J. H. Welch and W. Gutt, *J. Chem. Soc.*, 4442 (1961).
- (12) P. V. Riboud, *Bull. Soc. Chem. Fr.*, 1701 (1968).
- (13) A. F. Rogers, *J. Sci.*, **33**, 475 (1912); J. Ito, *Amer. Min.*, **53**, 890 (1968).
- (14) H. C. W. Skinner, *Mat. Res. Bull.*, **5**, 437 (1970).
- (15) N. W. Wikholm, R. A. Beebe, and J. S. Kittelberger, *J. Phys. Chem.*, **79**, 853 (1975).

Stability of Polymer Lattices Prepared Using Mixtures of Anionic and Nonionic Surfactants

Hiroshi Ono,* Eiki Jidai, and Akira Fujii

Central Research Laboratory, Mitsubishi Electric Corporation, 80 Nakano, Minamishimizu, Amagasaki, Hyogo, Japan, 661 (Received June 11, 1974; Revised Manuscript Received May 2, 1975)

Publication costs assisted by the Central Research Laboratory, Mitsubishi Electric Corporation

A series of poly(methylmethacrylate), acrylonitrile-methylmethacrylate copolymer, and acrylonitrile-styrene copolymer latex dispersions has been prepared by emulsion polymerization using various combinations of anionic and nonionic surfactants. The effect of surfactants present during the process of emulsion polymerization on the stability of latex dispersions has been investigated using simple electrolytes as coagulating agents. The particle diameter increases with an increase in the amount of nonionic surfactant in the surfactant mixture; the diameter also depends on the HLB value of the nonionic surfactant used. The values of critical coagulation concentration of latex dispersions increase with increasing proportion of nonionic surfactant in the surfactant blend, and also increase as the HLB values of the nonionic surfactants decrease. The ζ potential at critical coagulation concentration decreases with an increase in the proportion of nonionic surfactant.

Introduction

A considerable amount of experimental work on the stability of colloidal dispersions of organic substances has been carried out.^{1,2} However, most of this work has been centered on the study of polystyrene latex.³⁻⁷

On the other hand, most of the earlier work considering the effect of surfactant on the stability of colloidal systems was concerned with dispersions of inorganic substances.⁸⁻¹² Work concerning the effect of surfactants on the stability of polymer lattices has been limited to the study of surfactants added after the preparation of the dispersions.¹³ Little attention has been paid to the effect of surfactants present during the process of emulsion polymerization.

The present work was performed in order to study this aspect of the stability problem. For this purpose poly(methylmethacrylate) (MMA), acrylonitrile (AN)-MMA copolymer, and AN-styrene (ST) copolymer lattices were prepared by emulsion polymerization using mixtures of anionic and nonionic surfactants. The stability and electrophoretic behavior of these polymer lattices have been investigated using sodium chloride, magnesium chloride, and barium chloride as coagulating agents.

Experimental Section

Materials. Deionized water having a resistivity of more than $5 \times 10^6 \Omega \text{ cm}$ was used throughout. MMA, ST, and AN were purified by distillation at low temperature under reduced pressure in a stream of nitrogen. Potassium persulfate and sodium bisulfite were both Analar grade materials and were used without further purification. Sodium lauryl sulfate (SLS), hexaoxyethylene oleyl ether (EO), decaoxyethylenenonyl phenyl ether (ENP), and polyoxyethylene sorbitan monooleate (ESO) were purified by recrystallization. The characteristics of these surfactants are listed in Table I. The HLB value of SLS was calculated by Davies' method,¹⁴ using the following equation:

$$\text{HLB} = 7 + \frac{\sum (\text{hydrophilic group numbers})}{\sum (\text{lipophilic group numbers})} \quad (1)$$

On the other hand, HLB values for nonionic surfactants were calculated by Griffin's method,¹⁵ using the equation

$$\text{HLB} = E/5 \quad (2)$$

where E = weight percentage of oxyethylene content.

Methods

Preparation of Polymer Latex Dispersions. The latex dispersions were prepared by emulsion polymerization at 60° using potassium persulfate as an initiator. The concentration of the initiator was 0.5 g/l. for all lattices. A number of runs was made using an anionic surfactant and anionic/nonionic blends of surfactants. In this work, the anionic surfactant was SLS, while the nonionic materials were EO, ENP, and ESO. Poly-MMA and AN-MMA copolymer lattices were prepared using SLS, and selected ratios of SLS/EO: viz., SLS/EO ratio (by weight) = 8/2, 5/5, 3/7, 1/9. AN-ST copolymer lattices were prepared using 50/50 blends (by weight) of anionic/nonionic surfactants: viz., SLS/EO, SLS/ENP, and SLS/ESO. The total concentration of surfactant used for the preparation of the lattices was fixed at 0.4 g/l. for poly-MMA, and AN-MMA copolymer lattices, and at 1.0 g/l. for AN-ST copolymer lattices. A typical example of the preparation is as follows.

The reaction vessel, set in a water bath, was charged with 170 g of deionized water. Nitrogen was bubbled through the water for about 30 min with stirring in order to displace the dissolved oxygen. SLS (0.04 g), EO (0.04 g), and MMA (20 g) were introduced into the reaction vessel and the apparatus was brought to the polymerization temperature (60°). Potassium persulfate (0.1 g) and sodium bisulfite (0.03 g), dissolved in 10 g of deionized water, were inserted into the reaction vessel. Polymerization was allowed to proceed for about 4 hr at 60 ± 2° in a stream of nitrogen. The latex dispersion was then cooled with a water bath to room temperature and filtered through 100 gauge wire mesh to remove coagula. The polymer lattices thus prepared are listed in Table II.

Dialysis of Latex Dispersions. The latex dispersions ob-

TABLE I: Characteristics of the Surfactants Used

Abbreviated designation	Chemical structure	Mol wt	HLB	cmc, M
SLS	$C_{12}H_{25}OSO_3Na$	288	40.0	7.5×10^{-3}
EO	$C_{18}H_{35}O(CH_2CH_2O)_6H$	532	9.9	1.0×10^{-6}
ENP	$C_6H_5-O(CH_2CH_2O)_nH$	660	13.3	8.5×10^{-5}
ESO		1,748	15.1	1.0×10^{-3}

TABLE II: Listing and Modal Diameters of the Lattices Used

Latex desgn	Chemical compn, molar ratio	Surfactant, wt ratio	Modal diam, Å
MM 10	MMA	SLS/EO = 10/0	780
MM 82	MMA	SLS/EO = 8/2	900
MM 55	MMA	SLS/EO = 5/5	1040
MM 37	MMA	SLS/EO = 3/7	1160
MM 19	MMA	SLS/EO = 1/9	1260
AM 10	AN/MMA = 3/1	SLS/EO = 10/0	620
AM 82	AN/MMA = 3/1	SLS/EO = 8/2	680
AM 55	AN/MMA = 3/1	SLS/EO = 5/5	720
AM 37	AN/MMA = 3/1	SLS/EO = 3/7	880
AM 19	AN/MMA = 3/1	SLS/EO = 1/9	1020
EEO	AN/ST = 1/1	SLS/EO = 1/1	1160
EON	AN/ST = 1/1	SLS/ENP = 1/1	1030
EOS	AN/ST = 1/1	SLS/ESO = 1/1	820

tained contained residual monomer, free emulsifier, and miscellaneous free ions, which were removed by dialysis. About 1% w/v latex dispersions were placed in a Visking dialysis tube and dialyzed against deionized water for about 2 weeks. The dialyzate was changed every 24 hr. The dialysis was continued until a constant conductivity value was obtained.

Electron Microscopy. For electron microscope examination of latex dispersions, a supporting film of collodion coated with a thin layer of carbon mounted on copper gauze was used. Extremely dilute latex dispersions were sprayed from an injection syringe onto the supporting film. Modal diameters were determined by measuring the diameters of particles on electron micrographs. For each sample, approximately 200 particles were counted.

Mobility Measurement. The electrophoretic mobilities of latex dispersions were determined using a moving boundary apparatus based on the design of Kerker, Bowman, and Matijević.¹⁶

Determination of the Rates of Coagulation. The course of the early stages of coagulation of the lattices was followed turbidimetrically in order to determine the rates of coagulation. The change in turbidity with time was recorded continuously commencing 4–5 sec after the addition of the electrolyte solution. The rate constant, K , for the coagulation process was determined from the tangent of the turbidity curve at early stages.

Results

Modal Diameters of the Latex Particles. Electron mi-

TABLE III: Conductivity of the Lattices

Latex desgn	Specific conductivity, ^a $\Omega^{-1} \text{cm}^{-1}$	Latex desgn	Specific conductivity, ^a $\Omega^{-1} \text{cm}^{-1}$
MM 10	1.0×10^{-5}	AM 55	9.5×10^{-6}
MM 82	9.6×10^{-6}	AM 37	8.9×10^{-6}
MM 55	9.3×10^{-6}	AM 19	8.0×10^{-6}
MM 37	8.9×10^{-6}	EEO	1.0×10^{-5}
MM 19	8.3×10^{-6}	EON	1.4×10^{-5}
AM 10	1.1×10^{-5}	EOS	1.7×10^{-5}
AM 82	1.05×10^{-5}		

^a Concentrations of lattices are about 1% w/v.

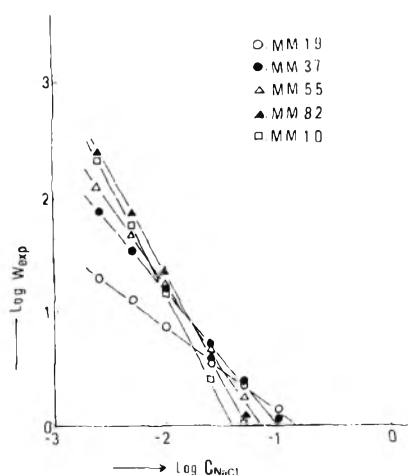
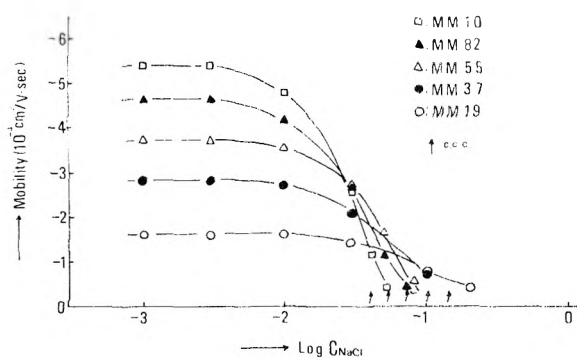
crographs of the lattices show that the latex particles are almost perfect spheres. As shown in the last column of Table II, the modal diameters of the latex particles for poly-MMA lattices increase uniformly with an increase in the proportion of nonionic surfactant present during the process of emulsion polymerization. The data of modal diameter for AN–MMA copolymer lattices indicate a similar tendency. Woods et al.¹⁷ reported that the particle diameters increase with increasing amount of nonionic surfactant. The results obtained in the present work are in accordance with their results. This trend would be expected from the micellar theory of emulsion polymerization. The modal diameter for AN–ST copolymer lattices follows the order EEO > EON > EOS. The results indicate that the modal diameters of the latex particles increase with increasing hydrophobic characteristics of the nonionic surfactants used.

Conductivity of Latex Dispersions. Values of specific conductivity of the dialyzed latex dispersions are shown in Table III. They increase uniformly with an increase in the anionic surfactant content of the surfactant blend for poly-MMA and AN–MMA copolymer lattices, whereas they increase with decreasing hydrophobic characteristics of the nonionic surfactant for AN–ST copolymer lattices. These results seem to indicate that the surface charge density of the latex particles decreases as the proportion of nonionic surfactant is increased.

Stability of Latex Dispersions. The change in turbidity with time after the addition of electrolyte solution was recorded. In the early stages of coagulation, these curves were always linear. The initial slopes of these curves are directly proportional to the rate of coagulation. For every latex, the value of K increased with increasing electrolyte concentration and reached a maximum at a specific concentration. Beyond this electrolyte concentration, the value of K becomes independent of electrolyte concentration. This maxi-

TABLE IV: Slopes of the Stability Curves and the ccc of the Lattices

Latex design	$-d \log W_{\text{expt}}/d \log C_e$			ccc, M		
	NaCl	MgCl ₂	BaCl ₂	NaCl	MgCl ₂	BaCl ₂
MM 10	1.93	1.85	1.70	3.98×10^{-2}	9.33×10^{-3}	1.15×10^{-2}
MM 82	1.85	1.78	1.68	5.25×10^{-2}	1.26×10^{-2}	1.35×10^{-2}
MM 55	1.45	1.40	1.33	7.08×10^{-2}	1.70×10^{-2}	1.78×10^{-2}
MM 37	1.18	1.10	1.06	1.00×10^{-1}	2.24×10^{-2}	1.91×10^{-2}
MM 19	0.75	0.69	0.71	1.41×10^{-1}	3.16×10^{-2}	2.04×10^{-2}
AM 10	2.82	2.70	2.50	5.01×10^{-2}	1.18×10^{-2}	1.62×10^{-2}
AM 82	2.53	2.45	2.32	6.61×10^{-2}	1.59×10^{-2}	2.29×10^{-2}
AM 55	1.92	1.80	1.64	8.91×10^{-2}	2.24×10^{-2}	3.16×10^{-2}
AM 37	1.55	1.43	1.33	1.26×10^{-1}	3.02×10^{-2}	3.39×10^{-2}
AM 19	0.85	0.75	0.83	1.78×10^{-1}	3.98×10^{-2}	3.55×10^{-2}
EOO	1.26	1.10	1.16	2.82×10^{-1}	6.31×10^{-2}	5.25×10^{-2}
EON	1.84	1.60	1.44	1.26×10^{-1}	2.51×10^{-2}	2.95×10^{-2}
EOS	2.15	2.05	1.70	6.31×10^{-2}	1.26×10^{-2}	1.78×10^{-2}

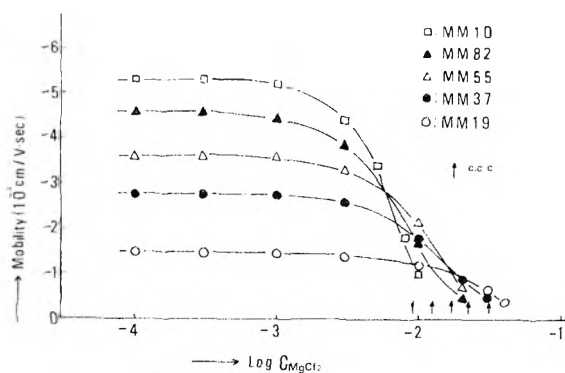
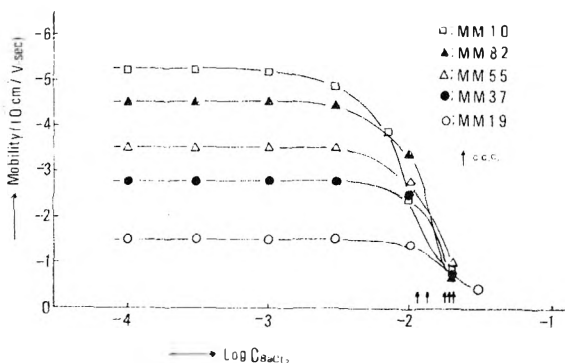
Figure 1. Log W_{expt} vs. $\log C_{\text{NaCl}}$ curves for poly-MMA lattices.Figure 2. Curves of electrophoretic mobility vs. $\log C_{\text{NaCl}}$ for poly-MMA lattices.

imum value of K is defined as K_0 , which corresponds to rapid coagulation. Thus, experimental W values are obtained from

$$W_{\text{expt}} = K_0/K$$

Therefore, W_{expt} becomes unity in the case of rapid coagulation.

An example of the stability curves thus obtained is given in Figure 1, in the form of a $\log W_{\text{expt}}$ vs. $\log C_e$ curve. C_e

Figure 3. Curves of electrophoretic mobility vs. $\log C_{\text{MgCl}_2}$ for poly-MMA lattices.Figure 4. Curves of electrophoretic mobility vs. $\log C_{\text{BaCl}_2}$ for poly-MMA lattices.

was taken as the molar concentration of the electrolyte. The curves were approximately linear over the range investigated and can be represented by an equation of form

$$\log W_{\text{expt}} = -K_1 \log C_e + K_2 \quad (3)$$

The values of the slope of the stability curve and the critical coagulation concentration (ccc) of the lattices for three electrolytes are given in Table IV. The values of the ccc were determined by extrapolating the $\log W_{\text{expt}}$ values down to $\log W_{\text{expt}} = 0$, and reading $\log C_e$ at the point of intersection.

Electrophoretic Mobility of Latex Dispersions in the

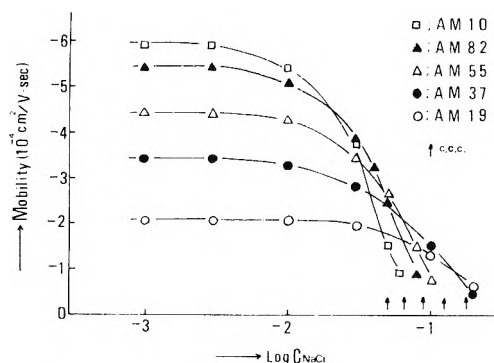


Figure 5. Curves of electrophoretic mobility vs. $\log C_{NaCl}$ for AN-MMA copolymer lattices.

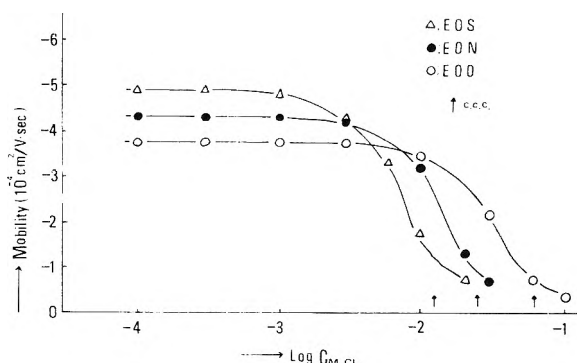


Figure 9. Curves of electrophoretic mobility vs. $\log C_{MgCl_2}$ for AN-ST copolymer lattices.

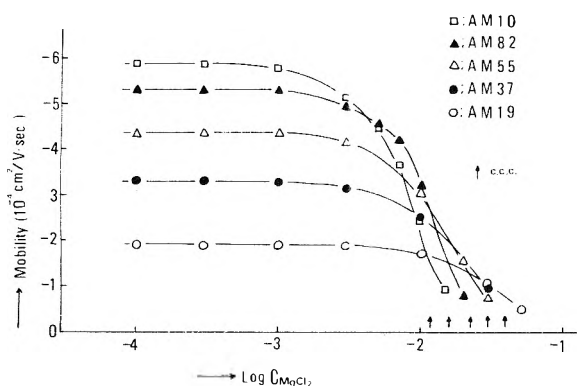


Figure 6. Curves of electrophoretic mobility vs. $\log C_{MgCl_2}$ for AN-MMA copolymer lattices.

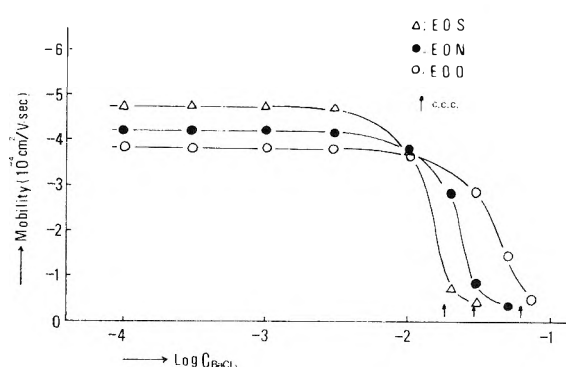


Figure 10. Curves of electrophoretic mobility vs. $\log C_{BaCl_2}$ for AN-ST copolymer lattices.

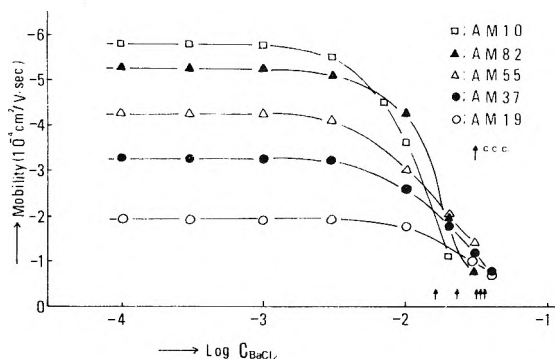


Figure 7. Curves of electrophoretic mobility vs. $\log C_{BaCl_2}$ for AN-MMA copolymer lattices.

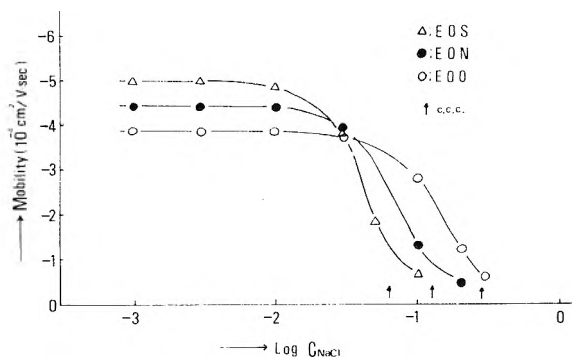


Figure 8. Curves of electrophoretic mobility vs. $\log C_{NaCl}$ for AN-ST copolymer lattices.

Presence of Inorganic Electrolytes. The electrophoretic mobility results obtained for poly-MMA, AN-MMA copolymer, and AN-ST copolymer lattices in the presence of inorganic electrolytes are given in Figures 2-10. C_e was taken as the molar concentration of the electrolytes.

Discussion

Effect of the Content of Nonionic Surfactant. The values of ccc for three electrolytes are summarized in Table IV. The order of the ccc values was found to be MM 19 > MM 37 > MM 55 > MM 82 > MM 10, and AM 19 > AM 37 > AM 55 > AM 82 > AM 10, for all electrolytes investigated. The values of ccc increase uniformly with an increase in the proportion of nonionic surfactant present during the process of emulsion polymerization, for both MM and AM series of lattices, and for all electrolytes investigated.

The values of the slopes of the stability curves are given in Table IV. They decrease as the proportion of nonionic surfactant increases, for both MM and AM series of lattices.

In order to obtain detailed information on the effect of nonionic surfactants, the electrophoretic mobilities in the presence of three different electrolytes have been investigated. As shown in Figures 2-7, the shapes of the mobility curves for each of these three electrolytes are quite alike for both MM and AM series of lattices. As shown in these figures, the mobility of the latex particles decreases uniformly with decreasing proportion of anionic surfactant in the region of low electrolyte concentration. These results seem to be caused by surface coverage of the latex particles by the nonionic surfactant. The rate of surface coverage seems to increase as the nonionic surfactant content of the surfac-

tant mixture increases. The concentration ranges over which the mobility remained almost constant increase with an increase in the nonionic surfactant content. A remarkable decrease in the mobility of the latex particles was observed just before ccc of the latex dispersions. The electrolyte concentration at which the mobility decreases suddenly shifts to higher values as the nonionic surfactant content is increased. The decrease in the mobility with increasing electrolyte concentration seems mainly to be due to the increase in ionic strength of the latex dispersions and partly due to the adsorption of the divalent counterions. Taking into account these experimental results, the degree of surface coverage or the thickness of the adsorbed layer of nonionic surfactant seems to increase with increasing nonionic surfactant content.

However, mobility results in the region of low electrolyte concentration given in Figures 2-7 show that all the lattices used in the present work have considerable negative surface charges.

Ottewill and Walker¹³ reported on the effect of nonionic surfactant on the stability of polystyrene latex dispersions. They considered the contribution of the enthalpy term, ΔG , to the stability of lattices having adsorbed layers, and presented the following equations:

$$V_T = V_R + V_A + \Delta G \quad (4)$$

$$\Delta G = \frac{4\pi C^2}{3v_1\rho_2^2}[\psi_1 - \chi_1] \left[\delta - \frac{H_0}{2} \right]^2 \left[3a + 2\delta + \frac{H_0}{2} \right] \quad (5)$$

In eq 4, V_T = total potential energy of interaction, V_R = electrostatic repulsion, V_A = van der Waals attraction, and ΔG = enthalpic stabilization term. In eq 5, c = concentration of adsorbed material in the adsorbed layer expressed in g/ml, v_1 = volume fraction of solvent molecule, ρ_2 = density of the adsorbed material, ψ_1 = entropy parameter, χ_1 = enthalpy parameter, δ = thickness of adsorbed layer, H_0 = distance between the surfaces of the particles, and a = particle radius.

Ottewill and Walker¹³ estimated V_T as a function of H_0 using specific values of c , v_1 , and ρ_2 , taking $\psi_1 = 0.5$, and assuming $V_R = 0$.

On the other hand, Napper et al.¹⁸⁻²⁰ have investigated the flocculation of sterically stabilized dispersions. For example, Napper¹⁸ studied the stability of polymer lattices which are stabilized solely by poly(ethylene oxide) moieties. He discussed the effect of such factors as the anchor polymer, the dispersion medium, the surface coverage, and the molecular weight of the stabilizing materials on the flocculation of the lattices. He concluded that entropic effects may govern the stability in nonaqueous dispersions, whereas enthalpic effects are dominant in aqueous systems. As mentioned above, for the lattices used in their work, electrostatic repulsion is not recognized.

For the lattices used in the present work, however, considerable negative charges are present, which must have an effect on the latex stability. Accordingly, V_T should be expressed by eq 4. For the present case, however, the thickness of the adsorbed layer, δ , and the concentration in the adsorbed layer, c , in eq 5 cannot be determined. Moreover, the determination of the values of ψ_1 and χ_1 is very difficult. Accordingly, the calculation of the total potential energy of interaction using eq 4 is impossible for the present systems. For lattices in both the MM and the AM series, V_R decreases with increasing nonionic surfactant content as shown in Figures 2-7. On the other hand, owing to the increase in the thickness of the adsorbed layer of nonionic

surfactant, V_A should decrease with increasing nonionic surfactant content. ΔG should be repulsive for the present systems and it seems to increase with increasing nonionic surfactant content.

Effect of the Kinds of Nonionic Surfactants. As shown in Table IV, the order of the ccc values for AN-ST copolymer lattices is EOO > EON > EOS for the three electrolytes investigated. The surfactants used for the preparation of these lattices are 50/50 blends of SLS/EO, SLS/ENP, and SLS/ESO, respectively, as described before. The HLB values of EO, ENP, and ESO are 9.9, 13.3, and 15.1, respectively, and therefore the values of the ccc were found to increase as the HLB value of the nonionic surfactant used decreased. That is, the ccc of the lattices increases with increasing hydrophobic characteristics of the nonionic surfactant used.

The values of the slopes of the stability curves given in Table IV show that the order of the slopes is EOS > EON > EOO for all three electrolytes.

As shown in Figures 8-10, the shapes of the mobility curves for the different nonionic surfactants are all quite similar to each other, for each of the three electrolytes. These figures show that the mobility of the latex particles decreases with decreasing HLB value of the nonionic surfactant in the region of low electrolyte concentration. They also show that lattices prepared using nonionic surfactants having low HLB values are more covered by the nonionic surfactant than those prepared with surfactants of high HLB. The concentration ranges over which the mobility remained almost constant increase with decreasing HLB value of the nonionic surfactant. A remarkable decrease in the mobility was also observed just before the ccc of the lattices. The electrolyte concentration at which this decrease in mobility occurs shifts to higher concentrations as the HLB value of the nonionic surfactant decreases. This indicates that a latex prepared using a nonionic surfactant which has a high HLB value is more strongly influenced by added electrolyte than one prepared using a nonionic surfactant having a low HLB value.

Taking into consideration these experimental results, the degree of surface coverage or the thickness of the layer of nonionic surfactant seems to increase with decreasing HLB value of nonionic surfactant.

References and Notes

- R. H. Ottewill and D. J. Wilkins, *Trans. Faraday Soc.*, **58**, 608 (1962).
- G. A. Johnson, J. Goldfarb, and B. A. Pethica, *Trans. Faraday Soc.*, **61**, 2321 (1965).
- R. H. Ottewill and J. N. Shaw, *Discuss. Faraday Soc.*, **42**, 154 (1966).
- R. H. Ottewill and J. N. Shaw, *J. Colloid Interface Sci.*, **26**, 110 (1968).
- A. Kotera, K. Furusawa, and K. Kudo, *Kolloid-Z. Z. Polym.*, **240**, 837 (1970).
- J. H. Schenkel and J. A. Kitchener, *Trans. Faraday Soc.*, **56**, 161 (1960).
- N. Dezelic, J. J. Petres, and Gj. Dezelic, *Kolloid-Z. Z. Polym.*, **242**, 1142 (1970).
- K. G. Mathai and R. H. Ottewill, *Trans. Faraday Soc.*, **62**, 750, 759 (1966).
- S. P. Jain and S. N. Srivastava, *Kolloid-Z. Z. Polym.*, **242**, 1201 (1970).
- R. H. Ottewill, M. C. Rastogi, and A. Watanabe, *Trans. Faraday Soc.*, **56**, 854 (1960).
- R. H. Ottewill and M. C. Rastogi, *Trans. Faraday Soc.*, **56**, 866, 880 (1960).
- R. H. Ottewill and A. Watanabe, *Kolloid-Z.*, **170**, 38, 132 (1960).
- R. H. Ottewill and T. Walker, *Kolloid-Z. Z. Polym.*, **227**, 108 (1968).
- J. T. Davies, *Proc. Int. Congr. Surface Activity*, **2nd**, **1**, 426 (1957).
- W. C. Griffin, *J. Soc. Cosmet. Chem.*, **5**, 249 (1954).
- M. Kerker, H. E. Bowman, and E. Matijević, *Trans. Faraday Soc.*, **56**, 1039 (1960).
- M. E. Woods, J. S. Dodge, and I. M. Krieger, *J. Paint Technol.*, **40**, 541 (1968).
- D. H. Napper, *J. Colloid Interface Sci.*, **32**, 106 (1970).
- D. H. Napper, *J. Colloid Interface Sci.*, **33**, 384 (1970).
- D. H. Napper and A. J. Netschey, *J. Colloid Interface Sci.*, **37**, 528 (1971).

Photohydrogenation of Ethyne and Ethene on the Surface of Titanium Dioxide

A. H. Boonstra* and C. A. H. A. Mutsaers

Philips Research Laboratories, Eindhoven, The Netherlands (Received March 31, 1975)

Publication costs assisted by Philips Research Laboratories

Titanium dioxide samples were illuminated in the near-uv in an atmosphere of ethyne. The reaction products were analyzed with a mass spectrometer. When the TiO_2 powder was previously outgassed at 90° the main products of the gas mixture after the illumination were methane, ethene, ethane, and propane. When the TiO_2 was outgassed at 500° the number of OH groups on the surface was strongly reduced. In this case no hydrogenated products could be observed after illumination but benzene was formed both in the dark as well as under illumination. In the presence of ethene, the irradiation of TiO_2 samples covered with a large number of Ti-O-H groups resulted in the formation of saturated hydrocarbons such as, methane, ethane, propane, and *n*-butane. However, after illumination of a TiO_2 sample outgassed at 500° , only the dimerization product, butene, was formed. In all the measurements no oxygen-containing hydrocarbons were detected. From the results it is concluded that under these circumstances the formation of hydrogen atoms is the governing factor in the mechanism of the photoreaction on titanium dioxide.

Introduction

Several studies have been made of the photocatalytic reactions of gases with TiO_2 powders. Under illumination in the near-uv an irreversible adsorption of O_2 was observed.¹⁻⁷ The up-take of oxygen during irradiation depends strongly on the pretreatment of the powder. It was found that the photoactivity of the TiO_2 for O_2 adsorption was determined by the number of OH groups remaining on the surface of the powder.⁷

A decisive mechanism for the photoreaction process on TiO_2 has not been reported. Some authors suggested the formation of hydroxyl radicals as the first step of the photoreaction of TiO_2 .^{8,9} Korsunovskii⁸ reported that hydroxyl radicals are formed as a result of the interaction of water and oxygen with illuminated TiO_2 . The existence of these radicals was determined by the hydroxylation of benzene. Völz⁹ interpreted his results of ESR measurements of illuminated TiO_2 in terms of the formation of OH radicals. However no H_2O_2 was observed when a suspension of TiO_2 ^{3,8,10,11} in water was illuminated in the near-uv whereas in the case of ZnO ^{10,12-15} H_2O_2 was easily detected under similar conditions. On TiO_2 powders illuminated in an oxygen atmosphere also no H_2O_2 was formed.¹⁶

Bickley et al.¹⁷ found that the photooxidation of 2-propanol to acetone on TiO_2 powder could only be sustained when oxygen was present in the gas phase. They suggested that the 2-propanol was oxidized by oxygen preadsorbed on the TiO_2 surface. Formenti et al.^{18,19} measured the photooxidation of alkanes on TiO_2 and concluded that in the absence of oxygen no reaction took place. The oxidation of the alkanes only occurred in the simultaneous presence of TiO_2 , oxygen, and uv irradiation.

Calvert et al.¹⁵ who studied the photochemical synthesis of H_2O_2 in ZnO suspensions, found, using ^{18}O enriched oxygen, that the oxygen in the hydrogen peroxide originated entirely from the oxygen gas. Therefore only the hydrogen of the H_2O_2 has to come from the solution or from the surface of the ZnO powder.

The role of hydrogen in the photoreaction of methanol and ethanol on the surface of ZnO and TiO_2 was shown in the experiments of Cunningham et al.²⁰ They described the

formation of formaldehyde and acetaldehyde as photo-assisted dehydrogenation processes. Besides ethene, methane and ethane were measured as main components formed during illumination. The presence of the last two compounds has to be considered as results of hydrogenation processes.

Comparing the properties of TiO_2 powders treated with small amounts of H_2O_2 with those of TiO_2 on which O_2 was photoadsorbed¹⁶ we concluded that the up-take of oxygen under illumination of TiO_2 was not caused by the formation of H_2O_2 . The photoreaction of TiO_2 was described as the formation of Ti_2O radicals on the surface and of hydrogen atoms which react immediately with the oxygen present to form water.

The aim of our studies was to investigate a possible existence of hydrogen atoms during the illumination in the near-uv of TiO_2 . The TiO_2 samples were therefore irradiated in an atmosphere of ethyne or of ethene which can trap hydrogen atoms liberated from the TiO_2 surface. By analyzing the reaction products in the gas mixture after illumination it should be possible to decide whether hydroxyl radicals or hydrogen atoms are the governing factor in the mechanism of the photoreaction of titanium dioxide.

Experimental Section

The illumination experiments were mainly carried out on the TiO_2 powder (P25) of the anatase modification supplied by Degussa, Frankfurt. The surface area of the powder was determined by the BET method at -195° using krypton. Assuming the area of a krypton atom to be 19.5 \AA^2 , the specific surface area of the powder was found to be $56 \text{ m}^2 \text{ g}^{-1}$.

Samples of about 2.0 g were placed in a bulb of fused silica, which was sealed to the vacuum system. During evacuation some samples were heated at 90° whereas, to decrease strongly the number of Ti-O-H groups on the surface, other samples were heated at about 500° . The rest of the system was heated during evacuation at about 150° . Ultimate vacuum of the order of 10^{-5} Nm^{-2} was attainable by the pumping unit consisting of a mercury diffusion pump backed by a rotary oil pump. The adsorption system²¹ was

protected against vapors of the pumping unit by a liquid N₂ trap. After about 2 hr of evacuation, pure oxygen at a pressure of about 10³ N m⁻² was admitted and the heating was continued for 30 min. Then the system was cooled to room temperature and evacuated again. By this procedure the Ti³⁺ ions formed on the surface of the sample during outgassing were reoxidized to Ti⁴⁺.

The gases used for the illumination experiments were supplied by the Matheson Co., N.J. The grade of purity was 99.98 mol % for ethene and 99.8 mol % for ethyne. The ethyne was purified in the vacuum system by freezing it out at 90°K and pumping off the volatile compounds. The ethyne was then slowly distilled to another trap and the residual gases were also pumped off. The gases were analyzed by a Perkin-Elmer Type 607-1000, partial pressure analyzer. To diminish the zero effect of the mass spectrometer, the analyzer was outgassed at 300° for several hours before each measurement.

After outgassing the TiO₂ samples, at room temperature a known amount of ethene or ethyne was admitted. Pressure changes were measured by a MacLeod manometer. After 30 min the sample was exposed to uv light of 320–390 nm from a water-cooled Philips P 500W spectrum lamp and pressure changes were measured again. During the illumination, the bulb containing the TiO₂ sample was vigorously shaken by a Vortex Genie mixer from Wilten Holland to ensure that all the powder was illuminated. A detailed description of the procedure is given elsewhere.⁷

After illumination, the gases were condensed in a liquid nitrogen trap. The amount of noncondensable gases was measured by a MacLeod manometer and analyzed. Then part of the system containing the TiO₂ sample was closed. The gases present in the liquid nitrogen trap were fractionated by a distillation process. The composition of each fraction was analyzed with the mass spectrometer.

Results

Photohydrogenation of Ethyne. After evacuating the TiO₂ sample at 90° for 2 hr, about 40 μmol of ethyne was admitted at room temperature. After 30 min both pressure and cracking pattern were unchanged. Then the sample was illuminated with 320–390-nm light for a period of 5 hr. Only a small decrease in pressure was observed. After illumination it was found that the TiO₂ powder had kept its white color. A section of the system was cooled with liquid nitrogen. Only part of the gas was condensed in the trap. The amount of the gas which was not condensable at 78°K was measured to be about 5 μmol. The gas was analyzed in the mass spectrometer and was found to be methane.²²⁻²⁴ After pumping off the methane the condensed gases were fractionally distilled. The fraction which was volatile at 90°K was distilled again. Then the amount of gas was measured at room temperature and was found to be 22 μmol. Mass spectrometric analyses indicate a mixture of ethene and ethane at a ratio of about 2:1. After evacuation, the next fraction (90–120°K) was measured. The total amount was about 12 μmol and consisted of a mixture of 70 vol % ethyne and 30 vol % propane. In the temperature range from 120°K to room temperature, water and small amounts of CO were observed. Because no CO was detected in the volatile gas mixtures, the carbon monoxide measured at higher temperatures was bound to be formed in the analyzer, probably due to a reaction of the water with a carbide layer on the filament. After the analyses of the gas mixture, the TiO₂ powder was slowly heated to 70° under evacua-

tion. During this outgassing the gases desorbed from the sample were analyzed. Only small amounts of H₂O and CO were detected. No indications were found of the existence of oxygen-containing hydrocarbon compounds in the desorbed gas.

Another TiO₂ sample was evacuated at 500° for 2 hr. After outgassing, the heating was continued for 30 min in oxygen at a pressure of 10³ N m⁻². The sample was then cooled in oxygen to room temperature and evacuated again. A known amount of ethyne was admitted to the sample and the pressure changes were measured as a function of time. In this case a considerable decrease in pressure was observed. After 30 min the gas was frozen out in the liquid N₂ baffle. Then the part of the system containing the sample was closed off. The baffle in the other part of the system was warmed to room temperature and the liberated gas was analyzed with the mass spectrometer. From the cracking patterns it was concluded that a large amount of the ethyne had been converted into benzene.

Another amount of ethyne was admitted to the sample and the illumination of the sample was started. After 5 hr irradiation no color change of the TiO₂ powder was observed. The gas was collected in the liquid N₂ trap. Only a very small amount of the gas could not be condensed and was found to be methane. The rest of the gas was analyzed following the same procedure as used for the 90° sample. From the cracking patterns it was concluded that the main gas formed during the reaction was benzene. Except a very small amount of methane no hydrogenated products of ethyne were observed.

When both powders were illuminated only for a few minutes then the same products were formed. Because of the small amounts of gases formed in this time no quantitative results could be obtained.

Photohydrogenation of Ethene. The illumination experiments on TiO₂ samples were repeated using ethene. After irradiation, the gas mixture was analyzed as described above. For the TiO₂ samples evacuated at 90° in the dark no pressure changes and no changes in cracking pattern were observed. Analyzing the gas, which was about 1 hr in contact with the powder, it was shown that the only gas present was ethene. During illumination a slow decrease in pressure was measured. After 5-hr illumination no color change of the white powder was observed. The gas was then analyzed as mentioned before.

The hydrogenation of ethene during the illumination of the TiO₂ sample covered with Ti–O–H groups on its surface resulted in the formation of the gases methane, ethane, propane, *n*-butane, and small amounts of pentane. It is clear that the hydrogenation was accompanied by dimerization and fragmentation processes. No oxygen-containing hydrocarbon products were detected in the gas mixture. Only small amounts of H₂O and CO were found in the last stage of the gas analysis. This means that small amounts of CO were formed on the filament of the mass spectrometer.

The reactivity of the TiO₂ sample, pretreated at 500°, with ethene was also investigated. In the dark a large decrease in pressure was observed. After 15 min the gas mixture was analyzed and butene was shown to be the main product. During the illumination a decrease in pressure of a fresh portion of ethene was also found. Here again, after 5-hr irradiation no color change of the TiO₂ powder was observed. The gas mixture was analyzed. Apart from ethene a considerable amount of butene was found. From the comparison of the measured cracking patterns of butene with

those given for butene-1, butene-2 and 2-methyl-1-propene,²²⁻²⁴ we concluded that in our case butene-1 was formed as the main product. Except for a small amount of methane, no hydrogenated products were detected on illuminating a TiO₂ sample outgassed at 500°.

Discussion

On the illumination of TiO₂ samples in an atmosphere of ethyne or ethene it was found that saturated hydrocarbon compounds were formed, only when Ti-O-H groups were present on the surface of TiO₂. The main compounds in the illumination process using ethyne were methane, ethene, ethane, and propane whereas in the case of ethene the compounds methane, ethane, propane, and *n*-butane were found. No oxygen-containing hydrocarbons could be detected even after warming the powders to 70°, which makes the formation of OH radicals very unlikely. The appearance of small amounts of CO was considered to arise mainly from the interaction of water with the carbide layer on the filament because the volatile fractions did not contain any CO.

During illumination no color changes of the powder were observed, so it was concluded that no carbon had been deposited on the TiO₂ surface. This was confirmed by the quantitative measurements of the reaction products in the experiments with ethyne. It was found that no hydrocarbons remained on the surface of TiO₂. Therefore the hydrogen used for the formation of saturated hydrocarbons must have originated from the Ti-O-H groups on the surface. In our opinion, as a result of the illumination of the TiO₂ powder, hydrogen atoms are formed which react immediately with the unsaturated hydrocarbons present.

Hardly any hydrogenation products were detected after illumination of a powder outgassed at 500°. This was due to the strong decrease in the number of Ti-O-H groups on the surface. In this case a fast polymerization of the unsaturated hydrocarbons was observed. Admitting ethyne at room temperature to the outgassed TiO₂ sample, benzene was formed in the dark as well as under illumination, whereas butene-1 was produced from ethene. No oxygen-containing hydrocarbon compounds were observed, which again excludes the formation of OH radicals.

These results are in agreement with those of Formenti et al.^{18,19} They found that the oxidation of alkanes took place only in the simultaneous presence of the TiO₂, uv irradiation, and oxygen.

The hydrogenation of olefins to form the corresponding paraffins was earlier reported by Lake and Kemball²⁵ who studied the deuteration of alkenes with TiO₂ as catalyst. They found that in the temperature range of 250–400°, the formation of the corresponding alkanes was the main product.

Ethene was hydrogenated even at room temperature when a mixture of hydrogen and ethene was exposed to ZnO as shown by Kokes et al.^{26,27}

Studying the photoreaction of TiO₂ with ethanol, Cunningham and coworkers²⁰ found acetaldehyde, ethane, and

ethene as the main components, whereas in the case of methanol, formaldehyde and methane were the main products. The formation of aldehydes was ascribed to the dehydrogenation capacity of the outgassed rutile surface. Ethene was formed as a result of a dehydration of ethanol. These reactions may result in an increase of the number of OH groups on the surface. The formation of ethane may be explained by the reaction of ethene with the hydrogen atoms formed during illumination.

It was demonstrated by Calvert et al.¹⁵ that the oxygen in the hydrogen peroxide, formed during the illumination of ZnO, originates entirely from the oxygen gas. This can be explained as the reaction of hydrogen atoms formed during illumination of ZnO with the oxygen gas.

Goetz and Inn²⁸ suggested a photographic process based on the photocatalytic behaviour of TiO₂ and ZnO in the reduction of silver ions whereas Jonker et al.²⁹ reported that a coating of TiO₂ illuminated in the near-uv can reduce metal ions such as, Cu²⁺, Ag⁺, Pd²⁺, Pt²⁺, and Au⁺, thereby creating a latent metallic image. The formation of hydrogen atoms during the illumination of TiO₂ or of ZnO can easily explain that only in the case of noble metal ions a reduction to metal was found.

Acknowledgment. We are indebted to Dr. J. C. M. Brokken-Zijp for many valuable discussions.

References and Notes

- (1) D. R. Kennedy, M. Ritchie, and J. Mackenzie, *Trans. Faraday Soc.*, **54**, 119 (1958).
- (2) R. D. Murley, *J. Oil. Colour. Chem. Assoc.*, **45**, 16 (1962).
- (3) I. S. MacLintock and M. Ritchie, *Trans. Faraday Soc.*, **61**, 1007 (1965).
- (4) G. Munuera and F. Conzalez, *Rev. Chim. Miner.*, **4**, 207 (1967).
- (5) R. I. Bickley and F. S. Stone, *J. Catal.*, **31**, 389 (1973).
- (6) R. I. Bickley and R. K. M. Jayanty, *Discuss. Faraday Soc.*, **58**, in press.
- (7) A. H. Boonstra and C. A. H. A. Mutsaers, *J. Phys. Chem.*, **79**, 1694 (1975).
- (8) G. A. Korsunovskii, *Russ. J. Phys. Chem.*, **34**, 241 (1960).
- (9) H. G. Volz, G. Kampf, and H. G. Fitzky, *Farbe Lack*, **78**, 1037 (1972).
- (10) M. C. Markham and K. J. Laidler, *J. Phys. Chem.*, **57**, 363 (1953).
- (11) G. Irick, *J. Appl. Polym. Sci.*, **16**, 2387 (1972).
- (12) E. Bauer and C. Neuweiler, *Helv. Chim. Acta*, **10**, 901 (1927).
- (13) G. Winter, *Nature (London)*, **163**, 326 (1949).
- (14) T. R. Rubin, J. G. Calvert, G. T. Rankin, and W. McNevin, *J. Am. Chem. Soc.*, **75**, 2850 (1953).
- (15) J. G. Calvert, K. Theurer, G. T. Rankin, and W. McNevin, *J. Am. Chem. Soc.*, **76**, 2575 (1954).
- (16) A. H. Boonstra and C. A. H. A. Mutsaers, *J. Phys. Chem.*, **79**, 1940 (1975).
- (17) R. I. Bickley, G. Munuera, and F. S. Stone, *J. Catal.*, **31**, 398 (1973).
- (18) M. Formenti, F. Juillet, P. Meriaudeau, *Bull. Soc. Chim. Fr.*, 69 (1972).
- (19) M. Djeghri, M. Formenti, F. Juillet, and S. J. Teichner, *Discuss. Faraday Soc.*, **58**, in press.
- (20) J. Cunningham, E. Finn, and M. Samman, *Discuss. Faraday Soc.*, **58**, in press.
- (21) A. H. Boonstra, *Philips Res. Rept. Suppl.*, **3** (1968).
- (22) Ch. Biguenet, *Vide*, **27**, No. 161 (1972).
- (23) A. Cornu and R. Massot, "Compilation of Mass Spectral Data", Heyden & Son, London, 1966.
- (24) "Eight Peak Index of Mass Spectra", Mass Spectrometry Data Centre, AWRE, Aldermaston, Reading, England, 1970.
- (25) I. J. S. Lake and C. Kemball, *Trans. Faraday Soc.*, **63**, 2535 (1967).
- (26) A. L. Dent and R. J. Kokes, *J. Phys. Chem.*, **73**, 3781 (1969).
- (27) W. C. Conner and R. J. Kokes, *J. Phys. Chem.*, **73**, 2436 (1969).
- (28) A. Goetz and E. C. Y. Inn, *Rev. Mod. Phys.*, **20**, 131 (1948).
- (29) H. Jonker, L. K. H. v. Beek, C. J. Dippel, C. J. G. F. Janssen, and E. J. Spiertz, *J. Photogr. Sci.*, **19**, 96 (1971).

Polarized Single-Crystal Spectra of the Phenazine–Iodine Charge-Transfer Complex¹

Basil G. Anex^{*2} and Govind Prasad

Department of Chemistry, New Mexico State University, Las Cruces, New Mexico 88001 and Department of Chemistry, University of New Orleans, New Orleans, Louisiana 70122 (Received July 24, 1974; Revised Manuscript Received June 4, 1975)

Publication costs assisted by the National Institutes of Health

Visible and quartz-ultraviolet single-crystal reflection spectra have been obtained with the incident radiation polarized along the *a*, *b*, and *c* crystallographic axes of the 1:1 complex of phenazine and iodine and the Kramers–Kronig analysis applied to yield the corresponding absorption spectra. It has thus been possible to locate and characterize an intermolecular charge-transfer transition that occurs in this crystal at 36.7 kK with a crystal extinction coefficient of $5.91 \times 10^4 M^{-1} \text{ cm}^{-1}$. The intramolecular phenazine transitions occurring in solution at approximately 40 and 28 kK have also been characterized in the crystal and both shown, in contrast to phenazine's hydrocarbon analog anthracene, to have predominantly long-axis polarization. This latter result is consistent with the general features of polyacene π -electron theory.

Introduction

As part of a continuing study of the polarized single-crystal spectra of charge-transfer complexes,^{3,4} an investigation of the phenazine–iodine system has been undertaken. This work has led to the characterization of the intermolecular charge-transfer band that occurs in the quartz-ultraviolet region of the spectrum for this crystal. At least equally important, however, is the fact that one has here an excellent vehicle for the study of the phenazine molecule as such, since the phenazine–phenazine interactions are significantly reduced over those found in the pure crystal and the crystal structure of the complex is relatively simple. Information has thus become available on a well-studied polyacene system so-substituted that the accidental zero-order degeneracy that plays a crucial role in the conventional description of the polyacene excited states is lifted.⁵ An interesting context is thus provided in which to evaluate in rather general terms the explanation that π -electron theory offers for the nature of the low-lying electronic transitions of the acenes.

This study constitutes an additional example of the utility of using charge-transfer crystals to study the spectra of their component molecules as such.⁶

Experimental Section

Preparation of Crystals. Phenazine and iodine were both obtained from Baker Chemical Co. as "analyzed reagents" and used without further purification. When these materials were dissolved in equimolar ratio in ethyl ether the reddish-brown complex at once precipitated. This product was filtered free of the mother liquor and recrystallized from chloroform to obtain well-formed crystals suitable for spectral study.

Spectral Measurements. The reflection spectra reported here were obtained using essentially the apparatus and procedures described previously.⁷

Results

Uchida⁸ reports that phenazine–iodine crystals prepared as described above belong to the orthorhombic *Pbcn* space group and have (100) as the well-developed face. The latter observation, combined with goniometric measurement of interfacial angles, led to the identification of another natu-

rally occurring face as (010). Reflection spectra were then obtained on the (100) and (010) faces, so that spectra corresponding to the *a*, *b*, and *c* crystallographic axes were available. These are reported in Figure 1 and the spectral parameters that characterized them summarized in Table I.

The Kramers–Kronig Analysis

The absorption spectra reported in Figure 2 have been derived from the reflection spectra through application of the Kramers–Kronig transformation. This method and the specific procedures followed here (including those used to approximate the effects of reflectivities in experimentally inaccessible regions) have been discussed elsewhere.⁷

Spectral parameters derivable from Figure 2 are summarized in Table II.

Discussion

The solution absorption spectrum of phenazine shows two strong, clearly allowed regions of absorption in the quartz-ultraviolet. One of these peaks near 250 $m\mu$ and the other near 360 $m\mu$.^{9–11} Clearly, the *a* and *c* spectra of Figures 1 and 2 possess regions of absorption that may be associated with these phenazine absorptions. In what follows, then, these allowed bands of phenazine will be discussed first. In a subsequent section the two absorptive regions observed in the *b* polarization will be examined.

The 250- and 360- $m\mu$ Bands of Phenazine. As is indicated in the Introduction, the phenazine molecule draws at least part of its significance from the fact that it is derived from an extensively studied conjugated hydrocarbon by rather straightforward aza substitution that does not change its symmetry. It thus provides an attractive system for testing one's understanding of the acenes and examining the transferability of methods developed for the study of hydrocarbons to analogous hetero systems.^{12–14}

It is clearly desirable to have the experimental situation with respect to such systems as phenazine characterized as precisely as possible. Such characterization should of course include polarization determinations, and thus Mikami¹⁵ and Zanker and Dreyer¹¹ have studied the strongly allowed bands of the phenazine single crystal in direct absorption. These studies were, however, complicated by two factors: the bands were obviously rather strongly perturbed

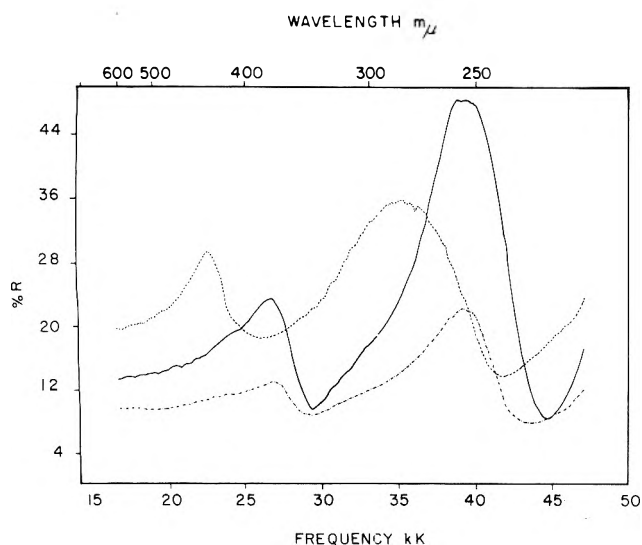


Figure 1. The polarized single-crystal reflection spectra obtained for phenazine-iodine when the incident radiation is so polarized that its electric vector vibrates parallel to the *a* axis (—), the *b* axis (---), and the *c* axis (· · · · ·). These reflectivities are relative values, having been taken vs. an aluminum mirror, and must be multiplied by approximately 0.9 to be placed on an absolute scale.

TABLE I: Characteristics of the Reflection Spectra of the Phenazine-Iodine Single Crystal

Crystal direction	Position of max		Max reflectivity, %
	Wavelength, $m\mu$	Energy, kK	
<i>a</i>	254	39.4	45
	374	26.7	21
<i>b</i>	284	35.2	33
	444	22.5	27
<i>c</i>	256	39.1	20
	373	26.8	12

in the crystal and the crystallographic face being studied was not fully identified. The present investigation involves a well-defined situation with minimal solid state perturbations in which to determine the polarization of the phenazine bands.

As pointed out previously, the 250- and 360- $m\mu$ phenazine bands both appear in the *a* and *c* polarizations. Since the *b* axis of the crystal and the short axis of the phenazine molecule coincide, the short axis transitions cannot appear on *a* and *c* in the orthorhombic system being dealt with here.⁸ One is thus immediately led to the conclusion that both phenazine absorptions must have, assuming $\pi \rightarrow \pi^*$ origins and thus in-plane transition moments, long-axis polarization.

The long-axis assignments for the phenazine transitions find confirmation in quantitative consideration of the intensities observed along the three crystal axes. In Table III, therefore, are presented the relative *a*, *b*, and *c* axis intensities expected on the basis of the crystal structure⁸ for transitions polarized along the *x* and *y* phenazine molecular axes.¹⁶ From these data one deduces a predicted *a/c* dichroic ratio of approximately 2.9 for long-axis polarized transitions. The comparable observed dichroic ratio (based on ϵ_{\max} values) for the 360- $m\mu$ band is 2.4 and that for the 250- $m\mu$ band is 2.3. The agreement for long-axis polariza-

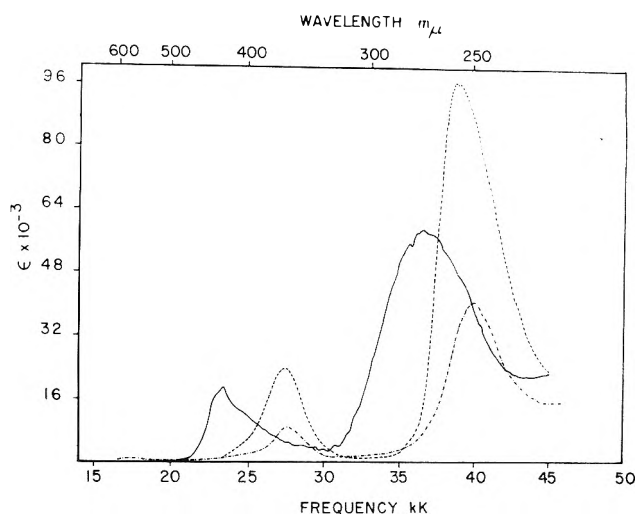


Figure 2. The Kramers-Kronig absorption spectra corresponding to the reflection spectra reported in Figure 1: (---) *a*-axis polarization; (—) *b*-axis polarization; (· · · · ·) *c*-axis polarization. (The reflection data were converted to an absolute basis prior to performing the analyses.)

TABLE II: Characteristics of the Kramers-Kronig Absorption Spectra of the Phenazine-Iodine Single Crystal

Crystal direction	Position of max		Crystal ϵ , $M^{-1} \text{ cm}^{-1}$
	Wavelength, $m\mu$	Energy, kK	
<i>a</i>	258	38.8	96,100
	363	27.5	23,800
<i>b</i>	272	36.7	59,100
	426	23.5	19,100
<i>c</i>	250	40.0	40,500
	362	27.6	8,800

tion is thus good, especially when one notes that the spectra in Figure 2 appear to suffer some baseline problems, and any correction for this situation would tend to affect the weaker *c*-axis spectrum more acutely.

The long-axis polarization of the 250- and 360- $m\mu$ phenazine bands indicates that the corresponding excited states are of B_{3u} symmetry¹⁶ and would thus be identified in Platt notation¹⁷ as the 1B_b and 1L_b states, respectively. That the lowest-energy strong absorption in this system is dominated by the 1L_b rather than the 1L_a band is markedly different than the situation that obtains for anthracene^{5,18} and consistent with previous single-crystal absorptive studies on phenazine.^{11,15,19} The results reported here are, moreover, relatively unambiguous, in that sufficient polarization data exist to make the assignments complete for an "oriented gas model" and the close correspondence between the solution and crystal spectra (compare Figure 2 of ref 15 and Figure 2 of this work) make such a model plausible.

The 1L_b band of phenazine has clearly undergone a marked increase in intensity in comparison to the corresponding band in anthracene. The *a* and *c* intensities reported in Table II for the 360- $m\mu$ band both correspond to solution ϵ values of about $11,000 M^{-1} \text{ cm}^{-1}$. The 1L_b band of anthracene, on the other hand, is usually taken to be

TABLE III: Projection of Unit Vectors Oriented along the Phenazine Molecular Axes onto the Principal Directions Studied in this Work^a

Phenazine axis	Projection on <i>a</i>	Projection on <i>b</i>	Projection on <i>c</i>
Short axis (<i>y</i>)	0	1	0
Long axis (<i>x</i>)	0.742	0	0.258

^a Projections are in terms of \cos^2 so as to be directly proportional to intensity.

buried under the 1L_a band,¹⁸ which in turn is highly structured and has an ϵ_{\max} in solution of $9000 M^{-1} \text{ cm}^{-1}$. A conservative estimate of the upper limit of ϵ_{\max} for the anthracene 1L_b band would probably be, judging in part from the situation that obtains for naphthalene,¹⁸ about 10% of the 1L_a band. The 1L_b band would thus appear to show at least a tenfold increase in intensity in phenazine compared to anthracene.

The growth in intensity noted for the phenazine 1L_b band is understandable in terms of the accepted description of the polyacene spectra.^{5,18} The 1B_b and 1L_b excited states of anthracene are thus viewed as corresponding essentially to those that arise from first-order configuration interaction between two low-lying configurations degenerate in the LCAO-SCF approximation^{5a} and whose transition moment matrix elements with the ground state configuration are parallel and equal in magnitude. The weakness of the 1L_b band then reflects a mutual cancellation of the zero-order transition moments in the first-order calculation. When one moves from anthracene to phenazine, the aza substitutions remove the zero-order degeneracy characteristic of the all-carbon analog, and one no longer expects either equal mixing of the crucial configurations^{12,13} or equal first-order transition moments. Since the essential features that lead to the weakness of the 1L_b band in anthracene are missing in phenazine, it is not surprising, within this theoretical context, that the intensity of this band is significantly enhanced in phenazine. This natural explanation of the effects of the observed changes in the 1L_b band in going from anthracene to phenazine provides additional support for the validity of the broad outlines of accepted π -electron theory of the acenes.

Bands of *b* Polarization. Figures 1 and 2 show two regions of strong *b*-polarized absorption, one having an ϵ_{\max} of 59,100 at 272 $m\mu$ and the other an ϵ_{\max} of 19,100 at 426 $m\mu$. These bands could have three origins: short-axis-polarized phenazine transitions, long-axis-polarized iodine transitions, and transitions involving charge-transfer between the phenazine and iodine moieties in the crystal.

Free iodine itself possesses an absorption band at about 500 $m\mu$ which has long-axis polarization.²⁰ It is well known that this band undergoes a typical blue shift when iodine is involved in charge-transfer complex formation, and Mulliken and Person²⁰ indicate its occurrence in the 410–430- $m\mu$ region in complexes involving *n*-nitrogen donors. It would thus appear that one may safely associate the *b*-polarized band peaking at 426 $m\mu$ in the crystal absorption spectra with the blue-shifted 500- $m\mu$ iodine band.

In addition to shifting to higher energies, the 500- $m\mu$ iodine band also typically undergoes an increase in intensity on complex formation, with Mulliken and Person quoting an ϵ range of 1000–2600 $M^{-1} \text{ cm}^{-1}$ for complexes involving *n*-nitrogen donors. The crystal ϵ value of 19,100 $M^{-1} \text{ cm}^{-1}$

reported in Table II for the 426- $m\mu$ band must be divided by three for comparison with the Mulliken–Person data, since the latter are for solution studies.²¹ Even then, the crystal value considerably exceeds the upper limit of the quoted solution range. The evaluation of this apparently large crystal intensification should, however, include recognition of the fact that the band in question is assumed to acquire its intensity via interaction with the strongly allowed band found at 180 $m\mu$ in iodine vapor and with the charge-transfer band.²⁰ That the details of such interactions may be different in the crystal than in solution would not be surprising, especially in light of the fact that in the crystal each iodine is interacting with two donors, instead of one as in solution. Moreover, mixing of crystal states of *b* polarization could provide a mechanism for intensification of the iodine transition completely lacking in solution.

The other prominent crystal absorptive feature appearing with *b* polarization is that peaking at 272 $m\mu$. This band has no obvious counterpart in either of the component spectra, and thus is reasonably assigned to charge transfer. This assignment is further supported by the fact that Mulliken and Person (see Table 10-2 of ref 20) report that the charge-transfer bands found in solution for a number of *n*-nitrogen donors fall in the range 229–278 $m\mu$ and possess ϵ values in the range 21,000–31,000 $M^{-1} \text{ cm}^{-1}$.²²

It is tempting to assume that the frequency of the charge-transfer band in the crystal provides information that is transferable to the 1:1 complex that occurs in solution. This may indeed be the case, in that there are examples where the crystal and solution charge-transfer transitions for the same complex correspond rather closely in energy.²³ Some caution must be observed in this regard, however, since in at least one case a rather significant energy difference has been observed for corresponding crystal and solution charge-transfer transitions.³ In addition to the various solid-state effects that may arise here, there is, of course, no guarantee that the donor and acceptor molecules even have the same mutual orientation in solution and crystal.

The short-axis-polarized 1L_a band of phenazine is also expected to occur in the *b*-axis crystal spectrum. While no obvious manifestation of the transition is apparent in Figure 2, the 426- $m\mu$ band does display a rather intense short-wavelength tail that could conceal a band of rather moderate intensity. Moreover, careful examination of the corresponding reflection spectrum reveals evidence of structure on its high-energy side.

Jaffé and Orchin^{18a} quote an ϵ_{\max} of about 9000 $M^{-1} \text{ cm}^{-1}$ for the 1L_a band of anthracene, which would lead to an expected crystal ϵ of about 27,000 $M^{-1} \text{ cm}^{-1}$. At 400 $m\mu$, where the solution spectra of phenazine in methanol⁹ and in ethanol^{10,11} reveal a shoulder of appreciable intensity, the *b*-axis spectrum still possesses a crystal ϵ value of 11,000 $M^{-1} \text{ cm}^{-1}$. This region could, therefore, if one is willing to assume something of an intensity loss on aza substitution of anthracene, contain the 1L_a band.

If the red shift of the low-energy portion of the 363- $m\mu$ phenazine band that Perkampus⁹ noted upon protonation is also a consequence of charge-transfer formation involving the nonbonding orbitals, then the 1L_a band may lie further to the red in the crystal than suggested above and reflect a concomitant less drastic loss of intensity on aza substitution. Such a location of the band would also, of course, tend to reduce the intensity of the blue-shifted iodine band and bring it somewhat more in line with the ϵ value pre-

vously reported for this transition. A definitive placement of the 1L_a band in this crystal, however, will have to await a somewhat higher resolution and probably low-temperature study of the type reported here. Moreover, the location of the 1L_a band in phenazine itself will have to rest on a more detailed study of the uncomplexed material than has been reported to date.^{11,15,19} Until such a study has been carried out, it is probably somewhat premature to speculate on the ordering of the 1L_b and 1L_a bands in phenazine on the basis of more-or-less qualitative observations of the crystal absorption of phenazine currently available.²⁴

References and Notes

- (1) This work has been partially supported by a grant from the National Institutes of Health.
- (2) Correspondence should be directed to this author at the University of New Orleans.
- (3) B. G. Anex and L. J. Parkhurst, *J. Am. Chem. Soc.*, **85**, 3301 (1963).
- (4) B. G. Anex and E. B. Hill, *J. Am. Chem. Soc.*, **88**, 3648 (1966).
- (5) (a) L. Salem, "The Molecular Orbital Theory of Conjugated Systems", W. A. Benjamin, New York, N.Y., 1966. (b) F. L. Pilar, "Elementary Quantum Chemistry", McGraw-Hill, New York, N.Y., 1968.
- (6) C. J. Eckhardt and J. Bernstein, *J. Am. Chem. Soc.*, **94**, 3247 (1972).
- (7) B. G. Anex, *Mol. Cryst.*, **1**, 1 (1966).
- (8) T. Uchida, *Bull. Chem. Soc. Jpn.*, **40**, 2244 (1967).
- (9) H. H. Perkampus, *Z. Phys. Chem. (Frankfurt am Main)*, **6**, 18 (1956).
- (10) F. Kummer and H. Zimmermann, *Ber. Bunsenges. Phys. Chem.*, **71**, 1119 (1967).
- (11) V. Zanker and P. Dreyer, *Z. Angew. Phys.*, **24**, 151 (1968).
- (12) N. Mataga and K. Nishimoto, *Z. Phys. Chem. (Frankfurt am Main)*, **13**, 140 (1957).
- (13) N. Mataga, *Bull. Chem. Soc. Jpn.*, **31**, 463 (1958).
- (14) W. R. Carper and J. Stengl, *Mol. Phys.*, **15**, 121 (1968).
- (15) N. Mikami, *J. Mol. Spectrosc.*, **37**, 147 (1971).
- (16) The x and y molecular axes of phenazine are here taken to be the in-plane long and short symmetry axes, respectively.
- (17) J. R. Platt, *J. Chem. Phys.*, **17**, 484 (1949).
- (18) (a) H. H. Jaffé and M. Orchin, "Theory and Applications of Ultraviolet Spectroscopy", Wiley, New York, N.Y., 1962. (b) J. N. Murrell, "The Theory of the Electronic Spectra of Organic Molecules", Wiley, New York, N.Y., 1963.
- (19) R. M. Hochstrasser, *J. Chem. Phys.*, **36**, 1808 (1962).
- (20) R. S. Mulliken and W. B. Person, "Molecular Complexes", Wiley-Interscience, New York, N.Y., 1969.
- (21) B. G. Anex and N. Takeuchi, *J. Am. Chem. Soc.*, **96**, 4411 (1974).
- (22) As was the case for the solid-state iodine band, the ϵ value of 59,100 $M^{-1} \text{ cm}^{-1}$ reported in Table II for the 272- $m\mu$ band must be divided by 3 for comparison with the results of solution studies.
- (23) H. Kuroda, T. Kunii, S. Hirota, and H. Akamatu, *J. Mol. Spectrosc.*, **22**, 60 (1967).
- (24) Narva and McClure, however, have recently placed the 1L_a band of phenazine some 2.13 kK to the red of the 1L_b band in studies on phenazine-biphenyl mixed crystals. (D. L. Narva, private communication.)

Carbon-13 Spin Relaxation and Methyl Rotation Barriers in the Methylethylenes

Scott W. Collins, Terry D. Alger, David M. Grant,* Karl F. Kuhlmann, and James C. Smith

Departments of Chemistry, University of Utah, Salt Lake City, Utah 84112 and Utah State University, Logan, Utah 84321
(Received March 4, 1975)

Publication costs assisted by the National Institutes of Health

Carbon-13 relaxation times (T_1) and nuclear Overhauser enhancement (NOE) factors are determined for a series of methylethylenes at field strengths of 15.1 and 25.1 MHz and temperatures of 40 and 60°. Subsequent separation of T_1 into contributions from dipolar (T_{1D}) and all other (T_{10}) relaxation mechanisms demonstrates that T_{10} is due essentially to spin-rotation effects (T_{1SR}). Isotropic motion is assumed in the molecules and values are calculated for the effective correlation times of the dipolar ($\tau_{c,eff}$) and spin-rotation ($\tau_{SR,eff}$) mechanisms. These are compared with the mean period of free rotation (τ_f) as computed by the equipartition principle to indicate that motions in these molecules are *not* in the diffusionally controlled limit. Rotations of 10–40° between intermolecular interactions and ratios of $\tau_{c,eff}/\tau_f \simeq 1$ are typical. Values of the barriers (V) to methyl rotation are estimated from the methyl dipolar relaxation contributions; and in those cases where the literature measurements or estimates are available, the NMR results are found to compare favorably with values obtained by other techniques. Data are presented which indicate that motions in all the methylethylenes (with the single exception of *trans*-2-butene) are quite similar and probably near isotropic in character. The results suggest that the motion in *trans*-2-butene is quite unique in that it possesses one very low moment of inertia about the principal axis which passes roughly through the double bond and the two *trans*-methyl groups. Rapid motion about this axis presumably results in considerable anisotropy of motion and in a much more efficient spin-rotation mechanism for *trans*-2-butene than observed in the other methylethylenes.

I. Introduction

Nuclear relaxation times can be used to characterize molecular motion in liquid systems.^{1–6} However, the significance of the motional parameters which are calculated de-

pends upon how well the relaxation data can be fit with an appropriate relaxation model. Within a structurally similar set of compounds, comparisons of similar molecular motions provide opportunities to substantiate the validity of the assigned model. Hence, carbon-13 relaxations in the methylethylenes provide an interesting set of compounds to examine since they possess a variety of motional features

* Address correspondence to this author at the University of Utah, Salt Lake City, Utah 84112.

which affect relaxation processes and yet are somewhat similar in structure.

The total spin-lattice relaxation time (T_1) for a carbon nucleus may be separated into its dipolar (T_{1D}) and all other (T_{10}) mechanistic contributions if the nucleus experiences a nuclear Overhauser enhancement (NOE). This is true since in the region of extreme motional narrowing:^{7,8}

$$T_{1D} = \gamma_S T_1 / 2\gamma_I \eta_{C(H)} \quad (1)$$

and

$$\frac{1}{T_{10}} = \frac{1}{T_1} - \frac{1}{T_{1D}} \quad (2)$$

where $\eta_{C(H)} = \text{NOE} - 1$, and γ_S and γ_I are the gyromagnetic ratios for the S and I nuclei, respectively. The NOE is determined by calculating the ratio between the proton irradiated and nonirradiated signal intensities of the carbon nucleus. The carbon-13-proton dipolar contribution (T_{1D}) to the relaxation time is dominated by intramolecular effects if hydrogens are attached directly to the carbon.^{8,9} Hence values of the molecular rotational diffusion constants (R_i) can be obtained directly from carbon-13 T_{1D} values in the methylethylenes by utilizing the following formulas for the calculation of intramolecular dipolar relaxation times for either isotropic or anisotropic motion:^{1,5,9,10}

$$\frac{1}{T_{1D}} = \frac{N_H \hbar^2 \gamma_C^2 \gamma_H^2}{r_{CH}^6} \tau_{c,\text{eff}} \quad (3)$$

where N_H is the number of directly bonded hydrogens and r_{CH} is the proton-carbon bond distance. For isotropic motion:

$$\tau_{c,\text{eff}} = 1/6R_{\text{iso}} \quad (4)$$

On the other hand, in a symmetrical top molecule:

$$\tau_{c,\text{eff}} = \frac{A}{6R_{\perp}} + \frac{B}{5R_{\perp} + R_{\parallel}} + \frac{C}{2R_{\perp} + 4R_{\parallel}} = \frac{1}{R_{\perp}} \left[\frac{A}{6} + \frac{B}{5 + \sigma} + \frac{C}{2 + 4\sigma} \right] \quad (5)$$

In eq 5, $\sigma = R_{\parallel}/R_{\perp}$ and for l equal to the directional cosine of the CH bond relative to the principal axis of the top:

$$\begin{aligned} A &= \frac{1}{4} (3l^2 - 1)^2 \\ B &= 3l^2(1 - l^2) \\ C &= \frac{3}{4} (l^2 - 1)^2 \end{aligned} \quad (6)$$

In the methylethylenes, internal methyl rotation also contributes to the relaxation. If the overall motion is isotropic, then eq 5 may be used to treat this case by recognizing that $R_{\perp} = R_{\text{iso}}$ and $R_{\parallel} = \rho$, an internal methyl jump rate.^{4,5} Internal rotation superimposed on the motion of a symmetrical top requires the more detailed expression given by Woessner et al.¹¹ for $\tau_{c,\text{eff}}$ as follows:

$$\tau_{c,\text{eff}} = \left[\frac{A_1}{6R_{\perp}} + \frac{A_2 + A_3}{6R_{\perp} + \rho_D} + \frac{B_1}{5R_{\perp} + R_{\parallel}} + \frac{B_2 + B_3}{5R_{\perp} + R_{\parallel} + \rho_D} + \frac{C_1}{2R_{\perp} + 4R_{\parallel}} + \frac{C_2 + C_3}{2R_{\perp} + 4R_{\parallel} + \rho_D} \right] \quad (7)$$

where

$$\begin{aligned} A_1 &= \frac{1}{16} (1 - 3m^2)^2 (1 - 3n^2)^2 \\ B_1 &= \frac{3}{4} m^2 (1 - m^2) (1 - 3n^2)^2 \\ C_1 &= \frac{3}{16} (1 - m^2)^2 (1 - 3n^2)^2 \\ A_2 &= \frac{9}{2} m^2 n^2 (1 - m^2) (1 - n^2) \\ B_2 &= \frac{3}{2} (4m^4 - 3m^2 + 1) n^2 (1 - n^2) \\ C_2 &= \frac{3}{2} (1 - m^4) n^2 (1 - n^2) \\ A_3 &= \frac{9}{32} (1 - m^2)^2 (1 - n^2)^2 \\ B_3 &= \frac{3}{8} (1 - m^4) (1 - n^2)^2 \\ C_3 &= \frac{3}{32} (m^4 + 6m^2 + 1) (1 - n^2)^2 \end{aligned} \quad (8)$$

The directional cosine of the methyl top axis relative to the principal axis is given by m , and n is the directional cosine of the C-H bond relative to the internal methyl top axis. An estimate of the energy barrier (V) to the internal rotation of a methyl group can now be calculated from ρ_D and the following rate equation:⁴

$$\rho_D = \rho_0 e^{-V/RT} \quad (9)$$

where ρ_0 is the mean jump rate of a freely rotating methyl group [$\rho_0 = \frac{3}{2}(kT/I)^{1/2} = 1.33 \times 10^{13}$ radians sec^{-1} at 40° where I is the moment of inertia of the methyl group about the axis of rotation].^{4,11}

Variations in field strength and temperature¹⁻⁹ with their concomitant effect upon T_{10} can be used to identify the origin of relaxation effects other than the dipolar mechanisms. If T_{10} is observed to be due to chemical shift anisotropy, no new motional parameters are introduced since this mechanism is controlled by the rotational diffusion constants affecting the dipolar mechanism. On the other hand, spin-rotational effects present in the methylethylenes require another motional parameter. Whereas, the dipolar correlation time¹²⁻¹⁴ effectively gives the time in seconds for dipoles to reorient approximately 1 radian, spin-rotation correlation times (τ_{SR}) roughly measure the time in seconds between "collisions" or interruptions of molecular rotation.¹²⁻¹⁴ Hubbard¹⁴ demonstrated that the two times are related for isotropic motion in the diffusional limit by

$$\tau_{\text{SR}} \tau_c = I/6kT \quad (10)$$

where I is the average moment of inertia about the three axes and $\tau_{\text{SR}} \ll \tau_c$. On the other hand, for a dilute gas where both τ_c and τ_{SR} are determined by brief collisions between molecules (inertial limit), τ_c is usually less³ than τ_{SR} . At intermediate conditions, various values between 1 and 6 have been substituted for the 6 in the denominator of eq 10¹⁵ to correct empirically for this deviation from the diffusion limit. However, the important point is that for any motion which is not diffusionally controlled, no unique relationship between τ_c and τ_{SR} is available and the reorientation and spin-rotation motional parameters must be treated as independent entities.

TABLE I: Spin Lattice Relaxation Times and Nuclear Overhauser Effects at 40 and 60° at 25.1 MHz and at 40° at 15.1 MHz

Compound	Carbon	MHz	t , °C	η	T_1 , sec	T_{1D} , sec	T_{10} , sec
<i>cis</i> -2-Butene	Me(1,4)	15.1	40	0.63 ± 0.15	24.0 ± 4	76 ± 10	35 ± 8
		25.1	40	0.62 ± 0.10	23.4 ± 2	75 ± 14	34 ± 7
		25.1	60	0.32 ± 0.10	14.3 ± 1	89 ± 20	17 ± 5
	2,3	15.1	40	0.63 ± 0.10	24.5 ± 4	78 ± 9	36 ± 8
		25.1	40	0.60 ± 0.11	25.1 ± 2	84 ± 13	36 ± 6
		25.1	60	0.32 ± 0.12	14.0 ± 1	88 ± 21	17 ± 5
<i>trans</i> -2-Butene	Me(1,4)	15.1	40	0.94 ± 0.10	23.0 ± 4	49 ± 12	43 ± 7
		25.1	40	0.99 ± 0.12	27.0 ± 2	54 ± 7	54 ± 7
		25.1	60	0.75 ± 0.10	17.9 ± 1	48 ± 11	28 ± 7
	2,3	15.1	40	0.31 ± 0.10	16.0 ± 4	103 ± 40	19 ± 6
		25.1	40	0.20 ± 0.12	14.5 ± 1	145 ± 60	16 ± 2
		25.1	60	0.15 ± 0.11	8.6 ± 1	115 ± 50	9 ± 2
Isobutene	Me(1,2)	15.1	40	1.31 ± 0.09	23.0 ± 4	35 ± 8	67 ± 5
		25.1	40	1.21 ± 0.12	25.8 ± 2	43 ± 5	65 ± 10
	2	15.1	40	0.31 ± 0.10	40.0 ± 8	258 ± 90	47 ± 25
		25.1	40	0.20 ± 0.18	40.0 ± 5	400 ± 200	44 ± 20
	3	15.1	40	1.21 ± 0.08	22.0 ± 4	36 ± 8	57 ± 5
		25.1	40	0.99 ± 0.17	20.6 ± 2	42 ± 4	40 ± 10
2-Methyl- <i>trans</i> -2-butene	Me(1)	25.1	40	1.43 ± 0.12	23.6 ± 2	33 ± 5	83 ± 10
	2	25.1	40	0.23 ± 0.12	49.6 ± 6	431 ± 200	56 ± 20
	3	25.1	40	0.88 ± 0.12	35.8 ± 2	81 ± 10	64 ± 6
	Me(4)	25.1	40	0.57 ± 0.13	22.0 ± 2	77 ± 4	31 ± 7
	Me(2)	25.1	40	0.88 ± 0.12	21.0 ± 2	48 ± 5	38 ± 5
2,3-Dimethyl-2-butene	Me(1,2,3,4)	25.1	40	1.42 ± 0.10	24.2 ± 2	34 ± 3	84 ± 8
	2,3	25.1	40	0.27 ± 0.10	79.3 ± 5	587 ± 220	92 ± 35

The equation for spin-rotation of a symmetric top is given in eq 11 from the work of Wang et al.⁴ where C is the spin-rotation constant (radians/sec),^{4-6,13-15} and I is the moment of inertia (g cm²). The spin-rotation moment-of-inertia product (CI) provides a measurement of the coupling between the *rotational* velocity of a molecule and the nuclear spin resulting in chemical shift variations and a spin-lattice relaxation mechanism. It is measured in units as radians ergs seconds.

$$\frac{1}{T_{1SR}} \approx \frac{2kT}{3\hbar^2} \left[(I_{\parallel}C_{\parallel})^2 \frac{\tau_{\parallel SR}}{I_{\parallel}} + 2(I_{\perp}C_{\perp})^2 \frac{\tau_{\perp SR}}{I_{\perp}} \right] \quad (11)$$

If one recognizes that $I_i C_i \approx \frac{1}{3} \sum_j^{x,y,z} (I_j C_j) = (IC)_{\text{trace}}$ for carbon-13 in many molecules,⁶ eq 11 can be simplified to

$$\frac{1}{T_{1SR}} \approx \frac{2kT(IC)_{\text{trace}}^2}{3\hbar^2} \left[\frac{\tau_{\parallel SR}}{I_{\parallel}} + \frac{2\tau_{\perp SR}}{I_{\perp}} \right] \quad (12)$$

This simplification is valid in part because of a nearly inverse dependence of I and C for anisotropic molecules. Thus $(IC)^2$ is seldomly as anisotropic as either C^2 or I^2 . Furthermore, if one assumes isotropic motion ($\tau_{\parallel SR}$, $\tau_{\perp SR}$ = $\tau_{SR,eff}$ and I_{\parallel} , I_{\perp} = I_{av}), eq 12 reduces to

$$\frac{1}{T_{1SR}} \approx \frac{2kT(IC)_{\text{trace}}^2 \tau_{SR,eff}}{\hbar^2 I_{av}} \quad (13)$$

The calculations of various τ_{SR} for symmetric top or spherical molecules can then be executed with eq 11-13 using appropriate spin-rotation relaxation data. Comparison of the τ_{SR} with τ_f , the mean period of free rotation for the molecule, permits determination of the average angular

displacement between effective intermolecular interactions and provides a means for determining whether or not the process is diffusion controlled ($\tau_{SR} \ll \tau_f$). The various $\tau_{f,i}$ are calculated from the equipartition principle as follows:

$$\tau_{f,i} = (I_i/kT)^{1/2} \quad (14)$$

II. Experimental Section

A. Materials. All samples were of reagent grade quality and were run as neat liquids after repeated freeze-thaw degassing. The compounds *cis*- and *trans*-2-butene, and isobutene are gases at room temperature and pressure. These compounds were condensed at liquid N₂ temperatures and sealed in a thick-walled NMR tube where they remain liquids under their own vapor pressure at room temperature. At ambient temperatures, the remaining compounds, 2-methyl-2-butene and 2,3-dimethyl-2-butene, are liquids.

B. Equipment and Methods of Measurement. All experiments were carried out at 15.1 and 25.1 MHz on Varian AFS-60 and XL-100-15 spectrometers, respectively. Temperature data at 40 and 60° were obtained. The equipment and experimental techniques have been described in previous papers.^{7,8} In addition to adiabatic rapid passage (ARP) techniques, the NMR parameters of the compounds also were measured by Fourier transform methods.

III. Results and Discussion

Table I contains the results of NOE and T_1 measurements on several methylethylene compounds at 15.1 and 25.1 MHz at 40°, and at 25.1 MHz at 60°. Since the results

at the two frequencies (15.1 and 25.1 MHz at 40°) are equal within experimental error, it must be concluded that chemical shift anisotropy is not a major relaxation process in the methylethylenes at the electromagnet field strengths utilized in this study. In contrast, observations at 40 and 60° (25.1 MHz) indicate that a spin-rotation mechanism is functioning. Note from Table I that η , T_1 , and T_{10} all decrease significantly with increasing temperature, while T_{1D} changes only slightly or remains essentially constant.¹ Further analyses are made, therefore, on the assumption that T_{1D} and T_{10} are dominated by intramolecular dipole-dipole and by spin-rotation mechanisms, respectively.

While the methylethylene compounds offer possibilities of methyl rotation and anisotropic motion, they unfortunately lack an adequate number of dipolar relaxation times to fit uniquely the four motional parameters present in these low symmetry molecules. To fit uniquely R_1 , R_2 , R_3 , and ρ_D ; four T_{1D} values would be needed. Nevertheless, most of the methylethylenes have only two values, T_{1D} (vinyl) and T_{1D} (methyl) (see Table I). Therefore, symmetry and other simplifying approximations have to be invoked in order to extract motional data from the relaxation measurements.

If motion in the methylethylene systems is assumed to be isotropic, the effective dipolar ($\tau_{c,eff}$) and spin-rotation ($\tau_{SR,eff}$) correlation times can be obtained from T_1 data on the vinyl carbons and compared with the mean period of free rotation (τ_f) to determine whether or not diffusional or inertial features dominate the motions which are characteristic of these molecules. Attention is therefore directed to eq 3 and 13 and the methods used to acquire the various parameters appearing in these expressions. A standard carbon-hydrogen bond distance of 1.09 Å was used in (3) for r_{CH} . The average moment of inertia and $(CI)_{trace}$ required by (13) pose more difficulty. The moments of inertia for these molecules are given in Table II along with an average inverse moment of inertia, $1/3(\sum_i 1/I_i)$, which is used in (13). Note, using a moment of inertia average of this form will give weight to those anisotropic components of motion which are most important to the spin-rotation relaxation mechanism. Nevertheless, it must be admitted that the approximation is rather severe for *trans*-2-butene where the moment of inertia tensor is very anisotropic. Because of this difficulty with *trans*-2-butene more attention will be given later to the problem of anisotropic motion in this molecule.

The spin-rotation moment-of-inertia product, $(CI)_{trace}$, is estimated using the relationship between spin-rotation and chemical shielding first proposed by Flygare¹⁶ and used by other workers.^{17,18} The expression is

$$[C^{(k)}I]_{ii} = \frac{\hbar^2 \gamma_k}{\beta} [\sigma_p^{(k)}]_{ii} + \frac{e\hbar \gamma_k}{c} \sum_l \frac{Z_l}{r_{kl}} \sin^2 \theta_{ikl} \quad (15)$$

where e , \hbar , c , and β (Bohr magneton) are the standard physical constants; γ_k is the gyromagnetic constant of the k th nucleus and $\sigma_{p,ii}^{(k)}$ is its localized paramagnetic screening term along the i th axis. The net formal charge of the other l atoms in the molecule is given by Z_l with r_{kl} the internuclear separation and θ_{ikl} the angle between the kl vector and the i th principle axis. It is to be noted that Z_l will be very small for the molecules considered in this work and thus the second term in (15) becomes negligible (<2%). For molecules with significant charge polarization, it may at times be desirable to make the formal charge correction embodied in the last term of (15). However, even then the

TABLE II: Moments of Inertia and Specific Weighted Averages ($\times 10^{39}$ g cm²)

	I_{xx}^a	I_{yy}	I_{zz}^a	I_{av}^b
<i>trans</i> -2-Butene	2.57	22.44	23.96	6.31
<i>cis</i> -2-Butene	6.00	14.24	19.19	10.38
Isobutene	8.98	10.77	18.69	11.64
2-Methyl-2-butene	15.15	17.85	30.30	19.35
2,3-Dimethyl-2-butene	13.35	19.66	33.01	19.22

^a The x axis lies along C=C double bond except in *trans*-2-butene where it is 39.8° from the double bond and in 2-methyl-2-butene where it is 24.0° from the double bond. The z direction is always perpendicular to the molecular plane and lies in the direction of the π orbitals. ^b $I_{av} = 1/\text{trace}(I_{ii})^{-1}$ is the effective inverse average.

corrections will be small if " k " is a carbon atom. Since an absolute chemical shift cannot be measured directly, it is necessary to reference $\sigma_{p,ii}^{(k)}$ in (15) using a known spin-rotation coupling constant. The spin-rotation coupling constant for carbon monoxide is available and as this compound has a chemical shift close to the vinyl carbons in the methylethylenes, it is used to standardize eq 15. Combining the value for $C_{\perp}^{CO} = 32.59 \times 10^3$ Hz (2.048×10^5 radians/sec) with the moment of inertia of $I_{\perp} = 1.516 \times 10^{-39}$ g cm² yields $(CI)_{\perp} = 4.942 \times 10^{-35}$ erg sec (3.105×10^{-34} radian erg sec). The C-O distance of 1.128 Å may be used with a dipole moment of 0.1 D to calculate a $Z_{O_x} = 0.019$. This give a component to $(CI)_{\perp}$ of 1.86×10^{-37} radian erg sec which is negligible compared with 3.105×10^{-34} for the last term in eq 15. Thus, the paramagnetic term along the perpendicular axis in carbon monoxide is

$$\sigma_{p,\perp}(CO) \approx \frac{\beta}{\hbar^2 \gamma_{CO}} (C_{\perp}^{CO})_{\perp} = 384 \text{ ppm} \quad (16)$$

The value of $\sigma_{p,\parallel}$ along the C-O axis is zero because of symmetry. Assuming that the difference in chemical shift between the methylethylenes and CO is due largely to the paramagnetic term, then one may write

$$\sigma_{p,ii}^{(k)} = \delta_{ii}^{(k)} - \delta^{(CO)} + \frac{2}{3} \sigma_{p,\perp}(CO) \quad (17)$$

The isotropic shielding of $\delta^{(CO)} = 182.6$ relative to the TMS scale, and $\frac{2}{3} \sigma_{p,\perp}(CO)$ is the trace of the paramagnetic shielding tensor ($\frac{2}{3} \times 384$). Thus, combining (17) with (15) one obtains

$$(C^k I)_{ii} = 8.063 \times 10^{-37} (\delta_{ii}^{(k)} + 73.4) \text{ radian erg sec} \quad (18)$$

where $\delta_{ii}^{(k)}$ given in parts per million is now the i th shielding component relative to TMS. The assumption of a constant diamagnetic term does not require that this term be small, only that it be mutually cancelling in the $\delta_{ii}^{(k)}$ and $\delta^{(CO)}$ terms thereby dropping out of eq 17. A judicious choice of coordinates is required if serious ill conditioning is to be avoided¹⁹ in relating the shielding and spin-rotation expressions. We used the experimental isotropic shifts, $\delta_{trace}^{(k)}$, given in Table III for the methylethylenes along with eq 18 which is appropriate for trace as well as subcomponents to calculate $(CI)_{trace}$. These values for $(CI)_{trace}$ appear in Table III along with the degree of anisotropy in shielding estimated from the theoretical methods of Strong, Ikenberry, and Grant.²⁰ The ratio of theoretical shielding components $\sigma_{p,xx}/\sigma_{p,zz}$ and $\sigma_{p,yy}/\sigma_{p,zz}$ was used to avoid overall magnitude errors intrinsic to all chemical

TABLE III: Experimental Shifts, Shielding Anisotropies, and Spin-Rotation Moment-of-Inertia Components

Compound	Carbons	$\delta_{\text{trace}}^{(k)}$ (expt)	$(CI)_{\text{trace}}$,	σ_{xx}/σ_{zz}	σ_{yy}/σ_{zz}	$(CI)_{xx}$,	$(CI)_{yy}$,	$(CI)_{zz}$,
			$\times 10^{35}$			$\times 10^{35}$	$\times 10^{35}$	radians
<i>trans</i> -2-Butene	1,4	17.4 ₆	7.38	1.031	0.939	7.69	7.00	7.46
	2,3	125.9 ₆	16.13	1.142	1.759	14.17	21.82	12.41
<i>cis</i> -2-Butene	1,4	11.7 ₂	6.92	1.009	0.940	7.10	6.62	7.04
	2,3	124.4 ₁	16.00	1.003	2.022	11.96	24.11	11.90
Isobutene	1,2a	23.4 ₅	7.87	1.007	0.899	8.18	7.30	8.12
	2	141.3 ₅	17.37	1.051	1.916	13.81	25.17	13.14
	3	110.5 ₇	14.89	1.006	2.225	10.62	23.49	10.50
2-Methyl- <i>trans</i> -2-butene	1	25.4 ₅	8.03	1.007	0.864	8.45	7.25	8.39
	2a	17.0 ₃	7.35	0.991	0.932	7.48	7.03	7.54
	4	13.2 ₄	7.04	0.993	0.934	7.17	6.74	7.22
	2	131.5 ₈	16.58	1.201	1.761	15.08	22.11	12.55
	3	118.8 ₅	15.56	1.155	2.048	12.83	22.75	11.11
2,3-Dimethyl-2-butene	1,2a,3a,4	20.2 ₆	7.61	1.042	0.936	7.99	7.18	7.67
	2,3	123.4 ₀	15.92	1.061	1.879	12.86	22.78	12.12

TABLE IV: Effective Correlation Times for Dipolar and Spin-Rotation Processes Compared with Periods of Free Molecular Rotation (All Values in Picoseconds) at 40°

Compound	$\tau_{c,\text{eff}}^a$	$\tau_{\text{SR},\text{eff}}^b$	$\tau_{f,x}$	$\tau_{f,y}$	$\tau_{f,z}$	$\tau_{f,z}/\tau_{f,x}$
<i>trans</i> -2-Butene	0.38	0.18	0.24	0.72	0.72	3.0
<i>cis</i> -2-Butene	0.58	0.14	0.37	0.57	0.67	1.8
Isobutene	0.60 ^c	0.12	0.46	0.50	0.60	1.3
2-Methyl-2-butene	0.58 ^c	0.14	0.59	0.64	0.84	1.4
2,3-Dimethyl-2-butene	0.59 ^d	0.11	0.56	0.67	0.87	1.6

^a For the diffusionally controlled limit, $\chi = \tau_{c,\text{eff}}/\tau_{f,i} \gg 1$. Since in this study $\chi \approx 1$ for all molecules about all axes, it must be assumed that the molecular motion is intermediary between the inertial and diffusional limits. ^b The maximum angles of rotation for all molecules occur about the x axis, and are approximately 43° for *trans*-2-butene, 22° for *cis*-2-butene, 15° for isobutene, 14° for 2-methyl-2-butene, and 11° for 2,3-dimethyl-2-butene; where $\theta = (\tau_{\text{SR},\text{eff}}/\tau_{f,x})$ (57.3°). ^c Obtained from C-3 T_1 data. If the C-2 T_1 data are used (quaternary carbons), a $\tau_{c,\text{eff}} \approx 0.8$ -0.9 psec is obtained. ^d This value was taken as the average of *cis*-2-butene, isobutene, and 2-methyl-2-butene since the vinyl carbons have no hydrogens directly attached. If the methyl hydrogens are used, a $\tau_{c,\text{eff}} \approx 0.70$ psec is obtained.

shielding calculations, and thereby improve the estimates of the $(CI)_{ii}$ components appearing in Table III. The following three equations are used to evaluate $(CI)_{xx}$, $(CI)_{yy}$, and $(CI)_{zz}$ from $(CI)_{\text{trace}}$, σ_{xx}/σ_{zz} , and σ_{yy}/σ_{zz} :

$$3(CI)_{\text{trace}} = (CI)_{xx} + (CI)_{yy} + (CI)_{zz}$$

$$(CI)_{xx} = (\sigma_{p,xx}/\sigma_{p,zz})(CI)_{zz} \quad (19)$$

$$(CI)_{yy} = (\sigma_{p,yy}/\sigma_{p,zz})(CI)_{zz}$$

Table III also contains a listing of the experimental $\delta_{\text{trace}}^{(k)}$ and theoretical quantities σ_{xx}/σ_{zz} and σ_{yy}/σ_{zz} used in these calculations.

Table IV contains the results from eq 3 and 13 on the effective dipolar and spin-rotation correlation times. Also contained in this table are the mean periods of free rotation about the principal axis used to diagonalize the moment of inertia tensor using eq 14. It is apparent from Table IV that the effective motions in all of the molecules are rather similar, although *trans*-2-butene does differ the most. The values for $\tau_{c,\text{eff}}$ in Table IV compare very well with a value of $\tau_c = 0.42$ psec calculated at 40° from the deuterium relaxation results of Assink and Jonas²¹ on deuterium-substituted isobutene. This agreement is unusually good when all the assumptions of both approaches are considered. As concluded early, the motions are not in the diffusionally controlled limit for any of the compounds. This conclusion

is supported by comparing $\tau_{c,\text{eff}}$ with any or all of the $\tau_{f,i}$ components. The ratio $\tau_c/\tau_f \gg 1$ if diffusion controls. In contrast, however, all such values in Table IV are of the order of unity. Moreover, the Hubbard diffusional relationship between τ_c and τ_{SR} , as expressed by eq 10, fails to correlate these two values. Finally, a comparison of $\tau_{\text{SR},\text{eff}}$ with the various values of $\tau_{f,i}$ indicates that relatively large angular rotations, 10–20°, will be realized during one τ_{SR} period for almost all motions of the molecules (especially about the x axis). A considerably greater angle of 40° is encountered if $\tau_{\text{SR},\text{eff}}$ is compared with $\tau_{f,x}$ for *trans*-2-butene (Table IV). All of these observations confirm that the rotational motion in these molecules is intermediate between the diffusion and inertia controlled limits.

Values for $R_{\perp} = (1/6\tau_{c,\text{eff}})^{3,14}$ determined from the vinyl carbon T_{1D} (vinyl) can now be used along with T_{1D} (methyl) in eq 5 to estimate the methyl jump rate $\rho_D = R_{\parallel}$. These values for R_{\perp} and ρ_D are presented in Table V along with the values of V obtained from eq 9.^{4,11} Agreement is relatively good between these NMR estimates for V and available literature values for V which are obtained from other physical methods. Furthermore, data on 2-methyl-2-butene and 2,3-dimethylbutene provide barriers not easily obtained by any other method.

Earlier, it was indicated that the methylethylenes lacked adequate dipolar relaxation times to fit uniquely all three

TABLE V: Calculation of Internal Methyl Rotation (Jump) Rates, ρ_D , and Barriers to Internal Methyl Rotation, V

Compound	R_{\perp} , ^a $\times 10^{-11}$ sec	ρ_D , ^b \times 10^{-11} sec	V_{calcd} , ^c kcal	V_{lit} , ^d kcal
<i>cis</i> -2-Butene	2.9	50.3	0.6	0.73 ^c
<i>trans</i> -2-Butene	4.4	7.8	1.7	1.95 ^d
Isobutene	2.8	6.0	1.9	2.21 ^c
2-Methyl-2-butene	2.9	6.2	1.9 (1-Me)	
		14.5	1.4 (2-Me)	
		43.5	0.7 (4-Me)	
2,3-Dimethyl-2-butene	2.8	4.9	2.1	

^a The value of R_{\perp} is calculated from $R_{\perp} = 1/6\tau_{c,\text{eff}}$. ^b The values of ρ_D are fit from T_{1D} (methyl) data using Woessner et al.'s formulation^{10,11} with $\rho_D = R_{\parallel}$ and $R_{\perp} = R_{\text{iso}}$. ^c See ref 22, 23, and 24. ^d See ref 25.

rotational diffusion parameters in these low symmetry molecules. Inclusion of spin-rotation relaxation data does not improve the situation as the relationships between dipolar and spin rotational parameters are strictly valid only for the diffusional rotation limit. For example, in *cis*-2-butene, there are four pieces of data T_{1D} (vinyl), T_{1D} (methyl), T_{1SR} (vinyl), T_{1SR} (methyl) to fit eight correlation times or diffusion constants describing the motional features [R_1 , R_2 , R_3 , ρ_D , τ_{SR1} , τ_{SR2} , τ_{SR3} , and ρ_{SR}]. Hence in order to calculate motional anisotropy from these four pieces of data, assumptions which reduce the number of motional parameters from 8 to 4 must be invoked. There are several approximations which might be used to avoid these difficulties. The first approach is utilized in constructing Table IV wherein isotropic symmetry was assumed in order to reduce the number of dipolar parameters in half thereby obtaining $\tau_{c,\text{eff}}$ and ρ_D from T_{1D} (vinyl) and T_{1D} (methyl), respectively. Moreover, $\tau_{SR,\text{eff}}$ was calculated from T_{1SR} (vinyl).

Some additional insight into the molecular motion of these systems is provided by testing these systems in the *inertial limit* of motion even though the data of Table IV clearly indicate that the motion is intermediate between the diffusional and inertial limits of motion.

In the *inertial limit*, the mean periods of free rotation about the major axis of rotation can be determined from eq 20^{6b} which is obtained from the equipartition principle

$$\tau_{f,i} = (I_i/kT)^{1/2} \quad (20)$$

The values for the three moments of inertia are given in Table II and the various $\tau_{f,i}$ appear in Table IV.

The principal axes have been ordered in every system such that $\tau_{f,x}$ and $\tau_{f,z}$ represent, respectively, the *smallest* and *largest* mean periods of free rotation about the principal axes. Hence, the ratio, $\tau_{f,z}/\tau_{f,x}$, gives the relative magnitude of the *maximum anisotropy* in the *mean periods of free rotation about the principal axes*, or similarly, the *maximum anisotropy in the mean angular velocities of free rotation about the principal axes*. In the case of four of the molecules, the ratios are quite uniform (<2). However, for *trans*-2-butene, the ratio is sizably larger (3.0) than for the remaining methylethylenes. This disparity results from the particularly small moment of inertia about the axis which runs roughly through the two methyls and the double bond of *trans*-2-butene. As one might expect,

motion about this one particular axis would be very rapid and might approach the *inertial limit of motion*. The almost identical values for $\tau_{f,x}$ (Table IV) and $\tau_{c,\text{eff}}$ for four of the molecules gives support to the isotropic assumption. Motion only in *trans*-2-butene appears to be sufficiently unique to warrant further consideration. Anisotropic motion would account for the fact that $\tau_{c,\text{eff}}$ is only 0.38 psec for *trans*-2-butene compared to a range of 0.58–0.60 psec for the other four methylethylenes (Table IV). Furthermore, it would explain why $\tau_{SR,\text{eff}}$ (the time roughly between effective intermolecular interactions or interruptions of molecular rotations) is quite large for *trans*-2-butene, 0.18 psec, compared to the range for the remaining molecules, 0.11–0.14 psec (Table IV). In other words, a very efficient rotation system about the unique axis in *trans*-2-butene could result in a very short period necessary for dephasing the dipole-dipole interaction ($\tau_{c,\text{eff}}$), but a relatively long period between interruptions of molecular rotations ($\tau_{SR,\text{eff}}$). One might therefore assume that the unique axis and rotation system in *trans*-2-butene would result in considerably more anisotropy of motion for *trans*-2-butene than for the other four molecules. Hence the 3.0 factor given in Table IV for this anisotropy would constitute a good lower limit for the two types of rotational motion.

Analyses of the molecular motion in the methylethylene molecules lead to the following general conclusions: (1) all of the molecules are efficient in their rotational relaxation due to their small size and lack of sizable dipole moments;⁶ (2) motions in four of the molecules (*cis*-2-butene, isobutene, 2-methyl-2-butene, and 2,3-dimethyl-2-butene) are remarkably similar and probably have very little anisotropy; and (3) motion in *trans*-2-butene is unique from the remaining molecules probably due to a unique and efficient rotation system about an axis which would be close to the principal inertia axis and which passes through the methyls and the double bond.

One of the focal points of interest resulting from this work is the prediction of rotational barriers, V , for the internally rotating methyl groups. It was indicated earlier that the values of V predicted by these NMR relaxation studies agreed favorably with literature values for *cis*-2-butene, *trans*-2-butene, and isobutene (see Table V).^{22–25} Calculated values agree within 15–20% (generally 0.1–0.3 kcal low) of reported literature values. The applicability of the method to more complex molecules where standard optical microwave techniques are not amenable however is emphasized. Thus, the NMR technique is particularly useful for approximating barriers in compounds with multiple rotating groups. For example, Table V presents barrier estimates for the 1-methyl (1.9 kcal), 2a-methyl (1.4 kcal), and 4-methyl (0.7 kcal) substituents in the compound 2-methyl-2-butene. A barrier is also predicted in Table V for 2,3-dimethyl-2-butene which along with 2-methyl-2-butene are presently the only experimental estimates now available. As previously stated, if these values are to be used, it should be noted that they may be low [by about 15–20% (0.1–0.3 kcal)] on the basis of variations of the values in Table V with the more accurate literature values found for the *cis*-2-, *trans*-2-, and isobutene molecules. These studies of methyl rotation barriers compliment the earlier work⁴ from this laboratory exhibiting the value of T_1 data in evaluating the energy parameters in such dynamical processes.

Acknowledgments. This work was supported by a Grant from the National Institutes of Health (GM 08521). S.W.C.

was a recipient of a NDEA Title IV Predoctoral Fellowship and this paper is based largely upon his thesis, submitted as partial fulfillment for the Ph.D. at the University of Utah.

References and Notes

- (1) A. Abragam, "The Principles of Nuclear Magnetism", Oxford University Press, London, 1961, Chapter 8.
- (2) J. S. Waugh in "Molecular Relaxation Processes", Academic Press, London, 1966.
- (3) D. K. Green and J. G. Powles, *Proc. Phys. Soc. (London)*, **85**, 87 (1965).
- (4) (a) K. F. Kuhlmann and D. M. Grant, *J. Chem. Phys.*, **55**, 2998 (1971); (b) T. D. Alger, D. M. Grant, and R. K. Harris, *J. Phys. Chem.*, **76**, 281 (1972); (c) J. R. Lyster, Jr., and D. M. Grant, *ibid.*, **76**, 3213 (1972).
- (5) J. R. Lyster, Jr., and D. M. Grant, *MTP Int. Rev. Sci., Ser. One*, **4**, 155 (1972).
- (6) (a) C. H. Wang, J. R. Lyster, Jr., and D. M. Grant, *J. Chem. Phys.*, **55**, 4674 (1971); (b) J. R. Lyster, Jr., D. M. Grant, and C. H. Wang, *ibid.*, **55**, 4676 (1971).
- (7) K. F. Kuhlmann, D. M. Grant, and R. K. Harris, *J. Chem. Phys.*, **52**, 3439 (1970).
- (8) T. D. Alger, S. C. Collins, and D. M. Grant, *J. Chem. Phys.*, **54**, 2820 (1971).
- (9) T. D. Alger and D. M. Grant, *J. Phys. Chem.*, **75**, 2538 (1971).
- (10) D. D. Woessner, *J. Chem. Phys.*, **37**, 647 (1962).
- (11) D. E. Woessner, B. S. Snowden, Jr., and G. H. Meyer, *J. Chem. Phys.*, **50**, 719 (1969).
- (12) (a) W. T. Huntress, Jr., *J. Chem. Phys.*, **48**, 3524 (1968); (b) D. Wallach and W. T. Huntress, Jr., *ibid.*, **50**, 1219 (1969).
- (13) K. T. Gillen and J. H. Noggle, *J. Chem. Phys.*, **53**, 801 (1970).
- (14) P. S. Hubbard, *Phys. Rev.*, **131**, 1155 (1963).
- (15) A. A. Maryott, T. C. Farrar, and M. S. Malmberg, *J. Chem. Phys.*, **54**, 64 (1971).
- (16) W. H. Flygare, *J. Chem. Phys.*, **41**, 793 (1964).
- (17) I. Ozier, L. M. Crapo, and N. F. Ramsey, *J. Chem. Phys.*, **49**, 2314 (1968).
- (18) P. Rigney and J. Viret, *J. Chem. Phys.*, **47**, 4645 (1967).
- (19) One avoids the difficult problems of gage and the separation of the first- and second-order perturbation terms (normally characterized as the diamagnetic paramagnetic shielding terms) by selecting the coordinate system at the *k*th carbon atom. All of the nonlocalized diamagnetic terms already have been incorporated along with the nuclear terms into the last term of eq 15. See ref 16 for details. It is the mutual cancellation of remote electron and nuclear terms which reduces the significance of this particular component of eq 15.
- (20) A. B. Strong, D. Ikenberry, and D. M. Grant, *J. Mag. Resonance*, **9**, 145 (1973).
- (21) R. A. Assink and J. Jonas, *J. Chem. Phys.*, **53**, 1710 (1970).
- (22) D. R. Linde, *J. Chem. Phys.*, **35**, 1372 (1961).
- (23) D. R. Linde and D. E. Mann, *J. Chem. Phys.*, **27**, 868 (1957).
- (24) D. R. Herschbach and L. C. Krisher, *J. Chem. Phys.*, **28**, 728 (1958).
- (25) J. E. Kilpatrick and K. S. Pitzer, *J. Res. Nat. Bur. Stand.*, **37**, 136 (1946).

Electron Spin Resonance of the [16]Annulene Anion Radical. Ion Association in Hexamethylphosphoramide

Jesus Gilberto Concepcion and Gershon Vincow*

Department of Chemistry, Syracuse University, Syracuse, New York 13210 (Received September 27, 1974; Revised Manuscript Received April 18, 1975)

Publication costs assisted by Syracuse University

The syn (2 + 2) dimer of cyclooctatetraene reacts with alkali metal producing the [16]annulene anion radical, which is in disproportionation equilibrium with its dianion and the neutral hydrocarbon. We have exploited this new method of preparing the [16]annulene anion to study ion association in hexamethylphosphoramide. The thermodynamic parameters controlling this disproportionation equilibrium have been obtained for three counterions (Li, Na, K) and the variation has been compared with previous results on the cyclooctatetraene anion and related systems. The variation in the thermodynamic parameters is ascribed to metal association with the [16]annulene dianion. This interpretation is based in part on ESR evidence that the [16]annulene anion occurs in hexamethylphosphoramide as a free ion. The *g* value and proton splittings are independent of counterion. The *g* value and line width are independent of temperature.

Introduction

Oth et al.¹ have prepared the radical anion and dianion of [16]annulene and have studied ESR, NMR, and electronic spectra in an effort to elucidate the geometrical and electronic configurations of these species.

In this paper we report a new and convenient approach for generating these species. We have investigated the ESR of the radical anion in hexamethylphosphoramide (HMPA) solvent using a number of alkali metal counterions. Thermodynamic parameters have been obtained for the disproportionation reaction



where π , π^{-} and π^{2-} denote the neutral molecule, anion

radical, and dianion respectively.² The results are discussed in terms of the extent of ion association in HMPA.

Experimental Section

A sample of the syn (2 + 2) dimer of cyclooctatetraene, syn-tricyclo[8.6.0.0^{2,9}]hexadeca-3,5,7,11,13,15-hexaene (see Figure 1; abbreviation to be used is DCOT), was kindly supplied by Dr. A. Anastassiou. Its melting point and NMR spectrum were consistent with those reported for this dimer (mp 53°; NMR singlets at 6.0, 5.65, and 3.25 ppm).³

Hexamethylphosphoramide (HMPA) was purchased from the Aldrich Chemical Co. It was dried over calcium hydride, distilled under reduced pressure, and stored over Linde 4A molecular sieves. Tetrahydrofuran (THF) and

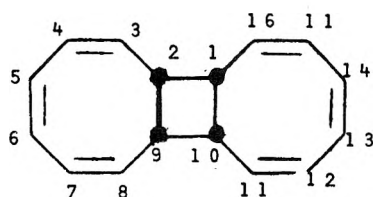


Figure 1. Structural formula for the syn (2 + 2) dimer of cyclooctatetraene.

1,2-dimethoxyethane (DME) were purchased from Eastman Chemicals. They were dried with lithium aluminum hydride, distilled under a nitrogen atmosphere, and stored under vacuum in a flask containing sodium pyrenide plus an excess of sodium metal.

Anion radical samples in HMPA were prepared under reduced pressure (10^{-5} Torr) as previously explained in ref 7. The solution formed was allowed to warm up to 5° and was stirred until all of the alkali metal dissolved. The time required for the metal to dissolve ranged from 4 hr for potassium to 12 hr for lithium. An aliquot of the resultant brownish solution was transferred to a side arm tube (3-mm o.d., Pyrex). These solutions of the [16]annulene anion radical are very stable. Over a period of 2 weeks a sample stored at room temperature showed only a very small decrease in the intensity of the ESR signal.

Preparation of samples with THF or DME as solvent followed along well-known lines.⁴ The reaction with the alkali metal mirror was conducted at -70° . At higher temperatures the mirror became covered with a brown precipitate preventing further reaction. Samples in these solvents typically yielded a large amount of a precipitate, presumably the [16]annulene dianion salt. In order to eliminate the occurrence of this precipitate the solution had to be dilute (10^{-3} M in DCOT) and only a very weak ESR signal was obtained. Thus only an order of magnitude of the disproportionation equilibrium constant could be obtained using these solvents.

X-Band ESR spectra were recorded using a Varian Associates E-9 spectrometer. The temperature in the ESR cavity was controlled using a constant flow of nitrogen gas and was measured with a copper-constantan thermocouple. Errors in relative values of temperature are $\pm 0.5^\circ$. To obtain hyperfine coupling constants, the magnetic field sweep was calibrated using a dual cavity with a sample of potassium naphthalenide in DME as standard.⁵ The g values were also determined using dual-cavity techniques. Potassium pyrenide in DME⁶ was the standard for the system $C_{16}H_{16}^-$ -HMPA-Na which was then used as the standard for $C_{16}H_{16}^-$ -HMPA-K and $C_{16}H_{16}^-$ -HMPA-Li.

The determination of thermodynamic parameters followed along previously described lines⁷⁻⁹ and is only briefly outlined here. The [16]annulene anion radical concentration was determined at room temperature by comparison of an overmodulated single-component spectrum to that of a standard sample of cyclooctatetraene (COT)-potassium in HMPA.¹⁰

The equilibrium constant for the disproportionation reaction of [16]annulene (eq 1) can be expressed in terms of readily measured quantities as in

$$K_{eq} = \frac{[\pi^{\cdot-}]^2}{\frac{1}{2}\{[DCOT][M] - \frac{1}{2}[M]^2\}} \quad (2)$$

where $[M]$ is the total concentration of metal added, $[DCOT]$ is the concentration of the dimer of COT, $[\pi]$,

$[\pi^{\cdot-}]$, and $[\pi^{2-}]$ are the concentrations of [16]annulene neutral molecule, anion radical, and dianion, respectively, and

$$[\pi^{2-}] = \frac{1}{2}\{[M] - [\pi^{\cdot-}]\} \quad (3)$$

$$[DCOT] = [\pi] + [\pi^{\cdot-}] + [\pi^{2-}] \quad (4)$$

$$[\pi^{\cdot-}] \ll [M] \quad (5)$$

The standard enthalpy change (ΔH°) of the disproportionation reaction was obtained from the temperature dependence of the ESR signal of the anion radical using a modified van't Hoff equation.^{7,8} Since $[\pi^{\cdot-}] \ll [\pi^{2-}]$, $[\pi]$, we plotted $\ln [h(\Delta w)^2]$ vs. $(RT)^{-1}$, which yielded a straight line with slope $-\Delta H^\circ/2$ (h is the peak height of the first-derivative ESR spectrum, and Δw is the line width between extrema). [The same value of ΔH° was obtained using either the central line of the resolved spectrum (line width and shape were independent of temperature) or an overmodulated single-component spectrum. A saturation study of [16]annulene anion was performed. All spectra used were taken at powers sufficiently low to avoid saturation.] The temperature range studied using HMPA as solvent was 0 – 40° . Below 0° the sample froze and above 60° the sample started to decompose.

Results and Discussion

When a solution of 0.5 mmol of DCOT (the syn (2 + 2) dimer of cyclooctatetraene) in 5.0 ml of HMPA reacts with 0.5 mg-atom of Li, K, or Na metal, a green brownish solution is produced with no evidence of precipitate formation. This solution exhibits an ESR spectrum which is essentially identical with that previously obtained by reduction of [16]annulene and ascribed to the [16]annulene anion radical¹ (see Table I).

Addition of more alkali metal to the anion radical solution described above results in a decrease in the ESR intensity. When 2 mol of alkali metal have reacted with 1 mol of the original COT dimer, the solution becomes diamagnetic. Addition of more DCOT to the diamagnetic solution under vacuum results in the return of the ESR signal. These experiments strongly suggest the formation of the [16]annulene dianion and the occurrence of an electron-transfer reaction between the dianion and DCOT to produce the [16]annulene anion radical.

There is also evidence for an electron-transfer reaction between DCOT and the anion radical. If we react DCOT with a small amount of alkali metal, the ESR spectrum observed for the anion radical is somewhat broadened. This broadening disappears upon reaction of equimolar amounts of DCOT and metal.

The completeness of the conversion of DCOT to species with the annulene framework is an essential requirement for the accuracy of the determination of thermodynamic parameters. This was checked using NMR. The NMR spectrum of a solution prepared using equimolar amounts of DCOT and metal in HMPA was compared to that of a solution of DCOT in HMPA. The DCOT spectrum is absent in the former case yielding a conservative upper limit of 10% unreacted.

Electron spin resonance has proven to be a very powerful technique in the study of ion association in liquid solution.^{11,12} The usual ESR evidence for ion pairing comes in a variety of forms: (1) occurrence of alkali metal hyperfine splitting, (2) occurrence of two or more spectra for the radical anion, one of which usually displays metal splittings, (3) variation of proton hyperfine splittings with counterion, (4)

TABLE I: ESR Spectral Parameters for the [16]Annulene Anion Radical^a

Solvent	Metal	a_1^b	a_2	a_3	Line width	g^c	Ref
HMPA	K	3.921	0.916	0.712	0.070	2.002608 ^d	<i>e</i>
HMPA	Li	3.902	0.909	0.708	0.070	2.002609 ^d	<i>e</i>
HMPA	Na	3.928	0.915	0.710	0.070	2.002612 ^d	<i>e</i>
DME	K	4.031	0.887	0.773	0.040		<i>e</i>
DMF	<i>f</i>	3.958	0.963	0.743	0.045	2.002611 ^e	<i>h</i>

^a All measurements were made at $20 \pm 1^\circ$. No alkali metal hyperfine splittings were observed. ^b Splittings are reported in gauss with an estimated error of $\pm 0.5\%$. No variation of the splittings was detected in the temperature range $0-60^\circ$. ^c Corrected for second-order shifts (-6×10^{-6} correction). Estimated error is $\pm 4 \times 10^{-6}$. ^d According to Allendoerfer⁶ these values should be decreased by 1.4×10^{-5} due to an error in the work of Segal et al.⁶ ^e This work. ^f Tetra-*n*-butylammonium perchlorate was used as supporting electrolyte. ^g Estimated error $\pm 5 \times 10^{-6}$. ^h Reference 1.

variation of g value with counterion, (5) temperature dependence of the g value, and (6) line-broadening effects.

Typically ion-pairing studies have been conducted in the ethereal solvents THF and DME. In contrast, HMPA, a powerful solvating agent for alkali metal ions,¹³ has been held to produce "free" hydrocarbon radical ions.¹⁴⁻¹⁷ The evidence consists of (1) absence of alkali metal splittings, (2) conductivity measurements, (3) absence of dimerizations of radical ions associated with contact ion pairs, and (4) enhanced electron-transfer rates.

In this work we have extended the above criteria for the occurrence of free hydrocarbon radical anions in HMPA through a series of very careful ESR measurements. As can be noted in Table I, the g value of the [16]annulene anion is the same within estimated error limits of $\pm 4 \times 10^{-6}$ for lithium, potassium, and sodium counterions. We have made a very careful attempt to measure a temperature dependence of the g value. The dual-cavity technique was employed with the [16]annulene anion at room temperature as the standard. No temperature dependence was observed; that is, $dg/dT < 0.2 \times 10^{-7} \text{ deg}^{-1}$. As a check on our technique we performed similar experiments for the cyclooctatetraene anion and tetramethylcyclooctatetraene anion radicals in HMPA and found $dg/dT = 2 \times 10^{-7}$ and 0.0 deg^{-1} , respectively. (These results will be discussed elsewhere.¹⁵) A third finding is that the proton splittings are also independent of counterion within experimental error.¹⁹ Finally, the ESR line width of 70 mG is independent of temperature and counterion. All of the above experimental results, plus the absence of metal hfs, point to the occurrence of free [16]annulene radical anions in HMPA.

Stevenson and Concepcion⁷⁻⁹ have introduced a sensitive probe of ion association effects for hydrocarbon systems in HMPA. Using ESR they studied the variation of the thermodynamic parameters controlling the disproportionation reaction (eq 1) with variation of alkali metal counterion. Such effects were demonstrated by these workers for cyclooctatetraene and substituted cyclooctatetraene anion radicals in HMPA and were ascribed to the occurrence of ion pairing for the anion radical and dianion, respectively.

In this work we have performed a similar study for the case of the [16]annulene disproportionation equilibrium. Values of the equilibrium constant for this reaction were obtained as described in the Experimental Section. These results are summarized in Table II. Also reported are values of ΔH° and ΔS° corresponding to the various alkali metal counterions. A typical plot from which a value of ΔH° was extracted is given in Figure 2.

When solutions of DCOT in THF or DME ($10^{-2} M$) react with potassium metal, a relatively large amount of

TABLE II: Thermodynamic Parameters for the Disproportionation Equilibrium of [16]Annulene

System	$K_{eq}^{a,b}$	$\Delta H^\circ, ^c$ kcal/mol	$\Delta S^\circ, \text{eu}$
HMPA-K ^a	$(2.3 \pm 0.8) \times 10^{-6}$	-3.9 ± 0.1	-39
HMPA-Na ^a	$(9.6 \pm 3.1) \times 10^{-6}$	-3.5 ± 0.1	-35
HMPA-Li ^a	$(3.8 \pm 1.1) \times 10^{-6}$	-4.5 ± 0.1	-40
THF-K	Ca. 10^{-9}		
DME-K	Ca. 10^{-8}		

^a At room temperature. ^b Six runs were made for each counterion. Error limits are the standard deviation of the mean. ^c ± 0.1 kcal/mol estimated precision measure.

precipitate is observed, probably due to the low solubility of the dianion salt in these solvents. Only order-of-magnitude estimates of the disproportionation equilibrium constants were obtained (cf. Table II). The occurrence of ion pairing is known to shift the disproportionation equilibrium toward the dianion salt.²⁰ The results of Table II are in agreement with this observation since the equilibrium constants decrease in order of increasing tendency of the solvents for ion-pair formation, namely, HMPA < DME < THF.

It is of interest to compare our thermodynamic parameters for $C_{16}H_{16}^-$ with those obtained previously for the smaller monocycle $C_8H_8^-$, both in HMPA. The COT⁻ results are given in Table III.

Qualitatively, we expect that variations of the thermodynamic parameters, and hence ion association effects, should be smaller for the larger radical since the charge on the anion and dianion is more dispersed. This is borne out by the results. For example, the variation of K_{eq} with counterions is much smaller in the case of $C_{16}H_{16}^-$ (factor of 4) than in the case of $C_8H_8^-$ (factor of 100).

Further, variations in ΔH° are only 1 kcal/mol for $C_{16}H_{16}^-$ as compared with 3 kcal/mol for $C_8H_8^-$. The maximum variation in ΔS° is 20 eu for COT⁻ but is only 5 eu for the [16]annulene anion.²¹ It is interesting to note that in both cases the same ordering of ΔS° values is obtained and in both cases the largest magnitude of ΔH° is found for lithium.

We conclude that even for a hydrocarbon framework of the size of [16]annulene, ion association effects in HMPA are still detectable using the thermodynamic parameters probe although the magnitude of the effect is quite small. In contrast with previous work⁷⁻⁹ we ascribe the variation in ion association with counterion to dianion species rather than to the radical ion. The ESR results obtained in this work as well as numerous previous studies¹⁴⁻¹⁷ argue

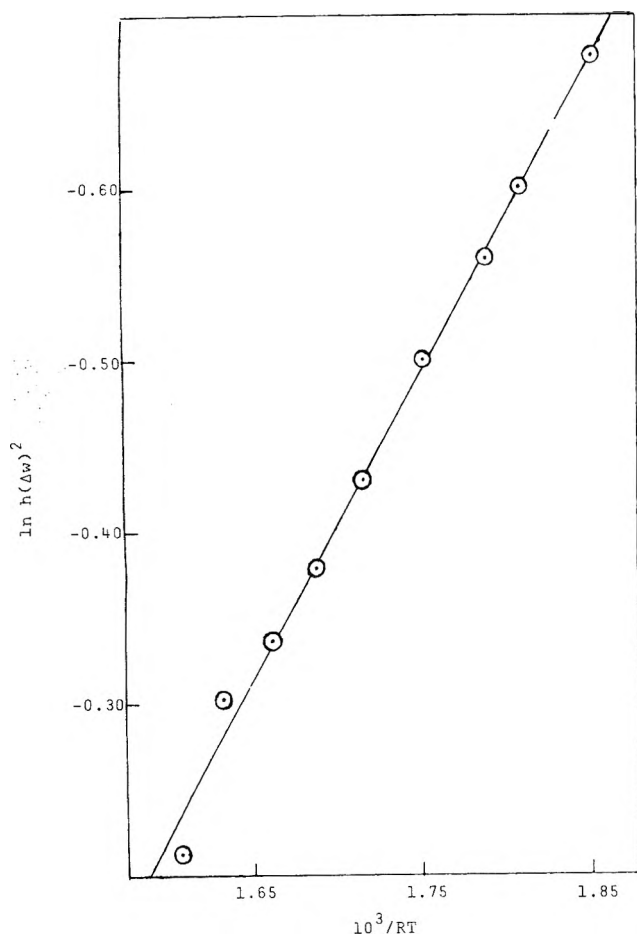


Figure 2. Plot of $\ln h$ vs. $10^3/RT$ for the system [16]annulene anion-HMPA-K. The line width Δw was constant over the temperature range studied.

TABLE III: Thermodynamic Parameters for the COT Anion Disproportionation Equilibrium in HMPA at 25^oa

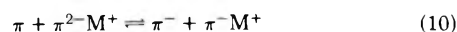
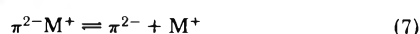
System	K_{eq}	ΔH° , kcal/mol	ΔS° , eu
HMPA-Li	5.0×10^{-4}	-7.8	-41
HMPA-Na	2.3×10^{-3}	-4.2	-26
HMPA-K	2.3×10^{-5}	-4.6	-37

^a Results from ref 7. The values given for ΔS° have been modified to correct for an arithmetic error in ref 7.

strongly against the occurrence of ion pairing for the hydrocarbon radical.

In an effort to have our analysis more directly reflect the actual physical situation in the HMPA solutions, we have explored various equilibria other than eq 1 and have attempted to reinterpret our data in terms of such expressions.²²

Let π denote [16]annulene and M denote the alkali metal. One can write a series of ionization and disproportionation equilibria as



We assume that the equilibrium constants K_6 and K_8 are very large and that the variation of K_7 with counterion gives rise to the variation in thermodynamic parameters which is observed. We focus attention on the disproportionation equilibria eq 9 and 10. There are three possibilities to be considered: (1) (case A) $[\pi^{2-}M^+]$ and $[\pi^{2-}]$ are of the same order of magnitude, (2) (case B) $[\pi^{2-}M^+] \gg [\pi^{2-}]$, and (3) (case C) $[\pi^{2-}] \gg [\pi^{2-}M^+]$.

Case A. Adding eq 8-10 we obtain

$$K_8K_9K_{10} = \frac{[\pi^-]^4[M^+]}{[\pi]^2[\pi^{2-}][\pi^{2-}M^+]} \quad (11)$$

Using mass and charge balance and neglecting $[\pi^-M^+]$, $[\pi^-]$, and $[\pi^{2-}M^+]$

$$K_8K_9K_{10} = \frac{[\pi^-]^4\{\frac{1}{2}[M] + [\pi^{2-}]\}}{\{[DCOT] - \frac{1}{2}[M]\}^2[\pi^{2-}]\{\frac{1}{2}[M] - [\pi^{2-}]\}} \quad (12)$$

Case B

$$K_8K_{10} = \frac{[\pi^-]^2[M^+]}{[\pi][\pi^{2-}M^+]} \quad (13)$$

Using mass and charge balance with $[\pi^{2-}]$ neglected

$$K_8K_{10} = \frac{[\pi^-]^2}{[\pi]} = \frac{[\pi^-]^2}{[DCOT] - \frac{1}{2}[M]} \quad (14)$$

Case C

$$K_9 = \frac{[\pi^-]^2}{[\pi][\pi^{2-}]} = \frac{[\pi^-]^2}{\{[DCOT] - \frac{1}{2}[M]\}\{\frac{1}{2}[M]\}} \quad (15)$$

(cf. eq 2).

An experimental test of the analysis given for case A would be desirable since it is the most general case. This would require an experimental determination of $[\pi^{2-}]$ and $[\pi^{2-}M^+]$ and is outside the scope of the present work.

From eq 14 and 15 it is seen that the dependence of $[\pi^-]$ on [DCOT] and [M] should be different for case B and case C. We have therefore considered the question, can we distinguish whether our experimental situation is closer to case B or case C. We have run a set of five additional determinations of the equilibrium concentration of the [16]annulene anion, $[\pi^-]$, for the system HMPA-K (20°) varying the values of [DCOT] and [M]. The data are given in Table IV. Also given is the disproportionation equilibrium constant calculated using eq 2 or 15 as before. The average value is 2.4×10^{-6} which is in excellent agreement with the value given in Table II, $(2.3 \pm 0.8) \times 10^{-6}$.

If case B holds, then $[\pi^-]$ is inversely proportional to the square root of $\{[DCOT] - \frac{1}{2}[M]\}$, but if case C is valid, then $[\pi^-]$ is inversely proportional to the square root of $\{[DCOT] - \frac{1}{2}[M]\}\{\frac{1}{2}[M]\}$. In Table V we compare the ratios calculated assuming that case B and case C hold with the experimental ratios for various pairs of runs from Table IV. For five of the seven entries in Table V, case C gives better agreement than case B. The average deviation between experimental and calculated ratios is 0.15 for case C and 0.40 for case B. Since the data are limited, we can only conclude that it seems probable that (1) we are close to the free-ion disproportionation equilibrium situation, thus supporting the use of eq 2 in this work, and by inference in the previous work of Stevenson and Concepción, and (2) the variation in the thermodynamic parameters of the disproportionation equilibrium for the [16]annulene anion in HMPA is not due to ion pairing for the radical but rather to

TABLE IV: Disproportionation Equilibrium Data for the System [16]Annulene-HMPA-K (20°C) with Varying Values of [DCOT] and [M]

Run	$10^2\{\frac{1}{2}[M]\}^a$	$10^2[\pi]_r^b$	$10^5[\pi^-]_r$	$10^6K_{eq}^{c,d}$
1	4.80	0.68	2.52	1.9
2	4.84	4.79	7.12	2.3
3	4.53	7.46	10.40	2.5
4	7.50	2.34	6.56	2.5
5	2.50	7.44	7.20	2.8

^a All concentrations are given in molar units. ^b The quantity tabulated is $[\text{DCOT}] - \frac{1}{2}[\text{M}]$. ^c Calculated using eq 2 or 15, both of which are identical. ^d The average value of K_{eq} equals 2.4×10^{-6} .

TABLE V: Comparison of Calculated and Experimental Ratios of $[\pi^-]_r/[\pi^-]_s$ for Various Runs Listed in Table IV

Run r	Run s	$[\pi^-]_r/[\pi^-]_s$		
		Calcd		Exptl ^c
		Case B ^a	Case C ^b	
5	4	1.79	1.03	1.09
5	3	1.00	0.74	0.68
5	2	1.24	0.90	1.01
5	1	3.38	2.43	2.86
4	3	0.56	0.72	0.63
4	2	0.70	0.87	0.92
4	1	1.89	2.35	2.60

^a Calculated using eq 14. ^b Calculated using eq 15. ^c The mean deviations of experimental from calculated ratios are 0.40 and 0.15 for case B and case C, respectively (mean deviation = $\Sigma|\text{Exptl} - \text{Calcd}|/n$).

changes in the concentrations of the free dianion, π^{2-} , and the corresponding singly metalated species $\pi^{2-}\text{M}^+$. A similar situation probably holds for other large systems with extensive charge delocalization.²³

Acknowledgments. This work was supported by the U.S. Army Research Office—Durham. J.G.C. gratefully acknowledges postdoctoral fellowship support by The Graduate School, Syracuse University. We wish to thank Professors M. Szwarc, J. Smid, and G. Levin for helpful discus-

sions and Professor A. G. Anastassiou for a generous gift of DCOT. We are grateful to the National Science Foundation (Chemistry Research Instrumentation Program) for the partial support of the purchase of the ESR spectrometer used in this work.

References and Notes

- (1) J. F. M. Oth, H. Baumann, J.-M. Gilles, and G. Schröder, *J. Am. Chem. Soc.*, **94**, 3498 (1972).
- (2) Equation 1 is written as the reverse of a conventional disproportionation reaction but is given as shown to maintain consistency with previous ESR studies to which comparisons are made (cf. ref 7–9).
- (3) R. M. Lazarus, Ph.D. Dissertation, Syracuse University, 1971.
- (4) J. R. Bolton and G. K. Fraenkel, *J. Chem. Phys.*, **40**, 3307 (1964).
- (5) J. R. Bolton and J. E. Wertz "Electron Spin Resonance Elementary Theory and Practical Applications", McGraw-Hill, New York, N.Y., 1972, p 63.
- (6) B. G. Segal, M. Kaplan, and G. K. Fraenkel, *J. Chem. Phys.*, **43**, 4191 (1965); R. D. Allendoerfer, *ibid.*, **55**, 3615 (1971).
- (7) G. R. Stevenson and J. G. Concepcion, *J. Phys. Chem.*, **76**, 2176 (1972).
- (8) G. R. Stevenson and J. G. Concepcion, *J. Am. Chem. Soc.*, **95**, 5692 (1973).
- (9) J. G. Concepcion, Ph.D. Thesis, University of Puerto Rico, 1973.
- (10) F. J. Smentowski and G. R. Stevenson, *J. Phys. Chem.*, **73**, 340 (1969).
- (11) J. H. Sharp and M. C. R. Symons, "Ions and Ion Pairs in Organic Reactions", Vol. 1, M. Szwarc, Ed., Wiley, New York, N.Y., 1972, Chapter 5.
- (12) J. L. Sommerdijk and E. de Boer, ref 11, Chapter 8.
- (13) H. Normant, *Angew. Chem., Int. Ed. Engl.*, **6**, 1046 (1957); D. A. Owensby, A. J. Parker, and J. W. Diggle, *J. Am. Chem. Soc.*, **96**, 2682 (1974).
- (14) A. Cserhegyi, E. Franta, J. Chaudhuri, J. Jagur-Grodzinski, and M. Szwarc, *J. Am. Chem. Soc.*, **89**, 7129 (1967).
- (15) G. Levin, J. Jagur-Grodzinski, and M. Szwarc, *J. Am. Chem. Soc.*, **90**, 6421 (1968).
- (16) A. Cserhegyi, J. Jagur-Grodzinski, and M. Szwarc, *J. Am. Chem. Soc.*, **91**, 1892 (1969).
- (17) G. Levin, J. Jagur-Grodzinski and M. Szwarc, *J. Am. Chem. Soc.*, **92**, 2268 (1970).
- (18) J. G. Concepcion and G. Vincow, *J. Phys. Chem.*, following article in this issue.
- (19) It is interesting to note that the proton splittings in HMPA are smaller in magnitude than those in DMF.¹ We have measured proton splittings for a number of hydrocarbon anions in HMPA (COT^- , Me_2COT^- , and $\text{C}_{10}\text{H}_8^-$). These are uniformly smaller in magnitude than splittings in the literature for other solvents: J. G. Concepcion and G. Vincow, unpublished results.
- (20) R. D. Allendoerfer and P. H. Rieger, *J. Am. Chem. Soc.*, **87**, 2336 (1965).
- (21) Such a decrease in the maximum variation of ΔS° has been found previously⁸ in a comparison of PhCOT and COT anions and was ascribed to extended conjugation in the larger species, decreasing electron–electron repulsion effects in the dianion.
- (22) The thermodynamic analysis of the disproportionation equilibrium developed previously^{7–9} and reviewed in the Experimental Section can be interpreted according to the suggestion of J. F. Garst and E. R. Zabolotny, *J. Am. Chem. Soc.*, **87**, 495 (1965), that one may use the equilibrium constant, K_{eq} , for eq 1 as an index of the position of a complex set of equilibria rather than as a measure of the very simple free-ion equilibrium.
- (23) Reported in part at the 168th National Meeting of the American Chemical Society, Atlantic City, N.J., Sept 1974; see Abstracts, No. PHYS 44.

Electron Spin Resonance Studies on the 1,3,5,7-Tetramethylcyclooctatetraene Anion Radical

Jesús Gilberto Concepción and Gershon Vincow*

Department of Chemistry, Syracuse University, Syracuse, New York 13210 (Received November 18, 1974; Revised Manuscript Received May 12, 1975)

Publication costs assisted by Syracuse University

The molecular geometries of cyclooctatetraene (COT), COT anion and dianion, and their alkyl-substituted analogs are of great interest in connection with the predictions of the Hückel $4n + 2$ rule and with anomalous ESR effects noted for orbitally near degenerate radicals. In this work the ESR of the anion radical of 1,3,5,7-tetramethylcyclooctatetraene (TMCOT) is investigated in order to shed light on molecular geometry and effects of orbital near degeneracy. Analysis of the ^{13}C hyperfine spectrum is consistent with a planar geometry. The first methyl-group ^{13}C hyperfine splitting for a hydrocarbon anion is reported and an empirical method for assigning such splittings is proposed. The temperature dependence of the proton splittings is measured. Analysis of these data in terms of a two-level statistical model and the HMO spin distribution yields an estimate of 1.8 kcal/mol for the lifting of molecular orbital degeneracy by alkyl substituents.

Introduction

We have previously conducted several ESR investigations of highly symmetrical hydrocarbon free radicals in order to elucidate the effects of vibronic near degeneracy.^{1,2} Some of the ESR results reported by us and others are not yet well understood.¹ One possible source of these "anomalies" would be the occurrence of nonplanarity in the seven- and eight-membered ring radicals.

Particular interest has been focused in the literature on the planarity of the 10π electron dianions of cyclooctatetraene (COT) and substituted cyclooctatetraenes. The Hückel $4n + 2$ rule prediction of aromaticity for such species has been a prime motivating factor. The pioneering work of Katz³ on the unsubstituted dianion and more recent NMR work by Paquette and coworkers on the dianion of 1,3,5,7-tetramethylcyclooctatetraene⁴ (Figure 1) and of several dimethyl-substituted cyclooctatetraenes⁵ have indicated that these are stable planar species. Very recent crystallographic work by Goldberg, Raymond, Harmon, and Templeton on the potassium diglyme 1,3,5,7-tetramethylcyclooctatetraene dianion has confirmed that the substituted cyclooctatetraene dianion is planar.⁶ Since cyclooctatetraene itself has a tub geometry it is of interest to ask whether, in the intermediate oxidation state, the anion radical is planar.

For these reasons we have studied the ESR of the 1,3,5,7-tetramethylcyclooctatetraene (TMCOT) anion and in particular the ^{13}C hyperfine spectrum. ^{13}C hyperfine couplings are known to be particularly sensitive to molecular geometry.

Very few methyl-group ^{13}C hyperfine splittings have been studied to date. In this work we report the first such splitting for a hydrocarbon anion. We also study the temperature dependence of the proton splittings and correlate this with the lifting of molecular-orbital degeneracy.

Experimental Section

1,3,5,7-Tetramethylcyclooctatetraene (TMCOT) was prepared by the methods of Mayo and Yip⁷ and Cotton et

al.⁸ Hexamethylphosphoramide (HMPA) was purchased from the Aldrich Chemical Co. It was distilled under vacuum from calcium hydride, and stored over Linde 4A molecular sieves. Spectroquality dimethylformamide (DMF) was obtained from Matheson Coleman and Bell. It was fractionally distilled under a nitrogen atmosphere and stored over Linde 4A molecular sieves.

The TMCOT anion radical was prepared in HMPA via alkali-metal reduction (K and Na),⁹ and in DMF via electrolytic reduction with the tetra-*n*-propylammonium ion (TNPA) serving as a counterion.¹⁰

X-Band ESR spectra were obtained using a Varian Associates E-9 spectrometer. The temperature in the cavity was measured with a copper-constantan thermocouple. Relative errors in the temperature were $\pm 0.5^\circ$, and absolute errors were $\pm 2^\circ$. The dual-cavity method used for the determination of g values and the measurement of the hyperfine splittings has been described previously.¹¹

Results and Discussion

The anion radical of TMCOT in HMPA was first prepared by Stevenson and Concepcion.² The larger coupling constant ($a_1 = 6.4$ G) was assigned to the 12 methyl protons, and the smaller one ($a_2 = 0.4$ G) to the four ring protons. They explained the observed behavior in terms of the lifting of the degeneracy in the nonbonding molecular orbitals of the cyclooctatetraene anion by the four electron-releasing methyl groups. Using a Boltzmann distribution analysis and following a Hückel MO model, these authors estimated an energy difference of 1.6 kcal/mol between the two electronic states.

We have confirmed the previously obtained proton couplings and have made a careful search for ESR manifestations of ion-pairing effects in HMPA. The proton couplings and g values measured in HMPA-K, HMPA-Na, and DMF-TNPA are given in Table I. Within error limits there is no discernible effect of the counterion on the measured parameters in HMPA. In addition, we have searched for a temperature dependence of the g value in the range of 0–

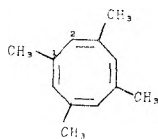


Figure 1. Structural formula for 1,3,5,7-tetramethylcyclooctatetraene.

TABLE I: Proton Coupling Constants and g Values for the TMCOT Anion Radical

System	a_1, G^a	a_2, G	Line width, mG	$g^{b,d}$
HMPA-Na	6.407	0.448	70	2.002654
HMPA-K	6.414	0.452	70	2.002655
Elect-DMF	6.551	0.528	180	

^a Errors in the proton couplings are less than 1%. ^b The uncertainty in the g value is ± 0.000002 . ^c These values are not corrected for second-order effects. ^d Measured relative to the g value of potassium pyrenide as primary standard. The value reported for that radical by Segal, Kaplan, and Fraenkel (*J. Chem. Phys.*, **43**, 4191 (1965)) was used. R. D. Allendoerfer has reported an error in this work which would lower all values by 14×10^{-6} (*J. Chem. Phys.*, **55**, 3615 (1971)).

65°. Within error limits for dg/dT of $\pm 1 \times 10^{-8}$ ($^{\circ}\text{K}$)⁻¹, there is no variation. These results, plus the absence of metal hyperfine splitting, tend to confirm the previously held view that HMPA, a powerful solvating agent for alkali metal ions,¹² produces free hydrocarbon radical ions.^{13,14}

Since power saturation has been used as an indicator of degeneracy,¹⁵ it was interesting to consider the power-saturation behavior of the TMCOT anion and compare it to that of anions which are known to be either degenerate or nondegenerate. For the degenerate systems we chose the cyclooctatetraene anion (C_8H_8^-) and the benzene anion (C_6H_6^-), and for the nondegenerate system the naphthalene anion ($\text{C}_{10}\text{H}_8^-$). A plot of the log of the relative intensity of the ESR signal of a particular system vs. the log of the microwave power is shown in Figure 2. From this figure it is clear that the saturation behavior of the TMCOT anion is close to that of the nondegenerate system.

Another indication of significant lifting of degeneracy in TMCOT anion is the small line width. When the alkali metal was in contact with a dilute solution of TMCOT (ca. 10^{-3} M) for a short period of time (10–15 sec) the component width of the ESR spectrum was 35 mG for both Na and K. At a modulation amplitude of 5–10 mG further structure was resolved which could be assigned to second-order effects in the large methyl-proton splitting.¹⁷ A simulated spectrum including second-order effects is in complete agreement with the experimental results and is shown in Figure 3. The minimum line width obtainable for the COT anion is approximately 350 mG. This large line width has been ascribed to effects of orbital degeneracy.

If the temperature of the above TMCOT anion sample is raised to 70°, the second-order structure broadens considerably. If the sample is allowed to react with metal for 30–45 sec or longer no such structure can be resolved. These observations are consistent with the occurrence on the ESR time scale of an electron transfer reaction between TMCOT anion and dianion. Similar results have been obtained previously for the COT anion.^{3,9}

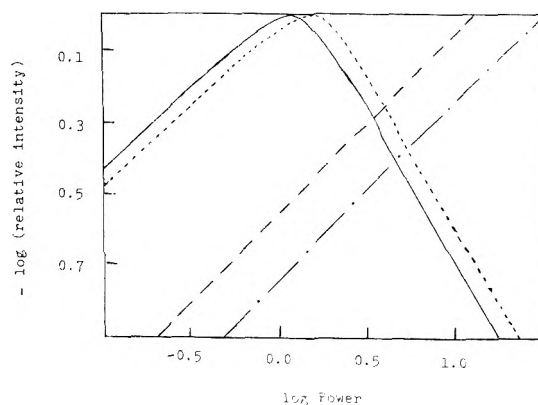


Figure 2. Power saturation study for the anion radicals of 1,3,5,7-tetramethylcyclooctatetraene (· · · · ·), naphthalene (—), cyclooctatetraene (- · - · -), and benzene (- - -). Plot of the log of the relative intensity of the ESR signal vs. the log of the microwave power. The power was monitored by the meter in the microwave bridge.

A careful study was made of the variation of the proton splitting constants with temperature. The magnitude of the 0.4-G ring-proton splitting increases by about 6% in the range 0 to 50° (Figure 4); i.e., the temperature coefficient is $d|a_2|/dT = +6 \times 10^{-4}$ G/ $^{\circ}\text{K}$. The methyl-proton hfs, which is large and positive in sign, decreases as the temperature is increased (Figure 4), with a temperature coefficient $da_1/dT = -(2.8 \pm 0.3) \times 10^{-3}$ G/ $^{\circ}\text{K}$.

Since the TMCOT anion is a nearly degenerate radical it is reasonable to fit these temperature dependences to a two-level model, as we have previously done for the *tert*-butyltropylenyl radicals.¹ If we make the usual approximation of a proportionality between splittings and π spin density, then the π spin density at any temperature ($\rho^\pi(T)$) can be represented as a statistical average of spin densities in the ground ($\rho^{\pi,G}$) and excited ($\rho^{\pi,E}$) states

$$\rho^\pi(T) = \frac{\rho^{\pi,G} + \rho^{\pi,E} \exp(-\Delta E/kT)}{1 + \exp(-\Delta E/kT)} \quad (1)$$

In eq 1, ΔE denotes the energy difference between the states. Differentiating and multiplying by the appropriate Q factor, one obtains

$$\frac{d\alpha(T)}{dT} = Q \frac{(\rho^{\pi,E} - \rho^{\pi,G})(\Delta E/kT^2) [\exp(-\Delta E/kT)]}{[1 + \exp(-\Delta E/kT)]^2} \quad (2)$$

In order to extract a value of ΔE from the temperature-dependence data, we must assume values for $\rho^{\pi,G}$, $\rho^{\pi,E}$, and Q . We consider first the methyl-proton case and use $Q^{\text{HCH}_3} = +25$ G. Spin densities are chosen according to the Hückel MO (HMO) theory with $\rho^{\pi,G} = 1/4$ and $\rho^{\pi,E} = 0$. This facilitates comparison with the previous work of Stevenson and Concepcion.² In addition, the Hückel model yields a fairly good approximation for the spin-density distribution in alkyl-substituted C_nH_n radicals. Two important factors, electron correlation and vibronic coupling, are neglected. Their contributions, however, tend to cancel.

A general expression for the spin-density distribution in the two nearly degenerate unpaired-electron MOs is

$$\rho_{kk}^\pi = \frac{1}{8} [1 \mp \gamma \eta \cos k\pi] \quad (3)$$

where γ and η are the electron correlation and vibronic coupling factors, respectively. For the HMO method, $\gamma = 1$. Moss¹⁶ has made detailed vibronic calculations for the alkylcyclooctatetraene anions. Using an approximate configu-

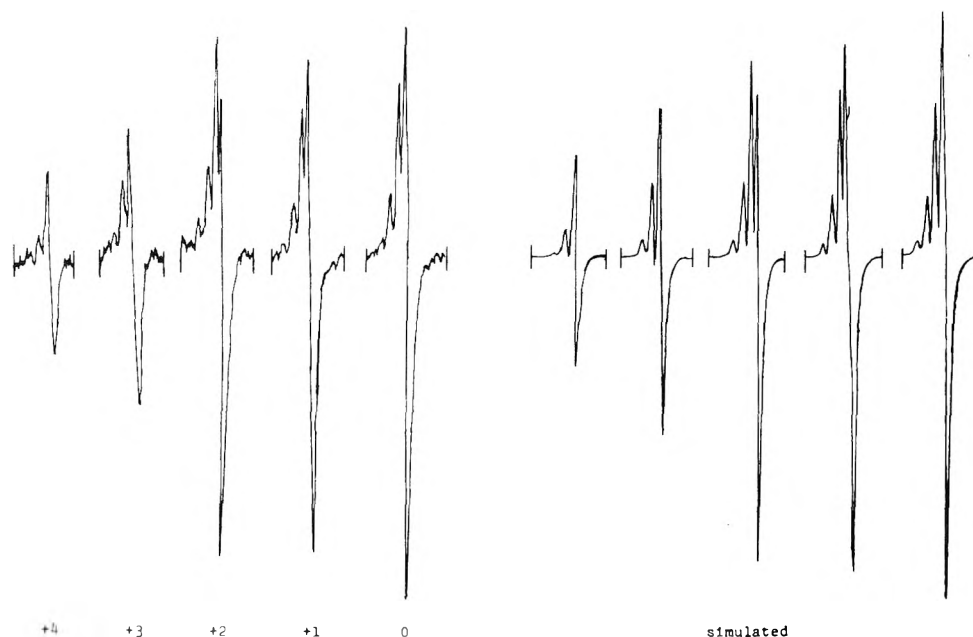


Figure 3. Center lines of the quintets in the proton spectrum of the TMCOT anion. The lines shown are due to $M_1 = 0, +1, +2, +3,$ and $+4$. The intensity of the lines arising from $M_1 = +2, +3,$ and $+4$ are increased for better visual presentation in both the experimental and simulated spectra.

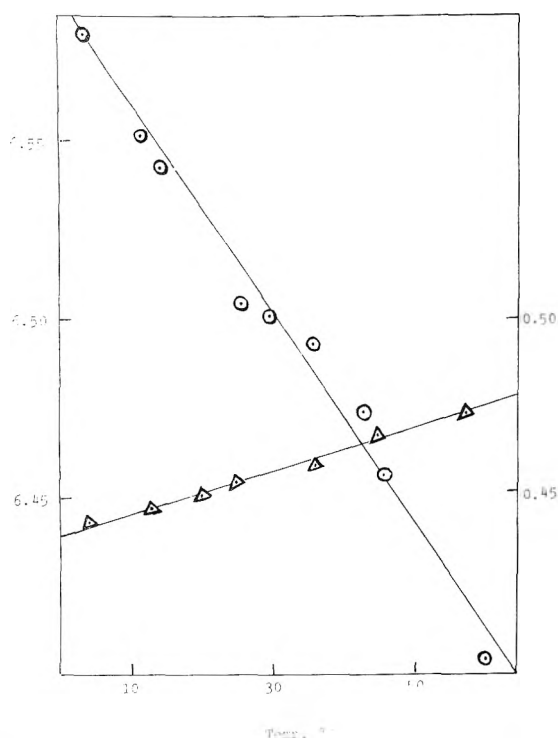


Figure 4. Plot of $|a_1|$ and $|a_2|$ vs. temperature for the TMCOT anion radical. The values of $|a_1|$ are denoted by \odot , while those of $|a_2|$ are represented by Δ (ordinate scale at the right).

ration-interaction method, he found $\gamma = 1.42$. In addition he developed a theory of vibronic coupling and found that the values of η , which depend on the electronic MO splitting, are significantly smaller than unity. The two factors thus tend to cancel in the product $\gamma\eta$. Similarly, Vincow and coworkers¹ studied alkyl-substituted cycloheptatrienyl radicals and found that $\gamma\eta = 1.0 \pm 0.1$ in excellent agree-

ment with the spin densities obtained from HMO theory ($\gamma = 1$).

To obtain ΔE , eq 2 is rearranged as follows:

$$\frac{T}{Q[\rho^{\pi,E} - \rho^{\pi,G}]} \frac{da(T)}{dT} = \frac{xe^{-x}}{(1 + e^{-x})^2} \quad (4)$$

$$x = \Delta E/kT$$

The right-hand side of eq 4 is plotted in Figure 5 vs. ΔE ($T = 293^\circ\text{K}$) and a graphical solution is easily found. There are two solutions $\Delta E = 0.3 \pm 0.05$ and 1.8 ± 0.1 kcal/mol. The smaller value can be eliminated since it predicts splittings of $a_1 = 3.9$ G and $a_2 = 2.3$ G, which are in poor agreement with experiment. The larger value is in excellent agreement with previous work,² in which $\Delta E = 1.6$ kcal/mol was obtained from an analysis of the magnitudes of the splittings at room temperature.

Next we consider the ring-proton temperature dependence and choose $Q^{\text{H}_{\text{CH}}} = -25.67$ G,³ $\rho^{\pi,G} = 0$, and $\rho^{\pi,E} = 1/4$. From an inspection of eq 2 and the similarity of $|Q^{\text{H}_{\text{CH}}}|$ and $|Q^{\text{H}_{\text{CH}_3}}|$, it is clear that the temperature coefficient of the ring splitting should be essentially the same as that of the methyl splitting, i.e., $da_2/dT \approx -3 \times 10^{-3}$ G/ $^\circ\text{K}$ for $\Delta E = 1.8$ kcal/mol. Assuming a negative value for a_2 , which is expected for $\Delta E = 1.8$ kcal/mol and a Hückel MO model, the experimental temperature coefficient is $da_2/dT = -0.6 \times 10^{-3}$, which is of the same sign but is considerably smaller in magnitude than the predicted value.

This discrepancy may be due to a contribution from another mechanism. Using a vibrational model to rationalize their results, Reddoch and coworkers¹³ have developed a semiempirical expression for the temperature dependence of ring-proton coupling constants in planar π -electron radicals

$$10^5(a_i)^{-1}(da_i/dT) = (-3.8 \pm 1.2) - (3.23 \pm 0.21)[(a_{i+1} + a_{i-1})/a_i] \quad (5)$$

where $a_i, a_{i\pm 1}$ are the hfs at the proton i of interest and at the neighboring protons, respectively. As can be readily

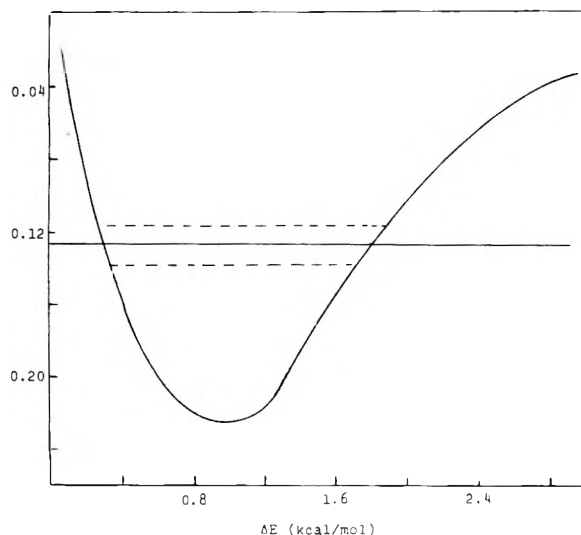


Figure 5. Combined plot of $[T/Q(\rho^{\pi,E} - \rho^{\pi,G})][da(T)/dT]$ (straight lines) and $[x \exp(-x)]/[1 + \exp(-x)]^2$ (curve) vs. ΔE (kcal/mol), where $x = \Delta E/kT$ and $T = 293^\circ\text{K}$. The dashed lines represent the error limits.

concluded from an examination of the second term in eq 5, this mechanism is most significant for the case of a position with a small splitting adjacent to positions of large spin density. This is precisely the case for a_2 of TMCOT anion.

Using eq 5, with $a_2 < 0$, one computes $da_2/dT = +4.4 \times 10^{-4} \text{ G}/^\circ\text{K}$. This is of the correct sign to partially cancel the value predicted from the statistical calculation, but does not account quantitatively for the entire discrepancy. This insufficiency may itself be related to the occurrence of near degeneracy. The Reddoch correlation was developed for the case of radicals with nondegenerate ground states. It is clear that in our case a complex averaging is required. If we focus on the ground state only, since this state dominates the statistics at room temperature with $\Delta E = 1.8 \text{ kcal/mol}$, we would expect a smaller value of a_2 , a larger value of $[(a_{i+1} + a_{i-1})/a_i]$, and consequently a larger magnitude of temperature coefficient based on eq 5. It is not possible to make a quantitative estimate of the ground-state contribution at present.

Now, we turn our attention to the ESR spectrum of the TMCOT anion with one carbon-13 atom in natural abundance. Due to the stability and concentration of the radical, the large separation of the quintets in the proton ESR signal and the fact that the ^{13}C spectrum falls essentially between those multiplets, it was possible to study the weak ^{13}C spectrum with this isotope present in natural abundance. An amplified experimental spectrum and a computer-simulated spectrum are given in Figures 6 and 7, respectively.

We first focused attention on this spectrum as a whole to see if it was possibly due to impurities in the hydrocarbon sample. This is not the case, since the signal observed was symmetric and since the same pattern repeats itself consistently between the quintets in the proton spectrum. In addition, the ratio of the intensity of each ^{13}C line to that of the corresponding proton line was 0.021. This compares well with the theoretical prediction of 0.022 for four equivalent ^{13}C nuclei (see below).

From an analysis of Figure 6 and extensive computer simulation it can be unambiguously concluded that the splittings arise from three different ^{13}C nuclei each corre-

TABLE II: ^{13}C Coupling Constants for the TMCOT Anion Radical

System	$a_{\text{CH}_3}^{\text{C}}$, G ^{a,b}	a_2^{C} , G	a_1^{C} , G
HMPA-Na	± 4.23	-6.37	+9.40
HMPA-K	± 4.27	-6.30	+9.37

^a Errors in the splitting constants are less than 2%. ^b The assignments and the signs of the splitting constants are discussed in the text.

sponding to four equivalent positions. We measured the ^{13}C coupling constants using two alkali metals, K and Na, in order to search for any dependence on counterion. No significant differences were observed. The results are listed in Table II.

There has been relatively little work to date on methyl-group ^{13}C splittings. Strauss and Fraenkel¹⁹ have studied the ^{13}C splittings due to the methyl-group carbons of a series of methyl-substituted *p*-benzosemiquinone anion radicals. Semiempirical calculations of both the MO and VB variety were performed. Both indicated a proportionality between $a_{\text{CH}_3}^{\text{C}}$ and $a_{\text{CH}_3}^{\text{H}}$. The data for four methyl-substituted semiquinones yield an average value of $|a_{\text{CH}_3}^{\text{C}}|/|a_{\text{CH}_3}^{\text{H}}| = 0.38$ or 0.71. Fessenden has measured the methyl group ^{13}C splitting for the ethyl radical. The magnitude is 13.57 G and the ratio of carbon to proton splitting is 0.51.

These empirical ratios are used to assign the ^{13}C splitting which corresponds to the methyl-group carbon in the TMCOT anion. For this radical we have three different splittings with magnitudes of 4.23, 6.37, and 9.4 G. Since $|a_{\text{CH}_3}^{\text{H}}| = 6.41 \text{ G}$, we obtain for the ratio $|a_{\text{CH}_3}^{\text{C}}|/|a_{\text{CH}_3}^{\text{H}}|$ the values 0.67, 1.0, and 1.5, respectively. The empirical range 0.4 to 0.7 mentioned above strongly suggests that the 4.23-G splitting is due to the methyl-group carbons.

There appears to be a discrepancy between theoretical predictions of the sign of methyl-carbon splittings. Strauss and Fraenkel¹⁹ performed semiempirical calculations based on the approach of Karplus and Fraenkel.²⁰ Using a VB method they predict a splitting of $-69\rho_c^\pi \text{ G}$ and a carbon to proton ratio of -2.5 . Using an MO approach they predict $-20.9\rho_c^\pi \text{ G}$ and a ratio of -0.67 . The latter ratio appears to agree in magnitude with their experiments. The question of sign is all important, however. Recently, Ellinger, Subra, Levy, Millie, and Berthier²¹ reported the results of nonempirical calculations of hyperfine splittings using gaussian basis sets within the framework of spin-restricted LCAO-SCF open-shell and first-order double-perturbation theories. For the methyl carbon of ethyl radical they predict a *positive* splitting, $a_{\text{CH}_3}^{\text{C}} = +11.8 \text{ G}$, the magnitude of which is in excellent agreement with the experimental value 13.57 G. Unfortunately we were not able to measure the sign of the 4.27-G splitting, and thus shed light on this discrepancy.

It is also of interest that the ratio of methyl carbon to proton splitting calculated by Ellinger et al. is 0.70.²¹ The concordance in values for this ratio, namely $0.4 \leq |a_{\text{CH}_3}^{\text{C}}|/|a_{\text{CH}_3}^{\text{H}}| \leq 0.7$, which is found for the methyl-substituted semiquinones, the ethyl radical, this work on the TMCOT anion, and the nonempirical calculations of Ellinger et al., point to its use as a valuable guide in assigning methyl-group ^{13}C splittings.

The remaining two coupling constants have been assigned with the aid of detailed consideration of the line

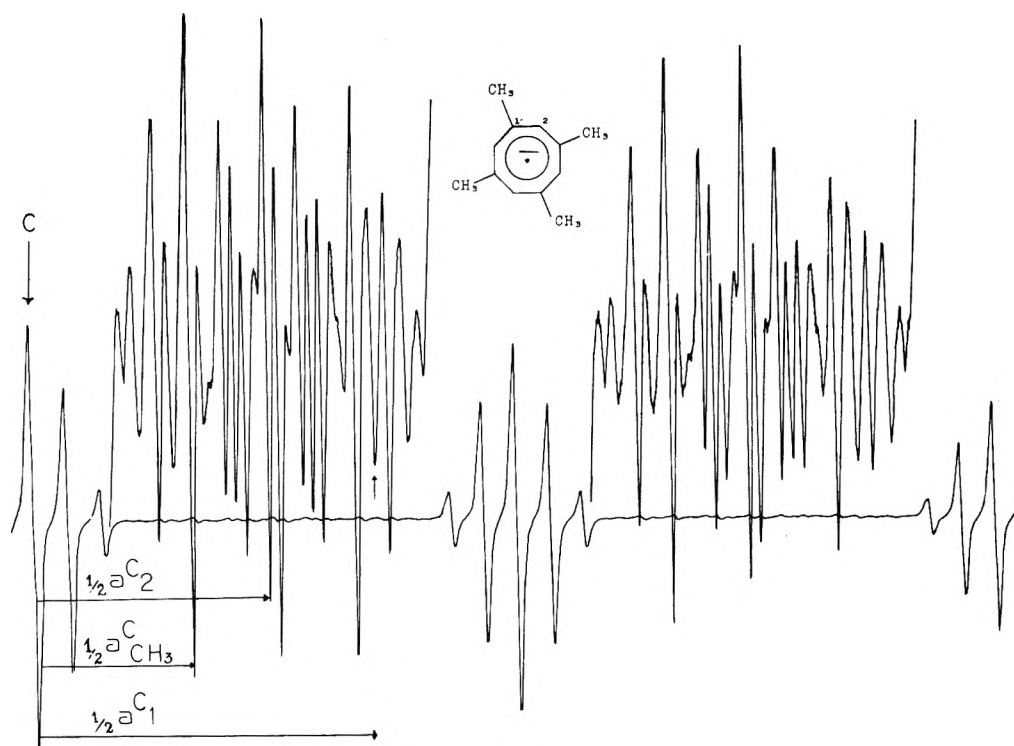


Figure 6. The ^{13}C spectrum for the TMCOT anion. Also shown are the quintets with $M_1 = 0, -1,$ and -2 in the proton spectrum. The ^{13}C spectrum is displayed at a much higher gain setting.

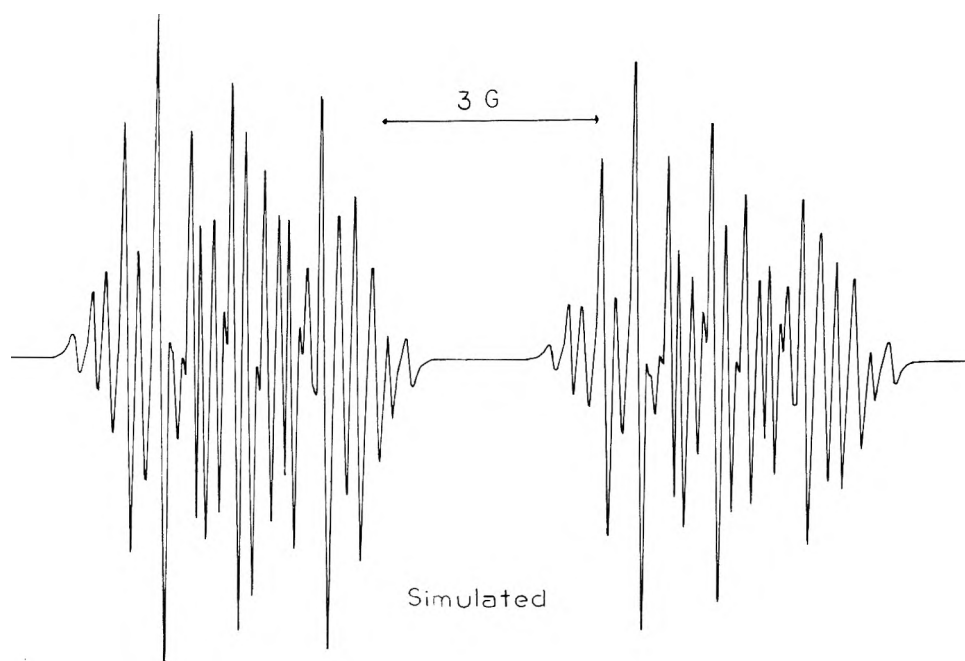


Figure 7. Computer-simulated ^{13}C spectrum of the TMCOT anion. The hyperfine parameters used in the simulation are given in Table II.

widths and peak intensities.²² Bolton and Fraenkel observed that the ^{13}C lines arising from different sets of nuclei, with each set having the same number of nuclei, quite often do not possess the same peak-to-peak intensity.²² They have explained this in terms of line width theory.

To illustrate the point, line width theory shows that the widths of the hyperfine lines in a radical containing a single magnetic nucleus with total spin angular momentum quantum number I and z -component quantum number m are

$$[T_2(m)]^{-1} = j^{(D)} \left[I(I+1) + \frac{5}{3} m^2 \right] + \frac{16}{3} j^{(DG_2)} B_0 m + x \quad (6)$$

where $j^{(D)}$ arises from the anisotropic intramolecular dipolar interaction and $j^{(DG_2)}$ from a cross term between this interaction and the effects of the g -tensor anisotropy. The quantity x includes other line width contributions which

presumably do not depend on m , as well as a contribution resulting from the g -tensor anisotropy, and B_0 is the external magnetic field.²² The spectral densities $j^{(D)}$ are roughly proportional to the square of the local spin density.²² It follows that, when the term $j^{(D)}$ is large enough to have a measurable effect on the widths, the lines from the nuclei of atoms bearing the larger spin density will have the larger width. From Figure 6 it can be readily observed that, at room temperature, the peak heights of the lines arising from the ^{13}C nuclei with $|a^c| = 9.4$ G are almost one-half those of the lines arising from the other two nuclei.

Both our experimental proton splittings and Hückel MO calculations indicate a π spin density of 0.25 at the 1,3,5,7 positions and a very small or zero spin density at the 2,4,6,8 positions. Thus, we would expect considerable broadening for the 1,3,5,7 positions and assign the 9.4-G splitting to those ^{13}C nuclei.

This type of analysis has been used by other authors in the assignment of carbon-13 splittings for the anthracene,²² *p*-xylene,²² and biphenylene²⁴ anion radicals. The magnitude of the line width effect observed in the case of the TMCOT anion is greater than that observed for the radicals mentioned above, due to a larger difference in π density between the carbons, and also to the higher viscosity of HMPA compared to the ethereal solvents used previously.²⁵

The remaining splitting, $|a^c| = 6.37$ G, is assigned to the 2,4,6,8 positions.

We have evidence that the sign of the 9.4-G splitting is positive. de Boer and Mackor²⁶ first showed that the signs of the ^{13}C hfs can frequently be determined by comparing the widths of the corresponding high- and low-field lines of a specific ^{13}C splitting. It can be shown^{27,28} that the product $a_i^c \rho_i^\pi$ will be positive if the high-field component is broader than the low-field component and vice versa. This method is only valid whenever the local spin density is not small compared to the spin density on the neighboring atoms. Examination of the spectrum in Figure 8 shows that for the lines arising from the 9.4-G splitting, the high-field components are less intense and therefore broader than the low-field components. Peak-to-peak height comparison between these low-field and high-field lines gives a ratio of 1.3, which yields a ratio of line widths equal to 0.9. The corresponding peak-to-peak ratio for the other splittings is almost one. This confirms the fact that the hfs of 9.4 G arises from a position of higher spin density in the TMCOT anion, and leads to the conclusion that the sign is positive, $a_1^c = +9.4$ G.

We next proceed to correlate the measured ^{13}C splittings of the TMCOT anion with theory, specifically the semiempirical expression of Karplus and Fraenkel.²⁰ For several hydrocarbon radicals the ^{13}C splittings calculated using their parameters agree well with experiment. In the case of the orbitally degenerate radicals (e.g., C_6H_6^- , C_7H_7^- , C_8H_8^-) the agreement is not as good.²⁰ For example, the value calculated for COT^- using the usual parameters is 0.98 G as compared with the experimental value of 1.28 ± 0.05 G. Possible origins of the discrepancy are effects of orbital degeneracy, nonplanarity, and variations in CCC bond angle.

In this work we have studied a related molecule, the TMCOT anion, in which orbital degeneracy is lifted. The effects of nonplanarity might be expected to be enhanced due to the four methyl substituents.

We have performed a number of calculations of the ^{13}C

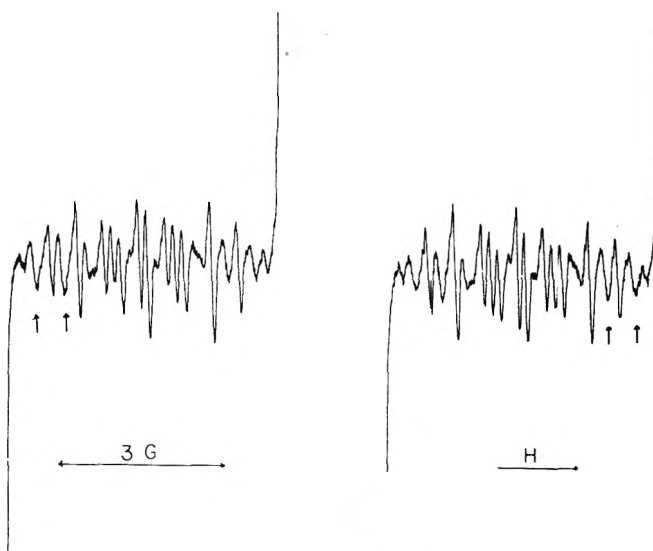


Figure 8. ^{13}C satellites flanking the $M_1 = 0$ quintet in the proton spectrum of the TMCOT anion. The arrows indicate pairs of ^{13}C lines arising from the 9.4-G splitting.

splittings using the HMO π spin distribution. The equation employed is that of Karplus and Fraenkel, in the notation proposed by Bolton²⁹

$$a^c = Q_c \rho_c^\pi + Q_c' \Sigma \rho_c^\pi \quad (7)$$

where the first term deals with the local spin density and the second term incorporates the contributions of the neighboring atoms.

Two values of the parameter Q_c might be used. Neither was derived for the case of a methyl group bonded to the π carbon framework. There is some empirical evidence to favor the value 35.6 G which holds for an aromatic carbon atom with an attached hydrogen atom. Specifically, the splitting of the α carbon of the ethyl radical (39.07 G) is almost the same as the ^{13}C splitting for methyl (38.34 G). If we use $Q_c = 35.6$ G,²⁰ the calculated splittings for the 1 and 2 positions are +8.9 and -7.0 G, respectively, as compared with the experimental values of +9.4 and $(\pm)6.37$ G. Assuming that the calculated sign of a_2^c is correct, the agreement is within 10% which is quite good.

Strom, Underwood, and Jurkowitz³⁰ have obtained an improved set of parameters Q_c and Q_c' . Using an empirical approach incorporating the data for CH_3^- and the anion radicals of benzene, cyclooctatetraene, *p*-xylene, anthracene, and naphthalene, they obtained $Q_c = 38.6$ G and $Q_c' = -11.6$ G. Using these parameters for TMCOT $^-$ we obtain +9.6 and -5.8 G which are in very good agreement with experiment.

From these comparisons of calculations with experiment we are led to conclude that the ^{13}C hfs of the TMCOT $^-$ anion, which should be quite sensitive to molecular geometry, does not reveal any significant deviation from planarity.

Bolton²⁹ has performed an interesting analysis of the ^{13}C data for benzene and *p*-xylene anion radicals, for which the spin distribution is considered well known. For *p*-xylene anion $\rho_{1,4}^\pi = 0$ and $\rho_{2,3,5,6}^\pi = 1/4$. Using $a_1^c = (\pm)5.3$ G and eq 7 and assuming a negative sign for Q_c' , we immediately obtain $Q_c' = -10.6$ G. With this value and $|a^c| = 2.8 \pm 0.1$ G for benzene anion, we readily compute $Q_c = 38 \pm 1$ G.

The agreement with the correlation of Strom et al. is quite good. As a check, Bolton used these parameters to calculate a_2^c for *p*-xylene anion. The result is 6.8 G in excellent agreement with the experimental value of 6.5 G.

We can perform a similar analysis using the anions of COT and TMCOT. From $a_2^c = -6.37$ G (sign chosen as discussed above) and the HMO spin distribution for TMCOT anion ($\rho_1^\pi = 1/4$, $\rho_2^\pi = 0$) we immediately obtain $Q_c' = -12.74$ G. Using this and $a^c = 1.28 \pm 0.05$ G for the COT anion, we compute $Q_c = +35.7$ G. As a check, these parameters can be used to predict the value of a_1^c for the TMCOT anion. The splitting obtained is +8.9 G in good agreement with experiment (+9.4 G).

An alternative approach is to use the two splitting constants of the TMCOT anion to obtain values of Q_c and Q_c' . With the HMO model for spin densities, $Q_c = 37.6$ G and $Q_c' = -12.7$ G. These parameters can be used to predict a splitting for the COT anion. The computed value is 1.5 G, which gives the closest agreement with experiment obtained to date.

Acknowledgments. This work was supported by the U.S. Army Research Office (Durham). One of us (G.C.) gratefully acknowledges postdoctoral fellowship support by the Graduate School, Syracuse University. The purchase of the ESR spectrometer was supported in part by a grant from the NSF Chemistry Research Instrumentation Program. We are grateful to a reviewer for many helpful suggestions, and in particular for the method of extracting ΔE (cf. eq 4).

References and Notes

- (1) G. Vincow, M. L. Morrell, F. R. Hunter, and H. J. Dauben, Jr., *J. Chem. Phys.*, **48**, 2876 (1968); W. V. Volland and G. Vincow, *ibid.*, **48**, 5589 (1968); *J. Phys. Chem.*, **73**, 1147 (1969); G. Vincow, *J. Chem. Phys.*, **47**, 2774 (1967); M. K. Carter and G. Vincow, *ibid.*, **47**, 292, 302 (1967); G. Vincow, M. L. Morrell, W. V. Volland, H. J. Dauben, Jr., and F. R. Hunter, *J. Am. Chem. Soc.*, **87**, 3527 (1965).
- (2) G. R. Stevenson, J. G. Concepcion, and L. Eschegoyen, *J. Am. Chem. Soc.*, **96**, 5452 (1974); G. R. Stevenson and J. G. Concepcion, *J. Phys. Chem.*, **78**, 90 (1974).
- (3) T. J. Katz, *J. Am. Chem. Soc.*, **82**, 3784, 3785 (1960); T. J. Katz and H. L. Strauss, *J. Chem. Phys.*, **32**, 1873 (1960).
- (4) L. A. Paquette, J. F. Hansen, and T. Kakihana, *J. Am. Chem. Soc.*, **93**, 168 (1971).
- (5) L. A. Paquette, S. V. Ley, R. H. Meisinger, R. K. Russell, and M. Oku, *J. Am. Chem. Soc.*, **96**, 5806 (1974).
- (6) S. Z. Goldberg, K. N. Raymond, C. A. Harmon, and D. H. Templeton, *J. Am. Chem. Soc.*, **96**, 1348 (1974).
- (7) P. de Mayo and R. W. Yip, *Proc. Chem. Soc.*, **84** (1964).
- (8) F. A. Cotton, J. W. Feller, and A. Musco, *J. Am. Chem. Soc.*, **90**, 1438 (1968).
- (9) G. R. Stevenson and J. G. Concepcion, *J. Phys. Chem.*, **76**, 2176 (1972).
- (10) D. H. Geske and A. H. Maki, *J. Am. Chem. Soc.*, **82**, 2671 (1960).
- (11) J. G. Concepcion and G. Vincow, *J. Phys. Chem.*, preceding article in this issue.
- (12) H. Normant, *Angew. Chem., Int. Ed. Engl.*, **6**, 1046 (1967); D. A. Owensby, A. J. Parker, and J. W. Diggle, *J. Am. Chem. Soc.*, **96**, 2682 (1974).
- (13) A. Cserhegyi, E. Franta, J. Chaudhuri, J. Jagur-Grodzinski, and M. Szwarc, *J. Am. Chem. Soc.*, **89**, 7129 (1967); G. Levin, J. Jagur-Grodzinski, and M. Szwarc, *ibid.*, **90**, 6421 (1968); A. Cserhegyi, J. Jagur-Grodzinski, and M. Szwarc, *ibid.*, **91**, 1892 (1969); G. Levin, J. Jagur-Grodzinski, and M. Szwarc, *ibid.*, **92**, 2268 (1970).
- (14) We have also confirmed this for the [16]annulene anion radical in HMPA (cf. ref 11).
- (15) For a review of the properties of orbitally degenerate radicals see G. Vincow in "Radical Ions", E. T. Kaiser and L. Kevan, Ed., Interscience, New York, N.Y., 1968, Chapter 4.
- (16) R. E. Moss, *Mol. Phys.*, **10**, 501 (1966).
- (17) R. W. Fessenden, *J. Chem. Phys.*, **37**, 747 (1962).
- (18) A. H. Reddoch, C. L. Dodson, and D. H. Paskovich, *J. Chem. Phys.*, **52**, 23 (1970).
- (19) H. L. Strauss and G. K. Fraenkel, *J. Chem. Phys.*, **35**, 1738 (1961).
- (20) M. Karplus and G. K. Fraenkel, *J. Chem. Phys.*, **35**, 1312 (1961).
- (21) Y. Ellinger, R. Subra, B. Levy, P. Millie, and G. Berthier, *J. Chem. Phys.*, **62**, 1,10 (1975).
- (22) J. R. Bolton and G. K. Fraenkel, *J. Chem. Phys.*, **41**, 944 (1964).
- (23) In order to obtain a good correspondence between the experimental and the simulated spectra, the line width due to that particular nucleus ($|a^c| = 9.4$ G) had to be increased to 1.4 times the line width of the other two ^{13}C nuclei. This is in good agreement with the peak-height results.
- (24) P. R. Hindle, J. dos Santos Veiga, and J. R. Bolton, *J. Chem. Phys.*, **48**, 4703 (1968).
- (25) Similar enhancement of line width effects due to solvent viscosity are mentioned by Bolton and Fraenkel (ref 22) for the case of a hydrocarbon cation radical in sulfuric acid.
- (26) E. de Boer and E. L. Mackor, *J. Chem. Phys.*, **38**, 1450 (1963).
- (27) F. Gerson, "High Resolution Electron Spin Resonance", Wiley, New York, N.Y., 1970.
- (28) J. H. Freed and G. K. Fraenkel, *J. Chem. Phys.*, **40**, 1815 (1964).
- (29) J. R. Bolton, *Mol. Phys.*, **6**, 219 (1962).
- (30) E. T. Strom, G. R. Underwood, and D. Jurkowitz, *Mol. Phys.*, **24**, 901 (1972).
- (31) Unpublished room-temperature data by L. M. Morrell and G. Vincow.

Rate of Electron Exchange between Ferrocene and Ferricenium Ion from Nuclear Magnetic Resonance Studies¹

Edward Shih Yang, Man-Sheung Chan, and Arthur C. Wahl*

Department of Chemistry, Washington University, St. Louis, Missouri 63130 (Received June 4, 1975)

Publication costs assisted by the National Science Foundation

The rate of electron exchange between bis(cyclopentadienyl)iron(II) (ferrocene) and bis(cyclopentadienyl)iron(III) ion (ferricenium ion) has been measured in acetonitrile and in methanol by the NMR line-broadening method over the temperature range 0–30°. The rate in acetonitrile depends on the first power of each reactant concentration; the rate has little dependence on electrolyte concentration in either solvent. For ionic strengths $\leq 0.1 M$, the rate constants at 25° are $(5.7 \pm 1.0) \times 10^6$ and $(5.4 \pm 1.0) \times 10^6 M^{-1} \text{sec}^{-1}$, and the experimental activation energies are 5 ± 1 and 3 ± 1 kcal/mol for acetonitrile and methanol, respectively, as solvents.

Introduction

The earliest investigations of electron exchange between ferrocene ($\text{Fe}(\text{cp})_2$) and ferricenium ion ($\text{Fe}(\text{cp})_2^+$) were by the isotopic-tracer method and showed that although exchange was too rapid near 25° to be measured in several nonaqueous solvents ($k > \sim 1 \times 10^4 M^{-1} \text{sec}^{-1}$),^{2,3} it was measurable between –75 and –65° in methanol ($k = (9 \text{ to } 35) \times 10^5 M^{-1} \text{sec}^{-1}$).⁴

In the first investigation of the exchange by the NMR line-broadening method Dietrich and Wahl⁵ found that the proton-absorption peak for the ferricenium ion was too broad to be observed; however, addition of small amounts of the ion to acetone solutions of ferrocene caused broadening and shifting of the ferrocene peak consistent with very fast exchange at ~25° ($k > \sim 1 \times 10^5 M^{-1} \text{sec}^{-1}$).

More recent investigations of the exchange rate by still other methods have given conflicting results. Ruff, Friedrich, Demeter, Csillag, and Korösi-Ódor⁶ reported observing that diffusion of the ferricenium ion into ~0.1 M HClO_4 solutions of methanol, ethanol, and 1-propanol was faster when ferrocene was present, as was also the diffusion of ferrocene when the ferricenium ion was present. They concluded that the electron-exchange reaction is very rapid at 25° ($k \approx 10^{10} M^{-1} \text{sec}^{-1}$).

Pladziewicz and Espenson⁷ employed the stopped-flow method to measure the rates of electron transfer between a number of derivatives of ferrocene and ferricenium ion. The measured rate constants in 1:1 v/v 1-propanol-water solutions ($\mu = 0.05$, adjusted with $\text{Ba}(\text{ClO}_4)_2$) ranged from $(4 \text{ to } 20) \times 10^6 M^{-1} \text{sec}^{-1}$. By use of the Marcus theory⁸ and the measured electrode potentials for the reactions investigated, the authors calculated that rate constant at 25° for electron exchange between ferrocene and ferricenium ion was $5.7 \times 10^6 M^{-1} \text{sec}^{-1}$.

Results

The initial objective of our investigation was to determine if the rate constant (k) for electron exchange between ferrocene and ferricenium ion, as well as the isotropic shift ($\delta\nu$) and line width for ferricenium ion ($W_P = (\pi T_2)_P^{-1}$, full width at half maximum in Hz), was measurable. The line widths (W_{DP}) for mixtures of the reactants⁹ were determined in acetonitrile at different total reactant concentra-

tions ($c = 0.02\text{--}0.10 M$) with a constant fraction ($f_P = 0.050 \pm 0.001$) of reactants as $\text{Fe}(\text{cp})_2^+$. The frequency shift was essentially constant (-138 ± 2 Hz) showing that the solutions were chemically stable during the measurements and allowing calculation of $\delta\nu \approx -138/0.05 = -2760$ Hz, since the frequency shift is proportional to f_P for fast exchange.^{5,10} The data were interpreted by use of¹¹

$$W_{DP} = f_P W_P + (1 - f_P) W_D + f_P(1 - f_P) 4\pi(\delta\nu)^2/kc \quad (1)$$

The symbol $W_D = (\pi T_2)_D^{-1} = 1.0 \pm 0.5$ Hz for ferrocene, and the other symbols have been defined above. A plot of W_{DP} vs. $1/c$ gave a straight line; a value of $W_P \approx 670$ Hz was derived from the intercept, and a value of $k \approx 7 \times 10^6 M^{-1} \text{sec}^{-1}$ was derived from the slope of the line.

Because of the possibility that k might vary appreciably with varying $\text{Fe}(\text{cp})_2\text{PF}_6$ concentration, the experiment was repeated at constant ionic strength ($\mu = 0.035$, adjusted with $\text{Co}(\text{cp})_2\text{PF}_6$) with f_P varying from 0.09 to 0.30 and for temperatures between 10 and 30°. The data were interpreted by use of eq 1 programmed as a subroutine for use with the ORGLS least-squares computer program,¹² values of f_P being calculated from the frequency shift $(\nu - \nu_0)$ divided by the isotropic shift, i.e., $f_P = (\nu - \nu_0)/\delta\nu$, a valid relationship for fast exchange. The values of W_P and k determined are listed in parentheses, columns 3 and 4, in Table I; the uncertainties listed for these and for other values reported in this article are the square root of the sum of the squares of the standard deviations obtained from the least-squares fit of eq 1 and of the average changes in k and W_P caused by changing $\delta\nu$, c , and W_D (and W_P for later experiments) one at a time by plus or minus their uncertainties.

The NMR absorption peak of the ferricenium ion was later observed directly by operating the Varian HA100 NMR spectrometer in the HR mode. Values of $\delta\nu$ and W_P were obtained directly at various temperatures for both $\text{Fe}(\text{cp})_2\text{PF}_6$ and $\text{Fe}(\text{cp})_2\text{BF}_4$ salts by use of the 2500-Hz modulation side bands of the solvent-proton absorption peak for calibration. The values from several separate experiments deviated from the average values by less than a few percent, and the average values plotted against $1/T$ were well represented by smooth curves. The values derived from the curves are listed in Table I along with uncertainties estimated from the spread of the data and from the small deviations from the curves. These $\delta\nu$ and W_P values

TABLE I: Exchange Rate Constant and NMR Absorption Parameters in Acetonitrile^a

Temp, °C	$\delta\nu$, Hz ^b (± 50)	W_P , Hz ^b (± 20)	k , $10^6 M^{-1} \text{sec}^{-1}$	
			($\mu = 0.035 M$) ^c	($\mu \approx 0.002 M$) ^d
0	-3120	810		2.7 \pm 0.2
10	-3000	730 (745 \pm 70) ^e	3.1 \pm 0.3 (3.2 \pm 0.9) ^e	3.7 \pm 0.2
20	-2930	690 (720 \pm 50)	4.1 \pm 0.5 (4.8 \pm 1.4)	4.9 \pm 0.3
25	-2900	680 (690 \pm 40)	5.3 \pm 0.8 (5.6 \pm 1.4)	6.0 \pm 0.5
30	-2880	670 (630 \pm 40)	6.4 \pm 1.2 (4.8 \pm 1.0)	7.1 \pm 0.7

^a $W_D = 1.0 \pm 0.5$ Hz. ^b Values derived from a smooth curve through averages of data obtained directly from NMR measurements with the spectrometer operating in the HR mode. ^c $c = 0.10 M$ ($\pm 3\%$), $f_P = 0.09$ -0.30, $\mu = 0.035 M$ adjusted with $\text{Co}(\text{cp})_2\text{PF}_6$, values of $\delta\nu$ and W_P used are listed in columns 2 and 3. ^d $c \approx 0.05 M$ ($\pm 3\%$), $f_P = 0.01$ -0.09, $\mu = 0.5$ -4.5 mM, anion is PF_6^- . ^e Values of W_P and k in parentheses were determined simultaneously from the same data.

TABLE II: Dependence of the Exchange Rate Constant on Reactant Concentrations in Acetonitrile^a

[Fe-(cp) ₂ PF ₆], mM	[Fe-(cp) ₂], mM	k , $10^6 M^{-1} \text{sec}^{-1}$	[Fe-(cp) ₂ PF ₆], mM	[Fe-(cp) ₂], mM	k , $10^6 M^{-1} \text{sec}^{-1}$
34.4	86.1	4.9	1.75	39.4	4.7
27.7	86.3	5.7	1.69	56.0	5.1
25.3	86.0	5.6	1.25	29.5	4.9
21.5	85.7	5.9	1.19	40.0	5.3
20.4	86.2	5.4	1.12	47.9	5.2
15.5	86.0	5.8	0.80	19.8	4.9
12.6	86.0	5.3	0.76	28.6	5.2
10.4	95.0	4.6	0.53	20.1	5.6
2.13	72.5	4.6			

(Av 5.2)

^a $\mu = 0.035 M$, adjusted with $\text{Co}(\text{cp})_2\text{PF}_6$, 25°.

agree, within experimental uncertainties, with those determined in the initial experiment at 25°, and the W_P values agree with those calculated along with k from the data obtained at $\mu = 0.035 M$ by use of eq 1 and the directly determined $\delta\nu$ values (column 2 of Table I).

As shown in Table II, the rate constant k derived from individual experiments does not change appreciably when reactant concentrations are varied, so the second-order rate law

$$\text{rate} = k[\text{Fe}(\text{cp})_2][\text{Fe}(\text{cp})_2^+]$$

assumed in the derivation of eq 1, is valid.

The rate constants measured at low reactant concentrations in acetonitrile are shown in the last column of Table I, and those measured in methanol are shown in Table III along with the $\delta\nu$, W_P , and W_D values used in calculating k . The estimated uncertainties listed were derived as has been described for data in Table I.

As can be seen from comparison of the last two columns of Tables I and III, there is little effect of ionic strength on the rate constants, as is to be expected when one of the reactants is neutral, so variations in ionic strength at low reactant concentrations should affect the rate constants very little.

Discussion

The measured rate constants at 25° are consistent with those deduced by Pladziewicz and Espenson⁷ of $5.7 \times 10^6 M^{-1} \text{sec}^{-1}$, but they are not consistent with those deduced by Ruff et al.⁶ of $\approx 10^{10} M^{-1} \text{sec}^{-1}$. Extrapolation of our rate constants obtained with methanol as solvent to -65,

-60, and -75° gives somewhat smaller rate constants than those measured by Stranks,⁴ but the ratios of the k values of 2 to 5 can be accounted for by the combination of experimental errors, e.g., the ± 1 kcal for our 3 kcal/mol activation energy and Stranks' 25-50% estimated experimental uncertainties in k .

The measured rate constants are consistent with those predicted by the Marcus theory⁸ as applied to spherical reactants in a continuous, unsaturated dielectric medium, but the smaller observed temperature dependence of the rate than predicted by the theory gives somewhat poorer agreement for the activation parameters as shown in Table IV. Since the activation energies determined for the exchange reaction in the two solvents differ by only 2 kcal/mol, the sum of the estimated experimental uncertainties, the differences the values of ΔH^* and ΔS^* may not be significant. The differences in the activation parameters determined from experiment and calculated from theory are not large, so the Marcus theory as applied to the simple model described above is a satisfactory representation of the ferrocene-ferrocenium-ion exchange system.

Dilute solutions of $\text{Co}(\text{cp})_2\text{PF}_6$ in acetonitrile and in methanol are highly conducting, so $\text{Co}(\text{cp})_2\text{PF}_6$ is largely dissociated into the ions, and, by analogy, we believe that the same is true for $\text{Fe}(\text{cp})_2\text{PF}_6$. Also, as is discussed in the Experimental Section, we found no evidence for the dimer, $[\text{Fe}(\text{cp})_2]_2^+$, reported by Lelievre, La Feuvre, Gaboriaud, and Champetier.¹³ Therefore, the reactants were mainly present as $\text{Fe}(\text{cp})_2^+$ and $\text{Fe}(\text{cp})_2$ in the solutions investigated, as we assumed in interpretation of the data.

Experimental Section

Ferrocene purchased from Alfa Inorganics was purified by two sublimations. Ferrocenium hexafluorophosphate was synthesized¹⁴ by dissolving 0.5 g of ferrocene in 10 ml of concentrated sulfuric acid in which oxidation occurred during a 15-60-min period, then the solution was poured into 150 ml of water. The dilute solution was filtered to remove sulfur, etc., and an aqueous solution of NaPF_6 was added. The resulting precipitate was filtered, washed several times with water, and dried under vacuum. Carbon and hydrogen analysis indicated that the compound was >99% pure. The molar extinction coefficient in acetonitrile measured in the absence of air at the absorption maximum, 6200 Å, was 446, a value close to the value of 450 determined for an ethanol-water mixture (1:1 v/v).¹⁵ Other reported values¹⁶⁻¹⁹ determined for water and several other solvents are generally smaller and may be in error due to partial decomposition of $\text{Fe}(\text{cp})_2^+$ in the presence of air.²⁰

Cobaltocenium hexafluorophosphate was synthesized by

TABLE III: Exchange Rate Constant and NMR Absorption Parameters in Methanol^a

Temp, °C	$\delta\nu$, Hz ^b (± 50)	W_p , Hz ^b (± 20)	k , $10^6 M^{-1} \text{sec}^{-1}$	
			($\mu \approx 0.003 M$) ^c	(0.1 M HClO ₄) ^d
0	-3070	830	3.7 \pm 0.2	3.2 \pm 0.2
5	-3030	770	3.9 \pm 0.3	3.5 \pm 0.2
10	-2990	720	4.2 \pm 0.3	3.8 \pm 0.3
15	-2950	680	4.7 \pm 0.3	4.1 \pm 0.3
20	-2910	660	5.4 \pm 0.5	4.5 \pm 0.3
25	-2870	640	6.0 \pm 0.5	4.8 \pm 0.4
30	-2830	620	6.6 \pm 0.6	5.3 \pm 0.4

^a $W_D = 1.0 \pm 0.5$ Hz. ^b Values derived from a smooth curve through averages of data obtained directly from NMR measurements with the spectrophotometer operating the HR mode. ^c $c = 0.04 M$ ($\pm 3\%$), $f_p = 0.04$ -0.09, $\mu = (1.6$ -3.6) $10^{-3} M$, anion is PF₆⁻. ^d $c = 0.04 M$ ($\pm 3\%$), $f_p = 0.06$ -0.10, $\mu = 0.10 M$, [PF₆⁻] = (2.4-4.0) mM.

TABLE IV: Comparison of Measured Rate Constants and Activation Parameters with the Marcus Theory

Parameter ^a	CD ₃ CN solvent		CD ₃ OD solvent	
	Measd ^b	Calcd ^c	Measd ^b	Calcd ^c
k , $10^6 M^{-1} \text{sec}^{-1}$	5.7 \pm 1.0	2.8	5.4 \pm 1.0	2.3
E_{act} , kcal/mol	5 \pm 1	7.0	3 \pm 1	7.1
ΔG^* , kcal/mol	5.8	6.2	5.8	6.3
ΔH^* , kcal/mol	4.4	6.4	2.4	6.5
ΔS^* , eu	-4.7	0.7	-11.4	0.7

^a Value for 25°. ^b Average of measurements at low and high ionic strengths; uncertainties are estimated to include spread in values and known systematic errors. ^c Values calculated using the Marcus theory⁸ as applied to spherical reactants in a continuous, unsaturated dielectric medium. It was assumed that the bimolecular collision number (Z) is $10^{11} M^{-1} \text{sec}^{-1}$, that the reaction distance was 7 Å, and that no internal reorganizational free energy of activation was required.

dissolving [Co(cp)₂]₂CoCl₄ purchased from Arapahoe Chemicals, Inc. in water and adding an excess of NaPF₆ solution. The Co(cp)₂PF₆ precipitate was filtered, washed several times with water, and dried under vacuum.

The solvents, CD₃CN ($\geq 99\%$ isotopic purity) and CD₃OD ($\geq 99.5\%$ isotopic purity), were purchased from Merck Sharp and Dohme Isotope Products. The CD₃OD was used without further purification, but CD₃CN was refluxed over P₂O₅ for several hours and then distilled.

In order to avoid the decomposition of Fe(cp)₂⁺ in solutions exposed to air, samples for all but the preliminary NMR measurements were prepared under high-vacuum conditions. Appropriate quantities of solid Fe(cp)₂ and solid Fe(cp)₂PF₆ were placed in small open ended tubes in the side arm of an apparatus attached to a vacuum line and to an NMR tube, containing 0.500 ml of solvent. After freezing the solvent and applying vacuum, then thawing and repeating the cycle several times to remove air, the apparatus was sealed off and tipped to dissolve the reactants in the solvent, then the solution was allowed to drain into the NMR tube, which was sealed off for measurements. Solutions prepared in this way were stable for several days and allowed NMR measurements to be made at a number of different temperatures, which were determined from the

chemical shift of CH₃OH. The NRM measurements were made with a Varian HA-100 spectrometer.

Two experiments were performed to look for evidence for the dimer, [Fe(cp)₂]₂⁺, reported to absorb at 6200 Å.¹³ In one experiment successive aliquots of (NH₄)₂Ce(NO₃)₆ solution were added to a cold methanol solution of Fe(cp)₂, 0.1 M in HClO₄. The intensity of absorption at 6200 Å increased linearly with the amount of Ce(IV) added until an equivalent amount had been added, then with excess Ce(IV), absorption decreased somewhat as Fe(cp)₂⁺ was oxidized and/or decomposed.²⁰ In the other experiment various amounts of Fe(cp)₂ were added to cold methanol solutions of Fe(cp)₂PF₆, 0.1 M in HClO₄; no appreciable change in absorption intensity at 6200 Å was observed during the first 10 min, then on being allowed to warm to 15-20° the absorption intensity decreased because of decomposition of Fe(cp)₂⁺.²⁰ The rate of decomposition decreased with increasing Fe(cp)₂ concentration.

Most of our experiments were done with Fe(cp)₂PF₆ because the solid is stable. Similar results were obtained with Fe(cp)₂BF₄ and with Fe(cp)₂ClO₄; however, Fe(cp)₂ClO₄ is a detonator and must be handled with care (i.e., no grinding or scraping of the dry compound), and only small amounts can be handled with relative safety.

References and Notes

- (1) Supported by the National Science Foundation under Grant No. GP-28260X.
- (2) G. P. Lang, M.S. Thesis, Washington University, St. Louis, Mo. 1956; A. C. Wahl, *Zeit. Electrochem.*, **64**, 90 (1960).
- (3) F. S. Dainton, G. S. Laurence, W. Schneider, D. R. Stranks, and M. S. Vaidya in "Radioisotopes in Scientific Research", Vol. II, Pergamon Press, New York, N.Y., 1958, p 305.
- (4) D. R. Stranks, *Discuss. Faraday Soc.*, **29**, 73 (1960).
- (5) M. W. Dietrich and A. C. Wahl, *J. Chem. Phys.*, **38**, 1591 (1963).
- (6) (a) I. Ruff, V. J. Friedrich, K. Demeter, and K. Csillag, *J. Phys. Chem.*, **75**, 3303 (1971); (b) I. Ruff and I. Korösi-Odor, *Inorg. Chem.*, **9**, 186 (1970).
- (7) J. R. Pladziewicz and J. H. Espenson, *J. Am. Chem. Soc.*, **95**, 56 (1973); *J. Phys. Chem.*, **75**, 3381 (1971).
- (8) R. A. Marcus, *J. Chem. Phys.*, **43**, 679 (1965).
- (9) Tris(4,4'-dimethyl-2,2'-bipyridyl)iron(III) hexafluorophosphate was used as an oxidizing agent, and tetramethylsilane was added as an internal reference standard.
- (10) H. S. Gutowsky and A. Saika, *J. Chem. Phys.*, **21**, 1688 (1953).
- (11) M.-S. Chan, J. B. DeRoos, and A. C. Wahl, *J. Phys. Chem.*, **77**, 2163 (1973).
- (12) L. A. Busing and H. A. Levy, Oak Ridge National Laboratory Report No. ORNL-TM-271, 1962 (unpublished).
- (13) J. Lelievre, C. Le Feuvre, R. Gaboriaud, and G. Champetier, *C. R. Acad. Sci., Paris, Ser. C*, **275**, 1455 (1972); **276**, 9 (1973).
- (14) W. L. Jolly, "The Synthesis and Characterization of Inorganic Compounds", Prentice Hall, Englewood Cliffs, N.J., 1970, p 487.
- (15) J. R. Pladziewicz, Ph.D. Thesis, Iowa State University, 1972, p 14.
- (16) G. Wilkinson, M. Rosenblum, M. C. Whitting, and R. B. Woodward, *J. Am. Chem. Soc.*, **74**, 2125 (1952).

- (17) Y. S. Sohn, D. M. Hendrickson, and H. Gray, *J. Am. Chem. Soc.*, **92**, 3233 (1970).
 (18) A. Horsfield and A. Wassermann, *J. Chem. Soc., Dalton Trans.*, 187 (1972).
 (19) M. D. Rowe and A. J. McCaffery, *J. Chem. Phys.*, **59**, 3786 (1973).
 (20) Many of the erratic results that we obtained in the early stages of our investigations, and possibly also some of the earlier results that have been reported,^{8,13,16-19} can be explained by the decomposition of $\text{Fe}(\text{cp})_2^+$ in solutions exposed to air. The yellow decomposition products have not been identified, but they are not entirely $\text{Fe}(\text{cp})_2$.

Spin-Orbit Coupling in Organic Molecules

C. A. Masmanidis, H. H. Jaffé,* and R. L. Ellis

Department of Chemistry, University of Cincinnati, Cincinnati, Ohio 45221 (Received November 4, 1974; Revised Manuscript Received June 20, 1975)

The application of CNDO/S wave functions to the calculation of spin-orbit matrix elements and their use in the study of molecular phosphorescence has been further explored. Calculations are reported on formaldehyde, formamide, and formic acid as prototypes of carbonyl compounds, amides, and acids. Further calculations on series of carbonyl compounds, aromatic hydrocarbons, and azines are reported. The results obtained are reasonably consistent with experimental observations.

In the framework of our continuing interest in the spectroscopic properties of triplet states, we have undertaken the calculation of spin-orbit coupling (SOC) effects in some selected classes of organic compounds, notably carbonyls, azines, and aromatic hydrocarbons.

It is generally recognized that organic molecules phosphoresce from the lowest triplet state.¹ In order for us to understand this process we must first abandon the concept of a pure spin state (i.e., the total spin angular momentum of the electrons (S) is no longer a good quantum number). The interactions which destroy the meaning of S are the coupling between the orbital and spin angular momenta of an electron. From the viewpoint of perturbation theory this coupling allows the phosphorescence process by permitting an admixture of small amounts of singlet character to the triplet wave functions and conversely some triplet character into the wave function that describes the singlet ground state; the two resulting "spin-impure" states can then couple through the electronic transition moment operator. This mixing of spin multiplicities is small for molecules containing only light atoms, and, therefore, the oscillator strength for the triplet-ground state transition is very small; as a result phosphorescence is a radiative process with very long lifetimes compared to the spin-allowed fluorescence,² and singlet-triplet absorption is observed only under special conditions.

McClure³ has presented a model for SOC in molecules which is an extension of the older treatment of many electron atoms.⁴ In a previous paper⁵ we reported SOC calculations on the lowest triplets of formaldehyde and azulene, applying McClure's treatment to molecular wave functions obtained by the CNDO/S method.⁶ We have now written a program to routinely perform SOC calculations based on CNDO/S wave functions. In the process of reworking the equations presented in our previous paper, we have discovered some minor inconsistencies which we shall correct here.

Our aim in this work is to evaluate the *natural radiative lifetime* of the lowest triplet state in a number of large molecules composed of first and second row elements, and to compare these to the experimentally measured phospho-

rescence lifetimes. This comparison will allow us to make an estimate as to the degree to which radiationless processes deplete the population of the triplet state. This information will help us to choose molecules to investigate in future studies of radiationless processes. Further it is hoped that the methods we present here can be used by experimentalists to evaluate their data for the phosphorescence lifetimes.

Theoretical Considerations⁷

Since the SOC effect is small in ordinary organic molecules we can use the Rayleigh-Schrödinger first-order perturbation theory to construct our "spin-impure" states from the zero-order wave functions, $^1\Psi_k$ and $^3\Psi_m$. In this way, the perturbed ground state is given by

$${}^1U_0 = {}^1\Psi_0 + \sum_m \sum_{\Gamma_r} \frac{\langle {}^3\Psi_m \Gamma_r | H | {}^1\Psi_0 \rangle} {E_0 - E_m} {}^3\Psi_m \Gamma_r \quad (1)$$

where m runs over all the triplet states available in the calculation and the summation over Γ_r includes the three spin components of the triplet states in question. Similarly, each component of the first-order perturbed triplet state is given by⁸

$${}^3U_{j\Gamma_r} = {}^3\Psi_{j\Gamma_r} + \sum_k \frac{\langle {}^1\Psi_k | H | {}^3\Psi_{j\Gamma_r} \rangle} {E_j - E_k} {}^1\Psi_k \quad (2)$$

where k runs over all singlet states, including the ground state ($k = 0$). The zero-order functions Ψ in eq 1 and 2, in the CNDO/S framework used in this paper, are given as linear combinations of a limited number of singly excited spin configurations, each a sum or difference of two Slater determinants:

$${}^1\Psi_k = \sum_a C_{ak} {}^{ij}V_a$$

$${}^3\Psi_m = \sum_b C_{bm} {}^{lk'}T_b$$

where V_a and T_b are singlet and triplet spin configurations, respectively. The superscripts refer to the molecular orbitals which are singly occupied. The unprimed index refers to

the MO which was doubly occupied in the ground state, the primed index to an MO which, in the ground state, was a virtual orbital. The unprimed and primed superscripts refer to the occupied and virtual MO's, respectively, that are involved in defining the single excitation of the configuration.

With the wave functions so defined, we obtain for the electronic transition moment between the "triplet" state j and the ground state:

$$\langle {}^1U_0 | \vec{M} | {}^3U_j \rangle = \sum_k \frac{\langle {}^1\Psi_k | H | {}^3\Psi_j \Gamma_r \rangle^* \vec{M}({}^1\Psi_0, {}^1\Psi_k) + \sum_m \frac{\langle {}^3\Psi_m \Gamma_r | H | {}^1\Psi_0 \rangle \vec{M}({}^3\Psi_j, {}^3\Psi_m)}{E_0 - E_m} \quad (3)$$

where $\vec{M}(\Psi_1, \Psi_2)$ is the transition moment between the two states Ψ_1 and Ψ_2 ; these transition moments are calculated within the CNDO/S program,^{6b} and for the purposes of this development may be assumed known. To evaluate transition moments according to eq 3 it is thus necessary to calculate the SOC matrix elements $\langle {}^1\Psi_k | H | {}^3\Psi_j \Gamma_r \rangle$ and $\langle {}^3\Psi_m | H | {}^1\Psi_0 \rangle$. To do so we must next consider the operator H' .

We assume that we can expand the spin-orbit perturbation operator H' as a sum of one-electron operators:⁹

$$H' = \sum_i h_i' \quad (4)$$

This assumption implies the neglect of spin-other-orbit interactions, which are known to be small.¹⁰ The one-electron operator h_i' is assumed to be of the form¹¹

$$h_i' = \frac{e^2}{2m^2c^2} \sum_k \frac{Z_k}{r_{ik}^3} \vec{l}_i \cdot \vec{s}_i = \sum_k \zeta_k(r_i) \vec{l}_i \cdot \vec{s}_i \quad (5)$$

where the summation over k runs over all atoms.

We now introduce the expansion of eq 1, 2, and 4 in the SOC matrix elements, and obtain for a typical element

$$\langle {}^3\Psi_j \Gamma_r | H | {}^1\Psi_k \rangle = \sum_a \sum_b \sum_i c_{bj} c_{ak} \langle {}^{mn'} T_b \Gamma_r | h_i' | {}^{op'} V_a \rangle \quad (6)$$

The integrals $\langle {}^{mn'} T \Gamma_r | h_i' | {}^{op'} V \rangle$, involving one-electron operators only, permit immediately the integration over the closed shell portion of the spin configuration, leading to

$$\sum_i \langle {}^{mn'} T | h_i' | {}^{op'} V \rangle = \langle |\psi_m(1)\psi_n(2)\rangle | h_i' + h_2' | |\psi_o(1)\psi_{p'}(2)\rangle \rangle \quad (7)$$

where the ψ are spin orbitals. At this point we can factor out spin and space functions, and obtain for the right-hand side of (7)

$$\langle (\psi_m \psi_n - \psi_n \psi_m) | \zeta_k(r_1) \vec{l}_1 | (\psi_o \psi_{p'} + \psi_{p'} \psi_o) \rangle \cdot \langle {}^3\omega | \vec{s}_1 | {}^1\omega \rangle + \text{an identical term with the operators } \vec{l}_2 \text{ and } \vec{s}_2 \quad (8)$$

where ${}^3\omega$ and ${}^1\omega$ are two-electron spin functions. For the singlet spin function we have

$${}^1\omega = \frac{1}{\sqrt{2}} [\alpha(1)\beta(2) - \alpha(2)\beta(1)]$$

For the three components of the triplet spin function we have an arbitrary choice: we choose¹²⁻¹⁴

TABLE I: Effect of Operation of the Spin Operator on the Symmetry Adapted Spin Functions^a

Spin function	Spin operator		
	$\hat{s}_x(1)^b$	$\hat{s}_y(1)^b$	$\hat{s}_z(1)^b$
${}^1\omega$	${}^3\omega_x$	${}^3\omega_y$	${}^3\omega_z$
${}^3\omega_x(\Gamma_-)$	${}^1\omega$	$-i{}^3\omega_z$	$i{}^3\omega_y$
${}^3\omega_y(\Gamma_+)$	$i{}^3\omega_z$	${}^1\omega$	$-i{}^3\omega_x$
${}^3\omega_z(\Gamma_0)$	$-i{}^3\omega_y$	$i{}^3\omega_x$	${}^1\omega$

^a In units of $\hbar/2$. ^b Operation on one electron of the two-electron spin functions.

$${}^3\omega_x = \frac{1}{\sqrt{2}} [\beta(1)\beta(2) - \alpha(1)\alpha(2)]$$

$${}^3\omega_z = \frac{1}{\sqrt{2}} [\alpha(1)\beta(2) + \alpha(2)\beta(1)]$$

$${}^3\omega_y = \frac{i}{\sqrt{2}} [\beta(1)\beta(2) + \alpha(1)\alpha(2)]$$

The singlet spin function ${}^1\omega$ always transforms like the totally symmetric representation of the point group of the molecule, while the three triplet functions transform like the three rotations.¹⁴

At this point we can operate with \vec{s}_i on the spin functions and evaluate the spin factor of eq 8. The effect of operating with \vec{s}_i on the one-electron spin functions α and β is well known.¹⁵ Thus, we can readily deduce the operation of $\vec{S} = \vec{s}_1 + \vec{s}_2$ on the two-electron functions ω the results of which are given in Table I; these may be substituted in eq 8. At the same time we recognize that the integrals (7), since they involve only one-electron operators, vanish identically unless either $m = o$ or $n' = p'$. Since the space functions of the configuration ${}^{mn'}T$ are antisymmetric, those of the configuration ${}^{op'}V$ symmetric,¹⁶ the integrals (7) also vanish if both $m = o$ and $n' = p'$. These facts may be expressed by adding to eq 7 a factor $(\delta_{n'p'} - \delta_{mo})$, where the δ are Kronecker deltas.

We must now return to the radial and angular momentum portions of the h_i' operators. In the present problem the result of the operation of the angular momentum operator for electron i , $\vec{l}(i)$, on a molecular orbital $\psi_p(i)$ is made tractable by the expansion of ψ_p in LCAO form. It can be shown that we may take $\vec{l}(i)$ to be independent of the origin of the coordinate system, and apply $\vec{l}(i)$ to each atomic orbital $\phi_p(i)$ as if the origin were at the atom on which ϕ_p is centered.¹⁷ We shall now also expand the operator h_i' as a sum of atomic terms:

$$h_i' = \sum_s h_{is}' = \left(\sum_s \zeta_s(r_i) \vec{l}_{is} \right) \cdot \vec{s}_i \quad (9)$$

As a consequence of the ZDO approximation, the result of the operation of \vec{l}_{is} on orbitals ϕ_r centered on any atom $r \neq s$ vanishes. Accordingly, we are now prepared to evaluate the first integral of eq 8. With the LCAO expansion, one term in this integral becomes

$$\left\langle mn' \left| \sum_s \zeta_s \vec{l}_1 \right| op' \right\rangle = \sum_\rho \sum_\sigma \sum_\tau \sum_\epsilon c_{m\rho} c_{n'\sigma} c_{o\tau} c_{p'\epsilon} \vec{l}(\rho\sigma\tau\nu)$$

with

$$\vec{l}(\rho\sigma\tau\nu) = \sum_s \langle \phi_\rho(1)\phi_\sigma(2) | \zeta_s \vec{l}_s(1) | \phi_\tau(1)\phi_\nu(2) \rangle$$

Under the CNDO approximations any terms with $\sigma \neq \nu$, and with ρ and τ centered on different atoms, vanish. Further, any terms in which orbitals ϕ_ρ and ϕ_τ are not centered on the atom, on which \hat{l}_{is} operates, also vanish. Consequently

$$\langle mn' | \sum_s \zeta_s \hat{l}_s | op' \rangle = \sum_s \sum_\sigma \sum_\rho \sum_\tau c_{m\rho} c_{n'\sigma} c_{o\rho} c_{p'\sigma} \langle \phi_\rho | \zeta_s \hat{l}_s | \phi_\tau \rangle \quad (10)$$

The operation of \hat{l}_s on ϕ_τ is well known.¹⁸ If ϕ_τ is one of the p orbitals of atom s , the result of the operation, in the cases of interest, is another p orbital of the same atom (multiplied by $i\hbar$); if ϕ_τ is an s orbital, $|\hat{l}_s|\phi_s\rangle = |\bar{0}\rangle$. Consequently, the integral on the right-hand side of eq 10 becomes

$$\langle \phi_\rho | \zeta_s(r) | (\hat{l}_s \phi_\tau) \rangle$$

This integral vanishes if $\phi_\rho \neq (\hat{l}_s \phi_\tau)$, otherwise gives

$$i\hbar \langle p_q | \zeta_s(r) | p_q \rangle = i\hbar \langle \zeta_s(r) \rangle$$

In keeping with the approximation made above, we assign the expectation value of $\zeta_s(r)$ the meaning of an atomic integral on the atom on which the orbitals are centered. Although we could readily use theoretically evaluated integrals,¹⁹ we have chosen, following McClure,³ to use empirical values. We may hope that some of the effects of the approximations made, particularly the neglect of spin-orbit coupling, are cancelled in this way. The values we have used are $\zeta_C = 28 \text{ cm}^{-1}$; $\zeta_N = 70 \text{ cm}^{-1}$; $\zeta_O = 156 \text{ cm}^{-1}$; $\zeta_F = 272 \text{ cm}^{-1}$. We now combine the results of this derivation into general algorithms for the SOC matrix elements; these are given in Table II.²⁰

We may now deduce a selection rule for phosphorescence, specific rules for the components of a triplet which can give rise to phosphorescence, and for the symmetry of the states that make phosphorescence allowed through SOC. First, the general selection rule for spin-orbit-allowed phosphorescence is

$$\Gamma_j \otimes \Gamma_R \otimes \Gamma_T \supset \Gamma_1 \quad (\text{SR1})$$

where Γ_j is the irreducible representation of the triplet spatial function, Γ_R and Γ_T are the reducible representations of the three rotations and the three translations, respectively, and Γ_1 is the totally symmetric representation of the molecular point group. The component(s) of the triplet which can give rise to phosphorescence are those which have spin functions, the irreducible representation(s) of which is/are contained in $\Gamma_j \otimes \Gamma_T$. The conditions that admixture of a given singlet state $^1\Psi_k$ be effective in making phosphorescence of a component with spin function ω spin-orbit allowed are

$$\Gamma_k \subset \Gamma_T \text{ and } \Gamma_k = \Gamma_j \otimes \Gamma_\omega \quad (\text{SR2})$$

Similarly, phosphorescence from the ω component of the triplet $^3\Psi_j$ becomes allowed by admixture of $^3\Psi_m$ to the ground state, if, and only if

$$\Gamma_m \subset \Gamma_j \otimes \Gamma_T \text{ and } \Gamma_m = \Gamma_\omega \quad (\text{SR3})$$

Methodological Considerations. In the present calculation, our zero-order wave functions and transition moments are taken from standard CNDO/S calculations.⁵ Experience^{6b} has shown that Coulomb integrals calculated by the Mataga-Nishimoto²¹ method give best results for singlet-singlet transition energies, whereas Pariser-Parr integrals²²

TABLE II: Matrix Elements of H' in Terms of MO's^{a,b}

Γ_τ	$\langle i^j V_a H' i^k T_b \Gamma_\tau \rangle$		$\langle i^k T_b \Gamma_\tau H' i^j \Psi_0 \rangle$
	$i = l$	$j' = k'$	
Γ_-	$-\langle j' A_x k' \rangle$	$\langle i A_x l \rangle$	$\sqrt{2} \langle k' A_x l \rangle$
Γ_+	$-\langle j' A_y k' \rangle$	$\langle i A_y l \rangle$	$\sqrt{2} \langle k' A_y l \rangle$
Γ_0	$-\langle j' A_z k' \rangle$	$\langle i A_z l \rangle$	$\sqrt{2} \langle k' A_z l \rangle$

^a In units of $(1/2)\hbar$. ^b $A_x = \sum_s \zeta_s \hat{l}_{xs}$, $A_y = \sum_s \zeta_s \hat{l}_{ys}$, $A_z = \sum_s \zeta_s \hat{l}_{zs}$.

give better results in the calculation of triplet states. In the present work, where both singlet and triplet states are involved, this difference on the preferred treatment of the two types of states leads to a dilemma. When each type of state is calculated with the different integrals, the spatial functions, i.e., the MO's, are no longer orthogonal, and the above development breaks down. Since the ultimate aim of these calculations is a singlet-triplet transition probability, we have now chosen arbitrarily to use Pariser-Parr Coulomb integrals throughout.²³

One drawback of using the standard CNDO/S calculation lies in the well-known degeneracy of singlet and triplet $n-\pi^*$ states.²⁴ Since the method was calibrated with singlet states, it may be assumed that the energy of triplet $n-\pi^*$ states is calculated too high by the singlet-triplet splitting. We have recently introduced a new method consisting of the direct SCF calculation of triplet states²⁵ which appears to account for the singlet-triplet splitting.²⁶ In some of the molecules treated here, the nature of the lowest triplet state is in doubt. Whenever our calculations lead to a near degeneracy of two or more states as the lowest triplet, we have attempted to resort to such SCF calculations to unravel the sequence. Unfortunately, this is not always uniquely feasible, since the SCF calculations, of necessity, ignore effects of configuration mixing, and good results are obtained only for states which are configurationally reasonably pure. We have also made use of the Extrapolation Method proposed in the same paper.²⁵ In some cases this has resulted in the conclusion that the state which actually has lowest energy, and hence is responsible for the phosphorescence, does not appear as the lowest triplet in the VO calculation. For consistency, the energies reported in the tables have been taken from the VO calculations, since only these readily permit calculation of the SO matrix elements; however, the state which we conclude to be responsible for the observed phosphorescence has been marked by placing a † over the corresponding energy.

As we mentioned above, the transition moments within each multiplicity manifold are routinely calculated by the CNDO/S program, using the ZDO and the central-field approximations.²⁷ To allow for nonzero $n \rightarrow \pi^*$ and $\sigma \rightarrow \pi^*$ transition moments, these approximations have been lifted by the introduction of polarization terms.^{6b} Thus, while many previous authors have resorted to experimental energies and oscillator strengths, all the quantities that we use in our SOC calculations are determined with respect to the same CNDO/S wave function.

Natural Radiative Lifetimes and Oscillator Strengths. The two quantities of interest to us in this work, the natural radiative lifetime, τ^0 , of the triplet, and the oscillator strength, f , of the ground-triplet absorption process, both can be expressed in terms of the transition moment of each component of the triplet to the ground state, given in eq 3:

$$(\tau^0)_{\Gamma_r}^{-1} = \frac{64\pi^4\sigma^3}{3h} |\langle {}^1U_0 | \bar{M} | {}^3U_1\Gamma_r \rangle|^2 \quad (11)$$

and

$$f_{\Gamma_r} = \frac{8\pi^2\mu c\sigma}{3e^2h} |\langle {}^1U_0 | \bar{M} | {}^3U_1\Gamma_r \rangle|^2 \quad (12)$$

where σ is the wave number of the transition in cm^{-1} .

At low temperature, i.e., in the absence of equilibrium between the triplet components by spin-lattice relaxation, this leads to three, usually different, lifetimes, one each for each component, and similarly to three oscillator strengths. These one component lifetimes and oscillator strengths can be converted into one another by

$$f_{\Gamma_r} = \frac{\mu c}{8\pi^2\sigma^2e^2} (\tau^0)_{\Gamma_r}^{-1} \quad (13)$$

At ordinary temperatures, where spin-lattice relaxation is very fast compared to emission, the populations of the three triplet components become equal, and kinetic analysis leads to the usual expression for the "natural radiative lifetime of the state", τ^0 :

$$(\tau^0)^{-1} = \frac{64\pi^4\sigma^3}{3h} (2S_i + 1)^{-1} \sum_{\Gamma_r} |\langle {}^1U_0 | \bar{M} | {}^3U_1\Gamma_r \rangle|^2 \quad (14)$$

Similarly, at high temperature, the apparent oscillator strength for the overall singlet \rightarrow triplet process is

$$f = \sum_{\Gamma_r} f_{\Gamma_r} \quad (15)$$

It should be noted that (14) and (15) are no longer related by eq 13.

The natural radiative lifetime τ^0 from eq 14 can be related to an experimentally measured lifetime τ_p by

$$(\tau^0)^{-1} = (\tau_p)^{-1} - k_Q \quad (16)$$

where k_Q is a comprehensive rate constant which is the sum of the rate constants for all first-order processes competing with emission in depleting the triplet (no processes of other orders are significant, or τ_p cannot be determined). According to eq 16, τ_p is a lower limit to τ^0

$$\tau^0 \geq \tau_p$$

Error Analysis. In our calculation of τ^0 , error may arise principally from three sources: (1) the values of the energy difference in the denominator of the SO coefficients, cf. eq 1-3; (2) in the calculation of the matrix elements of H' ; and (3) in the calculation of the transition moment integrals.

We estimate that our matrix elements H' and \bar{M} , because of the use of the approximations involved in the CNDO/S method and the techniques of integral evaluation, are affected with an uncertainty of a factor of about two. With considerable experience in comparing calculated and experimental spectra, we estimate the mean error in the energy terms to be of the order of 0.1 to 0.2 eV, probably nearer the lower limit for singlet states (for which the method was parametrized) and possibly somewhat larger for the triplets. Unless the energy difference is very small, these uncertainties do not lead to a significant contribution in the total error; and if the energy difference is that small, the perturbation technique is subject to question.

Based on these estimates of the errors in the individual terms, we are led to consider the uncertainty of our calculated $(\tau^0)^{-1}$ and f to be of the order of a factor not exceeding 3 or 4.

Results and Discussion

One of the problems facing the spectroscopist is the assignment of the orbital nature of the accessible spectroscopic states. In the case of phosphorescence, one is dealing with the lowest excited triplet and, therefore, in the organic molecules most frequently studied, the choice usually is between $\pi \rightarrow \pi^*$ and $n \rightarrow \pi^*$ (and, of course, $\sigma \rightarrow \pi^*$) states. The phosphorescence characteristics depend markedly on the orbital nature of the emitting state, and empirical rules have been established that help in the assignment of the nature of the phosphorescent state.²⁸

The SOC matrix elements for the interaction of singlet and triplet $\pi \rightarrow \pi^*$ states vanish identically since the operation of each component \hat{l}_q of the angular momentum operator on a p orbital represents just a rotation of 90° around the q axis. On the other hand, SOC matrix elements between singlet $\pi \rightarrow \pi^*$ and triplet $n \rightarrow \pi^*$ states (or vice versa) do not generally vanish. These arguments, known as El-Sayed's rules,²⁹ can commonly be used to predict the orbital nature of the states which can couple through SOC. However, care must be exercised because the rule that the $\pi \rightarrow \pi^*$ states of one multiplicity manifold can *only* spin orbitally couple with $n \rightarrow \pi^*$ (or $\sigma \rightarrow \pi^*$) states of the other does not imply the reverse. $n \rightarrow \pi^*$ states of one manifold can couple, not only with $\pi \rightarrow \pi^*$ states of the other, but also with $n \rightarrow \sigma^*$ states, and even with $\sigma \rightarrow \pi^*$ (including other $n \rightarrow \pi^*$) states provided the n and σ orbitals involve different p orbitals. The contribution of such terms, however, is usually not too important since the interacting states are usually of high energy and the transition moments are usually not large.

From the foregoing discussion we can see that $n \rightarrow \pi^*$ triplets will, in principle, have higher probability of emitting than $\pi \rightarrow \pi^*$ triplets. This happens because the former state couples with low-lying $\pi \rightarrow \pi^*$ singlets and borrows intensity from them, while the $\pi \rightarrow \pi^*$ triplet will have to borrow intensity from much higher $\sigma \rightarrow \pi^*$ singlets (including, of course, $n \rightarrow \pi^*$ singlets), which usually have low oscillator strengths. Furthermore, in carbonyls, the $n \rightarrow \pi^*$ state arises from excitation of a p electron localized on the oxygen atom to a delocalized π^* orbital. Because of the large amplitude of the n MO on the oxygen atom and since the SOC constant ζ_0 for oxygen is about 5.5 times larger than that for carbon, it is not surprising that the SOC effect is larger in carbonyls than in isoelectronic compounds containing atoms no heavier than carbon.

The emission from $\pi \rightarrow \pi^*$ triplets is, according to first-order perturbation theory, always polarized out of plane, since these states couple only with $n \rightarrow \pi^*$ (or $\sigma \rightarrow \pi^*$ and $\pi \rightarrow \sigma^*$) states. On the other hand, according to the above discussion, emission from $n \rightarrow \pi^*$ triplets can be polarized in any direction or have components of different polarization; however, since the predominant contribution in their spin-orbit coupling usually comes from $\pi \rightarrow \pi^*$ transitions, which are polarized in the molecular plane, we normally expect the phosphorescence to be in-plane polarized.

Carbonyl Compounds. Results of our calculation for a series of carbonyl compounds are summarized in Table III. The prototype carbonyl molecule is *formaldehyde*, and has been the subject of many previous theoretical studies.³⁰ The lowest triplet, by common consent of all workers, is an $n \rightarrow \pi^*$ state of symmetry A_2 . Our calculated lifetime for this state, 4.4×10^{-3} sec, is in fair agreement with other typical calculations which have obtained values in the range of 10^{-2} to 10^{-3} sec.³⁰ Experimental values for formal-

TABLE III: SOC in Carbonyls

Molecule	State ^{a,b}	$\Gamma_{c,d}$	Γ	Γ_0	τ^c	Polrzn ^f	τ_{lit}^g	τ_{expt}^h
Formaldehyde	$^3A_2, n \rightarrow \pi^*, 3.79^\dagger$	0.054 (x) [0.15 <i>f</i>] SF	3.84 (y) [0.017 <i>f</i>] 0.0085 (x) [0.16 <i>f</i>]	0.0015 (z) [0.86 <i>k</i>] SF ^j	0.0044	z	0.01 ^t	
	$^3A_1, \pi \rightarrow \pi^*, 6.64$				0.026	x	0.46 (x) ^k	
Fluoroformaldehyde	$^3A'', n \rightarrow \pi^*, 4.93^\dagger$	0.0031 (x,y) [0.24 <i>f</i> + 0.33 <i>f</i>]	0.00086 (x,y) [0.42 <i>f</i> + 0.64 <i>f</i>] 0.017 (z) [0.11 <i>k</i>]	0.017 (z) [0.17 <i>k</i>] 0.0	0.0020	x, y		
	$^3A', \pi \rightarrow \pi^*, 6.86$	0.0069 (z) [0.17 <i>k</i>]	0.004 (y) [0.25 <i>f</i>] SF	0.00027 (z) [0.28 <i>k</i>] SF	0.0074	z	0.0016-0.0035 ^k	
Difluoroformaldehyde	$^3A_2, n \rightarrow \pi^*, 6.21^\dagger$	0.023 (x) [0.11 <i>f</i>]	0.0059 (x,y) [0.43 <i>f</i> + 0.86 <i>f</i>] 0.011 (z) [0.15 <i>k</i>]	0.0197 (z) [0.17 <i>k</i>] 0.0	0.0013	x, y	0.15 (z), 0.06 (x) ^t 0.07 (z), 0.04 (x) ^t 0.28-0.37 (z) ^t	1.3 ^t
	$^3A_1, \pi \rightarrow \pi^*, 7.23$	0.0034 (y) [0.22 <i>f</i>]	0.0021 (x,y) [0.26 <i>f</i> + 0.44 <i>f</i>] [0.12 <i>k</i>]	0.0197 (z) [0.18 <i>k</i>] 0.0	0.0012	x, y		
Formic acid	$^3A'', n \rightarrow \pi^*, 4.82^\dagger$	0.0017 (x,y) [0.23 <i>f</i> + 0.57 <i>f</i>]	0.0005 (x,y) [0.38 <i>f</i> + 1.0 <i>f</i>] 0.0091 (z) [0.21 <i>k</i>]	0.0197 (z) [0.18 <i>k</i>] 0.0	0.0012	x, y		
	$^3A', \pi \rightarrow \pi^*, 6.18$	0.34 (z) [0.034 <i>k</i>]			0.027	z		
Formamide	$^3A'', n \rightarrow \pi^*, 4.61^\dagger$							
	$^3A', \pi \rightarrow \pi^*, 5.40$							
Acetone	$^3A_2, n \rightarrow \pi^*, 3.94^\dagger$	212.3 (x) [0.0021 <i>f</i>]	0.077 (y) [0.11 <i>f</i>] SF	0.0015 (z) [0.80 <i>k</i>] SF	0.0045	z	0.0078 (z) ^m	0.02-0.0006, ⁿ 0.00002-0.00008 ^o
	$^3A_1, \pi \rightarrow \pi^*, 6.32$	0.085 (y) [0.053 <i>f</i>]			0.068	y		
<i>p</i> -Benzoquinone	$^3B_{1u}, n \rightarrow \pi^*, 3.14$				SF			
	$^3A_0, n \rightarrow \pi^*, 3.22^\dagger$	2615. (x) [0.0008 <i>f</i>]	0.22 (y) [0.092 <i>f</i>]	0.00045 (z) [2.01 <i>k</i>]	0.0014 (49.4 × 10 ⁻⁷) ^q SF	z		z polarized ^r f = (6.3 × 10 ⁻⁷) ^r
Benzaldehyde	$^3B_{3g}, \pi \rightarrow \pi^*, 3.44$		0.77 (x) [0.04 <i>f</i>]	SF	2.30 (0.03) ^q	x		
	$^3B_{1g}, \pi \rightarrow \pi^*, 3.45$		0.028 (z) [0.23 <i>k</i>]	0.025 (z)	0.0	0.040 (z)		
Benzoic Acid	$^3A', \pi \rightarrow \pi^*, 3.63$	0.028 (z) [0.21 <i>k</i>]	0.0017 (x,y) [0.18 <i>f</i> + 0.76 <i>f</i>]	9.64 (z) [0.01 <i>k</i>]	0.0028	x < y ^s	0.0015 ^t (x < y)	
	$^3A', \pi \rightarrow \pi^*, 3.74^\dagger$	0.75 (z) [0.04 <i>k</i>]	14.7 (z) [0.009 <i>k</i>]	0.0	2.14	z	2.5 ± 2 ^u	

^a Symmetry, nature, and energy (eV) of the triplet state. ^b A dagger indicates the assigned phosphorescent state. ^c Symbols (x, y, z) in parentheses indicate axis of polarization. ^d Numbers in brackets indicate the transition moment vector, × 20²⁰ esu cm. ^e Phosphorescence lifetime calculated in this work, in seconds. ^f Polarization, indicating the axis along which phosphorescence is strongest. ^g Lifetimes from previous calculations in the literature, in seconds. ^h Experimental lifetimes, in seconds. ⁱ Reference 30b. ^j Symmetry forbidden. ^k D. G. Carroll, L. G. Vanquickenborne, and S. P. McGlynn, *J. Chem. Phys.*, 45, 2777 (1966). ^l Reference 32. ^m Reference 30a. ⁿ Reference 33. ^o Reference 34, results from solution phosphorescence. ^p Reference 35. ^q Calculated ground-triplet absorption oscillator strength. ^r Experimental ground-triplet absorption oscillator strength, ref 35. ^s The y component is stronger than the x component. ^t Reference 37. ^u Reference 3.

dehyde are unfortunately not available, but are believed to be of the order of 10^{-2} sec.³¹

It is apparent from Table III that the primary contribution to the phosphorescence probability comes from the Γ_0 component of the 3A_2 , which has a lifetime of 1.5×10^{-3} sec, with a z polarized emission. Table IV shows some of the most important SOC matrix elements. It is interesting to note that the mutual intermixing of the ground and 3A_2 states make the largest single contribution to the transition moment, because of the large difference in dipole moment between the two states.

The $A_1 \pi \rightarrow \pi^*$ triplet (calculated at 6.6 eV) in formaldehyde lies well above the $n \rightarrow \pi^*$ state and therefore is of no interest for the phosphorescence process per se. However, it is of theoretical interest because it represents the simplest case of a $\pi \rightarrow \pi^*$ state in carbonyls. Our result is 0.026 sec, originating exclusively from the Γ_+ spin component, and hence out-of-plane polarized, as expected.

Substitution of fluorine in formaldehyde has a relatively small effect on SOC. The lifetimes appear, cf. Table III, to be reduced by a factor of approximately two per F atom introduced. The relative contributions are very similar to the results obtained in formaldehyde; however, it is interesting to note that, in difluoroformaldehyde (carbonyl fluoride), the dipole moment changes direction between the ground and 3A_2 states, and hence the two separate contributions (cf. eq 3) from the mixing of each of these two states with the other have equal sign and reinforce one another, rather than partially cancelling. Although the Γ_0 component still provides the dominant contribution in difluoroformaldehyde, as it did in the parent molecule, the Γ_+ component has become much more nearly competitive. This occurs because of the mixing of the ground state with high triplets which involve heavy contribution from fluorine orbitals, and the relatively larger value of the SOC constant $\zeta_F = 272$ ($\zeta_C = 28$).

Even though the experimental data are confused³² or nonexistent, we report calculations for *formic acid* and *formamide* as prototypes of carboxylic acids and amides. The lowest triplet in both cases is calculated to have $n \rightarrow \pi^*$ nature, and resembles the 3A_2 state of formaldehyde closely. Given the lower symmetry of these compounds, the polarization is not as simple as in formaldehyde, but in both molecules is almost exclusively in the molecular plane. McGlynn and coworkers³² have measured a lifetime of 1.3 sec for formic acid, and are at a loss to explain this finding. Our calculated value of 1.3×10^{-3} sec certainly bears no resemblance to the measured result. The suggestion³² that the lowest triplet has $\pi \rightarrow \pi^*$ character seems unacceptable in view of our calculations.²⁵ Even the calculated lifetime of the $\pi \rightarrow \pi^*$ triplet is 0.02 sec, almost two orders of magnitude shorter than the reported value. If the measured τ_p is correct, this implies some kinetically slow mechanism for the formation of the triplet population. However, we have been unable to find any suggestion of this possibility in the literature. It seems clear that more detailed analyses of both τ^0 and τ_p for formic acid are called for.

For the $^3A_2 n \rightarrow \pi^*$ state of *acetone* at 3.9 eV, the calculated τ^0 is 4.5×10^{-3} sec, polarized along the C=O axis. Previous calculations gave a value of 7.8×10^{-3} , with the same polarization.^{30a} Early experimental determinations in EPA glass of τ_p and τ^0 were 6×10^{-4} and 1.2×10^{-2} sec, respectively.³³ Recent experimental work in solution has yielded lifetimes in the range of 2.1×10^{-5} to 8.1×10^{-5} . Because of their temperature and solvent dependency, these values contribute no new information about τ^0 .

TABLE IV. Details of Calculations in Formaldehyde

Triplet state component	$^1\Psi_k^{a,b}$	$^1E_k^c$	$\vec{M}(\Psi_0, \Psi_k)^d$	$^3\Psi_k \Gamma_+$	$^3\Psi_k \Gamma_+$	\vec{M}^f	$^3\Psi_m$	$\vec{M}(\Psi_m, \Psi_0)^g$	\vec{M}^f
1A_2	Γ_0	0.0	-3.14k	-57.8		-0.59k	1A_2	57.8	0.19k
	$2^1A_1, \pi$	9.71	-3.12k	48.5		-0.32k	$2^1A_2, \sigma$	17.8	-0.05k
	$3^1A_1, \pi$	12.61	2.30k	-21.2	π^*	-0.07k			
2^3A_1	$1^1B_1, \sigma$	9.18	-0.53k	45.4	σ^*	-0.12k	$1^3B_1, \sigma$	54.6	0.04k
	Γ_+				σ^*				

^a Perturbing singlet state. ^b States are classified by ascending symmetry. ^c Orbital nature of state is also shown. ^d State energy, in eV. ^e Multiplicity allowed transition moments, in Debyes. ^f Values of SOC matrix elements, in cm^{-1} . ^g Contribution to the singlet-triplet transition moment, $\times 10^{20}$ esu cm. ^h Perturbing triplet state.

TABLE V: SOC in Aromatic Hydrocarbons^a

Molecule	State ^b	$\Gamma_0^{c,d}$	τ^e	Polrzn ^f	$\tau_{lit.}^g$	τ_{expt}^h
Benzene	${}^3B_{1u}, \pi \rightarrow \pi^*, 3.43$					
Toluene	Cf. Table VI					
Naphthalene	${}^3B_{2g}, \pi \rightarrow \pi^*, 2.65$	33.7(x) [0.0099i]	101	x	10 ^j	75 ± 25 ^k
Azulene	${}^3B_2, \pi \rightarrow \pi^*, 1.71$	105(x) [0.011i]	315	x		

^a Only the Γ_0 components are shown. The Γ_- and Γ_+ components are symmetry forbidden for all molecules presented here, cf. Table VI. ^b Symmetry, orbital nature, and energy (eV) of triplet state. ^c Symbols in parentheses indicate polarization. ^d Numbers in brackets indicate the triplet-ground state transition moment vector, $\times 10^{20}$ esu cm. ^e Phosphorescence lifetime calculated in this work, in seconds. ^f The symmetry axis along which phosphorescence is strongest. ^g Phosphorescence lifetime from previous calculations found in the literature, in seconds. ^h Experimental lifetime, in seconds. ⁱ Symmetry forbidden. ^j Reference 42. ^k Reference 39a.

The singlet-triplet absorption of *p*-benzoquinone has been studied in hexane, and the oscillator strength for this transition was reported as $f = 6.3 \times 10^{-7}$,³⁵ and was found to be polarized along the O-O axis.³⁶ Our calculations show the four lowest triplets, 3A_u , ${}^3B_{1u}$, ${}^3B_{1g}$, and ${}^3B_{3g}$, to be very closely spaced.²⁵ Since SOC does not mix states of different parity, the usual spectroscopic selection rule $g \leftrightarrow g$ and $u \leftrightarrow u$ holds, in first order, also in phosphorescence and singlet-triplet absorption. Accordingly calculated oscillator strength and phosphorescence rate constants vanish for the two g states. The two $n \rightarrow \pi^*$ states, 3A_u and ${}^3B_{1u}$, are calculated so close in energy²⁵ that a decision on their order cannot be made. The observed absorption and its polarization suggest that the 3A_u state is the lowest. Our calculated oscillator strength for the ${}^3A_u \leftarrow {}^1A_g$ transition is the largest in this group of closely spaced states, and hence it appears likely that this is the transition observed. The calculated oscillator strength is 4.9×10^{-6} .

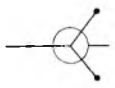
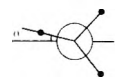
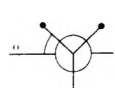
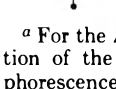
On the basis of both recent calculations²⁵ and experimental work³⁷ it seems likely that the lowest triplet state of *benzaldehyde* is an $n-\pi^*$ (A'') state. The calculated oscillator strength for the singlet-triplet absorption is 6×10^{-7} , the value measured in hexane at -47° is 1.8×10^{-7} .³⁶ The calculated τ^0 is 2.8×10^{-3} and τ_p in glass was reported as 1.45×10^{-3} . The calculated polarization of this transition is in the molecular plane, nearly parallel the long axis, in agreement with experiment.³⁸ The ${}^3A'$ $\pi \rightarrow \pi^*$ state has a computed lifetime of 0.04 sec and is out-of-plane polarized.

For *benzoic acid* the lowest triplet is calculated to be ${}^3A'$ $\pi \rightarrow \pi^*$ at 3.74 eV, with the $n \rightarrow \pi^*$ state being the fourth calculated triplet (by the VO-CI method) at 4.65 eV. The A' state has a calculated τ^0 of 2.14 sec, vs. an experimental τ_p of 2.5 ± 0.2 sec.³ In this molecule, unlike in *benzaldehyde*, the $\pi \rightarrow \pi^*$ state is mostly localized on the ring, with a very small amplitude on the oxygen atoms.

Aromatic Hydrocarbons. The lowest triplet states of aromatic hydrocarbons have $\pi \rightarrow \pi^*$ character, and consequently their phosphorescence must steal intensity from the multiplicity allowed $\sigma \rightarrow \pi^*$ and $\pi \rightarrow \sigma^*$ transitions. Since these transitions are weak and also since their energy is well above the low lying $\pi \rightarrow \pi^*$ triplet, aromatics are expected to have long emission lifetimes, and this indeed is observed experimentally. Based on careful measurement of τ_p and of the phosphorescence quantum yield (ϕ_p), and using estimates of the intersystem quantum yield (ϕ_r), it is currently thought that the natural lifetime of $\pi \rightarrow \pi^*$ triplets of aromatic hydrocarbons is of the order of 30 sec and larger.³⁹ Some typical calculations are shown in Table V.

In *benzene* the lowest triplet is a ${}^3B_{1u}$ state calculated at 3.43 eV. Application of the symmetry rules discussed above

TABLE VI: Phosphorescence of Various Conformers of Toluene^a

Con-formation	Sym-metry	α^b deg	τ^c	\vec{M}^d
	C_s	0	1310	$[1.9\hat{k}]$
	C_1	10	585	$[2.2\hat{i} + 0.1\hat{j} + 1.6\hat{k}]$
	C_2	20	314	$[3.6\hat{i} + 1.0\hat{k}]$
	C_s	30	268	$[4.1\hat{i}]$ $[9.0\hat{j} + 0.9\hat{k}]$

^a For the A' $\pi \rightarrow \pi^*$ triplet, calculated at 3.40 eV. ^b Angle of rotation of the methyl group, defined under Conformation. ^c Phosphorescence lifetime, in seconds. ^d Singlet-triplet transition moment, $\times 10^{23}$ esu cm. ^e Principal spin component.

shows that emission from this state via a first-order spin-orbit coupling is forbidden. To account for the benzene phosphorescence one would have to consider higher order mechanisms, such as spin-vibronic coupling.⁴⁰

Recently, τ_p has been reported for a series of deuterium-substituted *toluenes*.⁴¹ The values given vary from 8.02 sec for $C_6H_5CH_3$ to 10.54 sec for $C_6D_5CD_3$, and the substitution of D for H in the ring is the major factor in the variation of τ_p . Our calculations give a value for τ^0 much larger than any of the τ_p , and show a considerable variation with the orientation of the methyl group, cf. Table VI. In the computationally most convenient conformation, in which one of the methyl hydrogens lies in the molecular plane, the calculated lifetime is 1300 sec, the polarization is out of plane. These values are so large that the transition might as well be considered forbidden in the first order and the observed intensity must find its explanation in some second-order process. In the other extreme conformation, the lifetime is reduced to 270 sec, polarized along the short in-plane axis; intermediate conformations of C_1 symmetry give intermediate lifetimes and polarizations.

Until recently, *naphthalene* was considered to have a phosphorescence lifetime of 2.6 ± 0.2 sec.³ Recent experimental work has permitted to deduce an estimate of τ^0 of 75 ± 25 sec³⁹; our calculated value is 101 sec, compared with older calculations which gave 10 sec.⁴² Considering the estimates of error attached to both the experimental and our calculated values, the agreement is good.

The calculated lifetime for *azulene* is 316 sec, with an oscillator strength for absorption of 7.5×10^{-11} . Previous au-

TABLE VII: SOC in Azines

Molecule	State ^a	Γ_-^b	Γ_+	Γ_0	τ^c	Polariz ^d	$\tau_{\text{lit.}}^e$	τ_{expt}^f
Pyridine	$^3A_1, \pi \rightarrow \pi^*, 3.70$	SF ^g	0.51(x) [0.049 \hat{i}]	SF	1.52	x	1.54 ^h	
	$^3B_1, n \rightarrow \pi^*, 4.53$	SF	0.0079(z) [0.29 \hat{k}]	0.40(y) [0.040 \hat{j}]	0.023	z	0.012 ^h 0.005 ⁱ	
Pyridazine	$^3B_2, \pi \rightarrow \pi^*, 3.62$	SF	SF	0.28(x) [0.068 \hat{i}]	0.84	x		
	$^3B_1, n \rightarrow \pi^*, 3.66$	SF	0.0056(z)	0.095(y)	0.0158	z	0.02(z), 0.2'(x) ⁱ 0.0146(z) ^h	<0.05 ^j
Pyrimidine	$^3B_1, \pi \rightarrow \pi^*, 4.24$	SF	[0.47 \hat{k}] SF	[0.11 \hat{j}] 0.0087(y) [0.30 \hat{j}]	1.49	y		
	$^3B_2, n \rightarrow \pi^*, 4.53^\dagger$	0.013(xz)	SF	0.0038(x)	0.0088	x	0.004(x) ⁱ 0.07(z)	0.01–0.02 ^k (z)
Pyrazine	$^3B_{3u}, n \rightarrow \pi^*, 3.39^\ddagger$	SF	1.33(z) [0.034 \hat{k}]	0.0078(y) [0.43 \hat{i}] [0.45j]	0.023	y	0.007(x) ^h 0.001(y) ⁱ 0.0148 ^h	0.018 ^l
	$^3B_{1u}, \pi \rightarrow \pi^*, 3.40$	SF	0.0024(x) [0.81 \hat{i}]	SF	0.0071	x	0.0026 ^h	
3-Cyano-pyridine	$^3A_1, \pi \rightarrow \pi^*, 3.80^\ddagger$	1.01(z)	0.93(z) [0.03 \hat{k}]	SF [0.035 \hat{k}]	1.45			3.3 ^m
4-Cyano-pyridine	$^3B_1, n \rightarrow \pi^*, 4.33^\ddagger$	SF	0.0012(z) [0.80 \hat{k}]	4.71(y) [0.013 \hat{j}]	3.5×10^{-3}	z		0.004 ^m
2,6-Luti-dine	$^3A_1, \pi \rightarrow \pi^*, 3.70^\ddagger$	1.78(y) [0.026 \hat{j}]	SF	SF	5.36	y		3.2 ^m

^a Cf. footnotes a, b, Table III. ^b Cf. footnotes c, d, Table III. ^c Cf. footnote e, Table III. ^d Cf. footnote f, Table III. ^e Cf. footnote g, Table III. ^f Cf. footnote h, Table III. ^g Symmetry forbidden. ^h Reference 50. ⁱ Reference 51. ^j Reference 48. ^k Reference 49. ^l Reference 52. ^m Reference 44.

thors calculated τ^0 as 118 sec.^{42b} The fact that no phosphorescence has been observed⁴³ could be due either to a low quantum yield of the triplet state or to an effective competition of nonradiative transitions to the ground state.

Azines. In Table VII, we are reporting lifetimes of the lowest triplets of pyridine, substituted pyridines, and the diazines. These molecules are characterized by very closely spaced lower triplet $n \rightarrow \pi^*$ and $\pi \rightarrow \pi^*$ states. Also, the lone pair orbitals are different from those in the carbonyl compounds, in that they involve strong s-p hybridization.

Hoover and Kasha⁴⁴ have communicated preliminary results on the phosphorescence of three substituted pyridines measured in EPA glass at 77°K. The principal purpose of their study was to determine the nature of the lowest triplet in these compounds. For 2,6-lutidine and 3-cyanopyridine they conclude that the phosphorescing state has $\pi \rightarrow \pi^*$ character, and obtained values of τ_p of 3.2 and 3.3 sec, respectively. Our calculated values of τ^0 for these compounds are 5.36 and 1.45 sec, respectively. On the other hand, they found that 4-cyanopyridine phosphoresces from an $n-\pi^*$ (3B_1) state with $\tau_p = 4 \times 10^{-3}$ sec, compared with our calculated τ^0 of 3.5×10^{-3} . The close agreement between calculated τ^0 and observed τ_p in these compounds suggest that the ratio of intersystem and phosphorescence quantum yield is not far from unity, i.e., that most molecules reaching the triplet state emit, and that competing processes are not very effective.

In the same paper, Hoover and Kasha⁴⁴ were concerned with the nature of the lowest triplet of pyridine, and with the reasons that no phosphorescence is observed from this compound. Recent calculations⁴⁵ and experimental re-

sults⁴⁶ are in good agreement for the energy of the lowest triplet states (cf. Table VII for part of our results). Evans⁴⁷ has reported an oscillator strength of 0.11×10^{-7} for the singlet-triplet absorption of pyridine, which fortuitously coincides with our calculated value.

The lifetime τ^0 for the lowest triplet state of pyridine is calculated as 1.52 sec, which suggests that this compound should behave much like 2,6-lutidine and 3-cyanopyridine. The absence of phosphorescence in pyridine thus cannot be ascribed to an extremely long natural radiative lifetime; it must then be found either in quenching processes or in a low intersystem crossing yield.

The experimental oscillator strength for singlet-triplet absorption in pyridazine is $>5 \times 10^{-8}$ sec.⁴⁸ Our calculated result for the same quantity is 1.1×10^{-7} , in good agreement with experiment.

The singlet-triplet absorption spectrum of pyrimidine has been observed in solution and a visual estimate of the triplet lifetime has been made (0.01–0.02 sec).⁴⁹ The polarization of the absorption is along the C_2 axis. Previous calculations⁵⁰ assumed the phosphorescent state to be of $n \rightarrow \pi^*$ nature, and found a lifetime of 0.007 sec with the same polarization. In another calculation⁵¹ Goodman and Krishna computed two components both polarized in-plane. This is the one molecule for which our calculations²⁵ failed to give reasonable triplet state energies. Calculated lifetimes are 0.026 sec for the $^3B_1 \pi-\pi^*$, and 0.0088 sec for the $^3B_2 n \rightarrow \pi^*$ states.

The emission from the lowest triplet state of pyrazine has received considerable attention recently, particularly by El-Sayed and his coworkers. The phosphorescence has

been studied in the temperature range from 1.6 to 77°K.⁵² At 77°K, the observed lifetime τ_p is 0.018 sec, compared to our calculated value of τ^0 of 0.023 sec. At the lowest temperatures the total emission can be decomposed into three components with τ_p values of 0.006, 0.070, and 0.320 sec. Polarization studies suggest that the short and medium lifetime components have different polarization, and that the 6-msec component is long-axis polarized.

Our calculations give τ^0 for the Γ_0 and Γ_+ components as 0.0078 (long-axis) and 1.33 sec (short-axis polarized). Emission from the Γ_- component is symmetry forbidden. The polarization allows us to assign the short lifetime component as Γ_0 ; the symmetry forbidden nature of Γ_- makes it a prime candidate for the long lifetime component, leaving Γ_+ as the middle one.

If we assume with El-Sayed⁵² that no spin-lattice relaxation of the triplet components occurs, we can make a kinetic analysis of the relaxation processes. Such an analysis leads to

$$\frac{I(\Gamma_0)}{I(\Gamma_+)} = \frac{k_i(\Gamma_0) \tau_p(\Gamma_0) \tau^0(\Gamma_+)}{k_i(\Gamma_+) \tau^0(\Gamma_0) \tau_p(\Gamma_+)}$$

where $I(i)$ is the intensity of phosphorescence from component i , the k_i 's are the corresponding intersystem crossing rate constants, and the τ 's have their usual meaning. Substituting the previously cited values for these τ 's, and inserting El-Sayed's estimate for the intensity ratio, we obtain $k_i(\Gamma_0)/k_i(\Gamma_+) \sim 2$, a ratio much lower than El-Sayed's estimate of 30, however, a value which still supports the symmetry arguments for preferential population of Γ_0 . The discrepancy between our estimate of $k_i(\Gamma_0)/k_i(\Gamma_+)$ and El-Sayed's arises from his assumption that the τ_p 's are τ^0 , and our finding that, while this assumption is not bad for Γ_0 , it seems quite far off for Γ_+ . The original assumption that no spin-lattice relaxation occurs seems justified by these results. Postulation of spin-lattice relaxation would lead to even lower estimates of $k_i(\Gamma_0)/k_i(\Gamma_+)$, which is unlikely in view of the symmetry arguments given by El-Sayed.⁵²

Calculations of the nature of the phosphorescent state of some azanaphthalenes have been given elsewhere.⁵³

Conclusions

In this paper we have further explored the application of CNDO/S wave functions to the calculation of spin-orbit coupling matrix elements and their use in the study of molecular phosphorescence. In general, the results obtained have been reasonably consistent with experiment, i.e., calculated τ^0 's have not been less than observed τ_p , and not been sufficiently larger to make observation of phosphorescence unlikely. However, we were unable to obtain results for formic acid in any reasonable relation to the results of McGlynn, nor were we able to shed any new light on the reason for the lack of phosphorescence in pyridine, other than to demonstrate that it is not due to a long radiative lifetime, as postulated by Kasha.⁴⁴

Finally, in favorable cases it is possible to analyze the difference between calculated τ^0 and experimental τ_p to obtain new information about intersystem crossing rates and the existence of nonradiative processes.

Acknowledgments. We wish to acknowledge many interesting and helpful discussions with Dr. C. J. Seliskar. We also acknowledge the help from the South Western Ohio Regional Computer Center in providing the computer time necessary for this work and for the courteous help of their

staff. One of us (C.A.M.) wishes to thank the Research Council of the University of Cincinnati for the award of a Summer Research Fellowship (1973).

References and Notes

- (1) G. N. Lewis and M. Kasha, *J. Am. Chem. Soc.*, **66**, 2100 (1944).
- (2) S. P. McGlynn, T. Azumi, and M. Kinoshita, "Molecular Spectroscopy of the Triplet State", Prentice-Hall, Englewood Cliffs, N.J., 1969.
- (3) D. S. McClure, *J. Chem. Phys.*, **17**, 665, 905 (1949).
- (4) E. U. Condon and G. H. Shortley, "The Theory of Atomic Spectra", 7th ed, Cambridge University Press, New York, N.Y., 1967, p 211.
- (5) R. L. Ellis, R. Squire, and H. H. Jaffé, *J. Chem. Phys.*, **55**, 3499 (1971).
- (6) (a) G. W. Kuehnlenz, C. A. Masmanidis, and H. H. Jaffé, *J. Mol. Structure*, **15**, 445 (1973); (b) R. L. Ellis, G. Kuehnlenz, and H. H. Jaffé, *Theor. Chim. Acta*, **26**, 131 (1972), and references cited therein.
- (7) The reader should be aware that the wave functions (many electron functions as well as orbitals) contain an undefined phase factor (which may be written as $e^{i\phi}$, but practically only takes the values ± 1 , or, perhaps, $\pm i$). As a consequence most of the integrals also have an undetermined phase factor, i.e., are undetermined with respect to sign.
- (8) Actually, the first-order expansion of ${}^3U_j^{1r}$ should, in addition, contain terms in ${}^5\Pi_{1g}^{1r}$, with $\Gamma_s \neq \Gamma_r$. These terms, however, do not contribute to the transition moment between the state ${}^3U_j^{1r}$ and the ground state, and consequently are neglected.
- (9) We shall use throughout capital letters for many electron functions or operators, lower case letters for one-electron functions or operators.
- (10) H. F. Hameka, "The Triplet State", A. B. Zahlan, Ed., Cambridge University Press, New York, N.Y., 1967.
- (11) It should be noted here that the operator i_j in a molecule has no clear meaning since the angular momentum is not well defined. We postpone a further discussion of the problem to the point at which we introduce the LCAO expansion.
- (12) S. I. Weissman, *J. Chem. Phys.*, **18**, 232 (1950).
- (13) The function ${}^3\omega_x$ differs in sign from that used in ref 6.
- (14) J. H. van der Waals and M. S. de Groot, "The Triplet State", A. B. Zahlan, Ed., Cambridge University Press, New York, N.Y., 1967.
- (15) F. L. Pilar, "Elementary Quantum Chemistry", McGraw-Hill, New York, N.Y., 1968, Chapter 11; see also ref 2, pp 191-193.
- (16) When the Slater determinants reduce to this simple two-electron case, the form of the spatial part of the configurations is given as:

$${}^{ij}V_a = \frac{1}{\sqrt{2}} [\phi(1)\phi_j(2) + \phi(2)\phi_j(1)]$$

$${}^{ik}T_b = \frac{1}{\sqrt{2}} [\phi(1)\phi_k(2) - \phi(2)\phi_k(1)]$$
 Analogously we can write the ground state simply as

$$V_0 = [\phi(1)\phi(2)]$$
- (17) The basis members of the LCAO expansion individually are eigenfunctions of I_i^2 , provided we are defining i in a molecule fixed coordinate system.
- (18) Reference 2, pp 193-196.
- (19) See, for example, T. M. Dunn, *Trans. Faraday Soc.*, **1441** (1961).
- (20) Note that this table includes some minor corrections of Table 3 of ref 5.
- (21) K. Nishimoto and N. Mataga, *Z. Phys. Chem. (Frankfurt am Main)*, **12**, 335 (1957); **13**, 140 (1957).
- (22) R. Pariser and R. G. Parr, *J. Chem. Phys.*, **21**, 767 (1953).
- (23) Note that in ref 5 we used Mataga-Nishimoto integrals.
- (24) R. Daudel and C. Sandorfy, "Semiempirical Wave-Mechanical Calculations on Polyatomic Molecules", Yale University Press, 1971.
- (25) H. M. Chang, H. H. Jaffé, and C. A. Masmanidis, *J. Phys. Chem.*, **79**, 1109 (1975).
- (26) Recent calculation by R. Lake in this laboratory indicate that INDO calculations give results quite similar to the SCF triplets.
- (27) R. S. Mulliken, *J. Chem. Phys.*, **7**, 14, 20 (1939).
- (28) R. S. Becker, "Theory and Interpretation of Fluorescence and Phosphorescence", Wiley-Interscience, New York, N.Y., 1969, p 156; cf. also ref 2, pp 246-247.
- (29) M. A. El-Sayed, *J. Chem. Phys.*, **38**, 2834 (1963).
- (30) (a) H. F. Hameka and L. J. Oosterhoff, *Mol. Phys.*, **1**, 358 (1958); (b) J. W. Sidman, *J. Chem. Phys.*, **29**, 644 (1958).
- (31) Reference 2, chapter 6; ref 28, chapter 12.
- (32) L. W. Johnson, H. J. Maria, and S. P. McGlynn, *J. Chem. Phys.*, **54**, 3823 (1971).
- (33) E. H. Gilmore, G. E. Gibson, and D. S. McClure, *J. Chem. Phys.*, **20**, 829 (1952); **23**, 399 (1955).
- (34) G. Porter, S. K. Dogra, R. O. Loutfy, S. E. Sugamori, and R. W. Yip, *J. Chem. Soc., Faraday Trans. 1*, **69**, 1462 (1973).
- (35) Y. Kanda, H. Kaseda, and T. Matsumura, *Spectrochim. Acta*, **20**, 1387 (1964).
- (36) J. W. Sidman, *J. Am. Chem. Soc.*, **78**, 2363 (1956); *J. Chem. Phys.*, **27**, 820 (1957).
- (37) V. L. Ermolaev, *Opt. Spektrosk.*, **1**, 523 (1956).
- (38) R. Shimada and L. Goodman, *J. Chem. Phys.*, **43**, 2027 (1965).
- (39) (a) J. Langelaar, R. P. H. Rettschnick, and G. J. Hoijtink, *J. Chem. Phys.*, **54**, 1 (1971); (b) E. C. Lim, *ibid.*, **36**, 3497 (1962); (c) W. Siebrand, *ibid.*, **47**, 2411 (1967).

- (40) A. C. Albrecht, *J. Chem. Phys.*, **38**, 354 (1963).
 (41) T. E. Martin and A. H. Kalantar, *Chem. Phys. Lett.*, **1**, 623 (1968).
 (42) (a) B. R. Henry and W. Siebrand, *J. Chem. Phys.*, **51**, 2396 (1969); (b) W. S. Veeman and J. H. van der Waals, *Mol. Phys.*, **18**, 63 (1970).
 (43) D. F. Evans, *J. Chem. Soc.*, 1735 (1960).
 (44) R. J. Hoover and M. Kasha, *J. Am. Chem. Soc.*, **91**, 6508 (1969).
 (45) H. H. Jaffé, C. A. Masmanidis, H. M. Chang, and R. L. Ellis, *J. Chem. Phys.*, **60**, 1696 (1974).
 (46) S. Japar and D. A. Ramsay, *J. Chem. Phys.*, **58**, 5832 (1973).
 (47) E. F. Evans, *J. Chem. Soc.*, 3885 (1957).
 (48) R. M. Hochstrasser and C. Marzocco, *J. Chem. Phys.*, **46**, 4155 (1967).
 (49) R. Shimada, *Spectrochim. Acta*, **17**, 30 (1961).
 (50) T. Yonezawa, H. Kato, and H. Kato, *Theor. Chim. Acta*, **13**, 125 (1969).
 (51) L. Goodman and V. G. Krishna, *Rev. Mod. Phys.*, **35**, 541, 735 (1963).
 (52) L. Hall, A. Armstrong, W. Moomaw, and M. A. El-Sayed, *J. Chem. Phys.*, **48**, 1395 (1968); M. A. El-Sayed, *Acc. Chem. Res.*, **1**, 8 (1968); **4**, 23 (1971); in "Molecular Luminescence", E. C. Lim, Ed., W. A. Benjamin, New York, N.Y., 1969, p 715.
 (53) H. H. Jaffé and C. A. Masmanidis, *Chem. Phys. Lett.*, **24**, 416 (1974).

Analysis of Free Diffusion in a Binary System When the Diffusion Coefficient Is a Function of the Square Root of Concentration

John G. Albright and Donald G. Miller*

Chemistry Department, Lawrence Livermore Laboratory, Livermore, California 94550 (Received April 24, 1975)

Publication costs assisted by Lawrence Livermore Laboratory

Diffusion of even a very dilute electrolyte into pure water is markedly skewed from the "ideal" case of a concentration-independent diffusion coefficient owing to the $c^{1/2}$ dependence of D . This makes uncertain the value of c to which the D calculated from experiment refers. The skewing is predicted by poor convergence of the Gosting-Fujita series solution of Fick's equation for this case, particularly when one boundary is at zero concentration. Convergence is too slow for accurate conclusions, but the theory suggests crossover point or averaging methods to determine $D(\bar{c})$. Numerical integration of Fick's equation yields accurate solutions for $0 \geq \beta(2c)^{1/2} \geq -0.9$. Analysis of these solutions shows that either crossover points or averages can be used to determine $D(\bar{c})$ from skewed Rayleigh fringe patterns. Averaging D_j for $0.27 \leq z^* \leq 1.04$ is recommended for the $c^{1/2}$ dependence to get $D(\bar{c})$ to 0.1%. Analysis of Gouy fringe patterns is not considered here.

1. Introduction

Optical methods are the most precise for determining differential diffusion coefficients. In such methods concentration differences are usually made small, and any concentration dependence of the diffusion coefficient is assumed to be so negligible that the diffusion coefficient D can be taken as constant and equal to that for the average concentration. This situation, where D is effectively constant, is called *ideal* diffusion. In these circumstances, Fick's second equation can often be solved in closed form, which permits extraction of the diffusion coefficient from experimentally obtained fringe patterns. Methods for such analyses are well established,²⁻⁴ and precision is commonly 0.1%. In this paper, we shall confine ourselves to one-dimensional free diffusion in a binary system, and our principal concern is with the analysis of Rayleigh fringe patterns.

For larger concentration differences, the concentration dependence of D cannot be ignored. Free diffusion in a binary system, where D can be represented by a polynomial in the concentration c (in moles/liter)

$$D = D_0(1 + \alpha_1 c + \alpha_2 c^2 + \alpha_3 c^3 + \dots) \quad (1)$$

has been examined in some detail for Gouy⁵ and Rayleigh^{6,7} fringe patterns. The results^{5,6} are series expansions in terms of the quantity ϕ , where

$$\phi = (c - \bar{c})/(\Delta c/2) \quad (2)$$

and \bar{c} is the mean concentration. We define

$$\bar{c} = (c_T + c_B)/2 \quad (3)$$

$$\Delta c = c_B - c_T \quad (4)$$

where c_T and c_B are concentrations at $x = -\infty$ and $x = +\infty$, corresponding ordinarily to the top and bottom portions of an infinitely extended cell.

The series based on eq 1 converges rapidly as Δc decreases. Moreover, the first-order Δc contribution cancels out completely both in the Gouy analysis⁵ and in the symmetric pairing of Rayleigh fringes recommended by Creeth.⁶ Consequently, the first contribution to skewness comes from a Δc^2 term which disappears rapidly as Δc approaches 0. The term skewness refers to any deviation away from the ideal diffusion situation (constant D), including the positions of fringes, the shape of the concentration distribution, and the shape of the concentration distribution derivative. Thus, theory shows that systems with the concentration dependence of eq 1 are consistent with the intuitive notion of treating D as constant whenever Δc is small. Moreover, experiment verifies that when Δc is small, skewness is indeed both small and cancels in Gouy and Creeth-Rayleigh analyses of data. Consequently, the resulting D is for the average concentration \bar{c} , and is denoted by \bar{D} .

However, dilute electrolyte solutions, where pure water is layered over the electrolyte solution, form a very impor-

tant class of systems where D cannot be assumed constant for small Δc . Here D depends on $c^{1/2}$, i.e.

$$D = D_0(1 + \beta c^{1/2}) \quad (5)$$

where β is negative by experiment and theory.^{8,9}

Such systems have very skewed fringe patterns¹⁰⁻¹² even in the dilutest solutions accessible to experiment. This is because the $c^{1/2}$ skewness does not go away fast enough as Δc approaches 0. Consequently, it is uncertain whether the numerical value of D calculated by the usual analyses refers to \bar{c} or not.

Figure 1 shows concentration distributions calculated by numerical integration for ideal diffusion ($\alpha_1 = \beta = 0$), linear concentration dependence ($\alpha_1 = -0.5$), and $c^{1/2}$ dependence ($\beta = -0.5$). For all cases $c_T = 0$, $c_B = 1$, $\bar{c} = 0.5$, $D_0 = 10^{-5}$ cm²/sec, $t = 8000$ sec, and the initial boundary is at $x = 1.5$. The α_1 and β were chosen so that D at c_T and D at c_B would be the same for both concentration-dependent cases. Clearly, the two concentration-dependent cases are different from one another and are skewed from the ideal case both by shape and position. In particular, the x position of \bar{c} was shifted away from the initial boundary position.

The $c^{1/2}$ skewness is best seen in Rayleigh patterns. In this case, the symmetric Creeth pairs (fringes j and $J - j$) for dilute solutions give an apparent D_j which is a function of the $f(j)$ or z_j^* defined below. This is in sharp contrast to the case of linear or polynomial c dependence, where D_j for all symmetric pairs are nearly identical for all values of $f(j)$ when Δc is small. Here, j is the fringe number of interest, J is the total number of Rayleigh fringes (not necessarily an integer), and $f(j)$ and D_j are given by eq

$$f(j) = \frac{2j - J}{J} \quad (6)$$

$$D_j = \left[\frac{x_j - x_{J-j}}{2t^{1/2}(z_j^* - z_{J-j}^*)} \right]^2 \quad (7)$$

$$z_j^* = -z_{J-j}^* = \operatorname{erfinv}(f(j)) \quad (8)$$

where erfinv is the inverse error function, and x_j and x_{J-j} are the positions of fringes j and $J - j$ in the fringe pattern measured from the initial sharp boundary between the top and bottom solutions.

Figure 2 shows the skewing of D_j/\bar{D} as a function of z_j^* for the same cases shown in Figure 1. The values of α_1 , β , and Δc were chosen sufficiently large to show the nature of skewing even for the linear case. It is clear that the $c^{1/2}$ dependence shows substantially more skewing than the linear one, with maximum deviations of 5 and 1.5%, respectively. Moreover it is in the opposite direction. Another example (not graphed) is for $\alpha_1 = \beta = -0.2$. Here the value D_j/\bar{D} is 1.000 within 0.1% everywhere for the linear case, whereas deviations reach 2% for the $c^{1/2}$ dependence.

The principal purposes of this paper are to investigate analytically and numerically (1) the effects of a $c^{1/2}$ dependence on skewness and (2) the possibility of determining \bar{D} from skewed Rayleigh fringe patterns. Gouy fringe patterns will be discussed only in passing.

We shall show analytically for dilute electrolytes in the experimental region that skewness does not disappear as Δc approaches 0 because the series expansion in terms of ϕ (eq 3) becomes a series in $(\bar{c})^{1/2}$, which converges too slowly. Because convergence is so poor, analytical results do not faithfully represent the phenomenon. However, they do indicate the skewness in the Rayleigh analysis and the nonidentity of D_A and \bar{D} in the Gouy analysis. There is also a

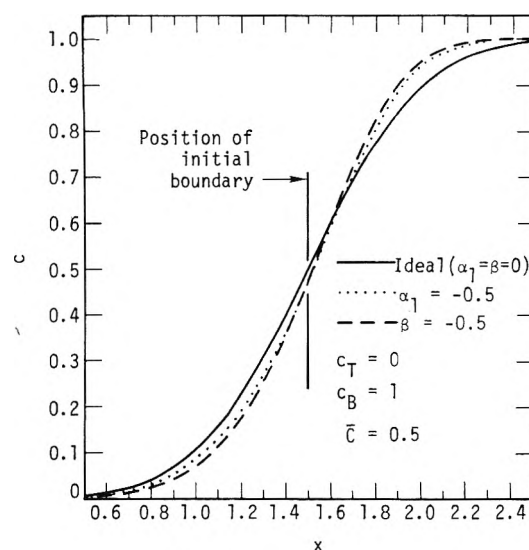


Figure 1. Concentration distribution obtained by numerical integration for free diffusion after 8000 sec for a system with $c_T = 0$, $c_B = 1$, $D_0 = 10^{-5}$ cm²/sec, and initial sharp boundary at $x = 1.5$ cm. Solid line is ideal diffusion ($\alpha_1 = \beta = 0$); dotted line is linear concentration dependence of D ($\alpha_1 = -0.5$); dashed line is $c^{1/2}$ dependence ($\beta = -0.5$).

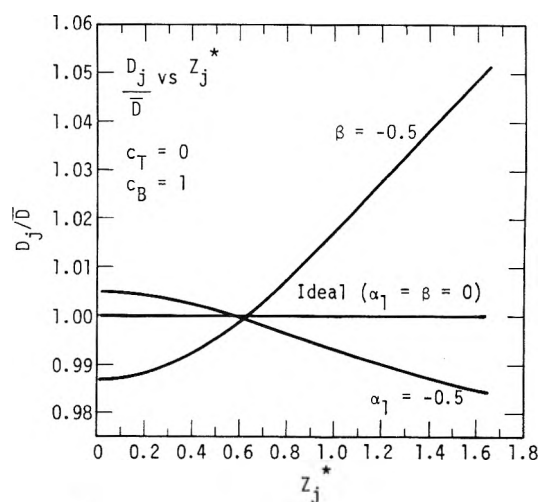


Figure 2. D_j/\bar{D} vs. z_j^* for the same system and conditions as in Figure 1. The skewing of the $c^{1/2}$ case is substantially greater than for the linear case, and deviates from ideal in the opposite direction from the linear case.

value of $f(j)$ for which the D_j of the symmetric Creeth pair is the same as \bar{D} . This value of $f(j)$ we call a *crossover point*, and it is a slowly varying function of $\beta(2\bar{c})^{1/2}$.

Numerical integrations for the $c^{1/2}$ dependence for Rayleigh quantities yield similar but more accurate results. There exist crossover points of $f(j)$ for which $D_j = \bar{D}$, which also form a slowly varying function of $\beta(2\bar{c})^{1/2}$ but which do not coincide with the ones from the poorly convergent analytical results. Since D_j is larger than \bar{D} on one side of the crossover point and less than \bar{D} on the other, there are also possible averages of selected values of j which could give

$$\bar{D} = \frac{1}{N} \sum_{j_a}^{j_b} D_j \quad 1 \leq j_a \leq j_b \leq J - 1 \quad (9)$$

where N is the number of D_j averaged.

Appropriate averages have been found which are valid to 1 part per 1000 for values of $0 \geq \beta(2\bar{c})^{1/2} \geq -0.9$.

Since this same kind of averaging is usually used to improve precision in the Creeth analysis for polynomial c dependence (where all D_j are the same to first order), the same method can be used with confidence generally without needing to know the actual c dependence.

2. Analytical Investigation

Because we wish to use the existing results of the Gosting-Fujita⁵ (GF) and Creeth⁶ theories, we summarize their equations. We also briefly review the application of their results to systems with the polynomial dependence of D on c . We will then turn to the case of $c^{1/2}$ dependence, noting differences and similarities.

A. *General Equations.* Fick's second law is

$$\frac{\partial c}{\partial t} = \frac{\partial}{\partial x} \left(D(c) \frac{\partial c}{\partial x} \right) \quad (10)$$

and the boundary conditions for free diffusion are

$$c = c_T = 0 \text{ when } x < 0 \text{ and } t = 0$$

$$c = c_B \text{ when } x > 0 \text{ and } t = 0$$

$$c = c_T \text{ when } x \text{ approaches } -\infty \text{ and } t > 0$$

$$c = c_B \text{ when } x \text{ approaches } +\infty \text{ and } t > 0 \quad (11)$$

The GF analysis⁵ is based on expanding \bar{D} in a Taylor series about \bar{c} ; namely

$$D = \bar{D} + \frac{\partial D}{\partial c}(c - \bar{c}) + \frac{1}{2!} \frac{\partial^2 D}{\partial c^2}(c - \bar{c})^2 + \dots \quad (12)$$

which can also be written

$$D = \bar{D} [1 + k_1(c - \bar{c}) + k_2(c - \bar{c})^2 + k_3(c - \bar{c})^3 + \dots] \quad (13)$$

with

$$k_n = \frac{1}{n! \bar{D}} \left(\frac{\partial^n D}{\partial c^n} \right)_{c=\bar{c}} \quad (14)$$

Gosting and Fujita transform eq 10 and 12 or 13, using new variables ϕ and z :

$$\phi = (c - \bar{c}) / (\Delta c / 2) \quad (2)$$

$$z = x / 2(\bar{D}t)^{1/2} \quad (15)$$

where ϕ is a reduced concentration variable (running from -1 to +1) and z is a reduced position variable. The resulting nonlinear differential equation can be solved in series form if Δc is small enough. The result is

$$\phi(z) = \Psi_0 + k_1 \Psi_1 \frac{\Delta c}{2} + (k_1^2 \Psi_2 + k_2 \Psi_3) \left(\frac{\Delta c}{2} \right)^2 + (k_1^3 \Psi_4 + k_1 k_2 \Psi_5 + k_3 \Psi_6) \left(\frac{\Delta c}{2} \right)^3 + \dots \quad (16)$$

where Ψ_0 is the error function with argument z as defined in eq 15, and the Ψ_i 's are complicated functions of Ψ_0 and its derivative.⁵ The functions Ψ_1 - Ψ_6 have both positive and negative values as well as zeroes other than at $z = 0$. Equation 16 has the same form for any $D(c)$ function, but different $D(c)$ functions yield different k_i expressions.

These equations can be substituted into expressions for the concentration dependence of the refractive index n , also Taylor-expanded about \bar{c} .⁵ We shall assume only a linear contribution to n so as to avoid complexities unrelated to the concentration dependence of D . In this case we have⁵

$$n(c) = n(\bar{c}) + R \frac{\Delta c}{2} \phi \quad (17)$$

where ϕ is given by eq 16 and R is the coefficient of the linear refractive index term. Since fringe displacements (Gouy) or fringes counted (Rayleigh) are proportional to $n - \bar{n}$, eq 17 is the starting point for optical investigations.

Creeth has extended the use of eq 16 and 17 to the Rayleigh system.⁶ His major result, omitting all but the linear term of n , can be written

$$z = z^* - k_1 R(z^*) \frac{\Delta c}{2} + \left(\frac{k_1^2}{2} S(z^*) - k_2 T(z^*) \right) \left(\frac{\Delta c}{2} \right)^2 + \dots \quad (18)$$

where z^* is the experimental quantity defined in eq 8, and R , S , and T are complicated functions of the Ψ_j functions and their derivatives.⁶ Creeth pointed out that since $R(z^*)$ was an *even* function of z^* , the symmetric pairing of fringes would cancel out the first-order dependence in Δc . Moreover, S and T are odd functions of z^* , so that with eq 8 we can write eq 18 as

$$z_j - z_{J-j} = z_j^* - z_{J-j}^* + [k_1^2 S(z_j^*) - 2k_2 T(z_j^*)] \left(\frac{\Delta c}{2} \right)^2 + \dots \quad (19)$$

If the second-order Δc term is small enough, the symmetric pairing gives $\Delta z = \Delta z^*$ and thus the direct calculation of \bar{D} from eq 15. Moreover, since z is a function of the single value \bar{D} , Δz_j^* from all such symmetric pairs should have exactly the same value for all values of j . Consequently, to smooth out random errors it is customary to average the Δz_j^* for all values of j . Exceptions are (1) those near the center of the pattern (near $J/2$) where the fringe pairs are so close together that comparator reading errors are significant and (2) those at the ends (near $j = 1$ or J) where curvature and tilt of the fringes makes their centers difficult to locate.

Finally, GF have derived an expression for the D_A used to determine \bar{D} in the Gouy method.⁵ Their result with numerical constants evaluated and in terms of $(\Delta c/2)$ is

$$\bar{D} = D_A \left[1 - (0.2819k_1^2 + 0.2064k_2) \left(\frac{\Delta c}{2} \right)^2 + \dots \right] \quad (20)$$

Thus, the first-order term in Δc also cancels out in the Gouy experiment.

B. *Polynomial c Dependence.* In this classical case,^{5,6} $D(c)$ is given by eq 1. To third order, the k_i expressions are

$$k_1 = \frac{D_0}{\bar{D}} (\alpha_1 + 2\alpha_2 \bar{c} + 3\alpha_3 \bar{c}^2)$$

$$k_2 = \frac{D_0}{\bar{D}} (\alpha_2 + 3\alpha_3 \bar{c})$$

$$k_3 = \frac{D_0}{\bar{D}} \alpha_3 \quad (21)$$

All of these quantities are finite and remain finite as \bar{c} approaches 0. Consequently, eq 16, 18, 19, and 20 converge as Δc approaches 0, and higher orders of Δc die away more rapidly than Δc . This supports the usual procedures for determining \bar{D} .

Let us now turn to situations where a linear dependence is strong enough to induce noticeable skewing. Stokes¹³

noted from numerical integrations of the purely linear case (all $\alpha_i = 0$ except α_1) that the plots of $d\phi/dz$ vs. z for arbitrary values of k_1 (or α_1) all seemed to intersect the ideal diffusion curve ($k_1 = \alpha_1 = 0$) at $z = \pm 0.66$. He called this intersection a "common point". Equation 16 shows that this can be true only if Ψ_1, Ψ_2, Ψ_4 , and all the higher order Ψ_i involving k_1 in higher order Δc terms vanish simultaneously at $z = \pm 0.66$. Krücke^{14,15} pointed out that this was in fact very nearly true to third order in Δc . Table I shows the "crossover" values of z where the functions $\Psi_1 \dots \Psi_6$ all vanish, and also shows the parity of these functions as odd or even functions of z . Since these functions (particularly Ψ_1, Ψ_2 , and Ψ_4) do not all vanish at exactly the same point, Krücke¹⁵ noted that strictly speaking there is no "common point". There is, however, a value of z for each value of $k_1\Delta c$ for which all terms to order Δc^3 except Ψ_0 cancel each other. These crossover values for z are a slowly varying function of $k_1\Delta c$, and are given by Krücke (Table I, ref 15, for $-3 \leq k_1 \Delta c \leq 3$). Quadratic or higher order c dependence would be more complex.

Similarly, Creeth⁶ noted in the pure linear Rayleigh case that $R(z^*)$ also vanished at $z = \pm 0.66$. Later he noted¹⁰ that $S(z^*)$ and $T(z^*)$ both seemed to vanish at $z^* = 0.6$ (actually ~ 0.57). If so, even with quadratic c dependence to second order in Δc , the square bracket terms of eq 19 would vanish at the crossover point. Thus, if we plot D_j from eq 7 vs. z_j^* and pick off the value at the crossover point $z_j^* = 0.57$, this value would be \bar{D} because $\Delta z_j = \Delta z_j^*$ there.

We have given more precise crossovers as well as the odd-even parity for R, S , and T in Table I, and note that S and T do not have exactly the same crossover point. Equation 19 also shows that (1) in the purely linear case to second order in Δc , the crossover point is independent of $k_1\Delta c$; and (2) with quadratic dependence of D on c and to second order in Δc , the crossover z^* will have a slight dependence on the relative values of k_1^2 and k_2 because of the different crossover points of S and T .

C. Square Root Dependence. We now turn to the main object of our analytical considerations, the $c^{1/2}$ dependence as given by eq 5. After evaluating the derivatives $(\partial^n D / \partial c^n)_{c=\bar{c}}$ and substituting for D_0 in terms of \bar{D} from eq 5, we find that

$$k_i = \frac{K[1 \cdot 1 \cdot 3 \cdot 5 \cdots (2i - 3)](-1)^{i-1}}{2^i (\bar{c})^i i!} \quad (22)$$

where

$$K = \frac{\beta \bar{c}^{-1/2}}{1 + \beta \bar{c}^{1/2}} \quad (23)$$

Consequently, eq 13, 16, 18, 19, and 20 become

$$D = \bar{D} \left[1 + \frac{K}{2} \frac{(c - \bar{c})}{\bar{c}} - \frac{K}{8} \frac{(c - \bar{c})^2}{\bar{c}^2} + \frac{3K}{48} \frac{(c - \bar{c})^3}{\bar{c}^3} - \dots \right] \quad (24)$$

$$\phi = \Psi_0 + \frac{K}{2\bar{c}} \Psi_1 \frac{\Delta c}{2} + \left(\frac{K^2}{4\bar{c}^2} \Psi_2 - \frac{K}{8\bar{c}^2} \Psi_3 \right) \left(\frac{\Delta c}{2} \right)^2 + \left(\frac{K^3}{8\bar{c}^3} \Psi_4 - \frac{K^2}{16\bar{c}^3} \Psi_5 + \frac{3K}{48\bar{c}^3} \Psi_6 \right) \left(\frac{\Delta c}{2} \right)^3 + \dots \quad (25)$$

$$z = z^* - \frac{K}{2\bar{c}} R(z^*) \frac{\Delta c}{2} + \left(\frac{K^2}{8\bar{c}^2} S(z^*) + \frac{K}{8\bar{c}^2} T(z^*) \right) \left(\frac{\Delta c}{2} \right)^2 + \dots \quad (26)$$

TABLE I: Properties of Gosting-Fujita and Creeth Functions

Function ^a	Crossover points		Parity
	z	$f(j)$	
Ψ_1	0.6586	0.6483	Even
Ψ_2	0.6447	0.6381	Odd
Ψ_3	0.5659	0.5765	Odd
Ψ_4	~ 0.67	~ 0.66	Even
Ψ_5	0.65-0.68	0.64-0.67	Even
Ψ_6	~ 0.82	~ 0.76	Even
R	0.6586	0.6483	Even
S	0.5806	0.5884	Odd
T	0.5659	0.5765	Odd

^a Values for $\Psi_1, \Psi_2, \Psi_3, R, S, T$, and z are interpolated from our computed values of these functions at 0.01 intervals of $f(j)$. Krücke's less accurate values¹⁴ are 0.6585, 0.644, 0.562, 0.6585, —, 0.562 from coarser values of z . The values for Ψ_4, Ψ_5 , and Ψ_6 are from Krücke.¹⁴

$$\Delta z_j = \Delta z_j^* + \left(\frac{K^2}{4\bar{c}^2} S(z_j^*) + \frac{K}{4\bar{c}^2} T(z_j^*) \right) \left(\frac{\Delta c}{2} \right)^2 + \dots \quad (27)$$

$$\bar{D} = D_A \left[1 - \left(\frac{0.28192K^2}{4\bar{c}^2} - \frac{0.20064K}{8\bar{c}^2} \right) \left(\frac{\Delta c}{2} \right)^2 + \dots \right] \quad (28)$$

We note that eq 5 leads to an infinite series for \bar{D} (eq 24), which converges slowly for $c - \bar{c}$ positive and still more slowly for $c - \bar{c}$ negative. Convergence was tested by comparing the series with the closed form derivable from eq 5 or 24:

$$D = \bar{D} \{ 1 + K[(1 + r)^{1/2} - 1] \} \quad (29)$$

where

$$r = (c - \bar{c})/\bar{c} \quad (30)$$

Slow convergence is not surprising, since a power series in c^n does not apply well to $c^{1/2}$.

If \bar{c} is large with respect to Δc , convergence of eq 24-28 will be adequate. Such will be the case for small Δc away from infinite dilution.

In the dilute electrolyte case, however, Δc and \bar{c} are of the same order of magnitude. In this circumstance the top solution is pure solvent so that

$$\bar{c} = c_B/2 \quad (31)$$

$$\Delta c = c_B \quad (32)$$

$$\bar{c} = \Delta c/2 \quad (33)$$

Clearly as Δc approaches 0, so does \bar{c} . In fact, \bar{c} and $\Delta c/2$ just cancel each other. Consequently, the convergence is now in terms of K , which by eq 23 and 33 goes to 0 as $(\Delta c)^{1/2}$, i.e., more slowly than Δc . Equation 24 is unchanged, but eq 25-28 in terms of K now become for the $c_T = 0$ situation:

TABLE II: Upper Concentration Limits for $\bar{D}/D_A = 1$ within ± 0.001 and ± 0.002 for Electrolyte Systems in Water (Eq 38)

Electrolyte type	Approximate β	Upper \bar{c} limit	
		± 0.001	± 0.002
1-1	-0.45	0.0060	0.0206
2-1	-1.0	0.0012	0.0042
3-1	-1.8	0.0004	0.0013
2-2	-1.8	0.0004	0.0013

$$\phi = \Psi_0 + \frac{K}{2} \left[\Psi_1 - \frac{1}{4} \Psi_3 + \frac{3}{24} \Psi_5 + \dots \right] + \left(\frac{K}{2} \right)^2 \left[\Psi_2 - \frac{\Psi_5}{8} + \dots \right] + \left(\frac{K}{2} \right)^3 \left[\Psi_4 + \dots \right] + \dots \quad (34)$$

$$z = z^* - \frac{K}{2} \left[R(z^*) - \frac{T(z^*)}{4} + \dots \right] + \left(\frac{K}{2} \right)^2 \left[S(z^*) + \dots \right] + \dots \quad (35)$$

$$\Delta z_j = \Delta z_{j^*} + \frac{K}{2} \left[\frac{T(z_{j^*})}{2} + \dots \right] + \left(\frac{K}{2} \right)^2 \left[S(z_{j^*}) + \dots \right] + \dots \quad (36)$$

$$\bar{D} = D_A \left[1 - \frac{K}{2} (0.05016 + \dots) + \left(\frac{K}{2} \right)^2 (0.28192 + \dots) + \dots \right] \quad (37)$$

Because $(\Delta c)^n$ cancels out, clearly each higher order Ψ_i function whose coefficient contains the first power of any k_n for arbitrary n will contribute to the $K/2$ terms of eq 34-37. Similarly coefficients containing k_n^2 will contribute to the $(K/2)^2$ term, etc.¹⁶ Since the higher order GF and Creeth functions are not known, *not even the $K/2$ term of any eq 34-37 is known with any confidence in the dilute solution case.*

As Δc approaches 0, so does K by eq 23 and 33. However, as noted before, it converges as $(\Delta c)^{1/2}$. This slower convergence is thus responsible for the persistence of terms which skew the fringe patterns. Because the higher order contributions to each term and their crossovers are not known, the crossover points of $\Psi_1, \dots, \Psi_6, R, S,$ and T are of no value here, in contrast to the case of polynomial dependence. Consequently, Creeth's suggestion to use the crossover in $T(z^*)$ with eq 36 for dilute electrolytes¹⁰ is unsatisfactory because it ignores those unknown higher order contributors to the $K/2$ term.

For the above reasons, analytical solutions should not yield results equivalent to a numerical integration. We have, however, explored eq 36 and 37 to the terms indicated, with the following suggestive results.

For Gouy systems which employ eq 37, the only way for D_A and \bar{D} to be the same (or equal to some tolerance) is for the expression

$$f = 0.02508K - 0.07048K^2 \quad (c_T = 0) \quad (38)$$

to be 0. A plot of f vs. K shows a shallow maximum at $K = +0.178$ with $f = 0.002$. For $f = 0 \pm 0.002$, we have $-0.069 \leq K \leq +0.425$ and for $f = 0 \pm 0.001$, we find $-0.036 \leq K \leq$

$+0.045$, $0.310 \leq K \leq 0.392$. Table II contains the upper limits to \bar{c} for various valence types, which can be found from K and from β crudely estimated from the aqueous-solution data in Harned and Owen.⁸ Since β for electrolytes are all negative, the limits of \bar{c} are very low. This results in Gouy fringes which are too few and too hard to read. Consequently, within the limitations of analytical approximations, it would appear unwise to use Gouy techniques for electrolyte solutions diffusing into pure solvent.

For Rayleigh systems, there are the possibilities of averaging and the use of crossover points. The quantities of interest are D_j/\bar{D} , an expression for which comes from eq 6, 7, 8, 15, and 36:

$$\frac{D_j}{\bar{D}} = \left(\frac{\Delta z_j}{\Delta z_{j^*}} \right)^2 = \left[1 + \frac{KT(z_{j^*})}{8z_{j^*}} + \frac{K^2S(z_{j^*})}{8z_{j^*}^2} \right]^2 \quad (c_T = 0) \quad (39)$$

Clearly, eq 39 as well as eq 34-38 depend only upon the parameter K which in turn is a function only of the parameter $\beta\bar{c}^{1/2}$.

Our results are reported for the proportional parameter A

$$A = \beta(2\bar{c})^{1/2} \quad (40)$$

which for the case of dilute solutions becomes

$$A = \beta(\Delta c)^{1/2} \quad (c_T = 0) \quad (41)$$

Table III contains crossover values of $f(j)$ and z^* for different negative values of A , since β and thus A are negative for dilute electrolyte systems. Figure 3 shows D_j/\bar{D} for $A = -0.5$ from the $T(z^*)$ term only and from both $T(z^*)$ and $S(z^*)$ terms. They are different from one another although having nearly the same crossover. The numerical integration curve is also shown. It has a different crossover point and form, although it coincides with curve 1 at very low z^* .

The different crossover points and shapes of the numerical integration curves hold true for all finite values of A . Consequently, the analytical results for the $c^{1/2}$ case have no practical value for calculations, although they are suggestive and indicate the proper parameter for numerical integration.

3. Numerical Integration Investigation

The lack of either a closed form or a valid series approximation for the $c^{1/2}$ dependence suggests a parameter study of the direct numerical integration of eq 10 with D from eq 5. In this paper, we consider only the Rayleigh analysis.

The numerical integration procedure used is based on that of Gear.¹⁷ Its results are c values at equally spaced x in a fixed length of 3, with the number of x points specified by a predetermined mesh size. The last-time t is scaled to be $0.08/D_0$. These parameters correspond to free diffusion for 8000 sec in 3 cm of a cell where the initial sharp boundary is at 1.5 cm and the solution has $D_0 = 10^{-5}$ cm²/sec. This corresponds to a plausible experiment in which diffusion has not yet affected the ends of the cell, but has gone on long enough to numerically smooth out the original discontinuity at $x = 1.5$.

For the Creeth-Rayleigh analysis, x values for symmetrically spaced values of c are required. We choose 100 equally spaced values for convenience; these are obtained by linear interpolation of the numerical integration output. Since a linear c dependence of n is assumed, each of the equally spaced c corresponds to an observed Rayleigh fringe in a

TABLE III: Crossover Points where $D_j = \bar{D}$ for Values of Parameter A of the Square Root Dependence Case ($c_T = 0$)

A	Analytical (eq 39)		Numerical integration	
	$f(j)$	z^*	$f(j)$	z^*
0	0.5765	0.5659	0.627	0.630
-0.01	0.5765	0.5659	0.627	0.630
-0.05	0.5764	0.5658	0.627	0.630
-0.1	0.5761	0.5655	0.6270	0.6300
-0.2	0.5756	0.5649	0.6272	0.6302
-0.3	0.5750	0.5641	0.6275	0.6306
-0.4	0.5741	0.5630	0.6281	0.6314
-0.5	0.5729	0.5616	0.6288	0.6323
-0.6	0.5711	0.5594	0.6300	0.6339
-0.7	0.5680	0.5556	0.6327	0.6375
-0.8	0.5618	0.5482	0.6382	0.6449
-0.9	0.5421	0.5249	0.6521	0.6638

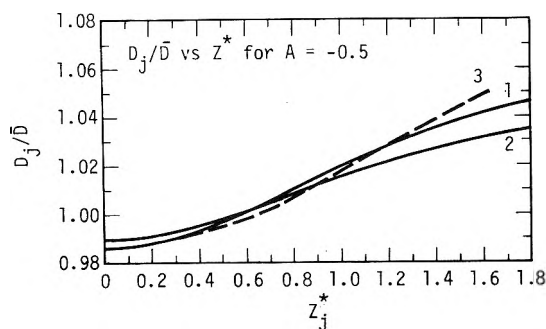


Figure 3. D_j/\bar{D} vs. z_j^* for the same system as in Figures 1 and 2, with all curves for the $c^{1/2}$ dependence with $A = -0.5$. Since $c_T = 0$ and $c_B = 1$, $A = \beta$ by eq 41. Curve 1 is the analytical result using just the $\mathcal{T}(z_j^*)$ of eq 39; curve 2 is the analytical result using both the $\mathcal{T}(z_j^*)$ and $S(z_j^*)$ terms of eq 39; curve 3 is the numerical integration for the same case.

100-fringe system. Thus, the j th value of c corresponds exactly to fringe j , with c_0 and c_{100} (c_T and c_B , respectively) corresponding to the horizontal fringes $j = 0$ and $j = 100$, respectively, and with

$$c_j = (c_{100} - c_0) \frac{j}{100} + c_0 \quad 0 \leq j \leq 100 \quad (42)$$

Consequently the index j corresponds to fringe j from a cell whose thickness has been adjusted to give exactly 100 fringes between c_T and c_B .

Given index j , the interpolated x_j associated with c_j , and the last-time t from the integration, we can calculate $f(j)$ from eq 6, z_j^* from eq 8, and D_j for the symmetric Creeth pairs from eq 7. Here $J = 100$. We obtain \bar{D} by substituting \bar{c} into eq 5, and it is divided into D_j , yielding values of D_j/\bar{D} , $1 \leq j \leq 49$.

The numerical integration was performed on a CDC 7600 for values of A (eq 40) ranging from 0.0 to -0.9 with a mesh size of 800 intervals (801 points) and an error tolerance of 10^{-5} . Trials with 100, 200, and 400 intervals had too much scatter to determine crossovers accurately. Trials with an error tolerance of 10^{-6} and 10^{-7} did not change the results significantly.

Representative plots of D_j/\bar{D} vs. z_j^* are given in Figure 4. The D_j/\bar{D} are clearly skewed from ideal diffusion ($A =$

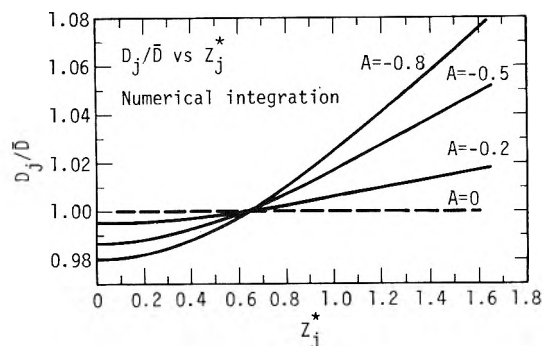


Figure 4. D_j/\bar{D} vs. z_j^* from numerical integration for the same system as previous figures but with varying values of the parameter A . All curves are for the $c^{1/2}$ dependence. Since $c_T = 0$ and $c_B = 1$, $A = \beta$ by eq 41.

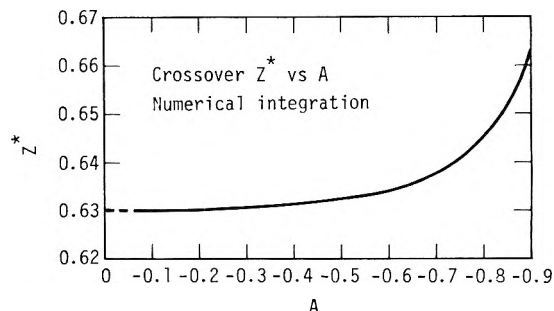


Figure 5. Crossover value of z^* vs. A for the $c^{1/2}$ dependence. At values of A between 0 and -0.6 , there is very nearly a "common point" at $z^* = 0.632 \pm 0.002$. Since $c_T = 0$ and $c_B = 1$, $A = \beta$ by eq 41.

0), and the function is not linear. Although skewness ultimately disappears if Δc is small enough, the 50- to 100-fringe experimental system $\text{ZnSO}_4\text{-H}_2\text{O}$ ($\beta \approx -2$) will have an $A = -0.4$ for $\Delta c = 0.04$. Even a 10- to 20-fringe ZnSO_4 system with $\Delta c \approx 0.01$ yields $A = -0.2$. Consequently, even in the most dilute systems accessible to reasonable measurement, Figure 4 and experiment show D_j/\bar{D} to be noticeably skewed.

The plots also show the expected crossovers. They all occur at $z^* \approx 0.63\text{--}0.66$, so that there is almost a "common point" for the $c^{1/2}$ dependence. The crossovers as a function of A are given in Table III in terms of z^* and $f(j)$ and are plotted in Figure 5. Owing to numerical noise in the integrations, these crossovers were determined by second- to fifth-order fits of D_j/\bar{D} as a polynomial in $f(j)$, the order chosen being the one with the lowest variance. Generally $\sigma \leq 0.0001$ for $-A \leq 0.2$. Crossovers were harder to determine at low values of A because of numerical noise. Consequently, 1601 point runs (error tolerance 10^{-6}) for $A = 0.0$ and -0.02 were done to verify that the numerical noise was indeed low enough and that the limiting crossover was in fact $z^* = 0.630$.

Because of the crossover, \bar{D} can be obtained by averaging the D_j over an appropriate interval of j , $f(j)$, or z^* , as described by eq 9. As mentioned in the Introduction and in section 2A, the D_j 's are averaged anyway to improve precision even where no skewness is expected. The interval usually chosen in this laboratory for binaries has been $z_j^* \leq 1.0$ and $\Delta x \geq 2$ mm. For ternaries, however, we use $0.25 \leq z_j^* \leq 1.0$ which in a 100-fringe system corresponds to averaging all j , $8 \leq j \leq 36$. With these limits, the average $\Sigma D_j/N\bar{D}$ for even the most skewed systems is within 0.2–0.3% of

TABLE IV: Averages $\Sigma_j D_j / (N\bar{D})$ from Numerical Integration for Various Intervals and Values of A for Square Root Dependence (100-Fringe System) ($c_T = 0$)

j limits	All (1-49)	8-36	8-36 EO ^a	7-35	7-35 EO ^a	8-32	8-32 EO ^a
$f(j)$ limits	0.98-0.02	0.84-0.28	0.84-0.28	0.86-0.30	0.86-0.30	0.84-0.36	0.84-0.36
z^* limits	1.64-0.02	0.99-0.25	0.99-0.25	1.04-0.27	1.04-0.27	0.99-0.33	0.99-0.33
No. of pairs	49	29	15	29	15	25	13
$A = -0$	1.0000	1.0000	1.0000	1.0000	1.0000	1.0000	1.0000
$= -0.05$	1.0000	0.9999	0.9999	1.0000	1.0001	1.0000	1.0000
$= -0.1$	1.0001	0.9998	0.9998	1.0000	1.0000	1.0001	1.0001
$= -0.3$	1.0003	0.9993	0.9994	0.9999	1.0000	1.0002	1.0003
$= -0.5$	1.0005	0.9988	0.9990	0.9998	1.0000	1.0003	1.0004
$= -0.7$	1.0006	0.9981	0.9983	0.9996	0.9998	1.0002	1.0004
$= -0.9$	1.0000	0.9973	0.9975	0.9986	0.9988	0.9991	0.9992

^a EO denotes averaging every other fringe.

1.0000, and for our ZnSO₄ example is within 0.1%. Consequently, other averages have been investigated, based on 100 fringes. The best ones are shown in Table IV. Also shown are the results of taking every other fringe in these intervals. This case, denoted by EO, also corresponds to taking every fringe in a 50-fringe system.

Averages 1-49, 7-35, 7-35 EO, 8-32, 8-32 EO are everywhere equal to 1.0000 within 0.1% for all $0 \geq A \geq -0.9$. Averages 6-36, 6-36 EO, 9-31, and 9-31 EO, which are not shown, are similar. Consequently, averaging is an appropriate way to determine \bar{D} . Our customary averages, 8-36 and 8-36 EO, are both equally as good as the above up to $A \geq -0.5$, but are poorer beyond that.

4. Discussion

In what follows, we emphasize that we are considering Rayleigh methods for the dilute electrolyte solution cases where $c_T = 0$.

In view of the slow convergence and lack of knowledge of higher Ψ_j functions, it is not surprising that the analytical results are in poor agreement with the numerical integration ones. The analytical results are an excellent guide for the polynomial dependence, but are at best suggestive for the square root dependence.

The numerical investigation of skewing indicated that \bar{D} can be obtained even in the square root case in two ways: (1) by the use of crossover points, and (2) by the use of proper averaging methods. Specific application to experiments follows.

The crossover point method is this. The usual analysis of fringe patterns is used to obtain a preliminary value of D and the Δt correction. For each value of j , the D_j are calculated from each fringe pattern exposure using eq 7 with the "true" time $t = t_{\text{meas}} + \Delta t$. These D_j are averaged to give a mean value \bar{D}_j for each j , and the \bar{D}_j 's are plotted against z_j^* for all values of j . If the value of A is known, \bar{D} will be the value of \bar{D}_j read off the smoothed curve at the crossover value of z^* for this A . Actually, knowledge of A is not really necessary, since the crossover z^* 's are 0.632 ± 0.002 to $A = -0.6$. Moreover even for $A = -0.8$, the error in choosing 0.632 does not exceed 0.1%.¹⁸ The problem with this method is that the inevitable errors of reading plates give rise to some scatter, and a "best" smoothed curve is subject to error. Least squaring is not fully satisfactory because, as we showed earlier, the proper analytical function is not known.

The averaging method is more convenient, because it gives \bar{D} directly and is the technique usually used to obtain the terms to calculate Δt and \bar{D} when there is either no

concentration dependence or a polynomial dependence. In dilute solutions the dominant contribution will be from the square root dependence. Consequently the best average to use should cancel out that square root skewness. Although the 7-35 or 8-32 averages appear equally good, preliminary examination of combined square root and linear dependence cases indicates that 7-35 may be preferable.

Problems in the averaging technique may arise because experiments seldom yield exactly 100 fringes. Thus, intermediate systems (e.g., $J = 69.3$) do not always have exactly the right number of terms to properly cancel skewness. However, for values $A > -0.5$, many other j intervals were found to average to \bar{D} within 0.1%. Consequently, setting $f(j)$ or z^* limits corresponding to 7-35 (see Table IV) will generally give satisfactory results.

In experimental work, 100 fringes will generally result from a 5-cm cell for $\Delta c \approx 0.08$. Since the approximate values of β shown in Table II can be ~ -2 , eq 41 indicates that A can reach -0.6 for a 2-2 or 3-1 electrolyte. To avoid any chance of the average deviating more than 0.1% from \bar{D} , it is recommended that Δc be arranged so that A never reaches -0.6 to -0.9 , even if fewer fringes result.

It is indeed reassuring that despite the marked skewing of $c^{1/2}$ -dependent D_j in dilute electrolyte solutions, the usual averaging technique eliminates most of this skewness. Because it is less subject to random errors, we believe that the averaging method is better than the crossover-point method. We recommend averaging D_j between $0.27 \leq z^* \leq 1.04$ ($0.86 \leq f(j) \leq 0.30$) which corresponds to the 7-35 case.

Acknowledgments. This work was performed under the auspices of the U.S. Energy Research & Development Administration. We are greatly indebted to Neil Madsen for his help in setting up the numerical integration codes.

References and Notes

- (1) "This report was prepared as an account of work sponsored by the United States Government. Neither the United States nor the United States Energy Research & Development Administration, nor any of their employees, nor any of their contractors, subcontractors, or their employees, makes any warranty, express or implied, or assumes any legal liability or responsibility for the accuracy, completeness or usefulness of any information, apparatus, product or process disclosed, or represents that its use would not infringe privately-owned rights."
- (2) L. J. Gosting in "Advances in Protein Chemistry", Vol. XI, Academic Press, New York, N.Y., 1956.
- (3) H. Svensson and T. E. Thompson, "A Laboratory Manual of Analytical Methods of Protein Chemistry", P. Alexander and R. Black, Ed., Pergamon Press, New York, N.Y., 1961, pp 57-118.
- (4) P. J. Dunlop, B. J. Steel, and J. E. Lane in "Physical Methods of Chemis-

- try", Vol. 1, Part IV, A. Weissberger and B. Rossiter, Ed., Wiley, New York, N.Y., 1972, Chapter IV, pp 207-349.
- (5) L. J. Gosting and H. Fujita, *J. Am. Chem. Soc.*, **79**, 1359 (1957).
 - (6) J. M. Creeth, *J. Am. Chem. Soc.*, **77**, 6428 (1955).
 - (7) The Rayleigh analysis is equally applicable to all integral fringe patterns, including those from Jamin, Mach-Zender, and holographic interferometers.
 - (8) H. S. Harned and B. B. Owen, "The Physical Chemistry of Electrolytic Solutions", 3rd ed, Reinhold, New York, N.Y., 1958.
 - (9) L. Onsager and R. Fuoss, *J. Phys. Chem.*, **36**, 3689 (1932).
 - (10) J. M. Creeth and B. E. Peter, *J. Phys. Chem.*, **64**, 1502 (1960).
 - (11) O. W. Edwards and E. O. Huffman, *J. Phys. Chem.*, **63**, 1830 (1959).
 - (12) J. D. Hatfield, O. W. Edwards, and J. L. Dunn, *J. Phys. Chem.*, **70**, 2555 (1966).
 - (13) R. H. Stokes, *Trans. Faraday Soc.*, **48**, 887 (1952).
 - (14) E. Krücke and H. Ley, *Z. Phys. Chem. (Frankfurt am Main)*, **26**, 187 (1960).
 - (15) E. Krücke, *Z. Phys. Chem. (Frankfurt am Main)*, **26**, 202 (1960).
 - (16) For example, the analogy with the *K* terms of eq 34 and 35, plus the definitions of *R* and *T* (ref 6), indicate that the next term in eq 35 will be $3\Psi_6/24 (d\Psi_0/dz)$, although Creeth did not carry his analysis this far. Since Ψ_6 and $d\Psi_0/dz$ are both even, this term will cancel out of eq 36.
 - (17) N. Madsen and R. Sincovec, *ACM Trans. Math. Software*, in press.
 - (18) Creeth¹⁰ suggested the point $z^* \approx 0.6$ based on his analytical considerations for the linear dependence. Our more exact analytical result is $z^* = 0.57$. Although the analytical basis is unsatisfactory, nonetheless the points $z^* = 0.6$ and $z^* = 0.57$ will yield a \bar{D} in error by less than 0.1% for all *A* more positive than -0.4 and -0.2 , respectively.

Enthalpy of Dilution of Aqueous Solutions of Some Bis Quaternary Ammonium Ganglionic and Neuromuscular Blocking Agents¹

S. Agharkar and S. Lindenbaum*

Pharmaceutical Chemistry Department, McCollum Laboratories, The University of Kansas, Lawrence, Kansas 66045

(Received May 7, 1975)

Heats of dilution are reported for aqueous solutions of bis quaternary ammonium chloride, bromide, acetate, and butyrate salts of the type $(\text{CH}_3)_3\text{N}^+(\text{CH}_2)_n\text{N}^+(\text{CH}_3)_3$. The heat of dilution, ΔH_D , for the chloride and bromide salts increases with increasing *n* until a maximum is reached at *n* = 5 and then drops with increasing *n*. The ganglionic blocking activity of these compounds also has a maximum value at *n* = 5. These results suggest that the biological activity of these compounds may be determined by their properties in aqueous solution.

Introduction

The polymethylene α,ω -bis(trimethylammonium) salts $(\text{CH}_3)_3\text{N}(\text{CH}_2)_n\text{N}(\text{CH}_3)_3\text{X}_2$ (*X* = univalent anion) are of great interest because of their ganglionic and neuromuscular blocking activity.²⁻⁵ A great deal of work has been published in which the effect of the distance between the quaternary nitrogen atoms on pharmacological activity is explored.⁴⁻⁶ The maximum ganglionic blocking activity for this series of compounds occurs for pentamethonium (*n* = 5) and hexamethonium (*n* = 6). The maximum neuromuscular blocking activity is obtained for decamethonium (*n* = 10).

On the basis of these results it has been suggested^{4,5} that the $\text{N}^+\text{-N}^+$ distances corresponding to the length of five or six methylene groups correspond closely to the distances between anionic acetylcholine receptor sites of the ganglionic receptor, and that the receptor sites of the muscle end plate receptor are separated by a distance corresponding to ten methylene groups.

This correlation is however not entirely consistent, and some potent blocking agents, not members of the "polymethonium" series do not have their positive charge sites separated by distances corresponding to those of pentamethonium or decamethonium.⁶ For this reason, the validity of this two point contact hypothesis has been questioned by several investigators.⁶⁻¹⁰ It has been suggested that the biological activity might be determined by the lipophilicity of these compounds,⁶ rather than by a specific fit to a two point contact receptor.

The results of a study of the thermodynamics of binding of a series of alkyltrimethylammonium salts to acetylcholinesterase have led Belleau⁹ to suggest that water is the determinant of the binding properties of these compounds. Belleau suggests that the binding of the quaternary ammonium ion to acetylcholinesterase (or the receptor) is facilitated by the formation of a hydrophobic bond between the quaternary ammonium ion and the receptor. The driving force for this interaction is taken to be the increase in entropy which accompanies the loss of a hydrophobic solute from the aqueous environment.^{11,12} On the basis of this suggestion, it might be expected that the relative affinities of these bis quaternary ammonium salts for the receptor will be determined largely by their properties in aqueous solution.

The present program of study was undertaken in order to determine the thermodynamic properties of these bis quaternary ammonium salts in aqueous solution, and to correlate these properties with their biological activity. The first of these properties reported here is the heat of dilution in aqueous solution at 25°.

Previous studies of tetraalkylammonium halides¹³⁻¹⁶ have suggested that the apparent molal heat content, ϕ_1 , is a measure of the hydrophobic nature, or water structure-making property of these solutes. If, as suggested, the biological activity, i.e., the binding of these compounds to a receptor, is determined by the hydrophobic bonding phenomenon, then a correlation between ϕ_1 and biological activity might be expected.

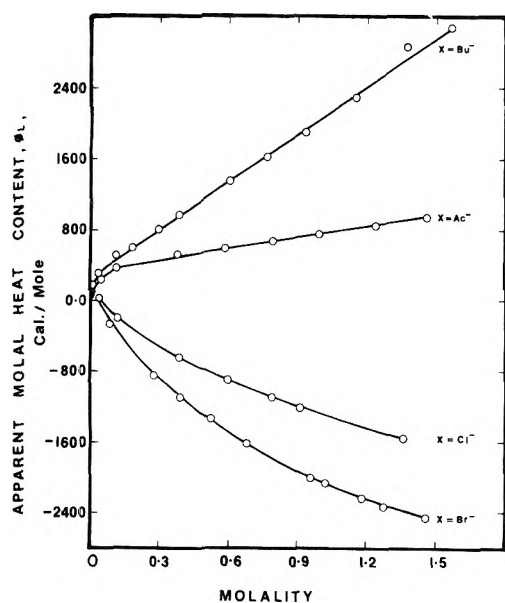


Figure 1. Apparent molal heat contents of aqueous solutions of tetramethonium salts at 25°.

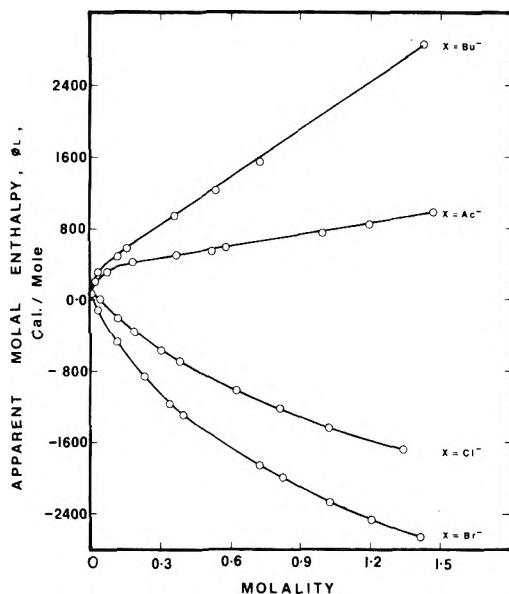


Figure 2. Apparent molal heat contents of aqueous solutions of pentamethonium salts at 25°.

Experimental Section

The synthesis of trimethonium dibromide ($n = 3$) was accomplished by refluxing 1,3-dibromopropane in a methanol solution with trimethylamine for 48 hr. The methanol was evaporated under vacuum, and the resulting solid was washed with diethyl ether. The product was recrystallized from a methanol-ether mixture and dried under vacuum at 40°.

Tetramethonium dibromide ($n = 4$), heptamethonium dibromide ($n = 7$), octamethonium dibromide ($n = 8$), and nonamethonium dibromide ($n = 9$) were synthesized in an analogous fashion. All compounds were obtained in 85% yield or better. Pentamethonium ($n = 5$), hexamethonium ($n = 6$), and decamethonium ($n = 10$) dibromides were obtained from K & K Laboratories, Inc., and used after recrystallization from a methanol-ether mixture.

The chloride, acetate (OAc), and butyrate (OBU) salts of

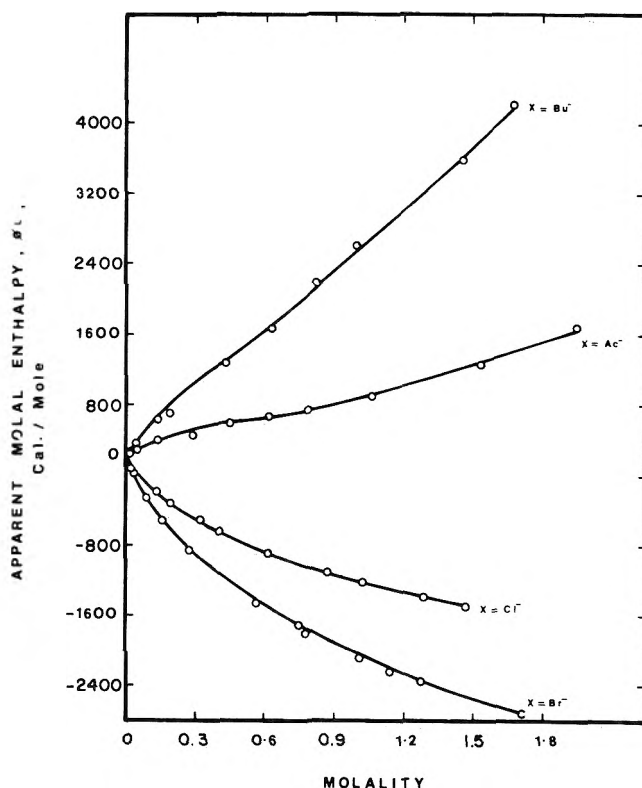


Figure 3. Apparent molal heat contents of aqueous solutions of hexamethonium salts at 25°.

these compounds were prepared as described previously.^{17,18}

The bromide and chloride salts were analyzed for their halide content by argentometric titration using a silver wire electrode and a calomel electrode with a potassium nitrate salt bridge. All compounds were found to be at least 99.9% pure with respect to halide content.

The acetate and butyrate salts were analyzed by cation exchange. Weighed quantities of acetate and butyrate salt solutions were passed through a strong acid cation exchange column (Dowex 50Wx8) in the hydrogen form. The resulting solutions were analyzed for acetic or butyric acid content by titration with standard sodium hydroxide. The results of the analyses were in good agreement ($\pm 0.5\%$) with the concentrations of the solutions calculated from the stoichiometry of the preparation from the halide salts.

The calorimeter employed for these studies was an LKB 10700-2 batch microcalorimeter. The operation of the calorimeter and the methods used have been described previously.¹⁹⁻²¹

Results and Discussion

A complete listing of the calorimetric data are available as supplementary materials in Tables I-IV of the microfilm edition of this journal.²² The corrections for the heat of dilution from the final concentrations to infinite dilution were carried out as previously described.¹⁸ Apparent molal heat contents, ϕ_L , are given in Figures 1-6 as a function of molality. At the highest concentrations most of the data has a precision of $\pm 10 \text{ cal mol}^{-1}$, and at the lower concentrations, $\pm 5 \text{ cal mol}^{-1}$. It was found that the ϕ_L data could be approximated by the equation

$$\phi_L = a + bm + cm^2 \quad (1)$$

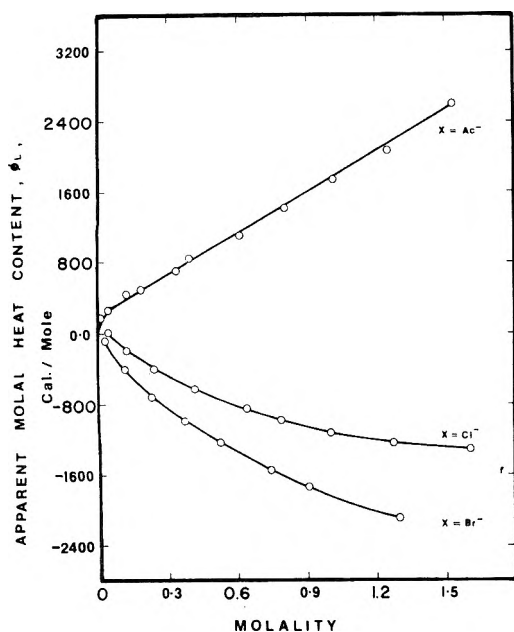


Figure 4. Apparent molal heat contents of aqueous solutions of octamethonium salts at 25°.

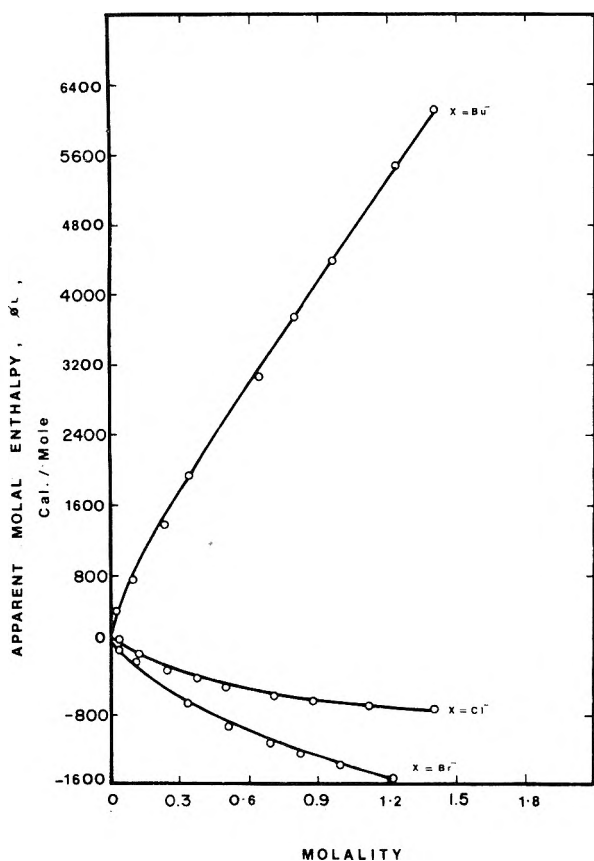


Figure 5. Apparent molal heat contents of aqueous solutions of nonamethonium salts at 25°.

where m is the molality (moles/kilogram of solvent) for m values ranging from 0.1 to 1.5. The values of the constants of eq 1 obtained by the method of least squares are summarized in Table V. The data for solutions more dilute than 0.1 M were not included in the fitting procedure since it is known that drastic changes in the slope of the ϕ_L vs. m

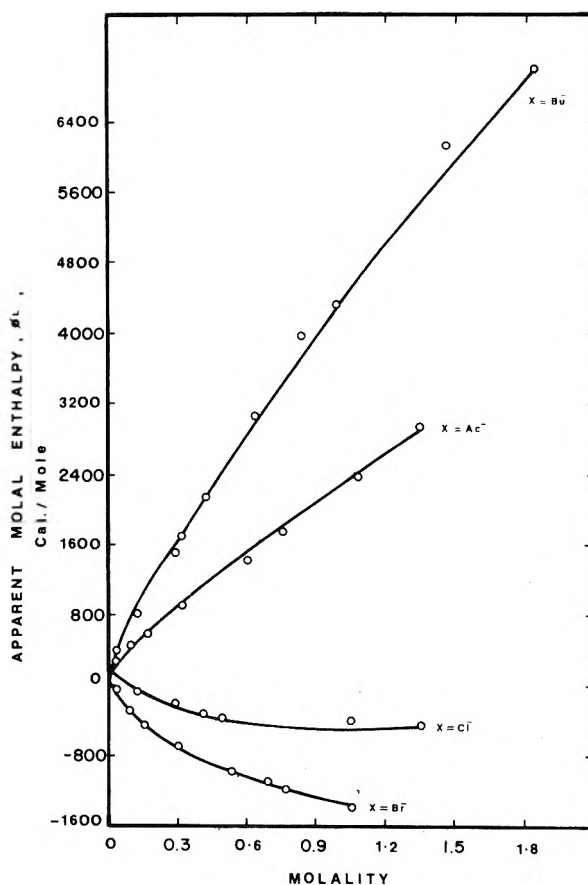


Figure 6. Apparent molal heat contents of aqueous solutions of decamethonium salts at 25°.

curve must occur in order to approach the Debye-Hückel limiting slope at infinite dilution.

For the acetate and butyrate salts the ϕ_L values are all positive, whereas for the chloride and bromide salts the values are negative. ϕ_L decreases in the order $\text{O}^-\text{Bu} > \text{O}^-\text{Ac} > \text{Cl}^- > \text{Br}^-$. This is the same order found previously for the sodium²³ and tetraalkylammonium salts.¹⁷

It has been suggested that the large exothermic heats of dilution of acetate and butyrate tetraalkylammonium salts are due in part to the structure-making effect of these anions on the aqueous solvent.^{17,23,24} Further support for this suggestion is also found in the fact that the butyrate and acetate salts of tetrabutyl- and tetraisoamylammonium ions also form stable clathrate hydrates.²⁵ Chloride and bromide ions, on the other hand, are water structure breakers,^{26,27} and would therefore be expected to contribute to a decrease in ϕ_L .

The effect of the length of the methylene chain separating the two nitrogen atoms on the heat of dilution is shown in Figure 7. A maximum is obtained in the graph of $\Delta H_D (= -\phi_L)$ vs. n at $n = 5$.

It may be speculated, that these maxima are due to the competition between two interactions with the solvent which contribute in opposite ways to the heat of dilution. The smaller members of this series are water structure breaking cations and this structure breaking effect increases as the size of the ion increases. As the size of the bis quaternary ammonium ion increases and the charged nitrogen atoms are sufficiently far apart, the solvent structuring effect of the hydrophobic methylene chain becomes important, and the heat of dilution decreases with increasing n .

TABLE V: Values of the Parameters of Eq 1

	<i>a</i>	<i>b</i>	<i>c</i>	σ^a	<i>a</i>	<i>b</i>	<i>c</i>	σ^a
	Bromides				Chlorides			
Trimethonium	-281	-2152	460	44				
Tetramethonium	-87	-2774	795	46	-7	-1785	480	25
Pentamethonium	-285	-2603	632	54	-10	-1980	566	25
Hexamethonium	-142	-2569	613	56	-8	-1706	484	23
Heptamethonium	-184	-2403	640	44	-1	-1735	489	43
Octamethonium	-133	-2541	810	38	-13	-1658	535	25
Nonamethonium	19	-2249	814	38	-3	-1149	461	28
Decamethonium	-137	-1959	744	35	3	-877	412	50
	Acetates				Butyrates			
Tetramethonium	342	418	-6	15	355	1498	170	69
Pentamethonium	405	179	151	20	296	1638	104	9
Hexamethonium	364	355	160	34	304	2213	53	39
Octamethonium	281	1268	153	33				
Nonamethonium					366	4411	-235	52
Decamethonium	261	1924	39	7	131	5074	-711	80

^a σ = standard error of fit.

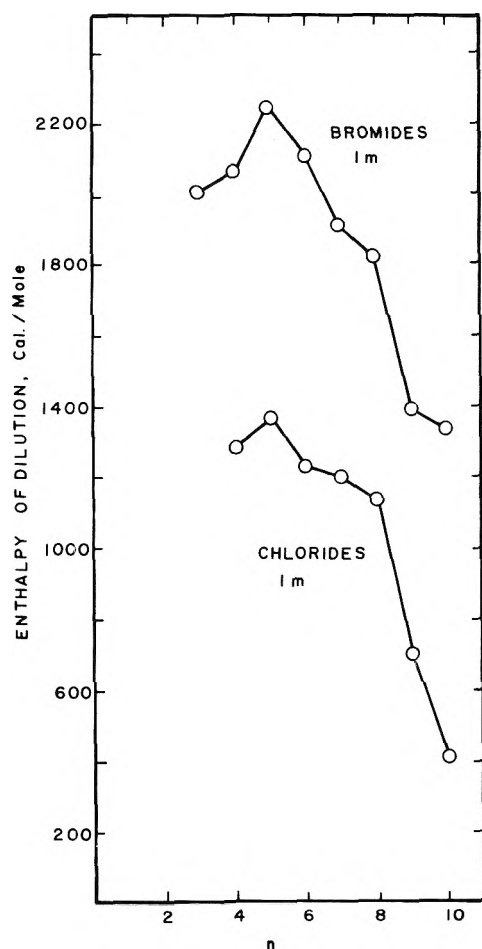


Figure 7. Heats of dilution ($-\phi_L$) of 1 *m* aqueous solutions of $(\text{CH}_3)_3\text{N}^+(\text{CH}_2)_n\text{N}(\text{CH}_3)_3$ chloride and bromide salts as a function of *n*, the number of methylene groups separating the nitrogen atoms.

For the acetate and butyrate salts, the heat of dilution decreases with increasing $-\text{CH}_2-$ chain length for all values of *n*. In these cases, the mutual cooperative water-structur-

ing effect of the cations and anions appears to be the predominant effect for all values of *n*, and maxima are therefore not obtained.

It is tempting to speculate that the factors responsible for the maximum at *n* = 5, in the ΔH_D vs. *n* graph are the same as those causing maximum ganglionic blocking activity for pentamethonium. If this were the case, this would imply that differences in the biological activity are largely caused by differences in aqueous solution properties, and to a much lesser extent by the specific structure of the receptor. Further studies on the thermodynamic properties of these compounds in aqueous solution and their binding to model receptor substances are in progress to elucidate the nature of the interaction between blocking agent and receptor site.

Acknowledgments. This work was supported by a Health Science Advancement Award (FRO 6147) granted to the University of Kansas by the National Institutes of Health, and by a grant from the University of Kansas General Research Fund.

Supplementary Material Available. Table I-IV containing calorimetric data for the heats of dilution of all of the α,ω -bis(trimethylammonium) chlorides, bromides, acetates, and butyrates at 25° will appear following these pages in the microfilm edition of this volume of the journal. Photocopies of the supplementary material from this paper only or microfiche (105 × 148 mm, 24× reduction, negatives) containing all of the supplementary materials for the papers in this issue may be obtained from the Business Office, Books and Journals Division, American Chemical Society, 1155 16th St., N.W., Washington, D.C. 20036. Remit check or money order for \$4.50 for photocopy or \$2.50 for microfiche, referring to code number JPC-75-2068.

References and Notes

- (1) Based on a thesis submitted by S. Agharkar in partial fulfillment of the requirements for the Ph.D. Degree, University of Kansas, 1975.
- (2) A. Goldstein, L. Aranow, and S. M. Kalman, "Principles of Drug Action", Harper and Row, New York, N.Y., 1969.

- (3) R. B. Barlow and H. R. Ing, *Nature (London)*, **161**, 718 (1948).
 (4) W. D. M. Paton and E. J. Zaimis, *Pharmacol. Rev.*, **4**, 219 (1952).
 (5) W. D. M. Paton and E. J. Zaimis, *Br. J. Pharmacol.*, **4**, 38 (1949).
 (6) R. A. Wiley, B. A. Faraj, A. Jantz, and M. M. Hava, *J. Med. Chem.*, **15**, 374 (1972).
 (7) M. P. Mertes, S. A. Nerurkar, and E. J. Walaszek, *J. Med. Chem.*, **11**, 106 (1968).
 (8) B. Belleau, H. Tani, and F. Lie, *J. Am. Chem. Soc.*, **87**, 2283 (1965).
 (9) B. Belleau, *Ann. N.Y. Acad. Sci.*, **144**, 705 (1967).
 (10) R. B. Barlow, *Br. J. Pharmacol.*, **51**, 413 (1974).
 (11) W. Kauzmann, *Adv. Protein Chem.*, **14**, 1 (1959).
 (12) C. Tanford, "The Hydrophobic Effect", Wiley, New York, N.Y., 1973.
 (13) S. Lindenbaum, *J. Phys. Chem.*, **70**, 814 (1966).
 (14) R. H. Wood, H. L. Anderson, J. D. Beck, J. R. France, W. E. deVry, and L. J. Soltzberg, *J. Phys. Chem.*, **71**, 2149 (1967).
 (15) W. Y. Wen, "Water and Aqueous Solutions, Structure, Thermodynamics and Transport Processes", R. A. Horne, Ed., Interscience, New York, N.Y., 1971.
 (16) W. Y. Wen, *J. Solution Chem.*, **2**, 253 (1973).
 (17) S. Lindenbaum, *J. Phys. Chem.*, **75**, 3733 (1971).
 (18) S. Lindenbaum, *J. Phys. Chem.*, **73**, 4334 (1969).
 (19) A. S. Levine and S. Lindenbaum, *J. Solution Chem.*, **2**, 445 (1973).
 (20) A. S. Levine and R. H. Wood, *J. Phys. Chem.*, **77**, 2390 (1973).
 (21) I. Wadso, *Acta Chem. Scand.*, **22**, 927 (1968).
 (22) See paragraph at end of text regarding supplementary material.
 (23) S. Lindenbaum, *J. Chem. Thermodyn.*, **3**, 625 (1971).
 (24) P. A. Leduc and J. E. Desnoyers, *Can. J. Chem.*, **51**, 2993 (1973).
 (25) G. Beurskens, G. A. Jeffrey, and R. K. McMullan, *J. Chem. Phys.*, **39**, 3311 (1963).
 (26) P. R. Philip and J. E. Desnoyers, *J. Solution Chem.*, **1**, 353 (1972).
 (27) S. Lindenbaum, L. Leifer, G. E. Boyd, and J. W. Chase, *J. Phys. Chem.*, **74**, 761 (1970).

Complexation and Form of Poly(vinylpyridine) Derivatives with Copper(II) in Aqueous Solution

Hiroshi Nishikawa and Eishun Tsuchida*

Department of Polymer Chemistry, Waseda University, Tokyo, 160 Japan (Received December 2, 1974; Revised Manuscript Received May 6, 1975)

The complexation of copper(II) with poly(4-vinylpyridine) (PVPy) and with partially quarternized PVPy (QPVPy) in aqueous solution was studied potentiometrically, spectroscopically, and viscometrically. From the formation curve computed from the titration data and spectroscopic results, it was found that four pyridine units coordinated with one cupric ion in the Cu-PVPy or Cu-QPVPy system. Overall formation constants of the polymer systems were much larger than those of the monomeric analog. This was caused by the enhancement of the successive stepwise formation constants due to the polymer effect. The four stepwise formation constants $\log K_i$ could be calculated directly from a least-squares curve-fitting method, and were 1.1, 2.2, 2.7, and 4.6 for the Cu-PVPy (Pn 19) system as contrasted with 2.5, 1.9, 1.3, and 0.8 for the binding of pyridine by Cu(II). When the PVPy ligand was partially quarternized by ethyl bromide, the formation constant decreased by the electrostatic effect. On the contrary, quarternization by benzil chloride did not affect the formation constant remarkably. This phenomenon can be explained by the affinity among benzyl groups. Visible and ESR spectra, however, did not vary with the change of the quarternizing reagent, which means that the structure of Cu complexes did not differ between the Cu-EBQPy system and the Cu-BCQPy system. From viscometric measurement data it was clear that the Cu-QPVPy complex had a very compact structure.

Introduction

It has been reported by many investigators that polymer-metal complexes show a high catalytic activity in redox reactions in solution, but the details of the catalysis have not been clarified because of the complexity of the catalytic system. In order to study the polymer-catalyst system it is necessary to clarify the form of the polymer-metal complexes in solution. In general, metal complexes which act as a catalyst are labile, so that analysis of the complex must be made in solution. The high catalytic activity of the copper(II) complex with poly(4-vinylpyridine) (PVPy) or partially quarternized PVPy (QPVPy) in the oxidation of phenols or ascorbic acid has been described previously.¹⁻³ In the present paper, the formation and form of complexes of PVPy or QPVPy with Cu(II) in aqueous solution were studied by potentiometric titrations, by spectroscopic measurements (visible, ESR), and by viscometric

measurements, and the effect of the polymer ligand on the formation process of the metal complex is discussed.

Experimental Section

Materials. Poly(4-vinylpyridine) was prepared by the radical polymerization of vinylpyridine and purified twice by reprecipitation. The average degrees of polymerization of PVPy used in this experiment were 19, 49, and 108, and were measured by vapor pressure osmometry. Partially quarternized PVPy (QPVPy) was obtained by quarternization of PVPy (PN 19 or 49) by benzil chloride or ethyl bromide. The percentage of quarternization (Q%) of QPVPy was determined by the measurement of the Cl⁻ or Br⁻ concentrations by means of the Volhard method. Copper(II) chloride and sodium chloride (analytical grade reagent) were used in order to rule out any effect of the counterion of pyridinium salt, and 0.1 M solutions of these were made

using distilled, CO₂-free water. The concentration of cupric ion in the stock solution was exactly determined by EDTA titration.

Solutions of CO₂-free sodium hydroxide were prepared according to the procedure described by Kolthoff and Sandell.⁴ The diluted solutions were standardized against freshly dried analytical grade potassium hydrogen phthalate and kept in polyethylene bottles. Diluted hydrogen chloride solution was prepared by dilution from analytical grade stock and was standardized with freshly standardized sodium hydroxide.

All solutions in this experiment were made using distilled, CO₂-free water.

Potentiometric Titrations. All titrations were made in the same way as reported by Gregor et al.⁵ under a nitrogen atmosphere in order to remove the effect of CO₂. No data above pH 5.5, where the hydrolysis of Cu(II) ion occurred, were used in the calculations. All titrations were made twice to check the reproducibility of the data. Hydrogen ion activities were determined with a Hitachi-Horiba M-5 type pH meter. Concentrations of hydrogen ion were calculated from the hydrogen ion activities by the assumption that the hydrogen ion activity coefficient was the same as the mean activity coefficient of supporting 1-1 electrolyte; γ^{\pm} was taken as 0.78 in 0.1 M sodium chloride and 0.82 and 0.05 M sodium chloride.⁶

Measurement of Spectra (Visible, ESR) and Viscosity of the Complex Solution. Measurements of visible spectra were limited to the Cu-QPVPy system which was always homogeneous under the experimental conditions. Visible spectra of the solutions were measured with a Simazu Model MPS-50L spectrometer and the ESR spectra were obtained with an electron spin resonance spectrometer (Japan Electron Optics JEP-1). The viscosities of the solution which were used for the spectroscopic measurement were measured by means of a modified Ubbelohde viscometer at 30.0°.

Calculations

Most of the polymer metal complexes behave as poly-electrolytes in aqueous solution, so that the calculation of formation constants introduced by Bjerrum must be modified for the binding of metals by polyelectrolytes. In this experiment, the modified Bjerrum method, which was reported by Gregor et al.,⁵ was used for the calculation and the method will be summarized herein. The average number of ligands bound per metal ion, \bar{n} , is determined as a function of the free ligand concentration to give the formation function of the system. For the PVPy-Cu(II) system, \bar{n} is expressed as

$$\bar{n} = \frac{[\text{PVPy}]_t - [\text{PVPy}] - [\text{PVPyH}^+]}{[\text{Cu}^{2+}]_t} \quad (1)$$

where $[\text{PVPy}]_t$ is the total base molar concentration of PVPy expressed in base moles per liter, $[\text{PVPy}]$ and $[\text{PVPyH}^+]$ are the concentrations of PVPy and protonated base groups, respectively, and $[\text{Cu}^{2+}]_t$ is the total copper(II) concentration.

From material balance equations and the electroneutrality requirement it can easily be shown that the pyridinium ion concentration is given by measurable quantities

$$[\text{PVPyH}^+] = [\text{PVPy}]_t (1 - \alpha) - [\text{H}^+] + [\text{OH}^-] \quad (2)$$

In the case of a polyacid, the acid dissociation "constant" is a function of the degree of chain charging. It was shown

empirically that over a wide range of α the titration of PVPy could be expressed as

$$K_a = \frac{[\text{H}^+][\text{PVPy}]}{[\text{PVPyH}^+]} \left(\frac{1}{Z}\right)^{n-1} \quad (3)$$

where Z is the ratio of charged to uncharged groups on the polymer chain and n is the Henderson-Hasselbach slope in the absence of added metal. For the presence of copper ions, information as to the species of complex present is required. As will be seen later, the principal coordination number N is four, with a small spreading factor, for the Cu-PVPy or Cu-QPVPy system, thus indicating the predominant species to be the 4:1 complex. Since in eq 3 the complexation does not itself alter the dissociation relation of the acid, eq 3 is expressed for the Cu-PVPy system as

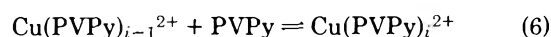
$$K_a = ([\text{H}^+][\text{PVPy}]/[\text{PVPyH}^+]) \times \{[\text{PVPy}]/([\text{PVPyH}^+] + \frac{1}{2}(\alpha[\text{PVPy}]_t + [\text{H}^+] - [\text{OH}^-] - [\text{PVPy}]))\}^{n-1} \quad (4)$$

and for the Cu-QPVPy system as

$$K_a = [\text{H}^+][\text{PVPy}]/[\text{PVPyH}^+] \times \{[\text{PVPy}]/([\text{PVPyH}^+] + \frac{1}{2}(\alpha[\text{PVPy}]_t - [\text{PVPy}] + [\text{H}^+] - [\text{OH}^-] + [\text{PVPyR}^+])\}^{n-1} \quad (5)$$

where $[\text{PVPyR}^+]$ is the concentration of quarternized PVPy unit. Equations 4 and 5 can be solved for the only unknown, $[\text{PVPy}]$, through an iterative procedure and \bar{n} obtained. Overall formation constants β_4 were obtained from \bar{n} -log $[\text{PVPy}]$ plots according to Bjerrum's theory.

Approximate values of the successive stepwise formation constants K_i which refer to the processes



can be calculated by an elegant procedure which was proposed by Scatchard and used by Edsall.⁷ In this method the parameter Y is introduced

$$Y = \bar{n}/(N - \bar{n})[A] \quad (7)$$

where N is the maximum coordination number. By plotting log Y vs. \bar{n} , one obtains approximate values of the formation constants.

$$\lim_{[A] \rightarrow 0} Y = K_1/4 \quad (8)$$

$$\lim_{[A] \rightarrow \infty} Y = 4K_4 \quad (9)$$

$$\lim_{\bar{n} \rightarrow 0} \frac{d \ln Y}{d \bar{n}} = \frac{8K_2 - 3K_1}{4K_1} \quad (10)$$

$$\lim_{\bar{n} \rightarrow 4} \frac{d \ln Y}{d \bar{n}} = \frac{8K_4 - 3K_3}{4K_3} \quad (11)$$

Since it is difficult to obtain accurate values as $\bar{n} \rightarrow 0$ and $\bar{n} \rightarrow 4$ experimentally, a linear extrapolation was used.

Between \bar{n} and $[\text{PVPy}]$, the relationship

$$\bar{n} = \frac{K_1[\text{PVPy}] + 2K_1K_2[\text{PVPy}]^2 + 3K_1K_2K_3[\text{PVPy}]^3 + 4K_1K_2K_3K_4[\text{PVPy}]^4}{1 + K_1[\text{PVPy}] + K_1K_2[\text{PVPy}]^2 + K_1K_2K_3[\text{PVPy}]^3 + K_1K_2K_3K_4[\text{PVPy}]^4} \quad (12)$$

is valid. Using this equation the formation constants K_1 , K_2 , K_3 , K_4 , and $\beta_4 (= K_1K_2K_3K_4)$ were also calculated directly on an IBM 370 Model 135 computer applying a least-squares curve-fitting technique.

Results and Discussion

The PVPy-Copper(II) System. The calculated forma-

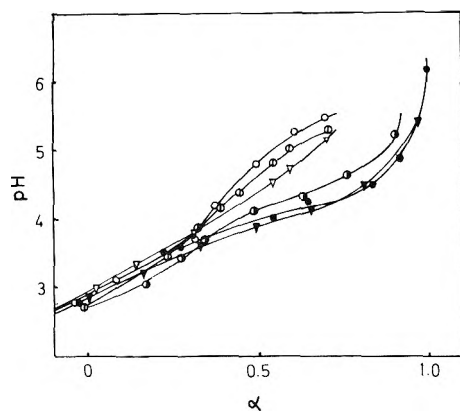


Figure 1. Titration of PVPy (circles) or quarternized PVPy by benzyl chloride (triangles) in 0.1 M sodium chloride with a copper(II) chloride concentration ($\times 10^{-3}$ M) of: 0 (—○—, —□—, —▽—), 2.0 (—●—, —▼—), and 4.0 (—○—). Polymer ligand concentration ($\times 10^{-2}$ M): 1.0 (—○—, —●—, —▽—, —▼—), 2.0 (—□—, —○—).

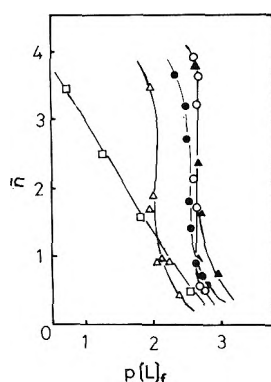


Figure 2. Formation curves for the Cu-PVPy and Cu-QPVPy complexes. Ligand concentration ($\times 10^{-2}$ M) of 1.0 (○, Δ, ▲) and 2.0 (●). Quaternizing reagents were ethyl bromide (Δ) and benzyl chloride (▲); pyridine-Cu(II) (□).

tion curve for the Cu-PVPy system is shown in Figure 2. This figure also shows the formation curve of Cu-QPVPy in 0.1 M sodium chloride. The formation curve of Cu-PVPy would appear to extrapolate to a maximum coordination number of $N = 4$. The steep slopes evidenced by the Cu-PVPy and Cu-QPVPy formation curves indicate spreading factors of less than unity between the stepwise formation constants.

Overall formation constants for the complexation of copper with PVPy under several experimental conditions are summarized in Table I, and the successive formation constants K_i calculated by a least-squares curve-fitting technique and those from Scatchard plots (Figure 3) are shown in Table II. The overall formation constants obtained by both the graphical method and direct calculation based on eq 12 are quite close. However the stepwise formation constants, especially K_1 and K_4 , obtained by both methods are fairly different. This difference between K_1 and K_4 is probably due to the error introduced by extrapolation in the Scatchard procedure. Thus, it is considered that the Scatchard procedure is unsuitable for polymer-metal complex systems in which the spreading factor is small. Overall formation constants β_4 for the Cu-PVPy system were 10^{2-4} times as large as that for Cu-Py system, which indicates that the $\text{Cu}(\text{PVPy})_4$ complex forms readily. The successive formation constants $\log K_i$ (Table II) show considerably greater successive increments with the Cu(II)-PVPy sys-

TABLE I: Overall Stability Constants of Cu(II)-PVPy Complexes

Pn	$[\text{PVPy}]_t, M$	$[\text{PVPy}]_t/[\text{Cu(II)}]_t$	μ	$\log \beta_4(\text{A})^b$	$\log \beta_4(\text{B})^c$
19	1×10^{-2}	5	0.10	10.8	10.5
49	1×10^{-2}	5	0.10	10.0	9.8
108	1×10^{-2}	5	0.10	10.0	9.7
19	2×10^{-2}	5	0.10	9.7	
19	1×10^{-2}	10	0.10	10.3	10.2
19	1×10^{-2}	20	0.10	10.0	
19	1×10^{-2}	5	0.05	8.6	
Py ^a			0.5	6.5	

^a R. T. Bruhlman and F. H. Verhoek, *J. Am. Chem. Soc.*, **70**, 1401 (1948). ^b Graphically obtained value. ^c Calculated value by a least-squares curve-fitting technique.

TABLE II: Successive Stepwise Stability Constants of Cu(II)-PVPy Complexes^a

Pn	$[\text{PVPy}]_t/[\text{Cu(II)}]_t$	Method ^b	$\log K_1$	$\log K_2$	$\log K_3$	$\log K_4$
19	5	A	2.2	2.3	3.0	3.1
		B	1.1	2.2	2.7	4.6
19	10	A	2.4	2.3	2.8	2.8
		B	1.2	2.1	2.7	4.3
108	5	A	2.0	2.0	3.0	3.0
		B	1.1	1.6	2.7	4.4
Py			2.5	1.9	1.3	0.8

^a $[\text{PVPy}]_t = 1 \times 10^{-2}$ M, $\mu = 0.10$, 20°. ^b Method A, Scatchard procedure. Method B, least-squares curve-fitting technique.

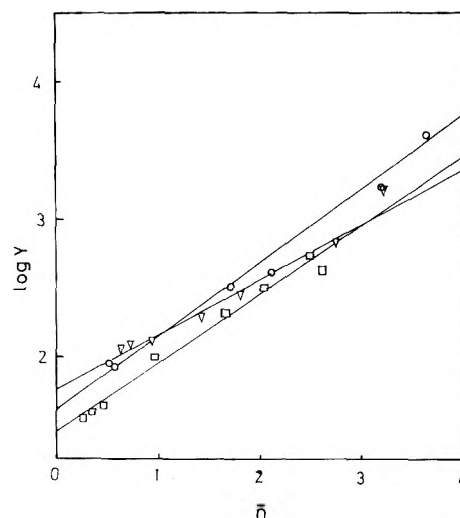


Figure 3. Scatchard Y plot for Cu(II)-PVPy complexes at ligand ratio $[\text{PVPy}]_t/[\text{Cu(II)}]_t$: 5.0 (○; Pn 19, □; Pn 108) and 10 (Δ; Pn 19).

tem than with the Cu-Py system. This phenomena appears to be general with the polymer complex system, and can be explained by the assumption that the concentration of ligand is higher in the polymer domain, so that once the metal ion is attached to one group on the polymer chain, the other ligands coordinate more readily. On the other hand, the K_1 value is always smaller in polymer systems than in analog monomeric systems. This is considered to be due to the electrostatic repulsion between the coordinating copper ion and the pyridinium ion or the cupric complex on

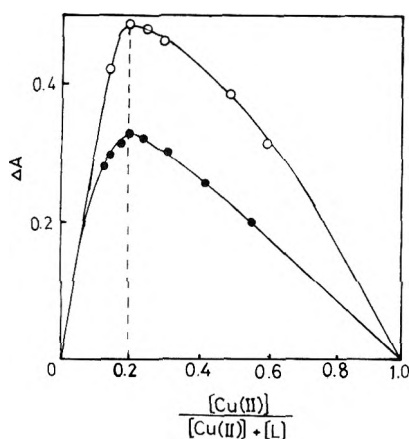


Figure 4. Continuous variations analysis of the Cu-QPVPy complex measured at 620 nm and pH 5.0. Quaternizing reagents were ethyl bromide (●) and benzyl chloride (○).

the polymer chain, and the steric hindrance of the coiling polymer chain. These reasons are supported by the fact that the difference between $\log K_1(\text{Cu-PVPy})$ and $\log K_1(\text{Cu-Py})$ decreased with increase ligand ratio $([\text{PVPy}]_t/[\text{Cu(II)}]_t)$, when the concentration of copper(II) complex per polymer chain decreased, and the electric repulsion and steric hindrance were lowered. On the contrary, K_3 and K_4 values decreased with increase of ligand ratio. This is probably due to the enhanced steric strain in the complexes by the decrease of the number of intrabridged points. On the whole, the stability of the $\text{Cu}(\text{PVPy})_4$ complex decreased with increase of ligand ratio. When the degree of the polymerization of the PVPy ligand increased, K_1 and K_2 values were lowered because of the enhancement of the electrical free energy. The ionic strength of the solution is a very important factor for the binding of a metal ion to a polymer. Since the decrease of the ionic strength increases the electrostatic repulsion among the pyridinium ions and Cu^{2+} complexes, the strain of coordination bond is increased; this can readily account for the observed result that $\log \beta_4 (\mu = 0.1) - \log \beta_4 (\mu = 0.05)$ is 2.2.

The QPVPy-Copper(II) System. Figure 4 shows the result of continuous variations analysis of the Cu(II)-QPVPy complexes measured at 630 nm and pH 5.4 using a 0.04 M total solution concentration. A sharp maximum was seen at the Cu(II) mole fraction of 0.2, and this indicated that the predominant species formed under these experimental conditions was a complex of four pyridine groups with one cupric ion. From these results it was clear that the partial quaternization had very little effect on the complex composition. Overall formation constants of the Cu-QPVPy complex calculated from the potentiometric titration data are listed in Table III. It is interesting to note that the effects of the quaternization on the complexation differ with the reagent used to quaternize. When the QPVPy quaternized by ethyl bromide (EBQPy) was used as a ligand, the overall formation constants decreased with the increase of $Q\%$ of EBQPy and $\log \beta_4$ at $Q\% = 35$ was 9.3 which was smaller by 1.5 than that of the Cu-PVPy complex. The electrical free energy term increased when a positive charge is added to polymer chain by quaternization; this is the reason for the observed decrease of $\log \beta_4$. With benzyl chloride being used as the quaternizing reagent, no effect of the quaternization on the stability of the polymer complex was observed. Since the benzyl group has a high hydrophobicity and a stacking effect, the BCQPy ligand readily ag-

TABLE III: Overall Stability Constants of Cu(II)-QPVPy Complexes^a

Quaternizing reagent	% Q	$\log \beta_4$
Benzyl chloride	10	10.7
Benzyl chloride	28	10.8
Benzyl chloride	43	10.5
Ethyl bromide	13	10.4
Ethyl bromide	25	9.5
Ethyl bromide	35	9.3

^a $[\text{QPVP}]_t = 1 \times 10^{-2} M$, $[\text{QPVPy}]_t/[\text{Cu(II)}]_t = 5$, $\mu = 0.1$, 23° .

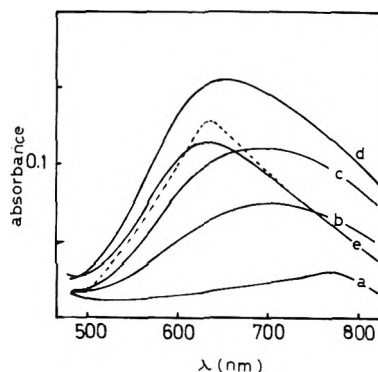


Figure 5. The visible spectra of Cu-QPVPy complex solutions containing $1.0 \times 10^{-2} M$ QPVPy by ethyl bromide (EBQPy) and $2 \times 10^{-3} M$ Cu(II) . The pH value of the solutions are 3.53 (a), 4.20 (b), 4.65 (c), 5.28 (d), and 8.30 (e). The dotted line is the spectrum of a Cu(Py)_4 solution.

gregates at rather high ionic strength where the electrostatic effects were shielded. At ionic strength 0.1 the electrostatic effect is not great so that the affinity among benzyl groups may be able to cancel the electrostatic strain of the polymer chain, allowing the polymer chain to bend easily. That is to say, the difference of the quaternization effect is probably due to the difference of the affinity among alkyl groups. Figure 5 shows that absorption spectra of the Cu(II)-EBQPy solution containing 0.02 M EBQPy and 0.002 M Cu(II) at various pH values. As \bar{n} was increased with pH, the absorptivity increased and the absorption maximum shifted toward shorter wavelengths. However the wavelength of the absorption maximum of the Cu(QPVPy)_4 complex solution (at pH 5.4) was longer by 10 nm than that of Cu(Py)_4 solution. The steric strain can readily account for this phenomenon. When the pH was increased beyond 5.4, at which the α value was 1.0, the absorptivity was lowered and the shape changed into that of the Cu(Py)_4 complex. This might be caused by hydrolysis of the complex region in which the strain of the polymer chain was large. The change of the viscosity of the Cu-PVPy complex solution with pH was illustrated in Figure 6 which also shows the change of \bar{n} . The viscosity decreased largely according to the increase of \bar{n} . This suggests the formation of the intramolecular chelate in the Cu-QPVPy complex and that the polymer complex takes a very compact structure as a whole. The viscosity of the solution, however, increased again beyond pH 5.4 due to the hydrolysis of the complex.

Some ESR spectra of Cu-QPVPy solution are shown in Figure 7, and the values of the parameters g and the splitting constant A , which express the interaction between unpaired electron and copper nucleus, are summarized in

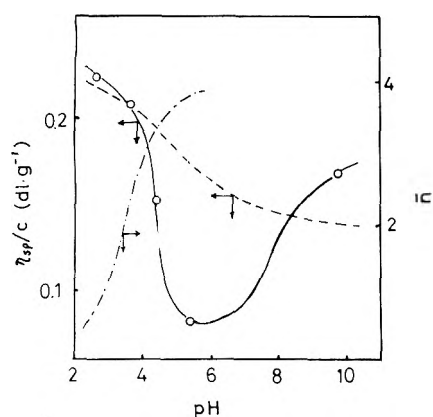


Figure 6. Change of viscosity (η_{sp}/c) and average coordination number of the Cu-EBQPy complex solution with pH. η_{sp}/c (Cu-EBQPy solution) vs. pH (—○—); η_{sp}/c (Cu(II) free EBQPy solution) vs. pH (---○---); \bar{n} vs. pH (- · -).

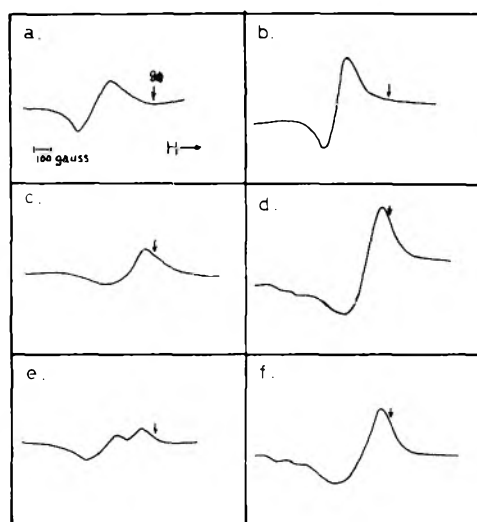


Figure 7. The ESR spectra of Cu-QPVPy complex solutions containing $5.0 \times 10^{-2} M$ Cu(II). a and b are QPVPy-free solutions, c and d contain $5.0 \times 10^{-1} M$ EBQPy, e contains $1.6 \times 10^{-1} M$ EBQPy, and f contains $5.0 \times 10^{-1} M$ BCQPy. a, c, and e are at ambient temperature, b, d, and f are at $77^\circ K$.

Table IV. The ESR spectra were very broad due to the interaction between protons from the solvent and the com-

TABLE IV: The g and A Parameters of Cu(II)-QPVPy Complexes^a

Complex	$[\text{QPVPy}]_t / [\text{Cu(II)}]_t$	$T, ^\circ K$	$g_\perp \pm 0.003$	$g_\parallel \pm 0.01$	$A_\parallel \pm 4, G$
Cu(II) _{aq}		293	2.170		
		77	2.157		
			2.155		
Cu-EBQPy	3.3	293	2.104		
		77	2.110	2.342	124
Cu-EBQPy	10	293	2.083		
		77	2.081	2.282	166
Cu-BCQPy	10	77	2.085	2.288	165

^a $\mu = 0.1, [\text{Cu(II)}]_t = 5 \times 10^{-2} M$.

plex. Especially at room temperature, the peak of the component of the horizontal direction was not found.

Comparing g or A values among $[\text{QPVPy}]_t / [\text{Cu}]_t = 0, 3.3,$ and 10 , it was found that g values were decreased and A values increased with the increase of the number of ligands interacting with Cu(II). For $[\text{QPVPy}]_t / [\text{Cu}]_t$ under 3.3 , two signals which correspond to the Cu(II)_{aq} ion and QPVPy complex were observed at room temperature, but at $77^\circ K$, only one signal appeared at an intermediate position; this suggests that the form of the complex changes with temperature at this condition. For a ligand ratio under 10 , the shape of the spectra did not change with temperature. This is probably due to the formation of $4:1$ complex of all cupric ions. There were no differences between ESR spectra of Cu-EBQPy and Cu-BCQPy; this suggests that the alkyl group does not affect the structure of the complex part of polymer-metal complex.

References and Notes

- (1) E. Tsuchida, H. Nishide, and T. Nishiyama, *J. Polym. Sci., Part C*, **47**, 35 (1974).
- (2) E. Tsuchida, H. Nishide, and H. Nishikawa, *J. Polym. Sci., Part C*, **47**, 47 (1974).
- (3) E. Tsuchida, H. Nishide, and H. Nishikawa, *Macromolecules*, in press.
- (4) I. M. Kolthoff and E. B. Sandell, "Textbook of Quantitative Inorganic Analysis", Macmillan, New York, N.Y., 1946.
- (5) E. H. Gold and H. P. Gregor, *J. Phys. Chem.*, **64**, 1464 (1960).
- (6) W. M. Latimer, "Oxidation Potentials", Prentice-Hall, Englewood Cliffs, N.J., 1956, p 356.
- (7) J. T. Edsall, G. Felsenfeld, D. S. Goodman, and F. R. N. Gurd, *J. Am. Chem. Soc.*, **76**, 3054 (1954).

**New concepts
new techniques
new interpretations**

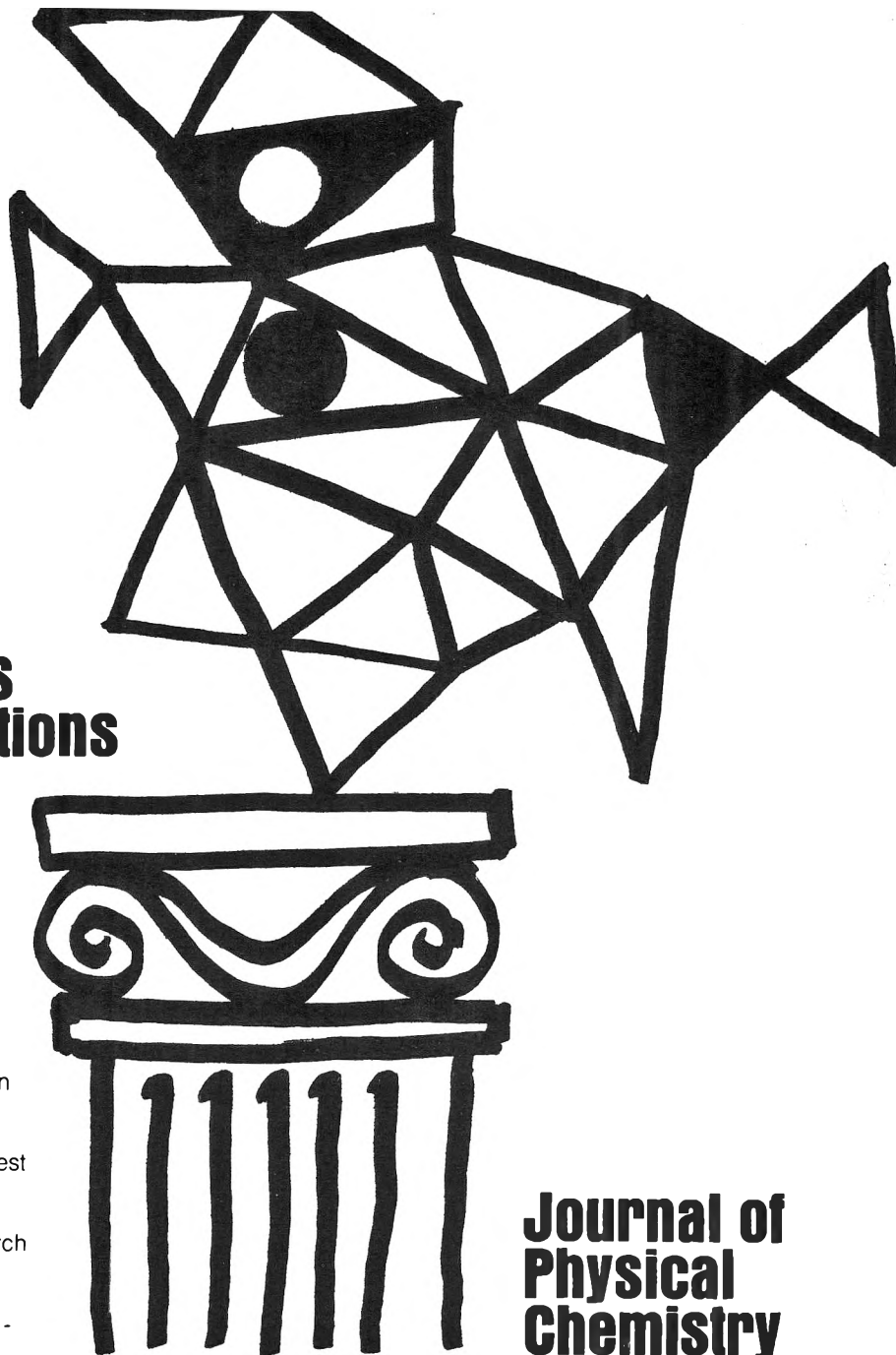
**... together
with valuable reports
on classical areas**

They are all waiting for you between the covers of our well-balanced JOURNAL OF PHYSICAL CHEMISTRY. Whatever your particular interest in physical chemistry, you'll find the JOURNAL's broad range of experimental and theoretical research reports are relevant and beneficial to your work. Each biweekly issue brings you an average of 30 authoritative, comprehensive reports on fundamental aspects of atomic and molecular phenomena, as well as timely notes, communications and reports plus the proceedings of selected symposia.

Join your fellow physical chemists who rely on JPC as an excellent biweekly source of data in both new and classical areas. Just complete and return the form to start your own subscription.



... another ACS service



Journal of Physical Chemistry

**The Journal of Physical Chemistry
American Chemical Society**

1155 Sixteenth Street, N.W.
Washington, D.C. 20036

1975

Yes, I would like to receive the JOURNAL OF PHYSICAL CHEMISTRY at the one-year rate checked below:

	<i>U.S.</i>	<i>Canada**</i>	<i>Latin America**</i>	<i>Other Nations**</i>
ACS Member One-Year Rate*	<input type="checkbox"/> \$20.00	<input type="checkbox"/> \$24.50	<input type="checkbox"/> \$24.50	<input type="checkbox"/> \$25.00
Nonmember	<input type="checkbox"/> \$80.00	<input type="checkbox"/> \$84.50	<input type="checkbox"/> \$84.50	<input type="checkbox"/> \$85.00

Bill me Bill company Payment enclosed

Air freight rates available on request.

Name _____

Street _____

Home
Business

City _____

State _____

Zip _____

Journal subscriptions start on January '75

*NOTE: Subscriptions at ACS member rates are for personal use only. **Payment must be made in U.S. currency, by international money order, UNESCO coupons, U.S. bank draft, or order through your book dealer.

New Volumes in . . .
PHYSICAL CHEMISTRY

An Advanced Treatise

edited by HENRY EYRING, DOUGLAS HENDERSON, and WILHELM JOST

VOLUME 6B
KINETICS OF GAS REACTIONS

edited by WILHELM JOST

CONTENTS: *A. Henglein*, Elastic and Reactive Scattering of Ions on Molecules. *H. Pauly*, Collision Processes, Theory of Elastic Scattering. *J. Wolfrum*, Atom Reactions. *A. B. Callear*, Relaxation Methods in Gases. *J. Troe*, Unimolecular Reactions: Experiments and Theories. *K. H. Hoyermann*, Interactions of Chemical Reactions, Transport, Processes, and Hydrodynamics.

1975, 538 pp., \$49.50/£23.75;
subscription price, \$42.00

VOLUME 11B
MATHEMATICAL METHODS

edited by DOUGLAS HENDERSON

CONTENTS: *N. W. Dalton*, Methods in Lattice Statistics. *D. A. McQuarrie*, Probability Theory and Stochastic Processes. *J. T. Hynes and J. M. Deutch*, Non-Equilibrium Problems—Projection Operator Techniques. *F. D. Peat*, Scattering Theory. *R. L. Somorjai*, The Solution of Integral and Differential Equations.

1975, 608 pp., \$47.00/£22.60;
subscription price, \$39.95

VOLUME 7
REACTIONS IN CONDENSED PHASES

edited by HENRY EYRING

CONTENTS: *S. H. Lin, K. P. Li, and H. Eyring*, Theory of Reaction Rates in Condensed Phases. *S. W. Benson and D. M. Golden*, Methods for the Estimation of Rate Parameters of Elementary Processes. *J. Michl*, Use of Correlation Diagrams for Interpretation of Organic Reactivity. *E. Grunwald and J. E. Leffler*, Perturbation of Reactions by Substituents. *R. G. Pearson and P. C. Ellgen*, Mechanisms of Inorganic Reactions in Solution. *E. S. Huyser*, Kinetics of Free-Radical Reactions. *M. Boudart*, Heterogeneous Catalysis. *M. E. Wadsworth*, Reactions at Surfaces. *A. G. Maddock*, Chemical Annealing Reactions in Solids. *M. S. Matheson*, Reactions of Solvated Electrons. *L. D. Spicer and C. D. Poulter*, Isotopes as Probes in Determining Reaction Mechanisms. *M. Kahlweit*, Nucleation in Liquid Solutions. *A. Mozumder and J. L. Magee*, Radiation Chemistry in Condensed Phases.

1975, 796 pp., \$58.00/£27.85;
subscription price, \$49.50

STRUCTURE OF METALLIC CATALYSTS

by J. R. ANDERSON

This is the first book which attempts a coherent account of the structure of metallic catalysts; in particular the author tries to relate general preparative methods and ultimate structure to the chemistry and physics of the materials concerned.

Many catalysts consist of chemical compounds containing a metal in a combined form, but only those where metal is present as a distinct and separate metallic phase are discussed here. There are chapters dealing with technical catalysts, and also with model catalysts which are a useful control for variables in the system and form a standard against which technical catalysts can be judged. Various techniques for the characterization of metallic catalysts are treated in some depth and a good deal of attention is given to support materials, which influence the dispersion of the metal and its accessibility to the reactant, as well as possibly providing catalytic activity of their own.

1975, 478 pp., \$33.75/£12.80

AN INTRODUCTION TO GROUP REPRESENTATION THEORY

by R. KEOWN

A Volume in the MATHEMATICS IN SCIENCE AND ENGINEERING Series

There are other books on representation theory, but newcomers to the field may have difficulty with them. This book, on the other hand, is specifically designed for the mathematician or scientist approaching representation theory for the first time. Its aim is to teach the reader how to calculate irreducible representations rather than just to develop theorems about them.

The book first reviews the algebraic facts needed in group representation theory. It then develops the complex representation theory of finite groups including that of the symmetric group, the finite-dimensional integral representations of the general linear groups and certain of their subgroups, as well as various ideas about the representation of Lie algebras and Lie groups. Computation is stressed throughout. An additional chapter attempts to satisfy some of the needs of students and research workers outside of mathematics for a quick presentation of various facts about the representation theory of special groups.

1975, 346 pp., \$21.00/£10.50

THERMAL CONDUCTIVITY OF SOLIDS

by J. E. PARROTT and AUDREY D. STUCKES

The aim of this book is to provide in a compact and accessible form a sound introduction to the subject. It reviews the underlying principles, systematically surveys the different measurement techniques, introduces the necessary theoretical concepts, analyzes theoretically experimental data, and provides a guide to the behavior of practical materials, with some insight into the possibility of "tailoring" thermal conductivity. The bibliography at the end of each chapter enables readers to follow up any points of individual interest.

The book is intended for final year undergraduates and postgraduates embarking on the study of heat conduction and for the applied scientists who have an interest in thermal conductivity, but the practical aspects dealt with in the book will be understood by engineers, chemists, and others not necessarily of graduate status.

1975, 163 pp., \$10.50/£4.00

Published by Pion, Limited. Distributed by Academic Press.

N.B.: Postage plus 50¢ handling on all orders not accompanied by payment.
Prices subject to change without notice.

ACADEMIC PRESS

A Subsidiary of Harcourt Brace Jovanovich, Publishers
111 FIFTH AVENUE, NEW YORK, N. Y. 10003
24-28 OVAL ROAD, LONDON NW1 7DX